Advances in Industrial Control

Péter Gáspár
Zoltán Szabó
József Bokor
Balázs Németh

Robust Control Design for Active Driver Assistance Systems

A Linear-Parameter-Varying Approach

Advances in Industrial Control

More information about this series at http://www.springer.com/series/1412

Péter Gáspár · Zoltán Szabó
József Bokor · Balázs Németh

Robust Control Design for Active Driver Assistance Systems

A Linear-Parameter-Varying Approach

Springer

Péter Gáspár
Computer and Automation Research Institute
Hungarian Academy of Sciences
Budapest
Hungary

József Bokor
Computer and Automation Research Institute
Hungarian Academy of Sciences
Budapest
Hungary

Zoltán Szabó
Computer and Automation Research Institute
Hungarian Academy of Sciences
Budapest
Hungary

Balázs Németh
Computer and Automation Research Institute
Hungarian Academy of Sciences
Budapest
Hungary

ISSN 1430-9491 ISSN 2193-1577 (electronic)
Advances in Industrial Control
ISBN 978-3-319-46124-3 ISBN 978-3-319-46126-7 (eBook)
DOI 10.1007/978-3-319-46126-7

Library of Congress Control Number: 2016951980

Printed on acid-free paper

This Springer imprint is published by Springer Nature
The registered company is Springer International Publishing AG
The registered company address is: Gewerbestrasse 11, 6330 Cham, Switzerland

Series Editors' Foreword

The series *Advances in Industrial Control* aims to report and encourage technology transfer in control engineering. The rapid development of control technology has an impact on all areas of the control discipline. New theory, new controllers, actuators, sensors, new industrial processes, computer methods, new applications, new design philosophies, new challenges. Much of this development work resides in industrial reports, feasibility study papers, and the reports of advanced collaborative projects. The series offers an opportunity for researchers to present an extended exposition of such new work in all aspects of industrial control for wider and rapid dissemination.

Road transportation has experienced significant control research and development over the last few decades. The introduction into vehicles and traffic-flow systems of reliable computing and information technologies along with robust sensor devices has produced a considerable change in the driving experience. Now prototype driverless vehicles are even appearing in the transport system. Creating a top-down view this control research in road transportation provides a useful framework for understanding the ongoing developments.

There are four major aspects to control research in road transport:

i. the classes of vehicles;
ii. the road transport infrastructure;
iii. the environmental conditions; and
iv. the issues arising from "human-in-the-loop" control.

These aspects then give rise to various interactions depending on the vehicle/traffic/environment situation being investigated. The "classes of vehicles" include: motor cycles, automobiles, light goods vehicles, heavy goods vehicles, and specialized vehicles (fire engines,and refuse-collection vehicles, for example). Each of these vehicle classes will have different travel objectives and quite different dynamics. However as more and more autonomy is introduced into vehicle control, the inclusion of the "human-in-the-loop" adds an addition level of complexity to

vehicle control. Road transport "infrastructure" includes urban road networks, rural road networks and then freeways, autobahns, or motorways. The quality of road surfaces, the density of traffic, the amount of roadside instrumentation, and the purpose of all these transport networks will differ considerably. Driving conditions as provided by the environment will depend on such factors as the weather, and the road topology. This type of overview can easily be transcribed into an interesting hierarchical diagram. Such an overview is useful to Series Editors as it enables them to place the many strands of road transport control research into a framework and allows them to identify new potential contributions for developing a well-balanced and up to date group of titles in the series.

One of the very few monographs in the *Advances in Industrial Control* series to deal with the characteristics of "human-in-the-loop" issues is the 1998 monograph *Modelling and Simulation of Human Behaviour in System Control* by Pietro C. Cacciabue (ISBN 978-3-540-76233-1, 1998). The practical issues of the balance between autonomy and human control intervention (from a driver, pilot, or operator) will undoubtedly receive more research input in future years across many different control application fields.

In the hierarchy of road transport, "infrastructure" is an important classifier with different types of network exhibiting different control requirements. The *Advances in Industrial Control* series has two monographs reporting developments in this growing field. The monograph *Feedback Control Theory for Dynamic Traffic Assignment* by Pushkin Kachroo and Kaan Özbay (ISBN 978-1-85233-059-0, 1998) is a seminal contribution (a second edition is currently in preparation) and the monograph *Hybrid Predictive Control for Dynamic Transport Problems* by Alfredo Núñez, Doris Sáez and Cristián E. Cortés (ISBN 978-1-4471-4350-5, 2012) reports some recent research on bus transport in urban road networks.

As evidenced by the frequent sessions at the IEEE control conferences, the exploitation of advanced control ideas for the automobile class of vehicles has received far more research input and the *Advances in Industrial Control* monograph series has several contributions:

- *Dry Clutch Control for Automotive Applications* by Pietro J. Dolcini, Carlos Canudas de Wit and Hubert Béchart (ISBN 978-1-84996-067-0, 2010);
- *Active Braking Control Systems Design for Vehicles* by Sergio M. Savaresi and Mara Tanelli (ISBN 978-1-84996-349-7, 2010); and
- *Optimal Control of Hybrid Vehicles* by Bram de Jager, Thijs van Keulen and John Kessels (ISBN 978-1-4471-5988-9, 2015).

In this same group of topics falls this monograph *Robust Control Design for Active Driver Assistance Systems: An LPV Approach* by Péter Gáspár, Zoltán Szabó, József Bokor and Balázs Németh. This particular monograph not only reports on control designs for driver-assist systems but is virtually a tutorial and case-study work on how to use the linear-parameter-variable method. This makes

the volume doubly welcome in the *Advances in Industrial Control* monograph series being both applications- and technique-oriented. The readership for this monograph will not only encompass the specialist engineer in automotive engineering but will undoubtedly include the broader control engineering community.

Michael J. Grimble
Michael A. Johnson
Industrial Control Centre
University of Strathclyde
Glasgow Scotland, UK

Contents

Abbreviations

DOF	Degrees of Freedom
FC	Full Control
FD	Finite Dimension
FDI	Fault Detection and Isolation
H_∞	H-infinity
H_∞/μ	H-infinity with μ
HIL	Hardware in-the-Loop
HJE	Hamilton-Jacobi Equations
HJI	Hamilton-Jacobi Inequalities
LFT	Linear Fractional Transformation
LMI	Linear Matrix Inequality
LPV	Linear Parameter Varying
LS	Least Squares
LTI	Linear Time Invariant
LTV	Linear Time Varying
MIMO	Multi-Input Multi-Output
NLTI	Nonlinear Time Invariant
OE	Output Estimation
OF	Output Feedback
PDLF	Parameter-Dependent Lyapunov Functions
qLPV	Quasi LPV
RS	Robust Stability
RLS	Recursive LS
RP	Robust Performance
SF	State Feedback
SIL	Software in-the-Loop
SISO	Single-Input Single-Output
SLF	Single Lyapunov Functions
SSR	State Space Representation

Chapter 1
Introduction

Driver Assistance Systems

Active driver assistance systems are able to assist the driver in enhancing passenger comfort, road holding, the efficiency and safety of transport, etc. At the same time the responsibility remains with the driver, since the driver is able to override the assistance. The demand for vehicle control methodologies that include the driver, the vehicle and the road arises at several research centers and automotive suppliers.

The book focuses on active driver assistance systems, which influence the dynamics of the vehicle. On the level of the individual vehicle components the control problem is formulated and solved by a unified modeling and design method provided by the linear parameter varying (LPV) framework. The requested global behavior is achieved by a judicious interplay between the individual components guaranteed by an integrated control mechanism. The integrated control problem is also formalized and solved in the LPV framework.

The main contributions of the book include

- application of the LPV paradigm in the modeling and control design methodology,
- application of the robust LPV design as a unified framework for setting control tasks related to active driver assistance,
- formulation and solution proposals for the integrated vehicle control problem,
- proposal for a reconfigurable and fault-tolerant control architecture.

Design Tools

Modeling and control of mechanical systems form an important class of nonlinear and linear systems, which have widespread application in science and industry. There are three approaches to describe the equation of motion for mechanical systems: Newtonian, Lagrangian, and Hamiltonian mechanics. Newtonian mechanics is used for simple mechanical systems because it is an intuitive and non-systematic method. By contrast, Lagrangian and Hamiltonian mechanics are used for complex multi-body mechanical systems because they are systematic approaches. A mechanical system

P. Gáspár et al., *Robust Control Design for Active Driver Assistance Systems*,
Advances in Industrial Control, DOI 10.1007/978-3-319-46126-7_1

is usually nonlinear in nature. Since the problem formulation of the output-feedback nonlinear control problem usually results in highly nonlinear partial differential equations and in a large number of theoretical and practical difficulties, it is difficult to solve in practice.

In modern control design, the approximation of nonlinear models with linear models is often based on a quasi LPV (qLPV) description. This approach is based on the possibility of rewriting the plant in a form in which nonlinear terms can be hidden by using suitably defined scheduling variables. For a successful analysis and design, it is crucial to obtain a model that captures the essential behaviors of the system under consideration. An advantage of qLPV models is that in the entire operational interval nonlinear systems can be defined while a well-developed linear system theory to analyze and design nonlinear control system can be used.

The purpose of modeling is control design, thus the model of the systems must be augmented with performance specifications and model uncertainties. Performance signals show the quantitative behavior of the controlled system, i.e., control systems are designed to maintain the system outputs at a desired value. In control systems usually a great number of predefined performance specifications must be formalized, e.g., passenger comfort, road holding, suspension deflection, tire load variation, energy consumption. The purpose of the control system is to guarantee the performance specifications. However, one of the properties might only be improved to the detriment of other properties, i.e., if one of the performance properties is enhanced at the same time another performance is usually degraded or hurt. For example, the performance demands of improving passenger comfort and road holding are in conflict. The conflict between different performance demands must be resolved in such a way that a balance between performances is achieved.

Uncertainties of the model are caused by neglected components, unknown or little-known parameters. The uncertainties are modeled by both unmodeled dynamics and parametric uncertainties. In the vehicle model there are unknown parameters which vary in normal operation both in a short time period, e.g., mass, and in a long time period, abrasion. The estimation of the uncertain interval around its nominal value is important in the control design. If the uncertain interval is selected too large, the designed controller will be conservative. In this case the controller is designed in such a way that it will guarantee performances even in extreme conditions that do not occur. The unmodeled dynamics must be reduced by using a more appropriate estimation of the difference between the model and the actual plant. If parametric uncertainties of mechanical components are known, the uncertainties for unmodeled dynamics can also be reduced.

Weighting functions are applied to the performance signals to meet performance specifications and guarantee a trade-off between performances. The uncertainties are modeled by both unmodeled dynamics and parametric uncertainties. As a result of this construction, a linear fractional transformation (LFT) interconnection structure, which is the basis of control design, is achieved.

In model-based controller synthesis, a model describing the physical system is used to determine the controller such that the specifications on the closed-loop system are satisfied. However, the model used in the controller synthesis is just an

approximation of the dynamics of the real physical system. In addition, there is always a presence of disturbances and measurement noises, which enter the system in an unpredictable way. The purpose of robust control methods is to design controllers with model uncertainties and disturbances, and at the same time they must satisfy the closed-loop system specifications.

Several control design methods have been proposed for linear or linearized models. In practice, the control design problem usually requires several control design methods, and the selection of the appropriate controller is carried out in the implementation phase. The robust control design methods which are usually applied fit in the so-called $\mathscr{H}_\infty$ and the $\mathscr{H}_\infty/\mu$ framework.

It is apparent that there is a great amount of analogy between classical adaptive schemes and the qLPV design philosophy. The parameters that are estimated during operational time and which are used to tune the actual controller in an adaptive scheme play the same role as the scheduling variables in the qLPV context. From this latter perspective the difference is in the acquisition of the scheduling variable, i.e., in the adaptive case the values of the scheduling variable are not directly available by measurement and need to be obtained by a specific estimation process based on the directly available data. This observation leads us to propose a unified view of both control design strategies cast in the qLPV design framework by extending the set of scheduling variables with parameters that might not be directly measured but estimated using a suitably designed procedure.

One of the advantages of the proposed general qLPV framework, i.e., a robust adaptive control scheme using dynamic output feedback based on an LPV methodology, is that besides the introduction of the (parametric) model uncertainties in the design the LPV method also makes it possible to consider the unknown parameter variation rate, providing a framework to answer the long-standing question of whether or not the adaptation is limited fundamentally to slowly varying systems.

The solution to the LPV control synthesis problem is formulated as a parameter dependent linear matrix inequality (LMI) optimization problem, i.e., a convex problem for which efficient optimization techniques are available. This control structure is applicable whenever the value of the parameter is available in real-time. The resulting controller is time varying and smoothly scheduled by the values of the scheduling variables. Therefore qLPV models with LMIs, as the main design tool, seem to be the most efficient approach to achieve robust and non-conservative results. The LMI constraint set for qLPV problems is convex, however, it is usually not easily dealt with, since it represents an infinite number of conditions. One way to overcome this difficulty is to approximate the exact set by a tractable one. By choosing appropriate inner/outer approximations one may develop computable lower/upper bounds for certain performances, e.g., stability margins.

This basic setting for the controller synthesis can be varied depending on the problem at hand and the actual demands. The information on the change rate of the measured scheduling variables can also be introduced in the design.

A practically relevant control design task contains nonlinear components, e.g., the dynamics of the dampers and springs and nonlinear actuator dynamics. In order to handle the high complexity of the problem the design of a two-level controller is

proposed in the integrated control framework. The required control force is computed by applying a high-level controller, which is designed using a LPV method. For the control design, the model is augmented with weighting functions specified by the performance demands and the uncertainty assumptions. The actuator generating the necessary control force is modeled as a nonlinear system for which a low-level force-tracking controller is designed. The proposed separation layers describe the intuitive structure of the different subsystems, i.e., the chassis and the actuators while keeping the complexity of the resulting control problems within reasonable bounds.

Each of the individual models is formulated in the LPV framework and contains the performance specifications and typical uncertainties. Thus, the primary models are augmented with the corresponding—preferably LPV—weights, which leads to the unified generalized plant structure, which is the starting point of the robust control design.

Integration of Vehicle Systems

Two different actuators might be able to influence the same vehicle dynamics. Thus, the role of the integrated vehicle control is to coordinate the local components and handle the interactions between them. Since the performance specifications of local controllers are often in conflict, they must also guarantee a balance or trade-off between them. This trade-off is formulated on the level of local controllers as a result of engineering knowledge. However, when an event occurs, the preferences, i.e., the trade-off levels, are subject to change.

The term configuration refers to a well-defined sensor and actuator set that is associated with a given functionality. Control reconfiguration is motivated by the following requirements: the achieved control performance in certain scenarios must be improved and increased reliability in the presence of sensor or actuator faults must be achieved. The term event is related to the occurrence of such a scenario. In a normal situation a baseline configuration is formed by a single local component, e.g., steering, otherwise it is composed of several local components that can cause the same functional behavior, e.g., steering and brake for generating yaw moment. The hierarchy of the configurations and corresponding scheduling variables ensure that the additional actuator(s) considered improve the stability properties of the given functionality.

The specification of the configuration sets and that of the corresponding reconfiguration policy are cornerstones of the proposed method and it may be a highly nontrivial task requiring considerable engineering knowledge. However, the analysis of the configurations, events, and possible reconfigurations is necessary for any reconfiguring control strategy.

The control solutions create a balance between driving (or road holding) and comfort and guarantee safety all the time. This balance often leads to compromises between vehicle functions, which may not be suitable for all the drivers. For example a driver who wants to minimize the length of the trajectory in the bend selects the curvature radius as small as possible, while the driver who requires comfort selects a larger curvature radius. At the same time, however, the selection of different curvature radiuses also corresponds to the possible speed selection, e.g., the larger radius allows

the driver to select larger speed. The control solutions in practice are based on the drivers' behavior, which is learnt by the system during the journey. The driver input is not only a function of the planned trajectory but it also affects the dynamics of the vehicle.

Consequently, a driver model must be combined with the vehicle model in order that the driver behaviors and requirements are incorporated in the design of the control system. In the driver assistance system the interaction between the vehicle and the driver is taken into consideration.

The main chapter of this part offers a detailed presentation of the integrated control framework. An integrated control system is designed in such a way that the effects of a control system on other control functions are taken into consideration in the design process by selecting the various performance specifications. In order to impose performance requirements, a tight coupling among the elements of the integrated structure is needed, which is realized through a set of well-defined additional monitoring signals.

The plant can be considered as a core system which communicates with the environment through different peripheral components, while the controller is a program that executes a given task on the core system function of the available set of peripheries. In this respect, there is an analogy between a modern computer with its operating system and application programs and which is equipped with a set of peripheries. An important point here is that the actual peripheral subsystem plugged into this architecture can fulfill its intended task and the applications can use it quite flexibly without previous knowledge of the operation system about the internal details of the specific subsystem. The only constraint is that the information flow between these components should respect some well-defined protocols. This plug-and-play paradigm has been proven to be very fruitful in computer science and is considered to be a model that can be applied to the design of control systems as well.

In the context of control systems a plug-and-play control architecture provides the possibility to use sensors and actuators supplied by different vendors interchangeably on a system by guaranteeing a performance level and leaving the global controller intact. If a new control component is added, an old control is replaced by a new one, or an old component is removed, the structure of the system (or the control) changes. In these cases, the conventional control should be redesigned, which is expensive and takes a long time. In the integrated concept the control logic must be modified on the highest level.

Once the local controllers have been designed it is possible to perform an analysis step in the robust control on a global level to prove both global stability and performance. The presence of competing multiobjective criteria makes the applicability of the global approach difficult. It is a great challenge for research since the proof of global performance leads to a highly computation-intensive procedure. Although the analysis of global stability is an intensively researched area there are only few theoretical results. Moreover, although the analysis is fundamental in terms of distributed control, it is a fully open research field.

The advantage of the integrated control is to provide reconfigurable and fault-tolerant structures. If a performance degradation or fault occurs in the system and it

has been detected, the role of the degraded controller may be substituted by another controller. The fault-tolerant local controllers also require components for monitoring fault information. Faults in the operation of an actuator can be usually detected by using a built-in self-diagnostic method. In this case, fault information is sent by the actuator itself to the supervisor. Any reconfiguration scheme relies on a suitable fault detection and isolation (FDI) component.

The basic objective of a fault detection methodology applied to dynamic systems is to provide techniques for the detection and isolation of failed components. Using a mathematical model of the system it is possible to exploit the principle of analytical redundancy, which allows to check discrepancies between the real behavior of the system and its idealized mathematical description or model. Model-based FDI relies on analytical redundancy to generate fault indicators, called residuals.

There are many analytical redundancy methods for linear and nonlinear systems available in the literature. While recent nonlinear approaches are useful for the analysis, and partly in the design of detection filters, they are largely incapable of solving synthesis problems because of the computational burden they usually pose to the implementation.

As a high-level approach, the FDI filter design problem can often be cast in the model matching framework. To achieve robustness in the presence of disturbances and uncertainty, multiobjective optimization-based FDI schemes can be proposed where an appropriately selected performance index must be chosen to enhance sensitivity to the faults and to simultaneously attenuate disturbances.

This is a typical worst-case filtering problem and the corresponding design criteria can be formulated as a convex optimization problem by using LMIs. The main problem here is that the sensitivity and robustness conditions are in conflict. In the linear time invariant (LTI) framework, it means that sensitivity to faults and insensitivity to unknown inputs cannot be achieved simultaneously at the same frequencies. Faults having similar frequency characteristics to those of disturbances might go undetected. While the design problem is nonconvex, in general, a scheme that can handle the problem by using LMI techniques is presented.

Structure of the Book

The book includes three parts and appendix. The first part focuses on the modeling and control of LPV systems. In Chap. 2, the construction of the LPV model of the physical system and the linearization methods are presented. Two examples are presented, i.e., the LPV modeling of the vertical dynamics and that of the yaw–roll dynamics. Since the parameters of the LPV models usually are not necessarily known, a gray-box identification method is applied. In Chap. 3 the model is augmented with the performance specifications and uncertainties in order to form a control-oriented LPV model. Both constant Lyapunov function and parameter varying Lyapunov functions are applied for stability and $\mathscr{L}_2$ performance. Finally, they are extended to LPV systems when the measured varying parameters do not exactly fit the real one. The theoretical part is extended by several important components in the Appendix.

In the second part of the book, the control methods for both vertical and longitudinal vehicle dynamics are presented. In Chap. 4 both the linear $\mathscr{H}_\infty$ methods and LPV

methods are applied for the control design. This chapter also presents the hierarchical structure of the control design. The high-level control focuses on the performance specifications and calculates a required control signal. The required signal is tracked by a low-level controller by setting the actuator dynamics. In Chap. 5, active anti-roll bars are applied for preventing the rolling over. It is combined with the active brake in order to improve the efficiency of the LPV control design method. Moreover, this combination guarantees the fault-tolerant operation of the control system. In Chap. 6, a classical control problem is presented, i.e., the adaptive cruise control in the longitudinal dynamics. In the robust control design both the driving and the braking systems are combined. The control algorithm is implemented in a SIL environment. An extension of the adaptive cruise control is the speed design in which several road and traffic conditions must be taken into consideration in order to reduce the control energy and keep the time requirement.

In the third part of the book, the control systems focus on the lateral dynamics. Since the control systems may affect the same vehicle dynamics, their operations must be integrated. An integrated control system is designed in such a way that the effects of a control system on other vehicle functions are taken into consideration in the design process by selecting the various performance specifications. The principles of the design methods are presented in Chap. 7. In this chapter, the operation of the integrated control is presented through trajectory tracking as a driver assistance system. In the integrated control three control components are applied simultaneously such as the brake, the steering and the suspension systems. Concerning the lateral vehicle dynamics the variable-geometry suspension system plays an important role. In Chap. 8, the modeling and control of the variable-geometry suspension system is presented. Moreover, the integration of the construction and the control design is also presented. In Chap. 9, the control design of the in-wheel motors for a trajectory tracking problem is presented. It leads also a hierarchical control, in which the retired longitudinal force and the yaw moment are calculated in the high-level while the torques of the in-wheel motors are designed in the low level. In Chap. 10, the drivers' behavior is analyzed. In the control design a simplified driver model is combined with the control-oriented vehicle model.

In the Appendix, further components of the modeling and robust control of LPV systems are included. The modeling part presents the basic terms of the analysis, the identifiability, the adaptive observers and the geometric approach of the FDI design. The robust control presents the structured uncertainty, the components of the nonlinear $\mathscr{H}_\infty$ methods and the LFT-based qLPV design.

Part I
Modeling and Control of LPV Systems

Chapter 2
Modeling of LPV Systems

Introduction

In general terms, control theory can be described as the study of how to design the process of influencing the behavior of a physical system to achieve a desired goal. An open-loop control is one in which the control input is not affected in any way by the actual (measured) outputs. If the system changes during the operational time then the control performance can be severely reduced. In a closed-loop system the control input is affected by the measured outputs, i.e., a feedback is being applied to that system. Very often a reference input is given, which is directly related to the desired value of system outputs, and the purpose of the controller will be to minimize the error between the actual system output and the desired (reference input) value.

There are two main features in the analysis of a control system: system modeling, which means expressing the physical system under examination in terms of a model (or models) which can be readily dealt with and understood, and the design stage, in which a suitable control strategy is both selected and implemented in order to achieve a desired system performance. Forming a mathematical model which represents the characteristics of a physical system is crucially important as far as the further analysis of that system is concerned.

Traditionally controllability and observability are the main issues in the analysis of a system before deciding the best control strategy to be applied, or whether it is possible to control or stabilize the system. Controllability is related to the possibility of forcing the system into a particular state by applying an appropriate control signal while observability is related to the possibility of reconstructing, through output measurements, the state of a system.

The model should not be over simple so that important properties of the system are not included, something that would lead to an incorrect analysis or an inadequate controller design. In some cases the nonlinear characteristics are so important that they must be dealt with directly, and this can be quite a complex procedure.

P. Gáspár et al., *Robust Control Design for Active Driver Assistance Systems*,
Advances in Industrial Control, DOI 10.1007/978-3-319-46126-7_2

Gain-scheduling is a technique widely used to control such systems in a variety of engineering applications. In the classical gain scheduling approach, having strong roots in flight control applications, the controller synthesis is based on local descriptions of the nonlinear system, that can most often be approximated by linear system properties. The gains of the gain-scheduled controllers are typically chosen using linear control design techniques and is a two step process. First, several operating points are selected to cover the range of system dynamics. At each of these points, the designer makes an LTI approximation to the plant and then, designs a linear compensator for each linearized plant. This process gives a set of linear feedback control laws that perform satisfactorily when the closed-loop system is operated near the respective operating points. A global nonlinear controller for the nonlinear system is then obtained by interpolating, or scheduling, the gains from the local operating point designs.

Since the synthesized controllers are guaranteed to satisfy specifications only locally, the designer typically cannot assess a priori the stability, robustness, and performance properties of gain-scheduled controller designs. While the local controller synthesis can be performed using the well established techniques of the linear system theory, it remains a non-trivial procedure to map the linear controllers such that non-local specifications of the closed loop system are kept.

The LPV paradigm provides a remedy to this problem, Shamma and Athans (1990), Shamma (1992). Initiated in Shamma and Athans (1991) LPV modeling techniques have gained a lot of interest, especially those related to vehicle and aerospace control, Becker and Packard (1994), Balas et al. (1997), Marcos and Balas (2001), Szászi et al. (2005). LPV systems have recently become popular as they provide a systematic means of computing gain-scheduled controllers. In this framework the system dynamics are written as a linear state-space model with the coefficient matrices functions of external scheduling variables. Assuming that these scheduling variables remain in some given range then analytical results can guarantee the level of closed loop performance and robustness. The parameters are not uncertain and can often be measured in real-time during system operation. However, it is generally assumed that the parameters vary slowly in comparison to the dynamics of the system. LPV based gain-scheduling approaches are replacing ad-hoc techniques and are becoming widely used in control design.

Many of the control system design techniques using LPV models can be cast or recast as convex problems that involve LMIs. Significant progress has been made recently in the use of LMI and $\mathscr{H}_\infty$ optimization in gain-scheduled control. One such control design technique, described by Apkarian et al. (1995), is the Lyapunov function/quadratic $\mathscr{H}_\infty$ approach wherein a single Lyapunov function is sought to bound the performance of the LPV system. Such a framework generally has a strong form of robust stability with respect to time-varying parameters. However, due to the continuous variation of scheduling parameters,such a synthesis approach is generally associated with a convex feasibility problem with infinite constraints imposed on the LMI formulation. This problem can be addressed by using affine LPV modeling that reduces the infinite constraints imposed on the LMI formation to a finite number.

Such a modeling approach has been used to solve design problems by Becker (1992), Sun and Postlethwaite (1998).

The above pure LPV model is not quite matched to the control problems where the scheduling variables are in fact system states (e.g., vehicle speed), rather than bounded external variables. An approach to this problem is to generate so-called quasi-LPV models, which are applicable when the scheduling variables are measured states, the dynamics are linear in the inputs and other states, and there exist inputs to regulate the scheduling variables to arbitrary equilibrium values.

These methods concentrate on robust performance, hence, robust stability of the controlled system. In this more general context such robust control problems—both analysis and synthesis—can be formulated using a generalized plant technique based on an LFT description of the uncertain LPV system, see, e.g., Iwasaki and Hara (1998), Iwasaki and Shibata (2001), Wu (2001). The controller synthesis leads to bilinear matrix inequalities (BMI) but often it is possible to reduce the problem to the solution of a finite set of LMIs, for details see, e.g., Scherer et al. (1997), Scherer (2001), Wu (2001).

2.1 LPV Model Structures

The mathematical model of a dynamic evolution of a nonlinear, non-autonomous physical system is usually formulated as a state space representation in terms of the input $u(t) \in \mathbb{R}^m$, output $y(t) \in \mathbb{R}^p$ and state signals $x(t) \in \mathbb{R}^n$ related by a first-order differential equation:

$$\dot{x} = f(x, u, w), \tag{2.1}$$

$$y = h(x, u, w), \tag{2.2}$$

subject to the initial condition $x(t_0) = x_0$. Usually the model also describes the effect of the outer disturbances, which are modeled through the signal $w(t) \in \mathbb{R}^d$. In what follows for the sake of simplicity we concentrate on the undisturbed system, i.e., w will be suppressed from the model.

According to the LPV paradigm, parameter-dependent systems are linear systems, whose state-space descriptions are known functions of time-varying parameters. While the time variation of each of the parameters is not known in advance, it is assumed to be measurable in real time. Thus, in the LPV controller synthesis step the parameters are regarded as freely varying parameters taking arbitrary values in the region Ω and, hence, the LPV description will differ from the nonlinear system. The larger this difference, the more conservatism is introduced in the LPV controller synthesis step. LPV descriptions of nonlinear systems are not unique: it is desirable to have an LPV description that in some sense is close to the nonlinear system for all parameter values.

Thus, the aim of the LPV modeling procedure is to find an LPV description of the nonlinear model on the form

$$\dot{x} = A(\rho)x + B(\rho)u \simeq f(x,u), \quad \rho \in \Omega \tag{2.3}$$
$$y = C(\rho)x + D(\rho)u \simeq h(x,u), \tag{2.4}$$

where ρ is the, possibly state dependent, parameter vector varying within a region Ω, such that the known relation $\rho = \sigma(y,r)$ depends only on the measured signals y and exogenous signals r whose values are known in operational time.

This guarantees that the parameter values are available to the controller and that an explicit nonlinear feedback controller can be obtained from the designed LPV controller. In order to ensure that trajectories of the original nonlinear system are equal or at least closed to the trajectories of the LPV description, (2.3) should be as close to the nonlinear system as possible for all parameter values in the region Ω.

Hence, an LPV model is defined as a linear model whose state-space matrices depend on a vector ρ of time-varying parameters of the form

$$\dot{x} = A(\rho)x + B(\rho)u, \tag{2.5}$$
$$y = C(\rho)x + D(\rho)u, \tag{2.6}$$

where it is often suppose that the parameter dependency has an explicit structure: namely either affine, polynomial, polytopic or an LFT dependency. Accordingly, if

$$S(\rho) = \sum_{i=0}^{n} \sum_{|\underline{j}|=i} \rho^{\underline{j}} S_{i,\underline{j}}, \tag{2.7}$$

where $\rho^{\underline{j}} = \rho_1^{j_1}\rho_2^{j_2}\cdots\rho_k^{j_k}$ with ρ_l are the components of the parameter vector ρ, $|\underline{j}| = \sum_{l=1}^{k} i_k$ and

$$S \sim \begin{pmatrix} A & B \\ C & D \end{pmatrix}, \quad S_{i,\underline{j}} \sim \begin{pmatrix} A_{i,\underline{j}} & B_{i,\underline{j}} \\ C_{i,\underline{j}} & D_{i,\underline{j}} \end{pmatrix},$$

then $n = 1$ corresponds to the affine models. Affine models are mostly involved in applications where geometric techniques are to be used.

For polytopic LPV models the system matrix $S(\rho)$ varies within a fixed polytope of matrices: it is a convex combination $S(\rho) \in \text{convex}\{ S_1, S_2, \ldots, S_k \}$ of the system matrices (vertex systems), i.e.,

$$S(\rho) = \sum_{i=1}^{k} \rho_i S_i, \quad \rho_i \geq 0, \quad \sum_{i=1}^{k} \rho_i = 1. \tag{2.8}$$

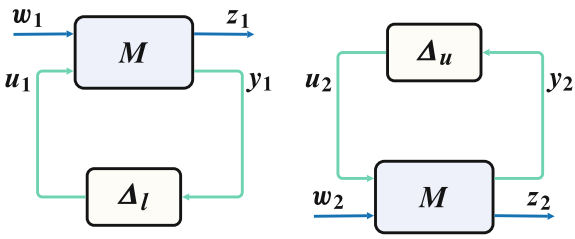

Fig. 2.1 Lower and upper LFT representations

Since polytopic models are well suited for Lyapunov-based analysis and design, they are very popular model candidates in the LPV framework.

A more general representation is the LFT, see Fig. 2.1. LFT is a representation of a system using a feedback interconnection between two operators, a known causal system

$$M = \begin{pmatrix} M_{11} & M_{12} \\ M_{21} & M_{22} \end{pmatrix}$$

and a causal bounded system Δ of proper dimension:

$$\mathcal{F}_L(M, \Delta) = M_{11} + M_{12}\Delta(I - \Delta M_{22})^{-1}M_{21} \tag{2.9}$$

$$\mathcal{F}_U(M, \Delta) = M_{22} + M_{21}\Delta(I - \Delta M_{11})^{-1}M_{12} \tag{2.10}$$

Δ is typically norm-bounded, $||\Delta||_\infty \leq 1$, but otherwise unrestricted in form (structured/un-structured) or type (nonlinear/time-varying/constant). If some of the components in the Δ operator are scheduling parameters an LPV system is obtained. This form is obtained by extracting a varying parameter from a system and placing it into a feedback loop, such that the remaining system, M, is time-invariant. Models with affine or polynomial parameter dependencies can be transformed exactly to a LFT. An important property of LFT systems is that their interconnection (e.g., sum, concatenation) and also the inversion, if it exists, always results in another LFT.

We emphasize that an LPV plant can be viewed either as an LTI plant subject to a time-varying parametric uncertainty $\rho(t)$, see, e.g., the LFT LPV structure or as a set of models of linear time-varying (LTV) plants, where each LTV system corresponds to a specific parameter trajectory. In the analysis and design process we chose the most convenient interpretation that fit the actual technique that we might use.

2.2 Linearization Through LPV Modeling

Practically, concerning the structure of the models, prior to the design and analysis phase there is no significant difference between LPV models and those used for gain scheduling. All of them can be obtained by using different, application specific,

methods. The direct linearization schemes applied to nonlinear systems can be roughly classified into the following types: linearization about an equilibrium, linearization about a parametrized state trajectory and global linearization. In the first case the system is represented as an LTI system locally around an equilibrium condition, while in the second approach the nonlinear system is to follow some prescribed trajectory around that it can be approximated by a family of parametrized linearizations. In the third case the original nonlinear system is approximated by a set of trajectories of a linear differential inclusion (LDI) which can represent it in the entire operation range. However, in this case there might be trajectories of the LPV model that are not actual trajectories of the original system. This might lead to a conservative analysis or design.

In what follows some of the most common techniques, e.g., classical, fuzzy and the off-equilibrium approaches, see, e.g., Leith and Leithead (2000), will be sketched.

2.2.1 Jacobian Linearization

Often in industrial settings, a finite collection of linear models is used to describe the behavior of a system throughout an operating envelope. The linearized models describe the small signal behavior of the system at a specific operating point and the collection is parametrized by one or more physical variables whose values represent this specific point. If the state variables have physical meaning, then it makes sense to develop polynomial least squares fits of the state-space matrices to get a continuous parameterization of the operating envelope.

The classical approach, using Jacobian linearization of the nonlinear model about a manifold of constant equilibria, constant operating points or set-points, is called linearization-based scheduling. When a corresponding scheduling variable ρ is chosen appropriately to parameterize the set of linear models, a parameterized family of linearized models representing the original nonlinear model results.

Considering the nonlinear plant dynamics an equilibrium or constant operating point (x_e, u_e) is defined by the equilibrium condition $f(x_e, u_e) = 0$. Assuming f is continuously differentiable at the equilibrium point, the nonlinear model is approximated by

$$\delta\dot{x} = A\delta x + B\delta u \tag{2.11}$$

$$\delta y = C\delta x + D\delta u, \tag{2.12}$$

where

$$\delta u = u - \tilde{u}, \quad \delta y = y - \tilde{y}, \quad \delta x = x - \tilde{x},$$

and

$$A = \partial_x f(x_e, u_e), \quad B = \partial_u f(x_e, u_e), \quad C = \partial_x h(x_e, u_e), \quad D = \partial_u h(x_e, u_e).$$

By considering an entire equilibrium family $(x_e, u_e) \in \Omega_e$ yields to a linear parameter-dependent linearization family $S(\rho_e)$, locally describing the nonlinear model:

$$\begin{aligned}\delta\dot{x} &= A(\rho_e)\delta x + B(\rho_e)\delta u\\ \delta y &= C(\rho_e)\delta x + D(\rho_e)\delta u.\end{aligned}$$

To obtain an LPV description for a nonlinear model, an interpolation of the stationary linearizations can be applied: e.g., by using a linear interpolation then system can be written as

$$\delta\dot{x}(t) = A(\rho)\delta x(t) \; + B(\rho)\delta u(t)$$

with

$$A(\rho) = \sum_{i=1}^{p} A_i\rho_i, \quad B(\rho) = \sum_{i=1}^{p} B_i\rho_i, C(\rho) = \sum_{i=1}^{p} C_i\rho_i, \quad D(\rho) = \sum_{i=1}^{p} D_i\rho_i, \tag{2.13}$$

where

$$\sum_{i=1}^{k} \rho_i = 1, \;\; \rho_i \geq 0, \;\; \delta x = x - x_e(\rho) \; , \delta u = u - u_e(\rho)$$

the points $(x_e^i, u_e^i) \in \Omega_e$ being stationary. The procedure, however, may give an LPV system that does not include the original nonlinear system. But if the stationary points can be chosen such that

$$\{(\partial f_x(x,u), \partial f_u(x,u))\} \subset \text{convex}\{(\partial f_x(x_e^i, u_e^i), \partial f_u(x_e^i, u_e^i))\}$$

then the LPV description (2.13) will include the nonlinear system.

A typical choice for Ω_e is to take a a specific trajectory $(\tilde{x}, \tilde{u}, \tilde{y})$, i.e., to perform the linearization of the nonlinear system (2.2) around a trajectory:

$$\begin{aligned}\delta\dot{x} &= \partial_x f(\tilde{x}, \tilde{u})\delta x + \partial_u f(\tilde{x}, \tilde{u})\delta u,\\ \delta y &= \partial_x h(\tilde{x}, \tilde{u})\delta x + \partial_u h(\tilde{x}, \tilde{u})\delta u,\end{aligned}$$

where

$$\delta u = u - \tilde{u}, \quad \delta y = y - \tilde{y}, \quad \delta x = x - \tilde{x}.$$

By taking the parameters of the specific trajectory (flight envelop) as measurable scheduling variables, the desired LPV model will be of the form

$$\dot{\xi} = A(\rho)\xi + B(\rho)\delta u$$
$$\delta y = C(\rho)\xi + D(\rho)\delta u.$$

A parameterized family of linearized models resulting from linearization-based scheduling or a number of black-box point-designs are only locally valid. In case an LPV model is based on such a set of linearized models, the accuracy of the resulting linear parameter-dependent model with respect to the original nonlinear model or plant is unknown. Classical gain scheduling is mainly restricted to local controller synthesis in stationary points. Even though nonlinear systems can be linearized along a trajectory, no gain scheduling approaches available in the literature that extends the stability region using a family of linearizations along different trajectories.

2.2.2 Off-Equilibrium Linearization

A disadvantage of classical linearization-based scheduling is the restriction to equilibrium-point modeling. Using the so-called velocity-based or off-equilibrium linearizations it is possible to enable linearization at every operating point: considering the nonlinear system

$$\dot{x} = f(x, u), \quad y = h(x, u),$$

the velocity linearization at a point (x_0, u_0) reads as

$$\dot{x} = \zeta$$
$$\dot{\zeta} = \partial f_x|_{(x_0,u_0)}\zeta + \partial f_u|_{(x_0,u_0)}\dot{u}$$
$$\dot{y} = \partial h_x|_{(x_0,u_0)}\zeta + \partial h_u|_{(x_0,u_0)}\dot{u}.$$

In this way there is a velocity-based linearization associated with every operating point of the original nonlinear system and the solutions may be pieced together. Thus, the resulting velocity-based linearization family, parameterized by ρ, globally approximates the trajectories of the nonlinear model to an arbitrary degree of accuracy. The velocity linearization is not limited to equilibrium points: as no restriction to equilibrium operating points is present, linear approximation of transient dynamics and operating points far from equilibrium operating points is also enabled.

Interpolation of linear controller based on velocity linearizations can be performed in a similar way to classical gain scheduling. However, since the velocity linearization is not an approximation in the same sense as a standard linearization scheme, it is easier to interpolate linearizations in a way such that the nonlinear system is included in the LPV description.

2.2.3 Fuzzy Linearization

One approach to gain scheduling, and thus, to LPV modeling, uses ideas from fuzzy systems, see Takagi and Sugeno (1985) to describe the nonlinear system: the plant dynamics is formulated as a blended multiple model representation such as a Takagi-Sugeno model or local model network of the form

$$\dot{x} = \sum_i f_i(x, u)\mu_i(\phi),$$
$$y = \sum_i h_i(x, u)\mu_i(\phi)$$

where the function $\phi(x, u)$ is the scheduling variable and the scalar blending weights $\mu_i \geq 0$ often are normalized to $\sum_i \mu_i = 1$.

After a linearization and blending of the individual components the typical form of the LPV model will be of the form:

$$\begin{pmatrix} \dot{x} \\ y \end{pmatrix} = S(\rho)\begin{pmatrix} x \\ u \end{pmatrix}, \tag{2.14}$$

with

$$S(\rho) = S_0 + \sum_{i \in I} \rho_i S_i, \tag{2.15}$$

where ρ_i will be the scheduling variables of the model.

2.2.4 qLPV Linearization

Quasi-LPV scheduling tries to overcome the general shortcomings of classical linearization schemes regarding local validity of the resulting model: the idea is to transform the nonlinear model to an LPV form hiding the nonlinear terms by including them in the scheduling variable. Since this process involves a transformation rather than a linearization, the resulting LPV model exactly equals the original nonlinear model.

A qLPV model may arise by considering state transformations on a class of nonlinear systems of the form:

$$\dot{x}_1 = f_1(x_1) + A_{11}(x_1)x_1 + A_{12}(x_1)x_2 + B_1(x_1)u,$$
$$\dot{x}_2 = f_2(x_1) + A_{21}(x_1)x_1 + A_{22}(x_1)x_2 + B_2(x_1)u,$$
$$y = x_1.$$

Assuming that there exist differentiable functions x_2^{eq} and u^{eq} such that for every x_1

$$0 = f_1(x_1) + A_{11}(x_1)x_1 + A_{12}(x_1)x_2^{eq} + B_1(x_1)u^{eq},$$
$$0 = f_2(x_1) + A_{21}(x_1)x_1 + A_{22}(x_1)x_2^{eq} + B_2(x_1)u^{eq}$$

is satisfied, then by applying the following state and input transformation:

$$\xi_1 = x_1, \quad \xi_2 = x_2 - x_2^{eq} \quad \nu = u - u^{eq},$$
$$\tilde{A}_{22}(\xi_1) = A_{22}(\xi_1) - \frac{dx_2^{eq}}{dx_1}|_{\xi_1} A_{12}(\xi_1) \quad \tilde{B}_2(\xi_1) = B_2(\xi_1) - \frac{dx_2^{eq}}{dx_1}|_{\xi_1} B_1(\xi_1)$$

one obtains the qLPV system

$$\dot{\xi}_1 = \tilde{A}_{12}(\xi_1)\xi_2 + \tilde{B}_1(\xi_1)\nu, \tag{2.16}$$
$$\dot{\xi}_2 = \tilde{A}_{22}(\xi_1)\xi_2 + \tilde{B}_2(\xi_1)\nu, \tag{2.17}$$
$$y = \xi_1. \tag{2.18}$$

While the system representation in (2.16)–(2.18) has a linearized appearance, it is not equivalent to a Jacobian linearization about an operating point still exactly represents the original nonlinear system. The representation is called qLPV since the exogenous parameter ξ_1 is actually a state.

If the system also depends on an exogenous parameter p, the final qLPV system will be of the form

$$\dot{\xi}_1 = \tilde{A}_{12}(\xi_1, p)\xi_2 + \tilde{B}_1(\xi_1, p)\nu, \tag{2.19}$$
$$\dot{\xi}_2 = \tilde{A}_{22}(\xi_1, p)\xi_2 + \tilde{B}_2(\xi_1, p)\nu + E_2(\xi_1, p)\dot{p}, \tag{2.20}$$
$$y = \xi_1, \tag{2.21}$$

where $E_2(\xi_1, p) = -\frac{dx_2^{eq}}{dp}|_{\xi_1}$. If no reliable measurement is available for the signal $\dot{p}$, then it can be treated as a disturbance signal which must be rejected.

In many cases it is possible to find a qLPV description of a nonlinear system more directly by hiding the nonlinearity in the parameter. As a trivial example let the nonlinear system be $\dot{x} = -\sin(x) + u$. This system can be represented by the qLPV system $\dot{x} = -\rho x$ with $\rho = \sin(x)/x$. Moreover, the resulting qLPV system exactly matches the original nonlinear system globally, provided the state x is measured. The same idea can be applied to obtain local models: e.g., take the nonlinear system $\dot{x} = -x^3 + u$, that can be described by the qLPV system $\dot{x} = -\rho x + u$, with the parameter satisfying $0 \leq \rho \leq M$. Clearly, the qLPV model become equal to the original one when $\rho = x^2$. In practice it is more likely to obtain local models, as in the combination of these cases: consider the nonlinear plant

$$\begin{aligned}\dot{x}_1 &= \sin x_1 + x_2,\\ \dot{x}_2 &= x_1^2 x_2 + u,\\ y &= x_1.\end{aligned}$$

Using $\rho_1 = \sin x_1/x_1$ and $\rho_2 = x_1^2$ the qLPV representation of the system is

$$\begin{aligned}\dot{x} &= A(\rho)x + Bu,\\ y &= Cx + Du,\end{aligned}$$

with $D = 0,\ C = \begin{pmatrix}1 & 0\end{pmatrix}$ and

$$A(\rho) = \begin{bmatrix}\rho_1 & 1\\ 0 & \rho_2\end{bmatrix} = \begin{bmatrix}0 & 1\\ 0 & 0\end{bmatrix} + \rho_1\begin{bmatrix}1 & 0\\ 0 & 0\end{bmatrix} + \rho_2\begin{bmatrix}0 & 0\\ 0 & 1\end{bmatrix},\quad B = \begin{pmatrix}0\\ 1\end{pmatrix}.$$

Concerning the vehicle dynamics models involved in this book in most of the cases first principle models of the form

$$J(\rho)\ddot{x} + b(\rho)\dot{x} + k(\rho)x = T(\rho)u \tag{2.22}$$

are available, where ρ depends only on measured signals, thus they are natural candidates to be choses as scheduling variables of a qLPV model. The advantage of these models are that they are global or they are valid at least on a domain on which the original first principle model was. A disadvantage might be the possible conservativity caused by the size of the domain Ω which ρ is supposed to belong when it turns to use the model for analysis or design.

We conclude this section by presenting a source of the LPV/qLPV models that is also of central importance concerning the topic of this book and it is related to the parameter varying choice of different weighting filters that enter in the formulation of the control problems.

2.2.5 Non-uniqueness of the LPV Models

An LPV description of a nonlinear system is not unique: as an example consider the nonlinear plant

$$\begin{aligned}\dot{x}_1 &= \sin x_1 + x_2,\\ \dot{x}_2 &= x_1 x_2 + u,\\ y &= x.\end{aligned}$$

Using $\rho_1 = \sin x_1/x_1$ and $\rho_2 = x_1$ the qLPV representation of the system is described by the system matrix

$$A(\rho) = \begin{bmatrix} \rho_1 & 1 \\ 0 & \rho_2 \end{bmatrix} = \begin{bmatrix} 0 & 1 \\ 0 & 0 \end{bmatrix} + \rho_1 \begin{bmatrix} 1 & 0 \\ 0 & 0 \end{bmatrix} + \rho_2 \begin{bmatrix} 0 & 0 \\ 0 & 1 \end{bmatrix},$$

while the choice $\rho_1 = \sin x_1/x_1$ and $\rho_2 = x_1$ leads to

$$A(\rho) = \begin{bmatrix} \rho_1 & 1 \\ \rho_2 & 0 \end{bmatrix} = \begin{bmatrix} 0 & 1 \\ 0 & 0 \end{bmatrix} + \rho_1 \begin{bmatrix} 1 & 0 \\ 0 & 0 \end{bmatrix} + \rho_2 \begin{bmatrix} 0 & 0 \\ 1 & 0 \end{bmatrix},$$

Different LPV descriptions of same nonlinear system may affect essential properties, such as controllability, observability and hence stabilizability of the system, i.e., we have different stability properties when the parameter varies freely without the connection to the state.

The nonlinear system

$$\begin{aligned} \dot{x}_1 &= -x_1 - x_1^3, \\ \dot{x}_2 &= -x_2 - x_1^2 x_2 \end{aligned}$$

can be either represented by the LPV system

$$\dot{x} = \begin{pmatrix} -1-\rho & 0 \\ 0 & -1-\rho \end{pmatrix} x, \tag{2.23}$$

with $\rho = x_1^2$, or

$$\dot{x} = \begin{pmatrix} -1-\rho_1^2+\rho_2 & -\rho_1 \\ \rho_2 & -1-\rho_1^2-\rho_1 \end{pmatrix} x, \tag{2.24}$$

with $\rho_1 = x_1$ and $\rho_2 = x_2$. In the first case it is assumed that the parameter ρ is bounded by $0 \leq \rho(t) \leq M$, where M is any fixed positive scalar; thus the nonlinear system is included in the domain $\{x \in \mathbb{R}^2 | -\sqrt{M} \leq x_1 \leq \sqrt{M}\}$. In the second case the parameter can be bounded by $-M \leq \rho_i \leq M$; thus the nonlinear system is included in the system in the domain $\{x \in \mathbb{R}^2 \mid -M \leq x_i \leq M,\ i = 1, 2\}$.

These LPV models have different properties: system (2.23) is LTI stable for all parameter values while the LPV system (2.24) is LTI unstable if $\rho_1 = 0$ and $\rho_2 > 1$. This fact out-rules constant matrix Lyapunov techniques to analyze stability of the system.

At this point it is time to recall the main goal of the LPV modeling, namely to obtain a control oriented model that facilitates the analysis and design process in the context of the available tools. At the time being these tools premises convexity, i.e., the convexity of the model set defined by the parameters Ω. Thus, the inherent non-uniqueness of the LPV modeling can be exploited in order to select those models that have this property. Moreover, in order to decrease the possible conservativeness of the design, we prefer the most compact representations.

Even the parameter set Ω is convex, it is usually not easily dealt with, since represents an infinity number of conditions. One way to overcome this difficulty is to approximate the exact set by a tractable one. By choosing appropriate inner/outer approximations one may develop computable lower/upper bounds for certain performances, e.g., stability margins.

As a possible solution, a uniformly and automatically executable tensor product (TP) model transformation method based based on the recently developed higher order singular value decomposition (HOSVD) concept has been proposed, see Zabó et al. (2008, 2010). The so called TP model transformation offers uniform, tractable and readily executable numerical ways and creative manipulations to generate convex (polytopic) representations of LPV models upon which LMI-based design techniques are immediately executable. The result of the TP model transformation is a model that belongs to the class of polytopic models, where the parameter-dependent weightings of the vertex systems are one-dimensional functions of the elements of the parameter vector.

This form offers a relatively simple way to describe various convex hull generations in terms of matrix operations. The obtained structures are not unique, however the framework provides an efficient background to introduce a set of rules, heuristics and algorithms that provide us with a set of candidate model structures on which further analysis and final model selection can be carried out.

After applying one of the modeling steps sketched in the previous sections one ends up with a parameter-varying state-space model of the form

$$\begin{pmatrix} \dot{x}(t) \\ y(t) \end{pmatrix} = S(\rho(t)) \begin{pmatrix} x(t) \\ u(t) \end{pmatrix} \tag{2.25}$$

with the parameter-varying system matrix

$$S(\rho(t)) = \begin{pmatrix} A(\rho(t)) & B(\rho(t)) \\ C(\rho(t)) & D(\rho(t)) \end{pmatrix}. \tag{2.26}$$

The time varying N-dimensional parameter vector $\rho(t) \in \Omega$ is an element of the closed hypercube $\Omega = [a_1, b_1] \times [a_2, b_2] \times \cdots \times [a_N, b_N] \subset \mathbb{R}^N$.

For practical reasons a finite element TP modeling is applied which uses a tensor defined by the values of $S(\rho(t))$ on a suitable discretization of Ω (usually a grid), i.e., a piecewise linear approximation of the multivariate map $S(\rho(t))$. Based on this data TP model transformation generates the HOSVD-based canonical form of LPV models, i.e.,

$$\begin{pmatrix} x(t) \\ y(t) \end{pmatrix} = \left(\mathcal{S} \otimes_{n=1}^{N} w_n(q_n(t)) \right) \begin{pmatrix} x(t) \\ u(t) \end{pmatrix}. \tag{2.27}$$

$\otimes_i$ denotes the i-mode tensor product as defined in Baranyi (2004), Baranyi et al. (2003).

One of the advantages of this model transformation is that it can be executed uniformly (irrespective of whether the model is given in the form of analytical equations

resulting from physical considerations, or as an outcome of soft computing based identification techniques such as neural networks or fuzzy logic based methods, or as a result of a black-box identification), without analytical interaction, within a reasonable amount of time. The obtained structure can be directly used for an LFT type modeling without any further preprocessing step.

According to defined by the ordering $(i_1, \ldots, i_N) \to r$ in the multi base number system defined by $(I_1, I_2, \ldots, I_N)$ the weighting functions are denoted by $w_r(\rho(t)) = \prod_k w_{k,i_k}(\rho_k(t)) \in [0, 1]$, where $w_{k,j}(\rho_k(t)) \in [0, 1]$ is the j-th one variable weighting function defined on the k-th dimension of Ω, while the corresponding vertex systems are $S_r = S_{i_1,i_2,\ldots,i_N}$. Using this index transformation one can write the model in the typical polytopic form:

$$S(\rho(t)) = \sum_{r=1}^{R} w_r(\rho(t)) S_r. \tag{2.28}$$

The convex hull of $S(\rho)$ might not be polytopic, however for design purposes a finite, polytopic (outer) approximation is needed. Convexity is ensured by the following conditions:

$$\forall n \in [1, N], i, \rho_n(t) : w_{n,i}(\rho_n(t)) \in [0, 1]; \tag{2.29}$$

$$\forall n \in [1, N], \rho_n(t) : \sum_{i=1}^{I_n} w_{n,i}(\rho_n(t)) = 1. \tag{2.30}$$

There are many ways to define the vertex systems and the type of the convex hull determined by the vertex system can be defined by the weighting functions. The applications of TP models specifies special requirements for the weighting functions.

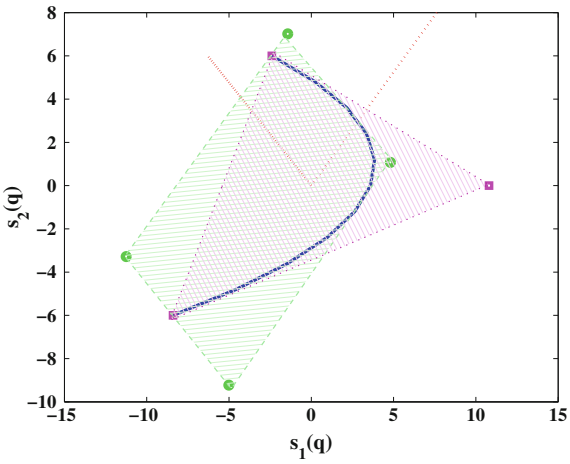

Fig. 2.2 Different convex approximations

For illustration purposes consider $S(\rho) = [\rho - \rho^2 \quad 2\rho]$ where $\rho \in [-3, 3]$. In Fig. 2.2 one can see the system $S(\rho)$ (in blue) while the dotted red lines depicts the directions given by the HOSVD while in green is depicted the smallest box that contains the convex hull $\tilde{S}$ of $S(\rho)$. Another convex hull is depicted in magenta, that corresponds to a TP model.

Often it is a non-trivial task to chose between the different model candidates. Then an important selection criteria is the solvability property of the design problems associated to the control tasks at hand.

2.3 Linearization by LFT Techniques

An LFT based model set is widely considered to be the most general representation adopted in robust controller design. From an analysis point of view the scheduling variables play the same role as the uncertainties and this fact can be reflected in the model structure. Both the Jacobian linearization and the LPV approximations lead to a parameter-dependent family of linear systems. Thus, the parameter dependence in the LPV system can be represented as an LFT. This representation provides a particular structure to the LPV system, also known as a $P - \Theta$ configuration, whereby the parameter-varying, uncertain or nonlinear terms are located in the Θ operator and the LTI part is described by the operator P.

Consider a feedback system, in which both the plant and the controller have a linear fractional dependence on Θ, see in the left-hand side of Fig. 2.3. In this representation P and K are known LTI models. The dependence of the plant and the controller are represented by the blocks Θ with input/output signals e_δ, d_δ and $\tilde{e}_\delta$, $\tilde{d}_\delta$. The block diagonal time-varying operator specifying the plant dynamics is denoted by

$$\Theta = \text{diag}(\rho_1 I_{r1}, ..., \rho_k I_{rk}), \qquad \text{where} \quad r_i > 1$$

whenever the parameter ρ_i is repeated and $r = \sum_{i=1}^{k} r_i$.

An LPV plant with a linear fractional dependence on Θ can be represented by the upper LFT interconnection:

$$\begin{bmatrix} z \\ y \end{bmatrix} = F_u(P, \Theta) \begin{bmatrix} d \\ u \end{bmatrix}. \tag{2.31}$$

The inputs and outputs of the augmented plant P is the following:

$$\left[\begin{array}{c} e_\delta \\ \hline z \\ y \end{array}\right] = \left[\begin{array}{c|cc} P_{\Theta\Theta} & P_{\Theta 1} & P_{\Theta 2} \\ \hline P_{1\Theta} & P_{11} & P_{12} \\ P_{2\Theta} & P_{21} & P_{22} \end{array}\right] \left[\begin{array}{c} d_\delta \\ \hline d \\ u \end{array}\right] \tag{2.32}$$

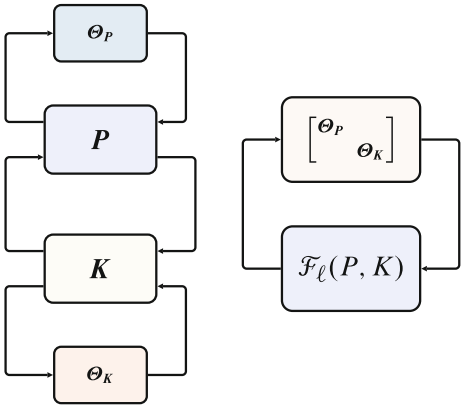

Fig. 2.3 The LPV control structure and its transformed form

Using the relation between d_δ and e_δ ($e_\delta = \Theta d_\delta$) the upper LFT interconnection structure is the following:

$$F_u(P,\Theta) = \begin{bmatrix} P_{1\Theta} \\ P_{2\Theta} \end{bmatrix} \Theta (I - P_{\Theta\Theta}\Theta)^{-1} \begin{bmatrix} P_{\Theta 1} & P_{\Theta 2} \end{bmatrix} + \begin{bmatrix} P_{11} & P_{12} \\ P_{21} & P_{22} \end{bmatrix}. \tag{2.33}$$

The feedback relation between u and y is

$$u = F_\ell(K,\Theta)y. \tag{2.34}$$

Note that while in most of the cases we use the same block Θ to schedule the plant and the controller, in general one may use blocks with a different structure. This fact is reflected in the notation of the Fig. 2.3. For the sake of simplicity in the formulas we use identical blocks.

The structure of the controller has the following relation:

$$\begin{bmatrix} u \\ \tilde{e}_\delta \end{bmatrix} = \begin{bmatrix} K_{11} & K_{1\Theta} \\ K_{\Theta 1} & K_{\Theta\Theta} \end{bmatrix} \begin{bmatrix} y \\ \tilde{d}_\delta \end{bmatrix}. \tag{2.35}$$

where the relation between d_δ and e_δ is $e_\delta = \Theta d_\delta$. The lower LFT interconnection structure is the following: $F_\ell(K,\Theta) = K_{1\Theta}\Theta(I - K_{\Theta\Theta}\Theta)^{-1}K_{\Theta 1} + K_{11}$.

The closed-loop operator from disturbance d to controlled output z is given by

$$T(P,K,\Theta) = F_\ell(F_u(P,\Theta), F_\ell(K,\Theta)). \tag{2.36}$$

The LFT structure can be transformed into a modified structure in which all parameter-dependent components are gathered into a single uncertainty block, see in the right-hand side of Fig. 2.3. Then the augmented plant is formalized in the following way:

$$\left[\begin{array}{c} \tilde{e}_\delta \\ \hline e_\delta \\ z \\ y \\ \hline \tilde{y} \end{array}\right] = \left[\begin{array}{c|c|c} 0 & 0 & I_r \\ \hline 0 & P & 0 \\ \hline I_r & 0 & 0 \end{array}\right] \left[\begin{array}{c} \tilde{d}_\delta \\ \hline d_\delta \\ d \\ u \\ \hline \tilde{u} \end{array}\right] \tag{2.37}$$

since $\tilde{y} = \tilde{d}_\delta$ and $\tilde{u} = \tilde{e}_\delta$. Here P is formalized using Eq. (2.32).

The closed-loop mapping from exogenous input d to controlled output z is expressed as

$$T(P, K, \Theta) = F_u\left(F_\ell(P_a, K), \begin{bmatrix} \Theta & 0 \\ 0 & \Theta \end{bmatrix}\right), \tag{2.38}$$

where P_a is formalized using Eq. (2.37). The original LPV problem can be viewed as a more classical robust performance problem in the face of the block-repeated uncertainty structure $\mathrm{diag}(\Theta, \Theta)$. This repeated structure is denoted by $\Delta \oplus \Delta$.

The approximation of the nonlinear system based on LFT structure is also found in Packard and Wu (1993), Packard (1994), Apkarian and Gahinet (1995).

2.4 Performance-Driven LPV Modeling

In a control design problem a control law has to be designed for a given system to reach the required performance specifications. The classical approach consists in building a mathematical model of the plant and this model is augmented with additional elements that reflect the different performance specifications. In most of the cases a given performance is modelled by the norm of a suitably selected set of signals. These signals—the performance signals—are related to the signals of the core model through some filtering. These filters are referred to as performance weights.

Recall the basic robust control paradigm: the design starts from a typical interconnection structure shown in Fig. 2.4. The Δ_m block contains the uncertainties of the system, such as unmodelled dynamics and parameter uncertainty. In this augmented plant unmodelled dynamics is represented by a weighting function W_r and a block Δ_m. The purpose of the weighting functions W_w and W_n is to reflect the disturbance and sensor noises.

In this framework performance requirements are imposed to signals z through a suitable choice of the weighting functions W_p. In contrast to the weights associated to control inputs and uncertainties, the role of these filters is not only to scale the signals but also to ensure a desired frequency separation between competing requirements, see, e.g., tracking and robustness. Thus, the performance weights are usually some dynamical systems, in a pure LTI setting transfer functions. In what follows we first list some of the typical control goals and the associated signals that are encountered in design problems.

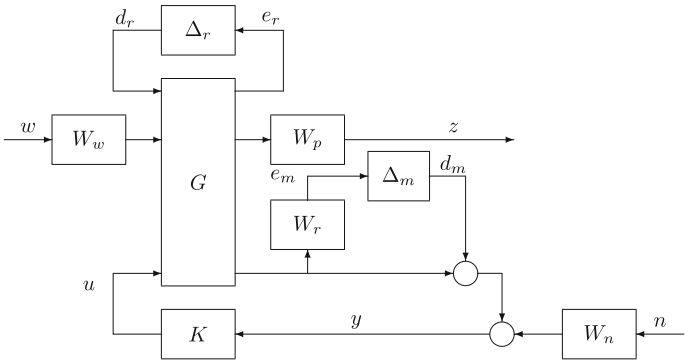

Fig. 2.4 The closed-loop interconnection structure

Yaw stability can be achieved by limiting the effects of the lateral load transfers. Then, the purpose of the control design is to minimize the lateral acceleration $z_a = a_y$, which can be chosen as a performance signal. Another control task is road tracking, i.e., to follow the road geometry. The purpose of the control is to minimize the difference between the yaw rate and the reference yaw rate: $z_e = |\psi_{act} - \psi_{ref}|$.

Roll stability is achieved by limiting the lateral load transfers on both axles to below the levels for wheel lift-off during various vehicle maneuvers. The lateral load transfer is $\Delta F_{zi} = k_t \phi_{ti}$, where ϕ_{ti} is the monitored roll angle of the unsprung mass at the front and the rear. The normalized lateral load transfer is introduced as $\rho_R = \Delta F_{zy}/(mg)$ and the aim of the control design is to reduce the maximum value of the normalized lateral load transfer if it exceeds a predefined critical value.

The pitch angle of the sprung mass may increase significantly during a sudden and hard braking. Thus a pitch stability requirement can be introduced which is achieved by limiting the longitudinal load transfers to below a predefined level. The normalized longitudinal load transfer is the normalized value of the pitch angle: $\rho_P = \theta/\theta_{max}$ where θ is the monitored pitch angle and θ_{max} is the maximal value of the pitch angle. The aim of the control design during braking is to reduce the pitching dynamics if the normalized longitudinal load transfer exceeds a critical value.

Finally, the control problem can be formulated in the general P-K-Δ structure, where P is the generalized plant and Δ contains both the uncertainties and the scheduling variables. In the design of local controllers the quadratic LPV performance problem is to choose the parameter-varying controller in such a way that the resulting closed-loop system is quadratically stable and the induced $\mathscr{L}_2$ norm from the disturbance and the performances is less than the value γ. The minimization task is the following (Fig. 2.5):

$$\inf_{K} \sup_{\Delta} \sup_{\|w\|_2 \neq 0, w \in \mathscr{L}_2} \frac{\|z\|_2}{\|w\|_2}. \tag{2.39}$$

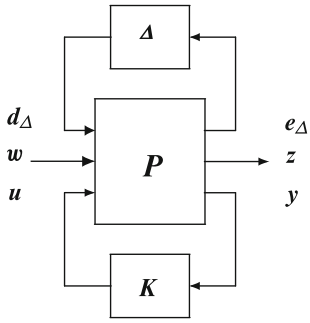

Fig. 2.5 The $P - K - \Delta$ structure

Nowadays there is a growing demand for vehicles with ever better driving characteristics in which efficiency, safety, and performance are ensured. In line with the requirements of the vehicle industry several performance specifications are in the focus of research, e.g., improving road holding, passenger comfort, roll and pitch stability, guaranteeing the reliability of vehicle components, reducing fuel consumption and proposing fault-tolerant solutions. An integrated control system is designed in such a way that the effects of a control system on other vehicle functions are taken into consideration in the design process by selecting the various performance specifications.

In a multi-layer supervisory architecture for integrated control systems the supervisor has information about the various vehicle maneuvers and the different fault operations by monitoring components and FDI filters. Thus, it is able to make decisions about the necessary interventions into the vehicle components and guarantee the reconfigurable and fault-tolerant operation of the vehicle. The role of the supervisor is to meet performance specifications and avoid the interference and conflict between components.

The advantage of the architecture for integrated vehicle control is that the complexity of the vehicle model is divided into several parts. In the formalism of the control-oriented model the messages of the supervisor must be taken into consideration. Consequently, the signals of monitoring components and FDI filters are built in the performance specifications of the controller by using parameter-dependent weighting. In this way the operation of a local controller can be extended to reconfigurable and fault-tolerant functions.

In the supervisory decentralized control the role of LPV methods is fundamental. In the formalism of the control oriented model, the selection of monitoring components and building them into signals, which are related to the performance requirements, are crucial points in the modeling. The proposed approach realizes the reconfiguration of the performance objectives by an appropriate scheduling of the corresponding weighting functions.

To illustrate the idea: consider a suspension system design where the performance weighting functions for heave acceleration and suspension deflections are selected as

$$W_{p,az} = \phi_{az} W_{0,az},$$
$$W_{p,sd} = \phi_{sd} W_{0,sd},$$

where ϕ_{az} and ϕ_{sd} are parameter varying gains. A large gain ϕ_{az} and a small gain ϕ_{sd} correspond to a design that emphasizes passenger comfort while choosing ϕ_{az} small and ϕ_{sd} large corresponds to a design that focuses on suspension deflection. A possible modeling choice is to select the suspension deflection as the parameter ρ that schedules these gains.

In order to sketch a possible choice for these scheduling variables two parameters are defined: c_1 and c_2. When the suspension deflection d is below c_1, the gain ϕ_a is selected to be constant and the gain ϕ_d is zero. When the deflection is between c_1 and c_2 the gains change linearly. When the value of the suspension deflection is greater than c_2, the gain ϕ_d is constant and the gain ϕ_a is zero, see Fig. 2.6.

We emphasize that in this way we obtain an LPV model and place the design into the LPV framework, even the original plant was modeled as an LTI system.

Since fault-tolerant control requires fault information in order to guarantee performances and modify its operation the presence of suitably designed FDI filters are needed. Then, the fault information provided by the FDI filter can be quantified as $\rho_D = f_{act}/f_{max}$, where f_{act} is an estimation of the failure (output of the FDI filter), that means the rate of the performance degradation of an active component, and f_{max} is an estimation of the maximum value of the potential failure (fatal error). Thus, the value of a possible fault is normalized into the interval $\rho_D = [0,\ 1]$.

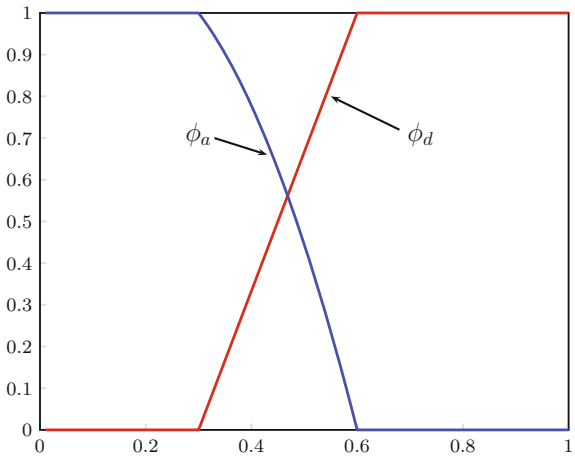

Fig. 2.6 Gains of the performance weights: ϕ_a and ϕ_d

The actuator reconfiguration is based on the fact that two actuators are able to influence the same vehicle dynamics. Thus, the fault-free actuator it is able to substitute for the operation of another actuator which has been affected by a failure or its performance has degraded. The control design is based on two factors: the failure or performance degradation have already been detected and the fault information ρ_D and the necessary intervention possibilities are built into its control design. This goal is achieved by a suitable scheduling of the corresponding W_p performance and W_a actuator weights.

As an example consider the design of the brake system the command signal is the difference in brake forces while the performance signal is the lateral acceleration: $z_b = \left[a_y, u_r\right]^T$. The weighting function of the lateral acceleration is selected as:

$$W_{pa} = \phi_a W_{0,pa},$$

where ϕ_a is a gain, which reflects the relative importance of the lateral acceleration and it is chosen to be parameter-dependent, e.g., the function of the normalized lateral load transfer ρ_R. When the vehicle is not in an emergency ρ_R is small ($|\rho_R| < R_b$), i.e., ϕ_a is small, indicating that the LPV control should not focus on minimizing acceleration. On the other hand, when ρ_R approaches the critical value, i.e., when $|\rho_R| \geqq R_b$, ϕ_a is large, it indicates that the control should focus on preventing the rollover.

Here the fixed parameter R_b defines the critical status when the vehicle is close to the rollover situation, i.e., all wheels are on the ground but the lateral tire force of the inner wheels tends to zero. Moreover, a parameter R_a can also be introduced to reflect how fast the control should focus on minimizing the lateral acceleration. These parameters guarantee the smooth transient of the signals, e.g., for the following choice:

$$\phi_a = \begin{cases} 1 & \text{if} \quad |\rho_R| > R_b \\ \frac{|\rho_R| - R_a}{R_b - R_a} & \text{if} \quad R_a \leq |\rho_R| \leq R_b \\ 0 & \text{if} \quad |\rho_R| < R_a \end{cases}$$

Moreover, in the presence of an anti-roll bar system, if a fault is detected in the operation of the anti-roll bars the brake system will be activated at a smaller critical value than in a fault-free case, i.e., when $|\rho_{Da}| > 0$. Consequently, the brake is activated in a modified way and the brake moment is able to assume the role of the anti-roll bars or the suspension actuator in which the fault has occurred. The modified critical value is

$$R_{a,new} = R_a - \alpha \cdot \rho_{Da},$$

where α is a predefined constant factor.

2.5 LPV Modeling of Two Subsystems

2.5.1 Modeling of the Vertical Dynamics

The full-car vehicle model, which is shown in Fig. 2.7, comprises five parts: the sprung mass and four unsprung masses. Let the sprung and unsprung masses be denoted by m_s, m_{uf}, and m_{ur}, respectively. All suspensions consist of a spring, a damper and an actuator, which generates a pushing force between the body and the axle. The front and rear suspension stiffnesses, the front and rear tire stiffnesses are denoted by k_{sf}, k_{sr}, and k_{tf}, k_{tr}, respectively. The front and rear suspension dampings are denoted by b_{sf}, b_{sr}, respectively. Let the front and rear displacement of the sprung mass on the left and right side be denoted by x_{1fl}, x_{1rl} and x_{1fr}, x_{1rr}, respectively. Let the front and rear displacement of the unsprung mass on the left and right side be denoted by $x_{2fl}, x_{2rl}, x_{2fr}$, and x_{2rr}, respectively. In the full-car model, the disturbances, $w_{fl}, w_{rl}, w_{fr}, w_{rr}$ are caused by road irregularities. The control forces, $F_{zfl}, F_{zrl}, F_{zfr}, F_{zrr}$ are generated by the actuators.

The full-car model is based on a seven degrees of freedom system. The sprung mass is assumed to be a rigid body and has freedoms of motion in the vertical, pitch and roll directions. Accordingly: x_1 is the vertical displacement at the center of gravity, θ is the pitch angle and ϕ is the roll angle of the sprung mass. The following linear approximations are applied to the front and rear displacements of the sprung mass on the left and right side:

$$\begin{aligned} x_{1fl} &= x_1 + \ell_f\theta + t_f\phi, \\ x_{1fr} &= x_1 + \ell_f\theta - t_f\phi, \\ x_{1rl} &= x_1 - \ell_r\theta + t_r\phi, \\ x_{1rr} &= x_1 - \ell_r\theta - t_r\phi. \end{aligned}$$

In the following the first principle based motion equations are formalized using the Lagrangian mechanics. Since in the model there exist seven degrees of freedom, define the generalized coordinates as

$$q = \left[x_1\ \theta\ \phi\ x_{2fl}\ x_{2fr}\ x_{2rl}\ x_{2rr}\right]^T. \tag{2.40}$$

When the kinetic energy for a moving rigid body is calculated from both the oscillation of the vehicle body and the vertical displacements of unsprung components are taken into consideration. Since the yaw motion compared to the steering movement is ignored and the roll angle is assumed to be small, the angular velocities are approximated in the following way:

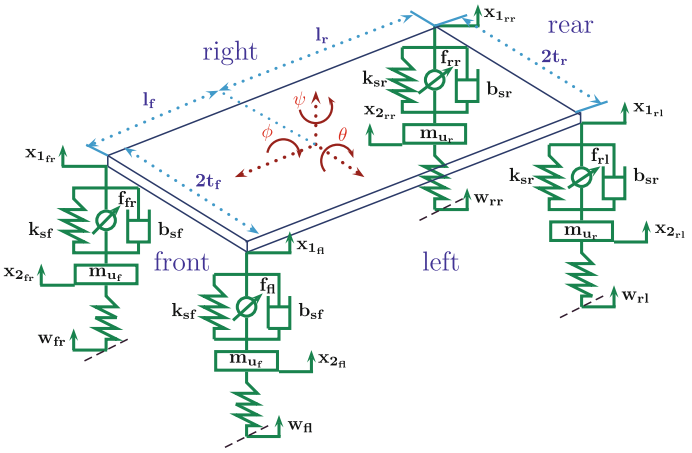

Fig. 2.7 The vertical dynamics of a full-car model

$$\Omega_x = \dot{\theta} sin\phi \approx 0,$$
$$\Omega_y = \dot{\theta} cos\phi \approx \dot{\theta},$$
$$\Omega_z = \dot{\phi}.$$

Thus, the kinetic energies contributed from the vehicle body and the unsprung components:

$$T_B = \frac{1}{2} M_s \dot{x}_1^2 + \frac{1}{2} I_\theta \dot{\theta}^2 + \frac{1}{2} I_\phi \dot{\phi}^2, \tag{2.41}$$
$$T_U = \frac{1}{2} m_{uf} (\dot{x}_{2fl}^2 + \dot{x}_{2fr}^2) + \frac{1}{2} m_{ur} (\dot{x}_{2rl}^2 + \dot{x}_{2rr}^2) \tag{2.42}$$

and the total kinetic energy is $T = T_B + T_U$.

The potential energy includes the deformations of springs and tires of the vehicle during vibrations. The deformations of the tires and that of the suspension components are:

$$d_{2fl} = x_{2fl} - w_{fl}, \quad d_{2fr} = x_{2fr} - w_{fr}, \quad d_{2rl} = x_{2rl} - w_{rl}, \quad d_{2rr} = x_{2rr} - w_{rr},$$

and

$$d_{1fl} = x_{1fl} - x_{2fl}, \quad d_{1fr} = x_{1fr} - x_{2fr}, \quad d_{1rl} = x_{1rl} - x_{2rl}, \quad d_{1rr} = x_{1rr} - x_{2rr},$$

respectively. The potential energy is the sum of two components: $U = U_S + U_T$, where U_S contains the potential energy stored in suspension systems and U_T contains the potential energy stored in tires:

$$U_S = \frac{1}{2}k_{sf}(d_{1fl}^2 + d_{1fr}^2) + \frac{1}{2}k_{sr}(d_{1rl}^2 + d_{1rr}^2), \tag{2.43}$$

$$U_T = \frac{1}{2}k_{tf}(d_{2fl}^2 + d_{2fr}^2) + \frac{1}{2}k_{tr}(d_{2rl}^2 + d_{2rr}^2). \tag{2.44}$$

The dissipation energy accounts for the effect of shock absorbers. Assuming that the forces produced by dampers vary linearly with the rates of change of deformations, the dissipation function is obtained as

$$D = \frac{1}{2}b_{sf}(\dot{d}_{1fl}^2 + \dot{d}_{1fr}^2) + \frac{1}{2}b_{sr}(\dot{d}_{1rl}^2 + \dot{d}_{1rr}^2). \tag{2.45}$$

The external forces are formalized for all generalized coordinates:

$$f_1 = -F_{zfl} - F_{zfr} - F_{zrl} - F_{zrr}, \quad f_2 = -l_f F_{zfl} - l_f F_{zfr} + l_r F_{zrl} + l_r F_{zrr}, \quad f_4 = F_{zfl},$$
$$f_3 = -t_f F_{zfl} + t_f F_{zfr} - t_r F_{zrl} + t_r F_{zrr}, \quad f_5 = F_{zfr}, \quad f_6 = F_{zrl} \text{ and } f_7 = F_{zrr}.$$

Then the Lagrangian equations of the full-car model are formalized as follows.

$$M_s\ddot{q} = LB_s(\dot{x}_u - \dot{x}_s) + LK_s(x_u - x_s) - Lf, \tag{2.46}$$

$$M_u\ddot{x}_u = B_s(\dot{x}_s - \dot{x}_u) + K_s(x_s - x_u) + K_t(w - x_u) + f, \tag{2.47}$$

where $q = \begin{bmatrix} x_1 & \theta & \phi \end{bmatrix}^T$, $x_s = \begin{bmatrix} x_{1fl} & x_{1fr} & x_{1rl} & x_{1rr} \end{bmatrix}^T$, $x_u = \begin{bmatrix} x_{2fl} & x_{2fr} & x_{2rl} & x_{2rr} \end{bmatrix}^T$, $w = \begin{bmatrix} w_{fl} & w_{fr} & w_{rl} & w_{rr} \end{bmatrix}^T$, and $f = \begin{bmatrix} F_{zfl} & F_{zfr} & F_{zrl} & F_{zrr} \end{bmatrix}^T$. The sprung mass ($M_s$), the unsprung mass ($M_u$), the suspension stiffness (K_s), the tire stiffness (K_t), suspension damping (B_s), geometry (L) matrices can be formulated as follows:

$$M_s = \begin{bmatrix} m_s & 0 & 0 \\ 0 & I_\theta & 0 \\ 0 & 0 & I_\phi \end{bmatrix}, \quad M_u = \begin{bmatrix} m_{uf} & 0 & 0 & 0 \\ 0 & m_{uf} & 0 & 0 \\ 0 & 0 & m_{ur} & 0 \\ 0 & 0 & 0 & m_{ur} \end{bmatrix}, \quad B_s = \begin{bmatrix} b_{sf} & 0 & 0 & 0 \\ 0 & b_{sf} & 0 & 0 \\ 0 & 0 & b_{sr} & 0 \\ 0 & 0 & 0 & b_{sr} \end{bmatrix},$$

$$K_s = \begin{bmatrix} k_{sf} & 0 & 0 & 0 \\ 0 & k_{sf} & 0 & 0 \\ 0 & 0 & k_{sr} & 0 \\ 0 & 0 & 0 & k_{sr} \end{bmatrix}, \quad K_t = \begin{bmatrix} k_{tf} & 0 & 0 & 0 \\ 0 & k_{tf} & 0 & 0 \\ 0 & 0 & k_{tr} & 0 \\ 0 & 0 & 0 & k_{tr} \end{bmatrix}, \quad L = \begin{bmatrix} 1 & 1 & 1 & 1 \\ l_f & l_f & -l_r & -l_r \\ t_f & -t_f & t_r & -t_r \end{bmatrix}.$$

The nominal parameters of the full-car model are in Table 2.1.

Using the kinematic relationship between x_s and q:

$$x_s = L^T q \tag{2.48}$$

and by substituting Eq. (2.48) for Eq. (2.46), the following differential equation is formalized:

Table 2.1 Parameters of the full-car model

Parameters (symbols)	Value	Unit
Sprung mass (m_s)	1400	kg
Pitch moment inertia (I_θ)	2100	kg m^2
Roll moment inertia (I_ϕ)	460	kg m^2
Unsprung masses (m_{uf}, m_{ur})	40, 40	kg
Suspension stiffness (k_{sf}, k_{sr})	23500, 25500	N/m
Front tire stiffness (k_{tf}, k_{tr})	190000, 190000	N/m
Suspension damping (b_{sf}, b_{sr})	1000, 1100	N/m/s
Actuator parameters (α, β, γ),	$4.515 \cdot 10^{13}$, 1, $4.969 \cdot 10^{12}$	
Area of piston (A_P)	$3.35 \cdot 10^{-4}$	m^2
Supply pressure (P_s)	10342500	Pa
Time constant (τ)	$\frac{1}{30}$	s

$$M\ddot{z} + B\dot{z} + Kz = K_r w + L_a f, \tag{2.49}$$

where $z = \begin{bmatrix} q^T & x_u^T \end{bmatrix}^T$, and the matrices are as follows:

$$M = \begin{bmatrix} M_s & 0 \\ 0 & M_u \end{bmatrix}, \quad B = \begin{bmatrix} LB_sL^T & -LB_s \\ -B_sL^T & B_s \end{bmatrix},$$
$$K = \begin{bmatrix} LK_sL^T & -LK_s \\ -K_sL^T & K_s + K_t \end{bmatrix}, \quad K_r = \begin{bmatrix} 0 \\ K_t \end{bmatrix}, \quad L_a = \begin{bmatrix} -L \\ I \end{bmatrix}.$$

Equation (2.49) can be represented as a state space form:

$$\dot{x} = Ax + B_1 w + B_2 u, \tag{2.50}$$

where $x = \begin{bmatrix} z^T & \dot{z}^T \end{bmatrix}^T$, $u = f$ and

$$A = \begin{bmatrix} 0 & I \\ -M^{-1}K & -M^{-1}B \end{bmatrix}, \quad B_1 = \begin{bmatrix} 0 \\ M^{-1}K_r \end{bmatrix}, \quad B_2 = \begin{bmatrix} 0 \\ M^{-1}L_a \end{bmatrix}.$$

The nominal parameters of the full-car model are in Table 2.1. From disturbances to performance signals the open-loop frequency responses of the full-car model, i.e., the heave, pitch, roll accelerations and suspension deflections, are illustrated in Fig. 2.8.

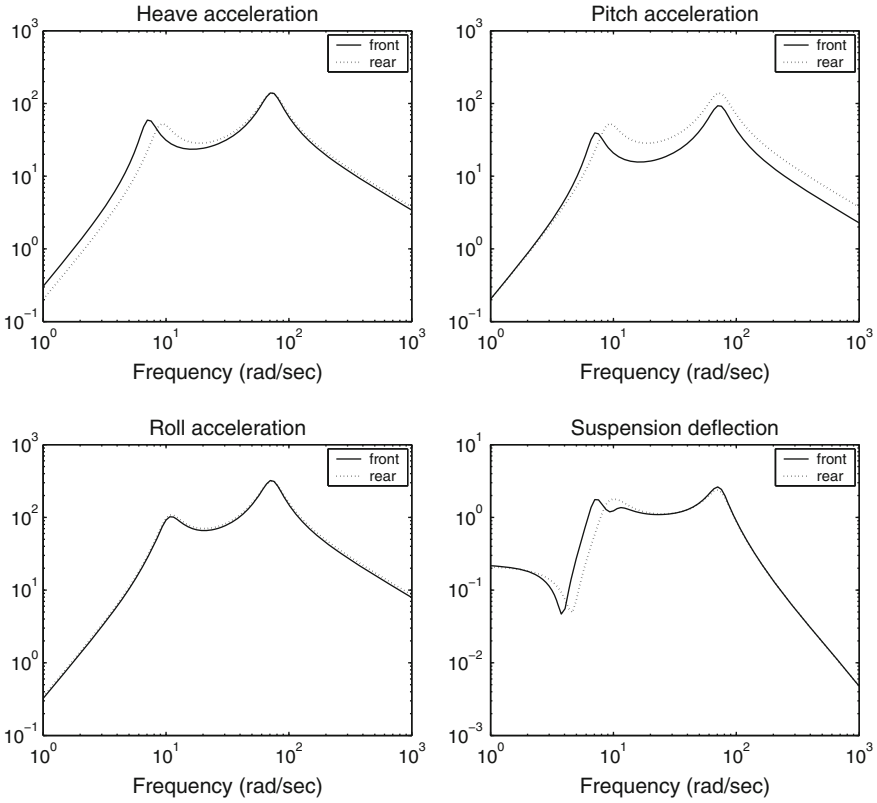

Fig. 2.8 Frequency responses of the full-car model to disturbances

2.5.2 Nonlinear Components of the Vertical Dynamics

In the full-char model presented in the previous section it was not explicitly expressed the nonlinearity of the suspension stiffness (K_s), the tire stiffness (K_t) and that of the suspension damping (B_s). Moreover the nonlinearity of the actuator was completely ignored. In what follows, we concentrate on these nonlinearities by developing the model of a relevant subsystem, the quarter-car.

The quarter-car vehicle model, which is shown in Fig. 2.9, is a two-degree-of-freedom model. $x_1 = q_1$ and $x_2 = q_2$ denote the vertical displacement of the sprung mass and the unsprung mass, respectively. In the modelling of suspension systems the nonlinear behavior of suspension components and the actuator dynamics are taken into consideration. The vertical dynamics of the suspension system is formalized in the following way:

$$m_s\ddot{x}_1 = F_{ks} + F_{bs} - F_{az}, \tag{2.51}$$

$$m_u\ddot{x}_2 = -F_{ks} - F_{bs} - k_t(x_2 - w) + F_{az}, \tag{2.52}$$

where F_{bs} is the suspension damping force, F_{ks} is the suspension spring force and F_{az} is the force of the actuator.

The force equation of the suspension stiffness is

$$F_{ks} = k_s^l(x_2 - x_1) + k_s^{nl}(x_2 - x_1)^3, \tag{2.53}$$

where parts of the nonlinear suspension stiffness (k_s) are a linear coefficient k_s^l and a nonlinear coefficient k_s^{nl}. The force equation of the suspension damping is

$$F_{bs} = b_s^l(\dot{x}_2 - \dot{x}_1) - b_s^{sym}(\dot{x}_2 - \dot{x}_1)sgn(\dot{x}_2 - \dot{x}_1) + b_s^{nl}\sqrt{|\dot{x}_2 - \dot{x}_1|}sgn(\dot{x}_2 - \dot{x}_1), \tag{2.54}$$

where $\dot{x}_1$ and $\dot{x}_2$ denote the vertical velocity of the sprung mass and the unsprung mass, respectively. Here, the nonlinear suspension damping b_s consists of a linear coefficient b_s^l and two nonlinear coefficients b_s^{nl} and b_s^{sym}. b_s^{nl} shows the nonlinear impact on the damping characteristics while b_s^{sym} describes its asymmetric behavior. Note that in the modelling of the suspension system a linearized model is often used instead of a nonlinear one. In the linearized version of the suspension system $F_{ks} = k_s^l(x_2 - x_1)$ and $F_{bs} = b_s^l(\dot{x}_2 - \dot{x}_1)$ are applied.

The hydraulic actuator operates nonlinearly, thus its force should be formalized in the following way, see Merritt (1967). The hydraulic actuator is controlled by electro-hydraulic servo-valves and is mounted parallel to the passive suspension system. Consider a four-way valve-piston system in which the force balance at the piston gives:

$$F_{az} = A_P P_L, \tag{2.55}$$

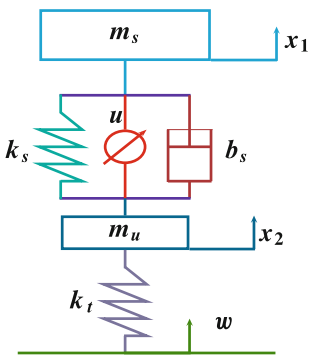

Fig. 2.9 Vertical dynamics of a quarter-car model

where A_P is the area of the piston and P_L is the pressure drop across the piston with respect to the front and rear suspensions. The derivative of P_L is given by

$$\dot{P}_L = -\beta P_L + \alpha A_P(\dot{x}_2 - \dot{x}_1) + \alpha Q, \tag{2.56}$$

in which $\alpha = \frac{4\beta_e}{V_t}$, $beta = \alpha C_{tp}$ and

$$Q = sgn[P_s - sgn(x_v)P_L]C_d S x_v \sqrt{\frac{1}{\bar{\rho}}|P_s - sgn(x_v)P_L|}, \tag{2.57}$$

and V_t is the total actuator volume, β_e is the effective bulk modulus of system, Q is the hydraulic load flow, C_{tp} is the total leakage coefficient of the piston, C_d is the discharge coefficient, S is the spool valve area gradient, x_v is the displacement of the spool valve, $\bar{\rho}$ is the hydraulic fluid density, P_s is the supply pressure. The cylinder velocity acts as a coupling from the position output of the cylinder to the pressure differential across the piston. It is considered a feedback term, which has been analyzed by Alleyne and Hedrick (1992), Alleyne and Liu (2000). The displacement of the spool valve x_v is controlled by the input to the servo-valve u:

$$\dot{x}_v = \frac{1}{\tau}(-x_v + u). \tag{2.58}$$

The state space representation of the nonlinear model is:

$$\dot{x} = f(x) + gu + hw, \tag{2.59}$$

in which the state vector x is as follows:

$$x = \begin{bmatrix} x_1 & x_2 & x_3 & x_4 & x_P & x_v \end{bmatrix}^T. \tag{2.60}$$

The components of the state vector are the vertical displacement of the sprung mass x_1, the vertical displacement of the unsprung mass x_2, their derivatives $x_3 = \dot{x}_1$, $x_4 = \dot{x}_2$, the pressure drop $x_P (= P_L)$, and the servo valve displacement x_v. The components of the Eq. (2.59) are

$$f(x) = \begin{bmatrix} x_3 \\ x_4 \\ \frac{1}{m_s}\left(F_{ks} + F_{bs} - A_P x_P\right) \\ \frac{1}{m_u}\left(-F_{ks} - F_{bs} - k_t x_2 + A_P x_P\right) \\ -\beta x_P + \alpha A_P(x_4 - x_3) + \alpha Q \\ -\frac{1}{\tau}x_v \end{bmatrix}, \quad g = \begin{bmatrix} 0 \\ 0 \\ 0 \\ 0 \\ 0 \\ \frac{1}{\tau} \end{bmatrix}, \quad h = \begin{bmatrix} 0 \\ 0 \\ 0 \\ \frac{k_t}{m_u} \\ 0 \\ 0 \end{bmatrix}.$$

In the following, an LPV model is constructed by selecting three scheduling variables, i.e., the square of the relative displacement, the signum of the relative velocity and a signal linked to the load pressure of the actuator.

$$\rho_{ks} = (x_2 - x_1)^2, \tag{2.61}$$

$$\rho_b = sgn(x_4 - x_3), \tag{2.62}$$

$$\rho_Q = sgn[P_s - sgn(x_v)P_L]C_d S\sqrt{\frac{1}{\bar{\rho}}|P_s - sgn(x_v)P_L|}. \tag{2.63}$$

Substituting ρ_Q into equation of the actuator (2.56), the differential equation is:

$$\dot{x}_P(\rho_Q) = -\beta x_P + \alpha A_P(x_4 - x_3) + \alpha\rho_Q x_v. \tag{2.64}$$

The parameter dependence of the load pressure differential equation is affine in ρ_Q. As a consequence of affine parameter dependence, quadratic stability and control performance are guaranteed in the whole parameter region, solving an optimization problem only at extreme points in the parameter region over the LMI constraints.

The nonlinear spring force is reformulated in the following way:

$$F_{ks}(\rho_{ks}) = k_s^l(x_2 - x_1) + k_s^{nl}\rho_{ks}(x_2 - x_1). \tag{2.65}$$

This force is expressed by a linear combination of states allowing the force to have nonlinear ρ_{ks} dependence. The nonlinear damping force is partitioned in the following way:

$$F_{bs}(\rho_b) = b_s^l(x_4 - x_3) - b_s^{sym}\rho_b(x_4 - x_3) + b_s^{nl}\rho_b\sqrt{\rho_b(x_4 - x_3)}, \tag{2.66}$$

where the first and the second terms are the linear parts and the third term is the nonlinear part of the damping force. The linear parts of the damping force can be expressed as a linear combination of the states, however, the the nonlinear part cannot. Thus, a fictitious signal u_{fict} must be introduced, and the nonlinear parts must be incorporated into the disturbance matrix when the LPV model is formalized.

In the LPV model of the active suspension system three parameters are selected. In practice, the relative displacement is a measured signal. The relative velocity is then determined by numerical differentiation from the measured relative displacement. The scheduling variable ρ_Q is linked to the load pressure of the actuator, which is assumed to be calculated directly from Eq. (2.57).

The state space representation of the LPV model is as follows:

$$\dot{x} = A(\rho)x + gu + \tilde{h}\tilde{w}, \tag{2.67}$$

where $\rho = [\rho_1\ \rho_2\ \rho_3]^T$ with $\rho_1 = \rho_{ks}, \rho_2 = \rho_b, \rho_3 = \rho_Q$ and $\tilde{w} = [w\ u_{fict}]^T$ includes both the disturbance and the fictitious signals. The matrix A is expressed in the following form

Table 2.2 Parameters of the quarter-car model

Parameters (symbols)	Value	Unit
Sprung mass (m_s)	290	kg
Unsprung mass (m_u)	40	kg
Suspension stiffness (k_s^l, k_s^{nl})	$235 \cdot 10^2, 235 \cdot 10^4$	N/m
Tire stiffness (k_t)	$190 \cdot 10^3$	N/m
Damping ($b_s^l, b_s^{nl}, b_s^{sym}$)	700, 400, 400	N/m/s
Time constant (τ)	$\frac{1}{30}$	s

$$
\begin{aligned}
A(\rho) &= A_0 + \rho_1 A_1 + \rho_2 A_2 + \rho_3 A_3 \\
&= \begin{bmatrix}
0 & 0 & 1 & 0 & 0 & 0 \\
0 & 0 & 0 & 1 & 0 & 0 \\
-\frac{k_s^l}{m_s} & \frac{k_s^l}{m_s} & -\frac{b_s^l}{m_s} & \frac{b_s^l}{m_s} & -\frac{A_P}{m_s} & 0 \\
\frac{k_s^l}{m_u} & -\frac{k_s^l}{m_u} - \frac{k_t}{m_u} & \frac{b_s^l}{m_u} & -\frac{b_s^l}{m_u} & \frac{A_P}{m_u} & 0 \\
0 & 0 & -\alpha A_P & \alpha A_P & -\beta & 0 \\
0 & 0 & 0 & 0 & 0 & -\frac{1}{\tau}
\end{bmatrix} + \rho_1 \begin{bmatrix}
0 & 0 & 0\,0\,0\,0 \\
0 & 0 & 0\,0\,0\,0 \\
-\frac{k_s^{nl}}{m_s} & \frac{k_s^{nl}}{m_s} & 0\,0\,0\,0 \\
\frac{k_s^{nl}}{m_u} & -\frac{k_s^{nl}}{m_u} & 0\,0\,0\,0 \\
0 & 0 & 0\,0\,0\,0 \\
0 & 0 & 0\,0\,0\,0
\end{bmatrix} \\
&+ \rho_2 \begin{bmatrix}
0\,0 & 1 & 0 & 0\,0 \\
0\,0 & 0 & 1 & 0\,0 \\
0\,0 & \frac{b_s^{sym}}{m_s} & -\frac{b_s^{sym}}{m_s} & 0\,0 \\
0\,0 & -\frac{b_s^{sym}}{m_u} & \frac{b_s^{sym}}{m_u} & 0\,0 \\
0\,0 & 0 & 0 & 0\,0 \\
0\,0 & 0 & 0 & 0\,0
\end{bmatrix} + \rho_3 \begin{bmatrix}
0\,0\,0\,0\,0 & 0 \\
0\,0\,0\,0\,0 & 0 \\
0\,0\,0\,0\,0 & 0 \\
0\,0\,0\,0\,0 & 0 \\
0\,0\,0\,0\,0 & \alpha\rho_Q \\
0\,0\,0\,0\,0 & 0
\end{bmatrix}
\end{aligned}
$$

and components g and $\tilde{h}$ are the following:

$$
g = \begin{bmatrix} 0 \\ 0 \\ 0 \\ 0 \\ 0 \\ \frac{1}{\tau} \end{bmatrix}, \quad \tilde{h} = \begin{bmatrix}
0 & 0 \\
0 & 0 \\
0 & \frac{1}{m_s} b_s^{nl} \rho_b \sqrt{\rho_b (x_4 - x_3)} \\
\frac{k_t}{m_u} & -\frac{1}{m_u} b_s^{nl} \rho_b \sqrt{\rho_b (x_4 - x_3)} \\
0 & 0 \\
0 & 0
\end{bmatrix}.
$$

The nominal parameters are in Table 2.2.

The performance signals of the suspension system, i.e., the heave acceleration of the sprung mass, suspension deflection, wheel displacement and the control force, are tested in two examples. The excitation signals are a bump on the road surface and a square wave input.

Firstly, the performance signals of the suspension system are tested by using a bump. The performance signals are illustrated in Fig. 2.10. The overshoots of the heave acceleration are larger about 10 % in the nonlinear case than in the linear one,

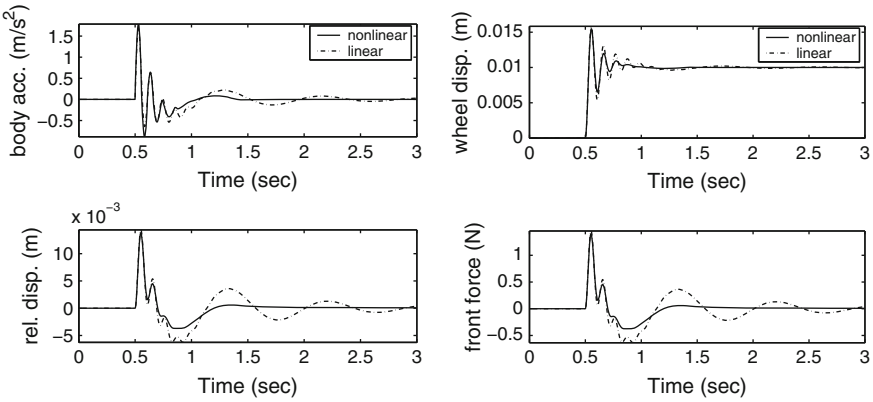

Fig. 2.10 Time responses of the vehicle to a bump

however, the transient duration of the nonlinear case is shorter than in the linear one. At the same time the values of suspension deflections are smaller in the nonlinear case than in the linear one. These properties are caused by the nonlinear damping characteristics, which are significantly different from the linear characteristics around the equilibrium point.

2.5.3 LPV Modeling of the Yaw–Roll Dynamics

The motion differential equations, i.e., the lateral dynamics, the yaw moment, the roll moment of the sprung mass, the roll moment of the front and the rear unsprung masses are the following. These equations were also formulated in Sampson and Cebon (2003), Gáspár et al. (2005c).

Figure 2.11 illustrates the combined yaw–roll dynamics of a vehicle, which is modelled by a three-body system, in which m_s is the sprung mass, $m_{u,f}$ is the unsprung mass at the front including the front wheels and axle, $m_{u,r}$ is the unsprung mass at the rear with the rear wheels and axle, and m is the total vehicle mass.

I_{xx}, I_{xz}, I_{zz} are the roll moments of the inertia of the sprung mass, the yaw–roll product, and the yaw moment of inertia, respectively. h is the height of CG of sprung mass and $h_{u,f}$, $h_{u,r}$ are the height of CG of unsprung masses and r is the height of the roll axis from ground. The total axle loads are F_{zl} and F_{zr}, respectively.

The roll motion of the sprung mass is damped by suspensions with damping coefficients b_{sf}, b_{sr} and stiffness coefficients k_{sf}, k_{sr}. The tire stiffnesses are denoted by k_{tf} and k_{tr}. The signals are the forward velocity v,the lateral acceleration a_y, the side slip angle of the sprung mass β, the heading angle ψ, the yaw rate $\dot{\psi}$, the roll angle ϕ, the roll rate $\dot{\phi}$, the roll angle of the unsprung mass at the front axle $\phi_{t,f}$ and at the rear axle $\phi_{t,r}$.

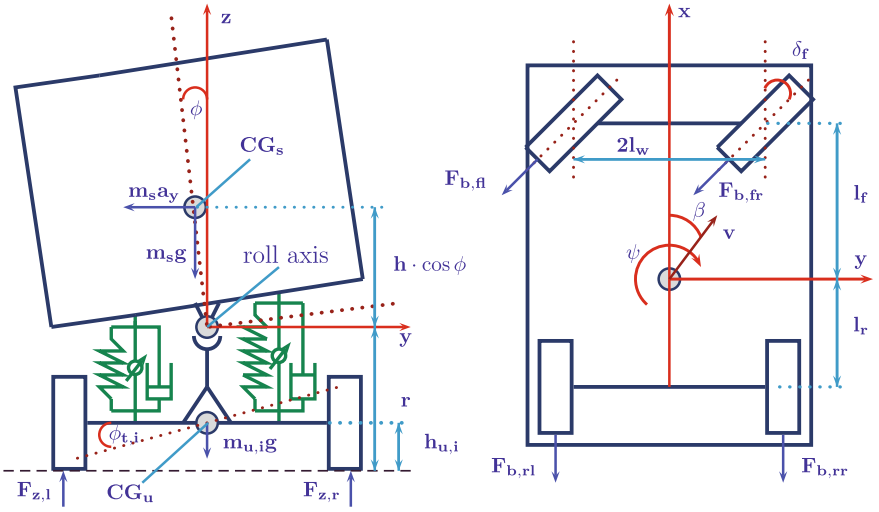

Fig. 2.11 Illustration of the vehicle model

δ_f is the front wheel steering angle and ΔF_b are the braking forces on the left and right hand side wheels. It is assumed that the difference between the brake forces ΔF_b provided by the compensator is applied to the rear axle. This assumption does not restrict the implementation of the compensator because it is possible that the control action be distributed at the front and the rear wheels at either of the two sides.

In vehicle modelling the motion differential equations of the combined yaw and roll dynamics of the single unit vehicle are formalized. The vehicle can translate longitudinally and laterally and it can also yaw. The sprung mass can rotate around a horizontal axis. The unsprung masses can also roll, permitting the vertical compliance of the tires. The motion is described using a coordinate system fixed in the vehicle: the roll axis is replaced by an x axis parallel to the ground, and the z axis passes downward through the center of mass of the vehicle. The suspension springs, dampers and active anti-roll bars generate moments between the sprung and unsprung masses in response to roll motions. The active roll control systems at each axle consist of a pair of actuators and a series of mechanical linkages in addition to the existing passive springs and dampers. The tires produce lateral forces that vary linearly with the side slip angles.

$$mv(\dot{\beta}+\dot{\psi}) - m_s h\ddot{\phi} = F_{yf} + F_{yr}, \tag{2.68}$$

$$-I_{xz}\ddot{\phi} + I_{zz}\ddot{\psi} = F_{yf}l_f - F_{yr}l_r + l_w \Delta F_b, \tag{2.69}$$

$$\begin{aligned}(I_{xx} + m_s h^2)\ddot{\phi} - I_{xz}\ddot{\psi} &= m_s g h\phi + m_s v h(\dot{\beta}+\dot{\psi}) - \\ -k_{f(r)}(\phi - \phi_{t,f}) - b_{f(r)}(\dot{\phi} - \dot{\phi}_{t,f}) &- k_{r(r)}(\phi - \phi_{t,r}) - b_{r(r)}(\dot{\phi} - \dot{\phi}_{t,r}),\end{aligned} \tag{2.70}$$

$$\begin{aligned}-rF_{yf} &= m_{uf} v(r - h_{uf})(\dot{\beta}+\dot{\psi}) + m_{uf} g h_{uf}\phi_{t,f} - \\ -k_{t,f(r)}\phi_{t,f} + k_{f(r)}(\phi - \phi_{t,f}) &+ b_{f(r)}(\dot{\phi} - \dot{\phi}_{t,f}),\end{aligned} \tag{2.71}$$

$$\begin{aligned}-rF_{yr} &= m_{ur} v(r - h_{ur})(\dot{\beta}+\dot{\psi}) - m_{ur} g h_{ur}\phi_{t,r} - \\ -k_{t,r(r)}\phi_{t,r} + k_{r(r)}(\phi - \phi_{t,r}) &+ b_{r(r)}(\dot{\phi} - \dot{\phi}_{t,r}).\end{aligned} \tag{2.72}$$

The lateral tire forces F_{yf} and F_{yr} in the direction of the wheel ground contact are approximated linearly to the tire slide slip angles α_f and α_r, respectively:

$$F_{yf} = \mu C_f \alpha_f, \quad F_{yr} = \mu C_r \alpha_r, \tag{2.73}$$

where μ is the side force coefficient (it is also called friction or cohesion co-efficient) and C_f and C_r are tire side slip constants. μ is also called friction or cohesion coefficient and by definition it is the ratio of the frictional force acting in the wheel plane and the wheel ground contact force.

The chassis and the wheels have identical velocities at the wheel ground contact points. The velocity equations for the front and rear wheels in the lateral and in the longitudinal directions are as follows:

$$v_{w,f}\sin(\delta_f - \alpha_f) = l_f \cdot \dot{\psi} + v\sin\beta \tag{2.74}$$

$$v_{w,f}\cos(\delta_f - \alpha_f) = v\cos\beta \tag{2.75}$$

$$v_{w,r}\sin\alpha_r = l_r \cdot \dot{\psi} - v\sin\beta \tag{2.76}$$

$$v_{w,r}\cos\alpha_r = v\cos\beta. \tag{2.77}$$

In stable driving conditions, the tire side slip angle α_i is normally not larger than 5° and the above equation can be simplified by substituting $\sin x \approx x$ and $\cos x \approx 1$. Thus, the classical equations for the tire side slip angles are then given as

$$\alpha_f = -\beta + \delta_f - \frac{l_f \cdot \dot{\psi}}{v}, \quad \alpha_r = -\beta + \frac{l_r \cdot \dot{\psi}}{v}. \tag{2.78}$$

By choosing the system states are the side slip angle of the sprung mass β, the yaw rate $\dot{\psi}$, the roll angle ϕ, the roll rate $\dot{\phi}$, the roll angle of the unsprung mass at the front axle $\phi_{t,f}$ and at the rear axle $\phi_{t,r}$, i.e.,

$$x = \left(\beta \;\; \dot{\psi} \;\; \phi \;\; \dot{\phi} \;\; \phi_{t,f} \;\; \phi_{t,r}\right)^T, \tag{2.79}$$

the differential algebraic model can be transformed into the following state space representation form:

$$E(v)\dot{x} = A_0(v)x + B_0\delta_f + B_1\Delta F_b \tag{2.80}$$

where $E(v)$ is an invertible matrix which also contains masses and inertias.

The system matrices are the following:

$$E(v) = \begin{bmatrix} mv & 0 & 0 & -m_s h & 0 & 0 \\ 0 & I_{zz} & 0 & -I_{xz} & 0 & 0 \\ -m_s vh & -I_{xz} & 0 & I_{xx} + m_s h^2 & -b_{f(r)} & -b_{r(r)} \\ -m_{uf} v(r - h_{uf}) & 0 & 0 & 0 & +b_{f(r)} & 0 \\ -m_{ur} v(r - h_{ur}) & 0 & 0 & 0 & 0 & +b_{r(r)} \\ 0 & 0 & 1 & 0 & 0 & 0 \end{bmatrix},$$

$$A_0(v) = \begin{bmatrix} -(C_f + C_r)\mu & \frac{(-l_f C_f + l_r C_r)\mu}{v} - mv & 0 & 0 & 0 & 0 \\ (-C_f l_f + C_r l_r)\mu & -\frac{(l_f^2 C_f + l_r^2 C_r)\mu}{v} & 0 & 0 & 0 & 0 \\ 0 & m_s vh & m_s gh - k_{f(r)} - k_{r(r)} & -b_{f(r)} - b_{r(r)} & k_{f(r)} & k_{r(r)} \\ -rC_f\mu & m_{uf} v(r - h_{uf}) - \frac{l_f r C_f \mu}{v} & k_{f(r)} & b_{f(r)} & A_{0(4,5)} & 0 \\ -rC_r\mu & m_{ur} v(r + h_{ur}) + \frac{l_r r C_r \mu}{v} & k_{r(r)} & b_{r(r)} & 0 & A_{0(5,6)} \\ 0 & 0 & 0 & 1 & 0 & 0 \end{bmatrix},$$

$$B_{10} = \begin{bmatrix} C_f\mu \\ l_f C_f \mu \\ 0 \\ rC_f\mu \\ 0 \\ 0 \end{bmatrix}, \quad B_{20} = \begin{bmatrix} 0 & 0 & 0 \\ 0 & 0 & l_w \\ 1 & 1 & 0 \\ 1 & 0 & 0 \\ 0 & 1 & 0 \\ 0 & 0 & 0 \end{bmatrix}.$$

using the notations $A_{0(4,5)} = -k_{t,f(r)} - k_{f(r)} + m_{uf} g h_{uf}$ and $A_{0(5,6)} = -k_{t,r(r)} - k_{r(r)} - m_{ur} g h_{ur}$.

By multiplying the left and right-hand sides of this equation by the $E^{-1}(v)$, the state space representation is yielded:

$$\dot{x} = A(v)x + B(v)\delta \tag{2.81}$$

where $\delta^T = \begin{bmatrix} \delta_f & \Delta F_b \end{bmatrix}$. If an active anti-roll bar system is also present, then one can introduce an additional control input $u_c = \begin{bmatrix} u_f & u_r \end{bmatrix}$ for the roll moments between the sprung and unsprung masses generated by the active anti-roll bars, i.e.,

$$\dot{x} = A(v)x + B(v)\delta + B_{rb}(v)u_c. \tag{2.82}$$

For the measured signals one can chose, e.g., the lateral acceleration, the yaw rate and the roll rate

$$y = \begin{bmatrix} a_y & \dot{\psi} & \dot{\phi} \end{bmatrix}^T, \tag{2.83}$$

where the lateral acceleration is $a_y = v\dot{\beta} + v\dot{\psi} - h\ddot{\phi}$.

Table 2.3 Parameters of the yaw–roll model

Params	Value
m_s	12,487 kg
m_{uf}, m_{ur}	706, 1000 kg
m	14,193 kg
h	1.15 m
$h_{uf} h_{ur}$	0.53, 0.53 m
r	0.83 m
C_f, C_r	$582 \cdot 10^3$ kN/rad, $783 \cdot 10^3$ kN/rad
k_f, k_r	$380 \cdot 10^3$ kNm/rad, $684 \cdot 10^3$ kNm/rad
b_f, b_r	$100 \cdot 10^3$ kN/rad, $100 \cdot 10^3$ kN/rad
$k_{t,f}, k_{t,f}$	$2060 \cdot 10^3$ kNm/rad, $3337 \cdot 10^3$ kNm/rad
I_{xx}	24,201 kg m^2
I_{xz}	4200 kg m^2
I_{zz}	34,917 kg m^2
l_f, l_r	1.95, 1.54 m
l_w	0.93 m
μ	1

In the linear yaw–roll models the forward velocity is considered a constant parameter. However, the forward velocity is an important stability parameter, so that it is considered to be a variable of the motion. Thus, the modelling of combined yaw and roll dynamics of road vehicles leads to a nonlinear model, since the Eq. (2.81) the the system matrices depend on the forward velocity of the vehicle and the side force coefficient nonlinearly.

The forward velocity is approximately equivalent to the velocity in the longitudinal direction while the side slip angle β is small. It can be assumed that the side slip angle is small under stable driving conditions. Hence the driving throttle is constant during a lateral manoeuvre and the forward velocity only depends on the brake forces. The forward velocity is assumed to be measured, however, the side force coefficient is usually not directly measured.

If v and μ are selected as scheduling variables, the differential equations of the combined yaw and roll motion are linear in the state variables:

$$\dot{x} = A(\rho)x + B_1(\rho)\delta_f + B_2(\rho)\Delta F_b \tag{2.84}$$

where

$$\begin{aligned} A(\rho) &= A_0 + \rho_1 A_1 + \rho_2 A_2 + \rho_3 A_3 + \rho_4 A_4 + \rho_5 A_5, \\ B_1(\rho) &= B_{10} + \rho_2 B_{11} + \rho_3 B_{12}, \\ B_2(\rho) &= B_{20} + \rho_1 B_{21}. \end{aligned}$$

where $\rho = [\rho_1\ \rho_2\ \rho_3\ \rho_4\ \rho_5]$ with $\rho_1 = \frac{1}{v}$, $\rho_2 = \mu$, $\rho_3 = \mu/v$, $\rho_4 = \mu/v^2$, $\rho_5 = v$.

Possible parameters for a nominal model that corresponds to a heavy-vehicle are included in Table 2.3.

2.6 Grey-Box Identification and Parameter Estimation

LPV models that are obtained by using first principle considerations are full with parameters whose values are not necessarily known a priori. Thus, a method is necessary in order to estimate these unknown parameters of the nominal model. In what follows we consider the (q)LPV systems, as a subclass of the input-affine nonlinear systems, that can be cast as:

$$\begin{aligned} \dot{x} &= A(p, \rho(t))x + B_u(p, \rho(t))u + B_\varphi(p)\varphi(\rho(t)), \\ y &= C(p, \rho(t))x, \end{aligned} \tag{2.85}$$

where p is a parameter vector, $\rho(t)$ is a known vector of time-varying scheduling parameters that eventually depends on measured outputs, i.e., $\rho(t) = \rho(y)$, and φ is a known, possibly nonlinear, function of its arguments.

The objective of our investigations is to compute the unknown parameter p for system (2.85) from input-output measurements, in other words, to solve a grey-box identification problem. A widely used idea to solve such an identification problem is to set a quadratic output error identification criterion, i.e., to minimize the problem as a function of the unknown parameter.

The objective function of this nonlinear least squares problem is usually given by

$$J(p) = \frac{1}{2}\|y - y(p)\|^2, \tag{2.86}$$

where $y(p)$ is the solution of (2.85) corresponding to input u and a suitable initial condition x_0. For practical reasons a norm induced by a discrete scalar product is used, e.g.,

$$\|v\|^2 := \frac{1}{N}\sum_{i=0}^{N-1} |v(t_i)|^2, \tag{2.87}$$

$v(t_i)$ being the samples of the signal v at the time instances t_i. In a practical identification experiment the sampling is uniform, the sampling time being τ, i.e., $t_i = t_0 + (i-1)\tau$. Usually, some additional box constrains

$$p_{i,l} \le p_i \le p_{i,u}, \quad i = 1, \cdots, n_p \tag{2.88}$$

on the parameter range are also available, permitting to set a constrained nonlinear least squares problem.

In a discrete-time setting there are several methods dedicated to the solution of this problem, see, e.g., Bamieh and Giarre (2002), Hori et al. (1992), Lee and Poola (1996, 1999), Ljung (2001), Verdult and Verhaegen (2002). In these approaches the optimization scheme in general is based on a Newton or quasi Newton type iteration process. Other methods, which are often termed as "adaptive" or "recursive", e.g., the Extended Kalman Filter (EKF) method, can be considered mainly as a recursive variant of these types of algorithms, where the main benefit, from an algorithmic point of view, is expected to be the low number of simulations needed. The general convergence properties of these type of methods, even in a theoretical setting, are little known.

In the continuous-time setting one can also apply these type of methods, all of them involving the integration of a system of type (2.85). This integration poses some problems that are new or are more stringent than the difficulties encountered in the discrete-time case.

The first problem is caused by the fact that the initial condition x_0 is often unknown in a practical setting. Besides the general theoretical question of identifiability one has to cope with the problem that in order to evaluate the functional (2.86), one has to integrate the system that contains the parameter p starting from the same initial condition as the original one. In a discrete time setting, at least in the case when sufficiently long data record is available, this problem can be solved by starting the simulation from a shifted initial time and by using the previous data as an initial condition. In order to overcome this difficulty we propose to set a modified identification problem. We propose to design a so called Luenberger type observer first, and then to perform the identification process for the observer system.

The simulation process, i.e., the method that computes $y(p, t_i)$, consists of a numerical algorithm, which performs an implicit discretization of the system. For a certain class of differential equations, i.e., stiff equations, these numerical methods are quite involved, containing implicit schemes with variable step length iterations. A closer analysis of this fact implies one of the inherent difficulties in the continuous-time parameter identification process.

To highlight the problem, note that in order to compute the solution with acceptable accuracy, the integration scheme needs the evaluation of the right hand of the differential equation in an intermediate time instance t, i.e., at $t_i \leq t \leq t_{i+1}$. The problem is, that values $\rho(t)$, $u(t)$ and $y(t)$, are not available during the simulation

process and they have to be replaced somehow, e.g., by interpolation or by a zero order hold strategy. Thus the quantization of the input u and of the scheduling variables ρ results in a modified differential equation. The solution of this equation might differ considerably from that of the original one.

2.6.1 Observer-Based Identification

If the system (2.85) is started from different initial states $\hat{x}_0$, the corresponding solution $\hat{y}$ will differ, in general, from the solution y. Moreover, for a nonlinear system this error is not an additive term with exponentially decay. It follows, that the objective functional will not vanish for the solution of the system determined by the nominal parameter p. Thus the applied optimization algorithms will fail to provide the correct parameter value.

If the initial condition x_0 is unknown, one has to extend the states of the original system with the unknown parameters, and add $\dot{p} = 0$ to the set of state equations. Observability of this extended system guarantees the uniqueness of the solution function corresponding to the pair $(p, x_0(p))$. However, the extended system is usually a full nonlinear system whose observability is hard to be tested in practice. In what follows it is assumed that identifiability under the condition of unknown initial condition holds.

In order to cope with the problem of unknown initial conditions, we propose to design a Luenberger type observer for the system, and then to perform the identification process for the observer system. The form of the observer is the following:

$$\begin{aligned}\dot{\eta} =&(A + KC)(\rho, p)\eta + (B_u + KD)(\rho, p)u + B_\varphi(\rho, p)\varphi - K(\rho, p)y\\ \varepsilon =& - C(\rho, p)\eta + y.\end{aligned} \tag{2.89}$$

By construction, for $p = p_0$ system (2.89) is an observer, i.e., for the nominal value of the parameters one has $\lim_{t\to\infty} \varepsilon(t) = 0$. That means that in practice the objective function (2.86) can be replaced by the function

$$\tilde{J}(p) = \frac{1}{2}\langle \varepsilon, \varepsilon\rangle_o, \quad \langle \varepsilon, \varepsilon\rangle_o := \frac{1}{N-L}\sum_{i=L}^{N-1} |\varepsilon(t_i)|^2, \tag{2.90}$$

with a properly chosen thread L. The choice of the thread depends on the convergence properties (time constants), of the observer, i.e., from the choice of observer gain K.

Concerning the question of stability, let us recall, that an LPV system is said to be quadratically stable if there exist a matrix $P = P^T > 0$ such that

$$A(\rho)^T P + PA(\rho) < 0 \tag{2.91}$$

for all the parameters $\rho \in \mathscr{P}$. A necessary and sufficient condition for a system to be quadratically stable is that the condition in Eq. (2.91) holds for all the corner points of the parameter space, i.e., one can obtain a finite system of LMI's that has to be fulfilled for $A(\rho)$ with a suitable positive definite matrix P, see Gahinet and Apkarian (1996), Fen et al. (1996).

In order to obtain a quadratically stable observer the LMI:

$$(A(\rho) + K(\rho)C)^T P + P(A(\rho) + K(\rho)C) < 0 \tag{2.92}$$

must hold for suitable $K(\rho)$ and $P = P^T > 0$. By introducing the auxiliary variable $G(\rho) = PK(\rho)$, one has to solve the following set of LMIs on the corner points of the parameter space:

$$A(\rho)^T P + PA(\rho) + C^T G(\rho)^T + G(\rho)C < 0 \tag{2.93}$$

By solving these LMIs one can obtain a suitable observer gain for a fixed, but arbitrary value of p.

2.6.2 Adaptive Observer-Based Approach

Adaptive observers are used mainly for fault detection and isolation and adaptive control purposes and they are meant to work on-line. In our identification setting the observer works off-line and it has to converge to acceptable values of the estimated parameters in the time given by the length of the measurements.

Our approach starts from the ideas from the general nonlinear theory, see Besancon (2000). It is assumed the existence of symmetric and positive definite matrix P, a gain matrix $K(t)$, a matrix M and $\mu > 0$ such that

$$PA_o(t) + A_o^T(t)P \leq -\mu I, \quad PB_p = C^T M, \tag{2.94}$$

where $A_o(t) = A(t) + K(t)C$ hold and that the signals φ are persistently exciting.

Then, the adaptive observer used for identification can be defined as:

$$\begin{aligned}\dot{\hat{x}} &= A(t)\hat{x} + B_u(t)u + B_p\varphi(t)\hat{p} + K(t)(y - C\hat{x})\\ \dot{\hat{p}} &= -\gamma\varphi^T(t)M^T(y - C\hat{x}),\end{aligned}$$

where M is assumed to meet conditions (2.94).

In an off-line identification setting the persistency condition

$$\int_t^{t+T} \varphi^T(\tau)B_p^T B_p\varphi(\tau)d\tau \geq \alpha I \tag{2.95}$$

is meant to be fulfilled in a finite time window determined by the measurement length and the value of T. The adaptive observer setting guarantees the exponential convergence rate. Knowing an estimation for this time constant one can determine the required measurement length in order to be able to estimate the parameters with sufficiently accuracy. Therefore an identification experiment is designed by considering these two factors, the persistency requirement and the desired convergence properties.

The performance properties of the observer depends heavily on the choice of the gain $K(t)$ and the parameter γ. By choosing γ properly, one can improve the convergence rate of the parameters. Further research is done in order to give a theoretically justified design procedure for these parameters.

Finding the unknown parameters requires the solution of certain differential equations, for an overview see Polak (1997). Although we embed the system in the class of (q)LPV systems, in general, we cannot exploit the linear structure in the solution process, and we have to use a general differential equation solver. For the observer design of the LTI system the effect of quantization is shown, e.g., in Sur and Paden (1998).

2.7 Parameter Estimation: Case Studies

2.7.1 Identification of a Suspension System

Model based suspension design relies on the knowledge of the physical parameters of the vehicle. For a given vehicle, however, these parameters are usually not known. Moreover the system is nonlinear and contains uncertain and time-varying components. Therefore the usual linear techniques are not suitable to handle this estimation problem. In what follows a nonlinear, quasi LPV (qLPV) model structure is used as a starting point for the identification. It is assumed that the accelerations of the sprung and unsprung masses and the relative displacement can be measured directly. For the complete identification of the model the knowledge of the road signal is indispensable.

Having found the identified model a method is presented for the reconstruction of the road disturbance. Due to the nonlinear nature of the model the unmeasured—but computable—relative velocity signal is also needed.

After the reconstruction of the road roughness signal one has a freedom in the choice of the post-processing method, which can be on-line or off-line and which aims to classify roads by their roughness. In the literature there are many papers with different approaches on the estimation of road roughness. The road surface can be examined as a stochastic process which can be estimated from a white noise source by using an appropriate transfer function Hac (1987), Sayers (1986).

The state space representation of the nonlinear model of a quarter car is written as:

$$\begin{bmatrix}\dot{x}_1\\ \dot{x}_2\\ \dot{x}_3\\ \dot{x}_4\end{bmatrix} = \begin{bmatrix} 0 & 0 & 1 & 0\\ 0 & 0 & 0 & 1\\ -\frac{k_s^l}{m_s} & \frac{k_s^l}{m_s} & \frac{b_s^l}{m_s} & \frac{b_s^l}{m_s}\\ \frac{k_s^l}{m_u} & -\frac{k_s^l}{m_u} - \frac{k_t}{m_u} & \frac{b_s^l}{m_u} & \frac{b_s^l}{m_u}\end{bmatrix}\begin{bmatrix}x_1\\ x_2\\ x_3\\ x_4\end{bmatrix} + \begin{bmatrix} 0 & 0 & 0\\ 0 & 0 & 0\\ \frac{k_s^{nl}}{m_s} & -\frac{b_s^{sym}}{m_s} & \frac{b_s^{nl}}{m_s}\\ -\frac{k_s^{nl}}{m_u} & \frac{b_s^{sym}}{m_u} & -\frac{b_s^{nl}}{m_u}\end{bmatrix}\begin{bmatrix}\rho_k^3\\ |\rho_b|\\ \sqrt{|\rho_b|}\,\mathrm{sgn}(\rho_b)\end{bmatrix} + \begin{bmatrix}0\\0\\0\\ \frac{k_t}{m_u}\end{bmatrix} w \tag{2.96}$$

where $\dot{x}_1 = x_3$ and $\dot{x}_2 = x_4$.

It is assumed that the accelerations $y_1 = \ddot{x}_1$ and $y_2 = \ddot{x}_2$ and the relative displacement $\rho_k = x_2 - x_1$ can be measured directly, and the relative velocity, i.e., $x_4 - x_3$ is then calculated with numerical integration from the measured signals. It is also assumed that the values for m_s and m_u are also known. Thus, in our case the relative velocity and the relative displacement can be selected as scheduling parameters:

$$\rho_b = x_4 - x_3 \quad \rho_k = x_2 - x_1 \tag{2.97}$$

Let us denote the column vector by $\phi(\rho_k, \rho_b)$

$$\phi(\rho_k, \rho_b) = \begin{bmatrix}\rho_k^3 & |\rho_b| & \sqrt{|\rho_b|}\,\mathrm{sgn}(\rho_b)\end{bmatrix}^T. \tag{2.98}$$

If one considers $\phi(\rho_k, \rho_b)$ as a fictitious input, then, the state space representation of the qLPV model is:

$$\dot{x} = \begin{bmatrix} 0 & 0 & 1 & 0\\ 0 & 0 & 0 & 1\\ -p_{11} & p_{11} & -p_{12} & p_{12}\\ p_{21} & -p_{21} - p_t & p_{22} & -p_{22}\end{bmatrix} x + \begin{bmatrix} 0 & 0 & 0\\ 0 & 0 & 0\\ p_{13} & -p_{14} & p_{15}\\ -p_{23} & p_{24} & -p_{25}\end{bmatrix}\phi(\rho_k, \rho_b) + \begin{bmatrix}0\\0\\0\\ p_t\end{bmatrix} w \tag{2.99}$$

where

$$\begin{bmatrix} p_{11} & p_{12} & p_{13} & p_{14} & p_{15}\\ p_{21} & p_{22} & p_{23} & p_{24} & p_{25}\end{bmatrix} = \begin{bmatrix} \frac{k_s^l}{m_s} & \frac{b_s^l}{m_s} & \frac{k_s^{nl}}{m_s} & \frac{b_s^{sym}}{m_s} & \frac{b_s^{nl}}{m_s}\\ \frac{k_s^l}{m_u} & \frac{b_s^l}{m_u} & \frac{k_s^{nl}}{m_u} & \frac{b_s^{sym}}{m_u} & \frac{b_s^{nl}}{m_u}\end{bmatrix} \tag{2.100}$$

$$p_t = \frac{k_t}{m_u} \tag{2.101}$$

Let us use the following formulae: $v(x_2, w) = p_t(x_2 - w)$, $\gamma = m_u/m_s$. From Eq. (2.99) follows, that

$$\gamma y_1 + y_2 = -v(x_2, w), \tag{2.102}$$

where

$$y_1 = p_{11}\rho_k + p_{12}\rho_b + [p_{13} \quad -p_{14} \quad p_{15}]\phi(\rho_k, \rho_b).$$

If one can determine ρ_b then the values of the parameters can be determined from Eq. (2.99) by using a least squares (LS) estimation. The values of ρ_b are estimated by using a second order scheme,

$$\dot{y}(t) = \frac{y(t + \Delta) - y(t)}{\Delta} - \frac{\Delta}{2}\ddot{y}(t),$$

i.e.,

$$\rho_b(t) = \frac{\rho_k(t + \Delta) - \rho_k(t)}{\Delta} - \frac{\Delta}{2}(y_2(t) - y_1(t)), \tag{2.103}$$

where Δ is the sampling time. To determine the value of p_t from Eq. (2.102), the value of the unsprung mass displacement x_2 is needed. Combining (2.99) and (2.102) after a simulation step x_2 can be obtained and then a value for p_t is yielded by carrying out an LS estimation. The signal x_2 can also be determined from the equation

$$\ddot{x}_2 = -p_{21}\rho_k - p_{22}\rho_b + [-p_{23}, p_{24}, -p_{25}]\phi(\rho_k, \rho_b) - \gamma y_1 - y_2, \tag{2.104}$$

by using two consecutive integration steps.

If there are no on board excitations the signal representing the effect of the road surface on the suspension system can be detected by using Eq. (2.102) as:

$$w = \frac{\gamma y_1 + y_2}{p_t} + x_2. \tag{2.105}$$

If the value of p_t for the qLPV model of the quarter car suspension system is known and the unsprung mass displacement x_2 can be determined, then the road signal w can be determined. The value of x_2 is computed by integrating the system (2.104). Due to the effect of the unknown initial value in the reconstructed road signal $\hat{w}$ there is a systematic error present in the form of a linear trend.

In order to classify different roads Hac (1987) has proposed a parameter based method. In this paper a slight modification of this model is used where the road signal is given by the following continuous time model:

$$\dddot{w} + (a_1 + a_3)\ddot{w} + (a_0 + a_1a_3)\dot{w} + a_0a_1w = \xi \tag{2.106}$$

where ξ is a white noise process and parameters a_1, a_2, a_3 depend on the forward velocity and the road type, given as follows:

$$a_0 = (\alpha_2^2 + \beta^2)^2 v^2 + 4\alpha_2^2 \beta^2 v^4, \quad a_1 = \alpha_1 v,$$
$$a_2 = 2(\alpha_2^2 - \beta^2)v^2, \quad a_3 = (a_2 + 2a_0)^{1/2}.$$

For example for a paved road the values of these parameters are defined by $\alpha_1 = 0.5$, $\alpha_2 = 0.2$ and $\beta = 2.0$.

In an identification setting the continuous time modelling is not suitable, hence the road characteristics should be given in terms of the parameters of a discrete time model set:

$$\omega_t + \delta_1 \omega_{t-1} + \delta_2 \omega_{t-2} + \delta_3 \omega_{t-3} = \xi_t \tag{2.107}$$

These parameters also depend on the velocity and the road type. In Fig. 2.12a this dependence is depicted in case of an asphalt road for the parameters δ_1, δ_2 and δ_3, respectively. Figure 2.12b also shows parameter δ_1 in the function of the velocity. Using these type of figures the task of the classification of the road can be performed by estimating coefficients δ_i if the value of the velocity is known.

The approach presented above gives a global characterization of roads by using a basic statistical identification process. In this case the aim of the road parameter estimation is to give a classification of a longer road segment. If local information about road quality is needed other methods should be used, e.g., wavelet based techniques, for details see Gáspár et al. (2003a).

In the first example the accelerations $y_1 = \ddot{x}_1$, $y_2 = \ddot{x}_2$, the relative displacement $\rho_k = x_2 - x_1$ and the road signal w are given from the simulated model described by the nominal parameters:

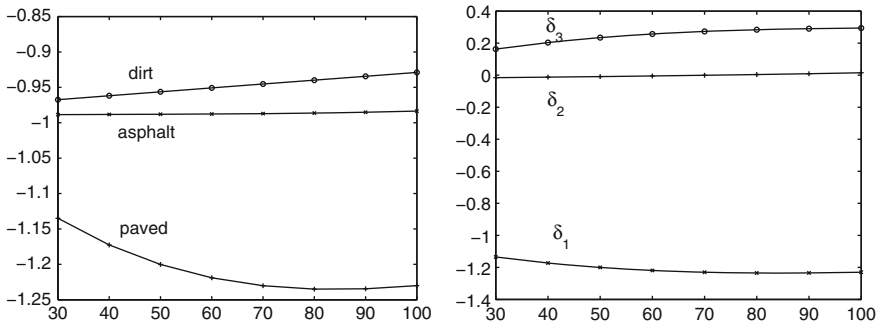

(a) δ_1 (b) paved road

Fig. 2.12 Values of parameters for different road conditions

Table 2.4 Reconstructed values of p

p	57.97	2.41	0.68	0.34	810.34	284.94	11.86	3.38	1.69	3983.1
$p_{0.001}$	57.97	2.41	0.68	0.34	810.65	284.95	11.85	3.38	1.70	3984.6
$r_{0.001}$	0	0	0	0	0.04	0	0.08	0	0.59	0.04
$p_{0.005}$	58.11	2.37	0.69	0.37	797.03	285.62	11.69	3.43	1.82	3917.6
$r_{0.005}$	0.24	1.66	1.47	8.82	1.64	0.24	1.43	1.48	7.69	1.64
$p_{0.01}$	58.39	2.38	0.70	0.36	755.6933	287.02	11.70	3.44	1.79	3714.4
$r_{0.01}$	0.72	1.24	2.94	5.88	6.74	0.73	1.35	1.78	5.92	6.75

Table 2.5 Reconstructed values of p_t

p_t	$p_{t,0.001}$	$p_{t,0.005}$	$p_{t,0.01}$
3220.3	3284.3	3363.1	2723.3
r_t	1.98	4.43	15.43

$$p = \begin{pmatrix} 57.97 & 2.41 & 0.68 & 0.34 & 810.34 \\ 284.94 & 11.86 & 3.38 & 1.69 & 3983.1 \end{pmatrix}.$$

The values for the masses are $m_u = 59$ kg and $m_s = 290$ kg. Different sampling times Δ are used in the simulation. The results of the identification are given in p_Δ and $p_{t,\Delta}$ and are summarized in Table 2.4 and Table 2.5, where r_Δ denotes the relative error.

The relative error of the estimation of $p_1 \ldots p_5$ is below 7 % and the estimation of p_t is below 16 % when the sampling time is selected $\Delta = 0.01$ sec. If we select smaller sampling time ($\Delta = 0.005$ s) the relative error is below 5 %. If the sampling time is $\Delta = 0.001$ s the relative error is below 2 %. The appropriate selection of the sampling time is significant in the sufficient estimation, however, the practice influences this selection.

As far as the road signal reconstruction is concerned the value of the estimate of p_t is decisive. The results show the importance of the choice of the sampling time. An estimation for the sampling time needed can be carried out by the Shannon theorem, which is only applied to the linear part of the model used in the identification process, i.e.,

$$\begin{bmatrix} 0 & 0 & 1 & 0 \\ 0 & 0 & 0 & 1 \\ -p_{11} & p_{11} & -p_{12} & p_{12} \\ p_{21} & -p_{21} & p_{22} & -p_{22} \end{bmatrix}.$$

Figure 2.13 shows the effect of the sampling time on the reconstruction of the unsprung mass displacement x_2, which also plays a central role in the reconstruction of the road signal.

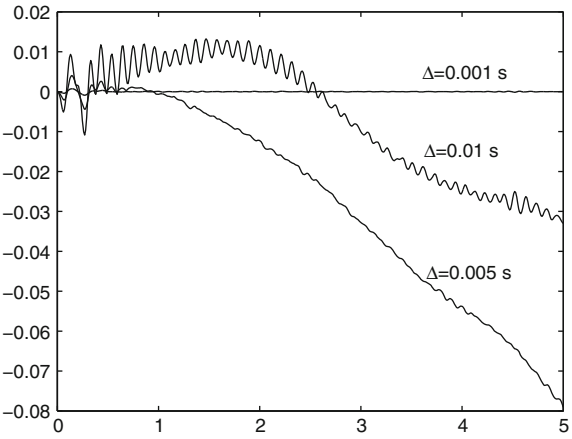

Fig. 2.13 Absolute errors for x_2 corresponding to different sampling times

Table 2.6 Identification results

v	Parameter	δ_1	δ_2	δ_3
40	Nominal	−0.988	−0.007151	0.00213
	Identified	−0.9878	0.007174	0.001743
60	Nominal	−0.9882	−0.006968	0.00618
	Identified	−0.9881	−0.006993	0.005798
80	Nominal	−0.9858	−0.007205	0.008486
	Identified	−0.9878	−0.007242	0.009956

In the second demonstration example three situations, which corresponds to an asphalt road and to different travelling velocities were simulated. The sampling time was set at 0.001 s. After reconstructing the road signal, the parameters δ_i of the discrete model (2.107) were estimated. The results are shown in Table 2.6.

2.7.2 Identification of the Yaw–Roll System

In rollover prevention methods in which the control design is based on the modelling of yaw–roll dynamics, the estimation of the CG is very important. In this section an estimation procedure for the position and height of the center of gravity (CG) is illustrated through a demonstration example. The real problem is that the physical model is of nonlinear continuous-time and the unknown parameter must be estimated by using a grey-box identification method. As a consequence of nonlinearity, the other difficulty is that the selection or estimation of the initial conditions is critical.

Figure 2.11 illustrates the combined yaw–roll dynamics of a vehicle. Recall that the qLPV model can be transformed into a state space representation form

$$\dot{x} = A(v)x + B(v)\delta, \quad x = \begin{bmatrix}\beta & \dot{\psi} & \phi & \dot{\phi} & \phi_{t,f} & \phi_{t,r}\end{bmatrix}^T, \quad \delta^T = \begin{bmatrix}\delta_f & \delta_b\end{bmatrix}$$

with $A(v) = E^{-1}A_0(v)$, $B_v = E^{-1}\begin{bmatrix}B_0 & B_1\end{bmatrix}$, where

$$E(v) = \begin{bmatrix} mv & 0 & 0 & -m_s h & 0 & 0 \\ 0 & I_{zz} & 0 & -I_{xz} & 0 & 0 \\ -m_s vh & -I_{xz} & 0 & I_{xx} + m_s h^2 & -b_f & -b_r \\ m_f v(r - h_f) & 0 & 0 & 0 & -b_f & 0 \\ m_r v(r - h_r) & 0 & 0 & 0 & 0 & -b_r \\ 0 & 0 & 1 & 0 & 0 & 0 \end{bmatrix},$$

$$A_0(v) = \begin{bmatrix} Y_\beta & Y_{\dot{\psi}} - mv & 0 & 0 & 0 & 0 \\ N_\beta & N_{\dot{\psi}} & 0 & 0 & 0 & 0 \\ 0 & m_s hv & a_{33} & -b_f - b_r & k_f & k_r \\ -rY_\beta & rY_f - m_f vh_f & -k_f & -b_f & k_{tf} & 0 \\ -rY_\beta & -rY_r - m_r vh_r & -k_r & -b_r & 0 & k_{tr} \\ 0 & 0 & 0 & 1 & 0 & 0 \end{bmatrix}$$

$$B_0 = \begin{bmatrix}Y_\delta & N_\delta & 0 & rY_\delta & 0 & 0\end{bmatrix}^T,$$

$$B_1 = \begin{bmatrix} -\delta_f & -d_1 - d_2\delta_f & 0 & 0 & 0 & 0 \\ -\delta_f & d_1 - d_2\delta_f & 0 & 0 & 0 & 0 \\ 0 & -\frac{l_w}{2} & 0 & 0 & 0 & 0 \\ 0 & \frac{l_w}{2} & 0 & 0 & 0 & 0 \end{bmatrix}^T.$$

The measured signals are the lateral acceleration, the yaw rate and the roll rate, i.e.,

$$y = \begin{bmatrix}a_y & \dot{\psi} & \dot{\phi}\end{bmatrix}^T, \tag{2.108}$$

where the lateral acceleration is $a_y = v\dot{\beta} + v\dot{\psi} - h\ddot{\phi}$. In the identification context the measuring of the roll rate seems to be obvious, since the parameter CG affects the roll dynamics rather than other dynamics: $y = \dot{\phi}$. The unknown parameters are the sprung mass m_s and the height h of CG. The real values of these parameters used in the simulation are $m_s = 12.48$ and $h = 1.15$.

The system does not depend affinely from the unknown parameters. Therefore it was necessary to manipulate the original system equations in order to obtain systems that might be useful from an identification point of view. Introducing the new variable $\zeta = I_{zz}\dot{\psi} - I_{xz}\dot{\phi}$ and considering the unknown parameter $\nu = 1/(m - m_s)$ one can obtain the system

$$\dot{x}_1 = A_{s,1}(\nu, v)x_1 + B_{s,1}(\nu, v)w \tag{2.109}$$

where $x_1 = \begin{bmatrix}\beta & \zeta\end{bmatrix}^T$ and $w = \begin{bmatrix}\delta_f & \delta_{b,r} & \dot{\psi} & \dot{\phi} & a_y\end{bmatrix}^T$. The matrices in (2.109) are the following:

$$A_{s,1}(v, v) = \begin{bmatrix} v\frac{Y_\beta}{v} & 0 \\ N_\beta & \frac{N_{\dot{\psi}}}{I_{zz}} \end{bmatrix}$$

$$B_{s,1}(v, v) = \begin{bmatrix} v\frac{Y_\delta}{v} & 0 & v\frac{Y_{\dot{\psi}}}{v} - 1 & 0 & -v\frac{m}{v} + \frac{1}{v} \\ N_\delta & -\frac{l_w}{2} & 0 & I_{xz}\frac{N_{\dot{\psi}}}{I_{zz}} & 0 \end{bmatrix}$$

Considering the unknown parameter $\alpha = m_s h$ one can write the equations

$$\dot{x} = A_{s,2}(v)x + B_{s,2}(v)\delta + \alpha B_{a,2}(v)\omega \tag{2.110}$$

where $A_{s,2} = E_2^{-1}A_2$, $B_{s,2} = E_2^{-1}B_s$ and $B_{a,2} = E_2^{-1}B_a$ with

$$E_2(v) = \begin{bmatrix} mv & 0 & 0 & 0 & 0 & 0 \\ 0 & I_{zz} & 0 & -I_{xz} & 0 & 0 \\ 0 & -I_{xz} & 0 & I_{xx} & -b_f & -b_r \\ m_f v(r - h_f) & 0 & 0 & 0 & -b_f & 0 \\ m_r v(r - h_r) & 0 & 0 & 0 & 0 & -b_r \\ 0 & 0 & 1 & 0 & 0 & 0 \end{bmatrix},$$

$$A_2(v) = \begin{bmatrix} Y_\beta & Y_{\dot{\psi}} - mv & 0 & 0 & 0 & 0 \\ N_\beta & N_{\dot{\psi}} & 0 & 0 & 0 & 0 \\ 0 & 0 & -k_f - k_r & -b_f - b_r & k_f & k_r \\ -rY_\beta & rY_f - m_f v h_f & -k_f & -b_f & k_{tf} & 0 \\ -rY_\beta & -rY_r - m_r v h_r & -k_r & -b_r & 0 & k_{tr} \\ 0 & 0 & 0 & 1 & 0 & 0 \end{bmatrix}$$

$$B_a = \begin{bmatrix} 0 & 0 & g & 0 & 0 & 0 \\ 1 & 0 & 0 & 0 & 0 & 0 \\ 0 & 0 & 1 & 0 & 0 & 0 \end{bmatrix}^T, \quad B_s = \begin{bmatrix} B_0 & B_1 \end{bmatrix}^T,$$

and $\omega = \begin{bmatrix}\phi & \ddot{\phi} & a_y\end{bmatrix}^T$.

Thus we obtain two qLPV systems that depend affinely on the unknown parameters, however, the expressions that corresponds to φ in (2.85) also contain unmeasured signals. It is difficult and yet unsolved problem to construct an adaptive observer in this general case. Therefore an estimation for the unmeasured signals β, ϕ and $\ddot{\phi}$ is needed. The signal ϕ is obtained by integrating the measured signal $\dot{\phi}$. The unknown integration constant $\phi(0)$ is introduced as an additional parameter that must be determined. For simplicity in our simulation example this value is set to zero.

The signal β is estimated from the equation

$$\dot{\zeta} = \frac{N_{\dot{\psi}}}{I_{zz}}\zeta + N_\beta\beta + \begin{bmatrix} N_\delta & -\frac{l_w}{2} & 0 & I_{xz}\frac{N_{\dot{\psi}}}{I_{zz}} & 0 \end{bmatrix} w, \tag{2.111}$$

where $\dot{\zeta}$ is estimated from ζ from a finite difference scheme. The signal $\ddot{\phi}$ is also estimated from $\dot{\phi}$ with another finite difference scheme.

The accuracy of the estimation of β is improved by using an unknown input estimation algorithm starting from (2.111):

$$\dot{\hat{\zeta}} = \frac{N_{\dot{\psi}}}{I_{zz}}\hat{\zeta} + N_\beta\hat{\beta} + \left[N_\delta \; -\tfrac{l_w}{2} \; 0 \; I_{xz}\tfrac{N_{\dot{\psi}}}{I_{zz}} \; 0\right]w - k(\hat{\zeta} - \zeta), \tag{2.112}$$

$$\hat{\beta} = \beta_0 - \delta(\hat{\zeta} - \zeta), \tag{2.113}$$

where β_0 is our initial estimate, for details. In our example the values $\delta = 500$ and $k = 700$ are used.

In order to fulfil the condition about persistent excitedness, the identification method is based on signals collected during in a cornering manoeuvre. The cornering manoeuvre starts at 1 s The steering angle applied in the simulation is a ramp signal. It reaches the maximum value in 0.5 s and filtered at 4 rad/s to represent the finite bandwidth of the driver. In the simulation experiment the forward velocity of the heavy vehicle varies between 40 and 65 km h due to a braking force. Two sampling times are applied, i.e., $T_{s1} = 0.01$ s, and $T_{s2} = 0.001$ s. The input and measured output signals are depicted in Fig. 2.14. The results of the identification are summarized in Table 2.7.

Figure 2.15 shows the convergence of the estimated parameters in our experiment for the given sampling times. As it is expected the convergence is smoother and quicker when the sampling time is smaller. However in practical applications the highest value of the sampling time, i.e., $T_s = 0.01$ s is used and the results show that this value is still acceptable in order to maintain a required accuracy of the estimated parameters.

In what follows we will use the notations of Sect. 2.5.3 and those of Fig. 2.11. Recall that the model equations can be expressed in a state space representation by considering the state vector:

$$x = \left[\beta \; \dot{\psi} \; \phi \; \dot{\phi} \; \phi_{t,f} \; \phi_{t,r}\right]^T \tag{2.114}$$

as

$$\dot{x} = A(\rho)x + B(\rho)u, \tag{2.115}$$

with

$$A(\rho) = A_0 + \rho_1 A_1 + \rho_2 A_2 + \rho_3 A_3, \quad B(\rho) = B_0 + \rho_1 B_1 + \rho_2 B_2 + \rho_4 B_4,$$

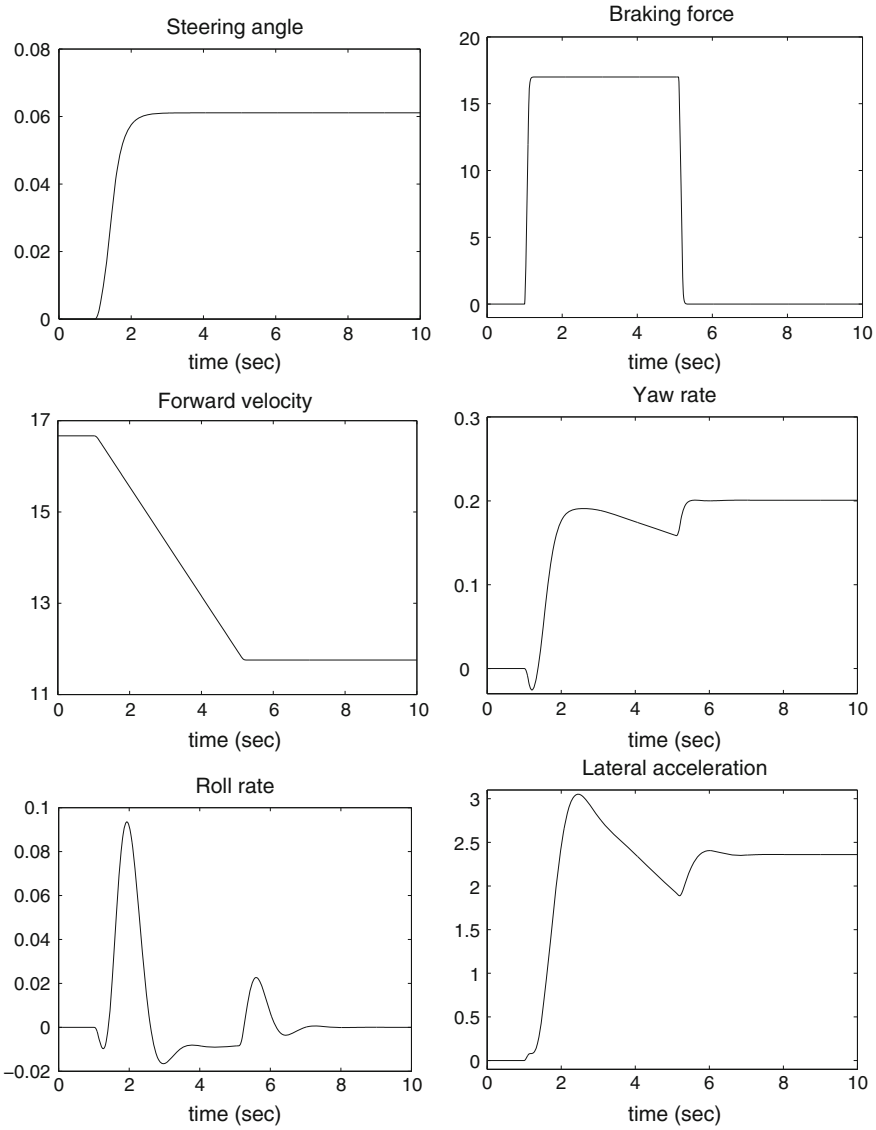

Fig. 2.14 Signals in the simulation example

where the components of the scheduling vector ρ are

$$\rho_1 = \mu, \quad \rho_2 = \frac{\mu}{v}, \quad \rho_3 = \frac{\mu}{v^2}, \quad \rho_4 = \frac{1}{v}.$$

Table 2.7 Results of the identification

T_s	$\hat{\alpha}$	$\hat{\nu}$	$\hat{m}_s$	$\hat{h}$
0.01	0.5807	14.3601	12.4709	1.1515
0.001	0.5822	14.3601	12.4754	1.1511

The real values: $m_s = 12.487$ and $h = 1.15$

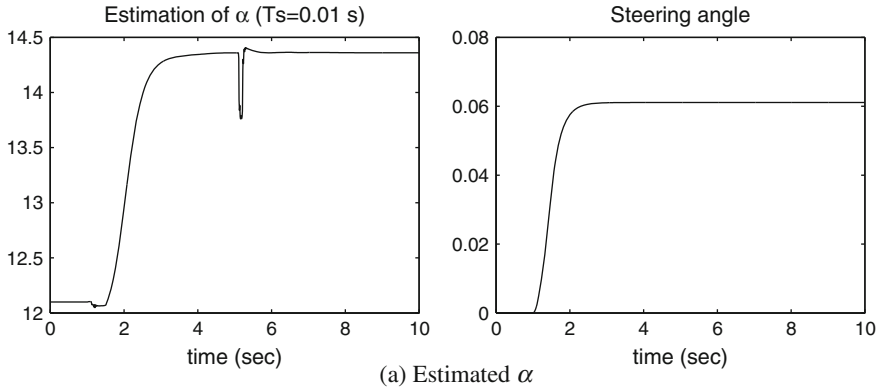

(a) Estimated α

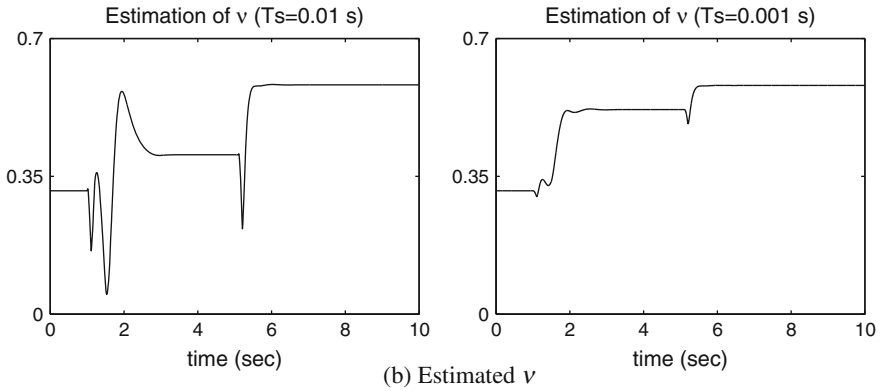

(b) Estimated ν

Fig. 2.15 Estimated parameters

The components of the state matrices are the following:

$$A_0 = \begin{bmatrix} 0 & -1 \\ 0 & 0 \end{bmatrix}, \qquad A_1 = \begin{bmatrix} 0 & 0 \\ \frac{(C_f+C_r)I_{xz}}{(m_s-m)hI_{zz}} & \frac{C_r l_r^2 - C_f l_f^2}{I_{zz}} \end{bmatrix},$$

$$A_2 = \begin{bmatrix} \frac{C_f+C_r}{m_s-m} & 0 \\ \frac{C_r l_r - C_f l_f}{I_{zz}} & \frac{(C_r l_r - C_f l_f)I_{xz}}{(m-m_s)hI_{zz}} \end{bmatrix}, \quad A_3 = \begin{bmatrix} 0 & \frac{C_r l_r - C_f l_f}{m-m_s} \\ 0 & 0 \end{bmatrix},$$

$$B_0 = \begin{bmatrix} 0 & 0 & 0 \\ \frac{m_s I_{xz}}{(m_s - m)h I_{zz}} & 0 & \frac{l_w}{I_{zz}} \end{bmatrix}, \qquad B_1 = \begin{bmatrix} 0 & 0 & 0 \\ 0 & \frac{C_f}{(m-m_s)h} & \frac{I_{xz}}{I_{zz}} + \frac{C_f l_f}{I_{zz}} & 0 \end{bmatrix},$$

$$B_2 = \begin{bmatrix} 0 & \frac{C_f}{m-m_s} & 0 \\ 0 & 0 & 0 \end{bmatrix}, \qquad B_4 = \begin{bmatrix} \frac{m}{m-m_s} & 0 & 0 \\ 0 & 0 & 0 \end{bmatrix}.$$

The measured signals are the lateral acceleration $a_y = v\dot{\beta} + v\dot{\psi} - h\ddot{\phi}$, the roll rate and the yaw rate while the control input signals are the steering angle and the difference in the brake forces. Later the lateral acceleration is also selected as a fictitious input. It is also assumed that the forward velocity is available.

The estimation of the unknown parameters in the model is based on the equations of the lateral and the yaw dynamics of the vehicle, see Eqs. (2.68) and (2.69). Since β and $\dot{\beta}$ are unknown and not measured, a direct estimation algorithm cannot be applied. Thus, it is necessary to manipulate the original system equations in order to obtain systems that might be useful from an estimation point of view.

Observe first, that the lateral acceleration is a measured signal, which has direct relation to $\dot{\beta}$. By eliminating both β and $\dot{\beta}$ we get

$$a_1\ddot{\phi} + a_2\ddot{\psi} = \mu(a_3\dot{\psi} + a_4\delta_f) + (a_5 a_y + a_6 \Delta F_b), \tag{2.116}$$

where

$$\begin{aligned} a_1 &= (m - m_s)h(l_r C_r - l_f C_f) - I_{xz}(C_f + C_r), \\ a_2 &= I_{zz}(C_f + C_r), \\ a_3 &= -\frac{1}{v} C_f C_r l^2, \\ a_4 &= C_f C_r l, \\ a_5 &= -m(l_r C_r - l_f C_f) \\ a_6 &= l_w(C_f + C_r). \end{aligned}$$

Equation (2.116) is transformed in the following form:

$$\dot{v} = \mu u_1 + u_2, \tag{2.117}$$

where

$$\begin{aligned} v &= a_1\dot{\phi} + a_2\dot{\psi}, \\ u_1 &= a_3\dot{\psi} + a_4\delta_f, \\ u_2 &= a_5 a_y + a_6 \Delta F_b. \end{aligned}$$

Assuming that the signals $\dot{\psi}$, $\dot{\phi}$, a_y, δ_f, ΔF_b, v are measured or calculated, the values of v, u_1, u_2 can be computed. Since the values $\dot{v}$ are not available, the least

squares (LS) method cannot be applied directly in this problem. Next, a possible method is proposed for the estimation of the parameter μ from the Eq. (2.117) where v, u_1, and u_2 are known.

Both sides of (2.117) are multiplied by $e^{\alpha t}$ and then an partial integration is performed. Using the partial integral form $v(t)$ can be expressed in the following way:

$$\begin{aligned} v(t) =& e^{-\alpha t} v(0) + \alpha e^{-\alpha t} \int_0^t e^{\alpha \tau} v(\tau) d\tau + \\ &+ \mu e^{-\alpha t} \int_0^t e^{\alpha \tau} u_1(\tau) d\tau + e^{-\alpha t} \int_0^t e^{\alpha \tau} u_2(\tau) d\tau. \end{aligned} \tag{2.118}$$

It is known that the solution of the system

$$\dot{w}(t) = -\alpha w(t) + v(t) \tag{2.119}$$

is $w(t) = e^{-\alpha t} w(0) + e^{-\alpha t} \int_0^t e^{\alpha \tau} v(\tau) d\tau$. Selecting $w = 0$ the filtered output of the system (2.119) is $v^f(t) = e^{-\alpha t} \int_0^t e^{\alpha \tau} v(\tau) d\tau$. Then the following relation is formulated:

$$\mu u_1^f(t) = v(t) - e^{-\alpha t} v(0) - \alpha v^f(t) - u_2^f(t), \tag{2.120}$$

where v^f, u_1^f, u_2^f are the filtered outputs of the systems with inputs v, u_1, u_2, respectively. Based on Eq. (2.120) one can construct different practical algorithms for the estimation of μ. Note that the choice $\alpha = 0$ corresponds to the case of the simple integration.

The equation, which is the basis of the identification, is the following:

$$\ddot{\psi} = \alpha_1 \ddot{\phi} + \alpha_2 u_f + \alpha_3 a_y + \alpha_4 \Delta F_b, \tag{2.121}$$

where the fictitious signal is $u_f = \delta_f - \frac{l}{v} \dot{\psi}$ and $\alpha_1 = -\frac{a_1}{a_2}$, $\alpha_2 = \mu \frac{a_4}{a_2}$, $\alpha_3 = \frac{a_5}{a_2}$, $\alpha_4 = \frac{a_6}{a_2}$.

Note, that the model which is applied both for the parameter estimation and the control design does not contain the adhesion coefficient, however it contains the multiplication of the tire side slip constant and the adhesion coefficient, $\tilde{C}_f = \mu C_f$ and $\tilde{C}_r = \mu C_r$. Thus, instead of the adhesion coefficient, this multiplication will be estimated. Applying an identification method to (2.121), the coefficients α_i are estimated. These coefficients are related to the unknown parameters I_{zz}, I_{xz}, $\tilde{C}_f$ and $\tilde{C}_r$, thus they can be expressed from the estimated values:

$$I_{zz} = \frac{l_w}{\hat{\alpha}_4}, \tag{2.122}$$

$$I_{xz} = I_{zz}\left(\hat{\alpha}_1 - \frac{m - m_s}{m} h\hat{\alpha}_3\right), \tag{2.123}$$

$$\tilde{C}_f = \frac{I_{zz}\hat{\alpha}_2 m}{l_f m + I_{zz}\hat{\alpha}_3}, \tag{2.124}$$

$$\tilde{C}_r = \frac{I_{zz}\hat{\alpha}_2 m}{l_r m - \hat{\alpha}_3 I_{zz}}. \tag{2.125}$$

In what follows, for the sake of simplicity, it is assumed that the value for I_{xx} is known. Based on the method outlined in this section it is possible to estimate its value, too.

The model used in the estimation of the side slip angle contains the adhesion coefficient, which is a time varying signal. These signals cannot be estimated simultaneously since the observer-based method assumes that the parameters in the LPV model are known and the scheduling variables are available in the estimation of the side slip angle. Thus, a three-step estimation procedure which is illustrated in Fig. 2.16 might be needed. In the initialization step the unknown parameters are estimated from Eqs. (2.122) and (2.124). In practice it is usually enough to calculate them only when the vehicle has started and already covered a certain distance. The estimated values of the adhesion coefficient is the initialization of the adaptive algorithm $\tilde{C}_{f0}$ and $\tilde{C}_{r0}$. The other parameters, i.e., the inertias can be considered constant in a long time period. Thus, the model initialization is rarely performed, e.g., after a maintenance or periodically depending on the distance traveled.

In the second step an adaptive identification method is carried out for the estimation of the changes of the adhesion coefficient in $\tilde{C}_f$ and $\tilde{C}_r$ by an adaptive observer scheme designed using (2.117). The procedure requires the vehicle to perform a manoeuvre, e.g., there must be a nonzero steering angle or a nonzero yaw rate so that the signal u_1 is not identically zero. In the third step an adaptive observer-based method is carried out for the estimation of the side slip angle. The method also gives an estimation of the roll angles of the unsprung masses, which are important in the monitoring of the pitching dynamics.

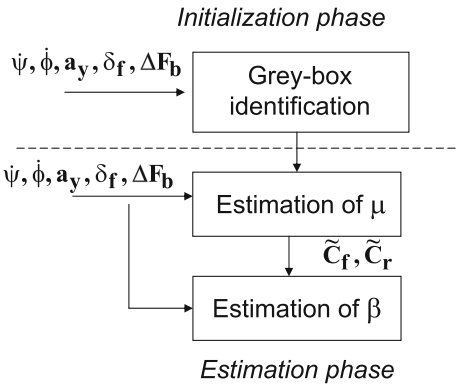

Fig. 2.16 The three-step estimation procedure

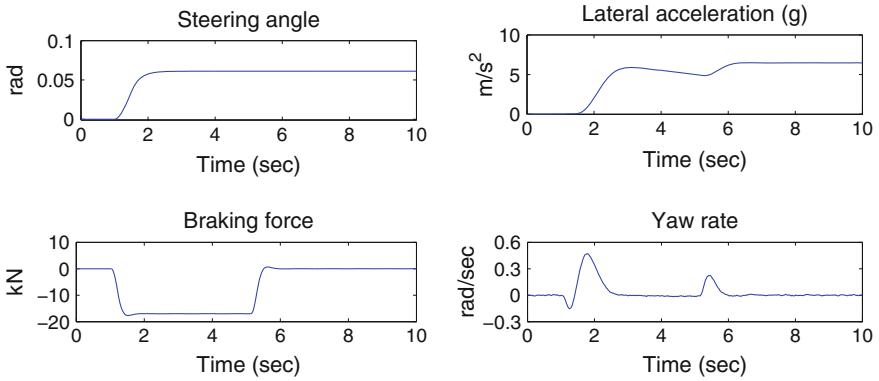

Fig. 2.17 Input and output signals in the identification step

Table 2.8 Result of the identification

Value	α_1	α_2	α_3	α_4
Actual	0.1174	26.6950	−0.0211	0.0266
Estimated	0.1116	26.6090	−0.0210	0.0266
Relative error	0.0491	0.0032	0.0048	0.0020
Value	I_{zz}	I_{xz}	μC_f	μC_r
Actual	34.9170	4.2	465.6	626.4
Estimated	34.9867	4.0062	465.0597	625.5661
Relative error	0.0020	0.0461	0.0012	0.0013

In what follows the three-step procedure is demonstrated through a simulation example. The preliminary estimation of the unknown parameters in the vehicle model is carried out in a vehicle manoeuvre in which the vehicle has started and already covered a certain distance. It is assumed that the manoeuvre has a short duration and the adhesion coefficient is constant. Using the measured signals the unknown parameters of the vehicle model are estimated. Obviously, when the model parameters are known, this step need not be performed.

Figure 2.17 presents the input and output signals of the simulation procedure, i.e., the steering angle, the lateral acceleration, the yaw rate and the difference between the brake forces. In the simulation example noise signals are added to the measured signals, which cause 2–3 % relative error. In the identification method it is assumed that the difference between the brake forces is available. Using the LS method four parameters are identified according to Eqs. (2.122) and (2.124) then the physical parameters are calculated. Table 2.8 shows the estimated values with their relative errors. In practice the difference between the brake forces is not always available. It is assumed, however, that if the brake forces are generated in a symmetrical way ΔF_b is approximately zero. In this case one of the estimated parameters must be known, e.g., the parameter I_{zz}.

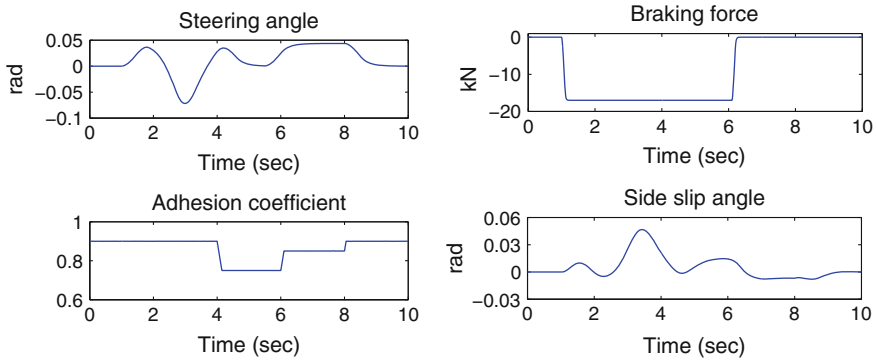

Fig. 2.18 Input and output signals in the estimation algorithm

Then the estimation of the side slip angle and the adhesion coefficient are carried out. The signals in the simulation procedure are illustrated in Fig. 2.18. The measured signals are the steering angle, the yaw rate, the roll rate, the difference in the braking forces and the lateral acceleration. In Fig. 2.18 the side slip angle and the adhesion coefficient are also illustrated. These signals, however, are used for validation purposes, and they are assumed not to be available in the identification procedure. The identification procedure is performed in an on-line way, i.e., the identification of both the adhesion coefficient and the side slip angle is performed during the vehicle manoeuvres.

Then two identification steps are carried out: first, the adaptive method using a partial integration method for the adhesion coefficient, second, the adaptive observer-based method for the side slip angle. The result of the estimation of the side force coefficient approximates the vary of the real side force coefficient below an acceptable limit. In order to filter out the noises from the estimated signal a filtering procedure is also performed, which is illustrated together with its relative error in Fig. 2.19a. The result of the estimation of the side slip angle is illustrated in Fig. 2.19b. The estimation of the side force coefficient tends to the actual side force coefficient within a predefined acceptable limit.

2.7.3 Fault Estimation in LPV Systems

Any reconfiguration scheme rely on a suitable FDI component. There are a lot of approaches to design a detection filter, see, e.g., Chen and Patton (1999). The LPV setting, however, narrows the available tools.

In contrast to the LTI case in the LPV framework stability cannot be guaranteed in algebraic terms, e.g., by requiring that the "frozen" LTI systems are stable. Besides the technical difficulties of the potential design process this fact implies that algebraic methods of the classical LTI FDI filter design, see, e.g., Gertler (1998), Varga (2008), are not suitable for the LPV setting. In the LPV framework the only practical solution

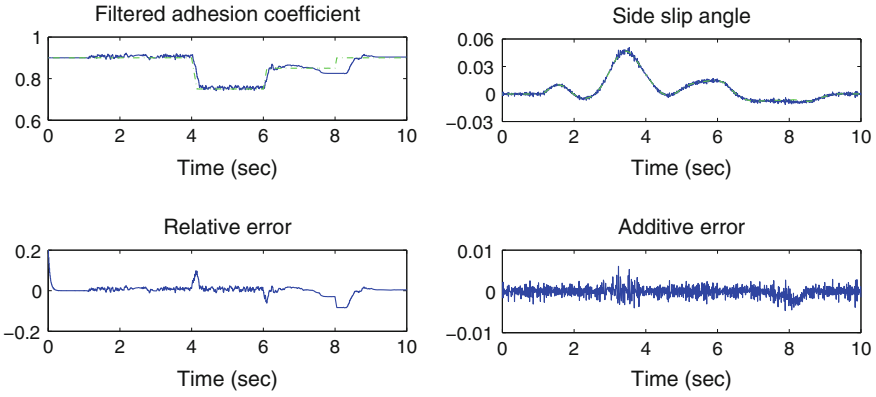

(a) side force coefficient (b) side slip angle

Fig. 2.19 Estimated signals through simulation

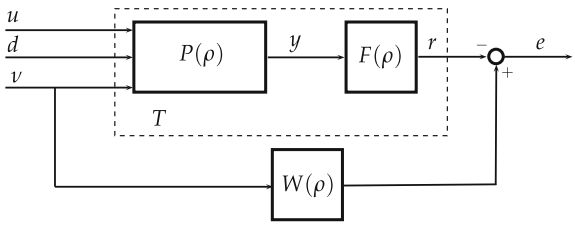

Fig. 2.20 Norm based detector design problem

is to require quadratic stability which can be cast as a set of LMI feasibility problems. The so called geometric approach of the FDI meets these requirements and often leads to successful detection filter design, for details see Balas et al. (2003), Bokor and Balas (2004), Edelmayer et al. (2004).

As a high level approach, the FDI filter design problem often can be cast in the model matching framework depicted on Fig. 2.20. The LPV paradigm permits to cast a nonlinear system as a linear time-varying (LTV) one, i.e., the residual can be expressed as

$$r = T_{ru}u + T_{rd}d + T_{rv}v. \tag{2.126}$$

Hence, to achieve robustness in the presence of disturbances and uncertainty, multi objective optimization-based FDI schemes can be proposed where an appropriately selected performance index has to be chosen to enhance sensitivity to the faults and simultaneously attenuate disturbances: the robust disturbance rejection condition is formulated as

$$\|T_{rd}\|_\infty = \sup_{\|v\|_2=1, \rho\in\mathscr{P}} \|r\|_2, \tag{2.127}$$

is to be minimized.

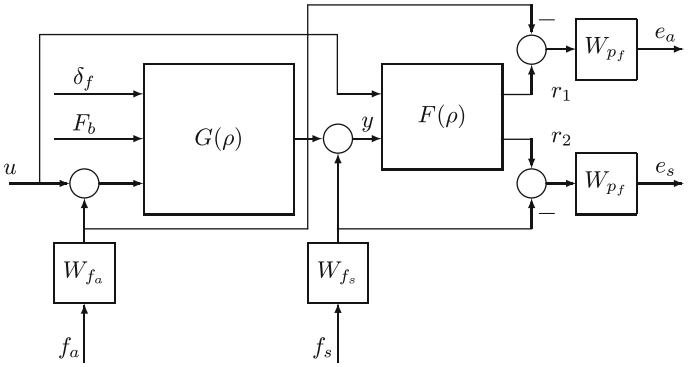

Fig. 2.21 Open loop interconnection structure for FDI filter design

This is a usual worst-case filtering problem and the corresponding design criteria can be formulated as a convex optimization problem by using LMIs. The main problem here is that the sensitivity and robustness conditions are conflicting. In the LTI framework it means that both sensitivity to faults and insensitivity to unknown inputs cannot be achieved at the same frequencies. Faults having similar frequency characteristics as those of disturbances might go undetected. While the design problem is non-convex, in general, Henry and Zolghadri (2004) proposes a scheme that can handle the problem by using LMI techniques.

A specific structure that fits the norm based approach, containing the weighted open-loop system, which includes the yaw–roll model $G(\rho)$ and the parameter-dependent FDI filter $F(\rho)$, and elements associated with performance objectives is depicted on Fig. 2.21. In the diagram, u is the control input, δ_f and F_b represent the disturbance signals, while y is the measured output. The FDI filter takes the measured outputs and the control inputs, thus, the effect of the control input is attenuated on residual outputs. In the figure, f_a is the actuator fault and f_s is the sensor fault. The e_a and e_s represents the weighted fault estimation errors associated with failures.

The weight W_{p_f} is the fault detection performance weight, which reflects the relative importance of the different frequency domains. The weighting function W_{p_f} chosen for fault estimation errors can be considered as penalty function, i.e., the weight should be large in the frequency range in which small errors are desired and small in which larger errors can be tolerated. The size of the frequency response of weight W_{p_f} should be large at low frequency to achieve the integral action for fault estimation. The weight W_{f_a} represents the size of possible fault in the actuator channel. The weight W_{f_s} takes sensor failure into consideration in the FDI filter design.

The augmented plant of the filtering problem has $w = \begin{bmatrix}\delta_f & F_b & f_a & f_s & u\end{bmatrix}^T$ as the disturbance input and $e = \begin{bmatrix}e_a & e_s\end{bmatrix}^T$ the performance output which are used to evaluate the estimation quality. The design requirement for $\mathscr{H}_\infty$ residual generation is to maximize the effect of the fault on the residual and simultaneously minimize the

effect of exogenous signals (δ_f, F_b, u) on the residual. Further details on the design can be found in Grenaille et al. (2008).

For illustrative purposes let us consider an FDI design for a suspension system, where possible faults of the actuators (loss of effectiveness) can be detected by reconstructing the actual suspension forces. Having measured the signals $y_1 = \dot{x}_3$, $y_2 = \dot{x}_4$ and $y_3 = x_2 - x_1$ an inversion based detection filter is designed.

Recall that the state space representation of the quarter-car model can be formalized with the state vector $x = \left[x_1\ x_2\ x_3\ x_4\right]^T$, where x_1 and x_2 denote the vertical displacement of the sprung mass and the unsprung mass, respectively, and x_3, x_4 denote their derivatives.

$$\dot{x}_3 = \frac{1}{m_s}(r_k(x_2 - x_1) + r_b(x_4 - x_3) + b_s^{nl}\rho_b\sqrt{\rho_b(x_4 - x_3)} - F), \tag{2.128}$$

$$\dot{x}_4 = \frac{1}{m_u}(-r_k(x_2 - x_1) - r_b(x_4 - x_3) - k_t(x_2 - d) - \\ - b_s^{nl}\rho_b\sqrt{\rho_b(x_4 - x_3)} + F), \tag{2.129}$$

where $r_b = b_s^l - b_s^{sym}\rho_b$ and $r_k = k_s^l + k_s^{nl}\rho_k$, while the chosen scheduling variables are $\rho_b = sgn(x_4 - x_3)$ and $\rho_k = (x_2 - x_1)^2$, respectively.

In the construction of the filter the first step is to express F from (2.128) and in these expression we plug in the known values y_i:

$$F = |z| + b_s^{nl}\rho_b\sqrt{|z|} + r_k y_3 - m_s y_1. \tag{2.130}$$

In this expression the value of the relative velocity z is not measured. The road disturbance is an unknown input signal but from the Eqs. (2.128) and (2.129) one has

$$m_s\dot{x}_3 + m_u\dot{x}_4 = -k_t(x_2 - d). \tag{2.131}$$

By plugging back the obtained expressions in the original equations one has the system $\dot{x}_3 = \frac{r_k}{m_s}(x_2 - x_1) - \frac{r_k}{m_s}y_3 + y_1$ and $\dot{x}_4 = -\frac{r_k}{m_u}(x_2 - x_1) + \frac{r_k}{m_u}y_3 + y_2$, where the relative velocity is not measured. The resulting LPV system

$$\dot{z} = -r_k m_e z + r_k m_e y_3 + y_2 - y_1, \tag{2.132}$$

with $m_e = \frac{m_u + m_s}{m_u m_s}$ will be observable.

For a semi-active actuator one can compare the value of the reconstructed force with the nominal value of the damper force given for the specific value of the damper velocity by the characteristics. If these two values differ considerably, a fault event must be signaled. For active actuators however, since the real actuators might present a saturation effect, it is necessary to check in addition, if the actual forces are lower then those corresponding to the saturation level of the actuators, i.e., it is not enough to compare the reconstructed forces with the force demands provided by the robust LPV controllers.

To obtain the final fault detection filter the equations of the actuator dynamics are used as:

$$\dot{\tilde{x}}_5 = -\beta\tilde{x}_5 + \alpha A_P\hat{z} + \gamma Q_{0,nom}(\hat{F})\tilde{x}_6, \tag{2.133}$$

$$\dot{\tilde{x}}_6 = -\frac{1}{\tau_{nom}}\tilde{x}_6 + \frac{1}{\tau_{nom}}u_a, \tag{2.134}$$

where $\hat{z}$ and $\hat{F}$ are the estimated damper velocity and damper force values, respectively. A possible actuator fault affects the terms Q_0 through a modified value of P_s and the time constant τ, respectively. The nominal values of these parameters (i.e., for the fault free case) are denoted by the subscript nom.

For the fault free case one should have $e_5 = x_5 - \tilde{x}_5 \approx 0$ and $e_6 = x_6 - \tilde{x}_6 \approx 0$, respectively. If $e = \|e_5\|_2 + \|e_6\|_2$ is greater than a given threshold, then a fault must be present in the system and a fault signal is emitted to the higher level controller, used in the controller reconfiguration process. Since the initial conditions are not known, an (LPV) observer need to be constructed for (2.132) and (2.133), (2.134) respectively. For a LPV system that depends affinely on the scheduling variables an LPV observer can be designed using LMI techniques: let us recall that an LPV system is said to be quadratically stable if there exist a matrix $P = P^T > 0$ such that $A(\rho)^T P + PA(\rho) < 0$ for all the parameters ρ. A necessary and sufficient condition for a system to be quadratically stable is that this condition holds for all the corner points of the parameter space, i.e., one can obtain a finite system of linear matrix inequalities (LMIs) that have to be fulfilled for $A(\rho)$ with a suitable positive definite matrix P.

In order to obtain a quadratically stable observer the LMI

$$A_o^T(\rho)P + PA_o(\rho) < 0 \tag{2.135}$$

must hold for suitable $K(\rho)$ and $P = P^T > 0$, with $A_o = A + KC$. By introducing the auxiliary variable $L(\rho) = PK(\rho)$, one has to solve the following set of LMIs on the corner points of the parameter space:

$$A(\rho)^T P + PA(\rho) - C^T L(\rho)^T - L(\rho)C < 0. \tag{2.136}$$

By solving these LMIs a suitable observer gain is obtained:

$$K(\rho) = P^{-1}L(\rho). \tag{2.137}$$

In the simulation example result the reconstructed force is illustrated by the solid blue line in the upper part of Fig. 2.22.

The force is compared with the force produced by a fault free suspension system (dashed line). The FDI filter gives the signals depicted in blue in the bottom part of Fig. 2.22, while the red signal is the chosen threshold level expressed in a given

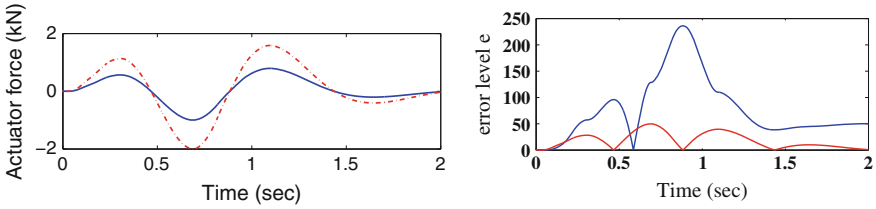

Fig. 2.22 The result of the FDI procedure

percent of the desired force. Since the obtained error level will be greater than this threshold, a fault signal is emitted indicating a faulty actuator.

The threshold level influences the fault-detection delay, i.e., high threshold level corresponds to increased delay. However, due to disturbances, sensor noises and the modeling uncertainties this level cannot be arbitrarily small and it is determined using engineering knowledge.

Chapter 3
Robust Control of LPV Systems

Introduction

LPV control synthesis is a controller design approach based on either LPV or LPV LFT which yields parameter-dependent controllers with a priori guaranteed stability and performance properties. The available real-time information of the parameter variation is used in the control synthesis method. Thus, in contrast to classical gain-scheduling methods the time-varying nature of the corresponding LPV dynamics is incorporated in the LPV control structure. The a priori stability and performance guarantees eliminate the need for validation of stability and performance characteristics afterwards by means of extensive simulations.

One of the main advantages of LPV control synthesis is that there exists a solid theoretical foundation guaranteeing a priori stability and performance for all parameters from a corresponding range and rate of variation. Moreover the corresponding controller design is global with respect to the parameterized operating envelope while, as opposed to the gain-scheduling approaches, the controller is synthesized directly, rather than its construction from a family of local linear controllers. While LPV control synthesis focuses on an linear model rather than a nonlinear model of the plant, but the resulting controller is a nonlinear one. Since LPV synthesis employs the induced $\mathscr{L}_2$-norm as a performance measure, the control synthesis is directly related to linear $\mathscr{H}_\infty$-techniques. As a disadvantage, the controller synthesis is much more involved and, generally, conservatism has to be introduced to arrive at a feasible and convex problem.

3.1 The Modeling of Performances

Control systems are designed to maintain the system outputs at a desired value. The outputs are linear combinations of the plant states and inputs that are important in terms of system performance. A number of factors influence the ability of the control system to maintain the desired output, e.g., initial conditions or external

P. Gáspár et al., *Robust Control Design for Active Driver Assistance Systems*,
Advances in Industrial Control, DOI 10.1007/978-3-319-46126-7_3

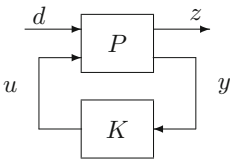

Fig. 3.1 The general *P-K* structure for control design

disturbance inputs. Quantitative performance criteria are required to evaluate control systems and to compare the merits of competing control system designs. The criteria can include closed-loop system parameters, the response of the closed-loop system subject to specific test conditions or the gain of the closed-loop system. The closed-loop interconnection structure, which includes the feedback structure of the model P and controller K, is shown in Fig. 3.1. In the diagram, d, u, y, and z are the disturbance, the control input, the measured output, and the performance output, respectively.

The main performance demands can be formulated easily. The sensitivity function $S = (I + PK)^{-1}$ must be small so that system disturbances and model errors have little influence on the output. The complementary sensitivity function $T = PK(I + PK)^{-1}$ must be small so that measurement noises have little influence on the output. However, there are several limitations and conflicts in the specifications. Example, both S and T cannot be small at the same frequency. Some of the performance limitations are: limitation of control effort, non-minimum phase plant, sensitivity versus complementary sensitivity. Weighting functions can be added to select frequency bounds of interest and the select times of interest. Input weighting functions are typically selected equal to the amplitude spectrum of disturbance inputs. Output weighting functions are typically selected equal to the inverse of the specifications on the outputs.

A standard weighting strategy is illustrated in Fig. 3.2. In the diagram u is the control input, y is the measured output, z_p is the performance output, z_u, and z_y are performances at the input and the output, w is the disturbance, n is the measurement noise. The aim of the weighting function W_p is to define the performance specifications. They can be considered as penalty functions, i.e., weights should be large in a frequency range where small signals are desired and small where large performance outputs can be tolerated. W_u and W_y may be used to reflect some restrictions on the actuator and on the output signals. The purpose of the weighting functions

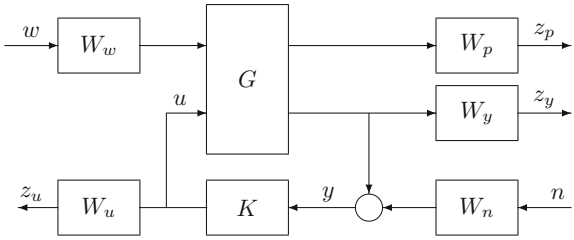

Fig. 3.2 The standard feedback configuration with weights

W_w and W_n is to reflect the disturbance and sensor noises. The disturbance and the performances in the general P-K structure are $d = \begin{bmatrix} w & n \end{bmatrix}^T$ and $z = \begin{bmatrix} z_u & z_y & z_p \end{bmatrix}^T$.

Next, the mixed sensitivity problem is formalized. The open-loop system P is given as

$$\left[\begin{array}{c} z \\ \hline y \end{array}\right] = \left[\begin{array}{c|c} P_{11} & P_{12} \\ \hline P_{21} & P_{22} \end{array}\right] \left[\begin{array}{c} d \\ \hline u \end{array}\right] \tag{3.1}$$

Using the feedback relation between u and y, i.e., $(u = -Ky)$, the closed-loop relationship taken from d to z can be derived as

$$T_{zd} = P_{11} - P_{12}(I + KP_{22})^{-1}KP_{21} \tag{3.2}$$

Using the weighting functions the transfer function T_{zd} can be obtained in the following form:

$$\left[\begin{array}{c} z_p \\ z_u \\ \hline y \end{array}\right] = \left[\begin{array}{c|c} 0 & W_pG \\ 0 & W_u \\ \hline I & G \end{array}\right] \left[\begin{array}{c} d \\ \hline u \end{array}\right] \tag{3.3}$$

Using Eq. (3.2) T_{zd} is as follows:

$$T_{zd} = \left\| \begin{bmatrix} W_pT \\ \upsilon W_uKS \end{bmatrix} \right\|_2 \tag{3.4}$$

Using (3.4) the $\mathscr{H}_2$ and $\mathscr{H}_\infty$ performances are formulated. The $\mathscr{H}_2$ criterion minimizes the expected energy of the performance z_p due to the disturbance d and the energy of the control signal z_u

$$\|z_p\|_2^2 + \upsilon^2\|z_u\|_2^2 = \left\| \begin{bmatrix} W_pT \\ \upsilon W_uKS \end{bmatrix} \right\|_2 \tag{3.5}$$

with the appropriate choice of weighting functions and scalar υ. The purpose of the first term is to make penalty functions for the performances, and the purpose of the second term is to avoid the saturation of the actuators. The parameter υ defines the trade-off between performance outputs and control effort. Using the $\mathscr{H}_2$ criterion the effect of disturbances on the performances is minimized, i.e., it solves the disturbance rejection problem. The main limitation of the $\mathscr{H}_2$ performance is the lack of the formal treatment of uncertainties of the plant.

The $\mathscr{H}_\infty$ criterion is to find a stabilizing controller that minimizes $\|T_{zd}\|_\infty$, i.e., minimizes the $\sup_{\|d\|_2 \le 1} \|z_p\|_2$ subject to some restrictions on the control energy $\sup_{\|d\|_2 \le 1} \|z_u\|_2$. The mixed criterion with a parameter υ is the following:

$$\sup_{\|d\|_2 \le 1} \{\|z_p\|_2^2 + \upsilon^2 \|z_u\|_2^2\} = \left\| \begin{bmatrix} W_p T \\ \upsilon W_u K S \end{bmatrix} \right\|_\infty . \tag{3.6}$$

If there is a bound on the $\mathscr{H}_\infty$ norm such that $\|T_{zd}\|_\infty < \gamma$ thens

$$\left\| \begin{bmatrix} W_p T \\ \upsilon W_u K S \end{bmatrix} \right\|_\infty < \gamma, \tag{3.7}$$

with a positive γ.

Hence the frequency-dependent weights W_p and W_u can be chosen to give bounds on the terms T and KS required to achieve the high and low frequency gains. In fact W_u must be a low pass filter while W_p needs to be a high pass filter. After selecting weighting functions to bound T and KS, the plant is augmented with these weights. The controller synthesis is carried out on this augmented plant while the $\mathscr{H}_\infty$ norm is minimized. The smaller γ is indicating a more robust design.

One of the main advantages of the $\mathscr{H}_\infty$ performance is that it guarantees maximum robustness against destabilizing uncertainties. In general, a slightly suboptimal $\mathscr{H}_\infty$ controller is preferred to an optimal one.

The mixed $\mathscr{H}_2/\mathscr{H}_\infty$ control synthesis treats the $\mathscr{H}_2$ and the $\mathscr{H}_\infty$ problems in a unified state space framework. This method provides a compensator that combines the $\mathscr{H}_2$ quadratic performance criterion for disturbance rejection with the $\mathscr{H}_\infty$ performance criterion for maximum robustness against destabilizing uncertainties.

The freedom of choice of suboptimal $\mathscr{H}_\infty$ controllers can be used to minimize the $\mathscr{H}_2$ performance index. Thus, the controller which minimizes the $\mathscr{H}_2$ performance index is selected from the suitable suboptimal $\mathscr{H}_\infty$ controllers. The performance $z_{p\infty}$ is associated with the $\mathscr{H}_\infty$ constraint, and the performance z_{p2} is associated with the $\mathscr{H}_2$ criterion.

A standard weighting strategy, which includes the feedback structure of the model G and controller K, is illustrated in Fig. 3.3. The weighting function W_{p2} is applied to the performance z_{p2} and $W_{p\infty}$ is applied to the performance $z_{p\infty}$. The disturbance and the performances in the general P-K structure in Fig. 3.1 are $d = \begin{bmatrix} w & n \end{bmatrix}^T$ and $z = \begin{bmatrix} z_{p2} & z_{p\infty} & z_y & z_u \end{bmatrix}^T$.

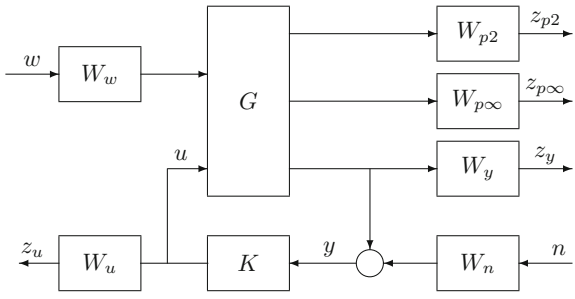

Fig. 3.3 The feedback configuration with mixed performances and weights

3.2 The Modeling of Uncertain Components

Usually, two types of uncertainty structure are applied in the control design, i.e., unstructured and structured uncertainties. An unstructured uncertainty is modeled by connecting an unknown but bounded perturbation to the plant. This type of uncertainty structure requires little information, i.e., only the bound and the type of connection. The perturbation is a bounded transfer function, where the bound is defined in terms of the system ∞-norm. An unstructured perturbation can be connected to the plant in numerous ways, e.g., in additive, output multiplicative, input multiplicative, coprime factor uncertainty way, etc.

The control design is based on the closed-loop interconnection structure, which is illustrated in Fig. 3.4. In this structure uncertainties of the unmodelled dynamics are represented by a block Δ_m and a weighting function W_r. It is assumed that the transfer function W_r is known, and it reflects the uncertainty in the model. The transfer function Δ_m is assumed to be stable and unknown with the norm condition, $\|\Delta_m\|_\infty < 1$. W_p, W_w, and W_n are weighting functions for performance specifications, disturbances, and sensor noises, respectively.

Stability robustness can be evaluated when the perturbations in the models are bounded: $\bar{\sigma}(\Delta(j\omega)) \leq \Delta_{max}(j\omega)$, where $\bar{\sigma}$ is the maximum singular value and Δ can be any of the perturbations. The bound given for the perturbation is in general frequency-dependent allowing the specification of plant uncertainties to vary over frequency. For example, in practice the plant model is accurate at low frequencies but less accurate at high frequencies. The standard form of the unstructured uncertainty structure is shown in Fig. 3.5. The small gain theorem provides a test for robust stability with respect to bounded perturbations.

Theorem 3.1 (Small gain theorem) *Suppose M_Δ general feedback system is a real rational subspace of $\mathscr{H}_\infty$ and $\gamma > 0$. Then M_Δ is well-posed and internally stable for all possible perturbations in $\mathscr{H}_\infty$, where the perturbation is bounded $\|\Delta\|_\infty \leq 1/\gamma$ if and only if*

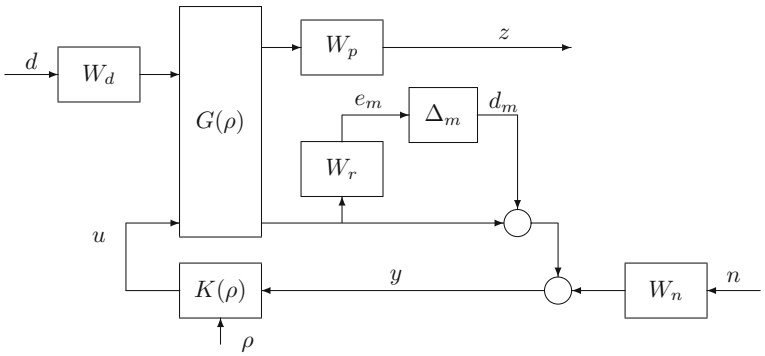

Fig. 3.4 The standard feedback configuration with performances and uncertainties

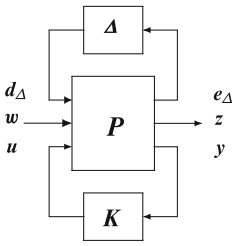

Fig. 3.5 The general *P-K-Δ* structure for control design

$$\|M_\Delta(s)\|_\infty < \gamma. \tag{3.8}$$

See Zhou et al. (1996).

The small gain theorem implies that the smaller the ∞-norm of the stable transfer matrix $M_\Delta(s)$, the larger the ∞-norm of the smallest stable perturbation Δ that destabilizes the interconnected system (M, Δ). If the system model is described by a set of additive perturbations (i.e., $G = G_{nom} + W_{r2}\Delta W_{r1}$), the closed-loop system is robustly stable for all $\|\Delta\|_\infty \leq 1/\gamma$ if $\|W_{r2}KSW_{r1}\|_\infty < \gamma$. If the system model is described by a set of output multiplicative perturbations (i.e., $G = (I + W_{r2}\Delta W_{r1})G_{nom}$), the closed-loop system is robustly stable if $\|W_{r2}TW_{r1}\|_\infty < \gamma$. These results can all be derived by the use of the small gain theorem.

3.3 Control Design Based on LPV Methods

In the LPV control design framework the basic setting is the following: it is assumed that the state space representations of the plant is:

$$\dot{x} = A(\rho)x + B_1(\rho)w + B_2(\rho)u, \tag{3.9}$$
$$z = C_1(\rho)x + D_{11}(\rho)w + D_{12}(\rho)u, \tag{3.10}$$
$$y = C_2(\rho)x + D_{21}(\rho)w, \tag{3.11}$$

while the controller is searched as

$$\dot{x}_c = A_c(\rho)x_c + B_c(\rho)y \tag{3.12}$$
$$u = C_c(\rho)x_c + D_c(\rho)y. \tag{3.13}$$

In the $\mathscr{L}_2$ LPV controller synthesis the objective is to find an LPV controller such that the $\mathscr{L}_2$ gain of the closed-loop system is minimized. This corresponds to the robust $\mathscr{H}_\infty$ control formulation known from the LTI framework.

The LPV system is regarded as a linear differential inclusion (LDI), and the relation between the state, or output, and the parameter is ignored in the LPV controller synthesis step. Thus, even the scheduling variable is known in operational time, in

the analysis/design stage basically it behaves as a mere uncertainty. Its knowledge at the implementation phase is exploited as a linearizing condition in the design: in contrast to the uncertain case, the full order LPV design can be cast as a convex problem.

In the basic setting, the gain in the LPV case is interpreted in terms of all possible trajectories allowed by the parameters within the set $\rho \in \Omega$ (usually bounding box conditions). This approach corresponds to the choice of a single Lyapunov function (SLF), in which the variation of the scheduling variables can be arbitrarily fast.

In later applications a parameter-dependent Lyapunov functions (PDLF) are applied. The motivation reason for that is that when the bandwidth of the actuators or the signals are disregarded it leads to an infinite rate bound on ρ in an impractical way. If the rate bound on ρ is assumed a less conservative result for the class of systems is yielded. Moreover, several examples show that a LPV system cannot be stabilized by applying any controller if the system is defined in an SLF way.

The tool used in the LPV synthesis is the robust extension to the bounded real lemma, see, e.g., Fen et al. (1996). In this formulation also the parameter derivative $\dot{\rho}$ enters in the consideration. Hence, it is necessary to have information about the rate of change of the parameter, i.e., the parameter derivative must be bounded by $\dot{\rho} \in \bar{\Omega}$.

3.3.1 Formulation of a Nonlinear Controller

When a LPV controller has been designed, the relation between the state, or output, and the parameter $\rho = \rho(x)$ is used in the LPV controller, such that finally a nonlinear controller is obtained and implemented

$$\dot{x}_c = A_c(\rho(x))x_c + B_c(\rho(x))y \tag{3.14}$$

$$u = C_c(\rho(x))x_c + D_c(\rho(x))y \tag{3.15}$$

Observe that it is an important assumption that $\rho(x)$ is measured or depends only on measured signals. According to the properties of the modeling assumptions the LPV system is equal to, or at least approximates well, the nonlinear model for all parameter and parameter derivative values in the bounding boxes, i.e., $\rho \in \Omega$ and $\dot{\rho} \in \bar{\Omega}$. In contrast to the gain-scheduling approach the LPV control framework guarantees to meet closed-loop system specifications in the validity domain even under transients.

Intuitively this indicates that the closed-loop LPV specifications also hold for the nonlinear closed-loop system with the nonlinear controller and the nonlinear model. Due to the underlying robustness paradigm, however, the design is conservative, in general. This is caused by the fact that Ω, and $\bar{\Omega}$, respectively, is much larger than the set spanned by the actual parameter trajectories.

3.3.2 Control Design Based on SLF Methods

Starting from a constant Lyapunov function the formulation of the analysis conditions for stability and $\mathscr{L}_2$ performance are rather straightforward based on the Lyapunov and dissipativity theory.

Concerning the question of stability, let us recall, that an LPV system is said to be quadratically stable if there exist a matrix $X = X^T > 0$ such that

$$A(\rho)^T X + X A(\rho) < 0 \tag{3.16}$$

for all the parameters $\rho \in \mathscr{P}$. Based on this concept an adaptation of the bounded real lemma leads to: if there is a matrix $X = X^T > 0$ such that

$$\begin{bmatrix} A(\rho)^T X + X A(\rho) & X B(\rho) & C^T(\rho) \\ B^T(\rho) X & -\gamma I & D^T(\rho) \\ C^T(\rho) & D(\rho) & -\gamma I \end{bmatrix} < 0, \quad \rho \in \mathscr{P} \tag{3.17}$$

is satisfied, then the $\mathscr{L}_2$ gain of the system described by

$$\begin{aligned} \dot{x} &= A(\rho)x + B(\rho)w \\ z &= C(\rho)x + D(\rho)w \end{aligned}$$

is less than γ, i.e., for zero initial conditions $x(0) = 0$ it guaranteed that

$$\sup_{\rho \in \mathscr{P}} \sup_{\|w\|_2 \neq 0, w \in \mathscr{L}_2} \frac{\|z\|_2}{\|w\|_2} < \gamma < \infty. \tag{3.18}$$

3.3.3 Polytopic Approach

Let us consider an LPV plant $S(\rho)$ given in a polytopic form, i.e.,

$$S(\rho) = \sum_{i=1}^{p} \rho_i S_i, \quad \rho_i \geq 0, \quad \sum_{i=1}^{p} \rho_i = 1. \tag{3.19}$$

with

$$S \sim \begin{pmatrix} A & B \\ C & D \end{pmatrix}, \quad \text{and vertex systems} \quad S_i \sim \begin{pmatrix} A_i & B_i \\ C_i & D_i \end{pmatrix}.$$

Let us suppose that a controller $K(\rho)$ of the form

$$\begin{bmatrix} A_K(\rho) & B_K(\rho) \\ C_K(\rho) & D_K(\rho) \end{bmatrix} = \sum_{i=1}^{p} \rho_i \begin{bmatrix} A_{Ki} & B_{Ki} \\ C_{Ki} & D_{Ki} \end{bmatrix},$$

is designed that leads to the closed-loop system

$$\begin{aligned} \dot{x} &= A_{cl}(\rho)x + B_{cl}(\rho)w, \\ z &= C_{cl}(\rho)x + D_{cl}(\rho)w. \end{aligned}$$

Considering a polytopic LPV model a necessary and sufficient condition for a system to be quadratically stable is that the condition in Eq. (3.16) holds for all the corner points of the parameter space, i.e., one can obtain a finite system of LMI's that has to be fulfilled for $A(\rho)$ with a suitable positive definite matrix P, see Gahinet and Apkarian (1996), Fen et al. (1996).

We apply this idea for a state feedback design first. In order to obtain a quadratically stable state feedback the LMI

$$(A(\rho) + B(\rho)K(\rho))^T X + X(A(\rho) + B(\rho)K(\rho)) < 0, \tag{3.20}$$

or equivalently

$$Y(A(\rho) + B(\rho)K(\rho))^T + (A(\rho) + B(\rho)K(\rho))Y < 0, \tag{3.21}$$

must hold for suitable $K(\rho)$ and $X = Y^{-1} > 0$. By introducing the auxiliary variable $M(\rho) = K(\rho)Y$, one has to solve the following set of LMIs on the corner points of the parameter space:

$$YA^T(\rho) + A(\rho)Y + M^T(\rho)B^T(\rho) + B(\rho)M(\rho) < 0 \tag{3.22}$$

If B is parameter independent, than one has the following design conditions for the vertex points of the parameter space:

$$YA_i^T + A_iY + M_i^T B^T + BM_i < 0, \quad i = 1, \ldots, p. \tag{3.23}$$

By solving these LMIs one can obtain a suitable observer gain for a fixed, but arbitrary value of p. The controller is given by

$$K(\rho) = \sum_{i=1}^{p} \rho_i M_i Y^{-1}.$$

Observe that if B is not parameter independent, then condition (3.22) is not linear in ρ. Thus, in order to linearize it, one need a reparametrization, which, in general, introduces a certain amount of conservativeness in the design.

Concerning the performance problem with dynamic output feedback, the starting point is the polytopic reformulation of the Bounded Real Lemma, i.e.,

Theorem 3.2 (Polytopic Bounded Real Lemma) *Suppose that there is a matrix* $X_{cl} = X_{cl}^T > 0$ *such that on each vertex the LMI*

$$\begin{bmatrix} A_{cl}(\rho_i)^T X_{cl} + X_{cl} A_{cl}(\rho_i) & X_{cl} B_{cl}(\rho_i) & C_{cl}^T(\rho_i) \\ B_{cl}^T(\rho_i) X_{cl} & -\gamma I & D_{cl}^T(\rho_i) \\ C_{cl}^T(\rho_i) & D_{cl}(\rho_i) & -\gamma I \end{bmatrix} < 0, \quad i = 1, \ldots, p \tag{3.24}$$

is satisfied.

Then the quadratic Lyapunov function $V(x_{cl}) = x_{cl}^T X_{cl} x_{cl}$ *guarantees the stability of the closed-loop system. Moreover, the performance level set by* γ*, i.e.,* $\|z\|_2 < \gamma \|w\|_2$*, holds.*

As in the state feedback case, in order to directly obtain a finite set of LMIs it is needed to assume that the matrices B_2, C_2, D_{12}, and D_{21} are constant, i.e., parameter independent, see the notations of (3.9)–(3.11). If this condition holds, then the controller can be designed based on the following result, see Apkarian and Gahinet (1995):

Theorem 3.3 (Polytopic $\mathscr{H}_\infty$ conditions) *Let us denote by* N_X *and* N_Y *the orthonormal bases of the null spaces* (B_2^T, D_{12}^T) *and* $(C_2, D_{21},)$*, respectively. The polytopic* $\mathscr{H}_\infty$ *control problem is solvable if and only if there exist pairs of symmetric matrices* X, Y *satisfying the following system of LMIs in each of the vertex points* $i = 1, \ldots, p$

$$N_X^T \begin{bmatrix} A_i X + X A_i^T & X C_{1i}^T & B_{1i} \\ C_{1i} X & -\gamma I & D_{11i} \\ B_{1i}^T & D_{11i}^T & -\gamma I \end{bmatrix} N_X < 0, \tag{3.25}$$

$$N_Y^T \begin{bmatrix} A_i^T Y + Y A_i & Y B_{1i} & C_{1i}^T \\ B_{1i}^T Y & -\gamma I & D_{11i}^T \\ C_{1i} & D_{11i} & -\gamma I \end{bmatrix} N_Y < 0, \tag{3.26}$$

$$\begin{bmatrix} X & I \\ I & Y \end{bmatrix} < 0. \tag{3.27}$$

Moreover, the problem is solvable with a k-th order LPV controller if and only if

$$\operatorname{rank}(I - XY) \leq k.$$

The controller can be synthesized using standard $\mathscr{H}_\infty$ techniques, see, e.g., Apkarian and Gahinet (1995) and Scherer and Weiland (2000).

3.3.4 An LFT-Based Design

An LPV system P mapping exogenous input d and control input u to controlled output z and measured output y are given. The state space representation of the plant P is the following:

$$\dot{x} = Ax + B_1 d + B_2 u, \tag{3.28}$$
$$z = C_1 x + D_{12} u, \tag{3.29}$$
$$y = C_2 x + D_{21} d. \tag{3.30}$$

The assumptions of the control design are the same as it was in the classical $\mathscr{H}_\infty$ control design. The problem is to find an LPV control structure K such that the closed-loop system is internally stable for all parameter trajectories with $\gamma^2 \Theta^T \Theta \leq 1$ and the induced $\mathscr{L}_2$-norm of the operator $T(P, K, \Theta)$, see in Eq. (2.36), satisfies

$$\max_{\|\Theta\|_\infty \leq 1/\gamma} \|T(P, K, \Theta)\|_\infty < \gamma \tag{3.31}$$

where γ is a prescribed performance level. The LPV problem can be interpreted as a robust performance problem for the nominal linear time invariant (LTI) plant P_a in the face of the norm-bounded uncertainty $\Delta \oplus \Delta$.

The structure of the uncertainty is the following: $\Delta = \text{diag}(\rho_1 I_{r1}, \ldots, \rho_k I_{rk})$, where $r_i > 1$ whenever the parameter θ_i is repeated. Consider the set of positive definite similarity scalings associated with Δ:

$$L_\Delta = \{L > 0 : L\Theta = \Theta L, \forall \Theta \in \Delta\}. \tag{3.32}$$

Given L_Δ the set of scalings commuting with the repeated structure $\Delta \oplus \Delta$ is readily deduced as

$$L_{\Delta\oplus\Delta} = \left\{ \begin{bmatrix} L_1 & L_2 \\ L_2^T & L_3 \end{bmatrix} > 0 : L_1, L_3 \in L_\Delta, L_2\Theta = \Theta L_2, \forall \Theta \in \Delta \right\}. \tag{3.33}$$

From small gain theory, a sufficient condition for robust performance in the face of the uncertainty $\Delta \oplus \Delta$, or equivalently for the existence of gain-scheduled controllers is as follows:

Theorem 3.4 (γ-suboptimal LPV $\mathscr{H}_\infty$ controller) *Consider an uncertainty structure Δ and the associated set of similarity scalings $L_{\Delta\oplus\Delta}$ defined in (3.33). If there exists a scaling matrix $L \in L_{\Delta\oplus\Delta}$ and an LTI control structure K such that the nominal closed-loop system $F_\ell(P_a, K)$ is internally stable and satisfies the following inequality:*

$$\left\| \begin{bmatrix} L^{1/2} & 0 \\ 0 & I \end{bmatrix} F_\ell(P_a, K) \begin{bmatrix} L^{-1/2} & 0 \\ 0 & I \end{bmatrix} \right\|_\infty < \gamma, \tag{3.34}$$

then $F_\ell(K, \Theta)$ is a γ-suboptimal gain-scheduled $\mathscr{H}_\infty$ controller. See Apkarian and Gahinet (1995).

The LMI approach applied for gain-scheduled $\mathscr{H}_\infty$ controller is based on the Scaled Bounded Real Lemma, which is formalized in the following:

Theorem 3.5 (Scaled Bounded Real Lemma) *Consider a parameter structure Δ, the associated scaling set L_Δ defined in (3.32) and closed-loop system. The following statements are equivalent.*

- *A is stable and there exists $L \in L_\Delta$ such that*

$$\left\| L^{1/2}(D + C(sI - A)^{-1}B)L^{-1/2} \right\|_\infty < \gamma \tag{3.35}$$

- *There exist positive definite solutions P and $L \in L_\Delta$ to the matrix inequality*

$$\begin{bmatrix} A^T P + PA & PB & C^T \\ B^T P & -\gamma L & D^T \\ C & D & -\gamma L^{-1} \end{bmatrix} < 0. \tag{3.36}$$

See Apkarian and Gahinet (1995).

Using Theorem 3.4 the solution of the scaled $\mathscr{H}_\infty$ controller problem is presented. In the next theorem, the scaled $\mathscr{H}_\infty$ problem is considered as LTI plants with arbitrary uncertainty structures Δ. The general statement of scaled $\mathscr{H}_\infty$ problems is as follows. Given are $\gamma > 0$, an uncertainty structure Δ and the associated scaling set L_Δ. Find $L \in L_\Delta$ and an LTI controller K such that the closed-loop system is internally stable and

$$\left\| L^{1/2} F_\ell(G, K) L^{-1/2} \right\|_\infty < \gamma. \tag{3.37}$$

Theorem 3.6 *Consider a plant G with uncertainty structures Δ and an associated scaling set L_Δ. Let N_X and N_Y denote orthonormal bases of the null spaces $(B_2^T, D_{12}^T, 0)$ and $(C_2, D_{21}, 0)$, respectively. The suboptimal scaled $\mathscr{H}_\infty$ problem is solvable, if and only if there exist pairs of symmetric matrices $X, Y \in \mathscr{R}^{n\times n}$ and $L, J \in \mathscr{R}^{r\times r}$ with $L \in L_\Delta$, $J \in J_\Delta$ satisfying the following system of LMIs:*

$$N_X^T \begin{bmatrix} AX + XA^T & XC_1^T & B_1 \\ C_1 X & -\gamma J & 0 \\ B_1^T & 0 & -\gamma L \end{bmatrix} N_X < 0, \tag{3.38}$$

$$N_Y^T \begin{bmatrix} A^T Y + YA & YB_1 & C_1^T \\ B_1^T Y & -\gamma L & 0 \\ C_1 & 0 & -\gamma J \end{bmatrix} N_Y < 0, \tag{3.39}$$

$$\begin{bmatrix} X & I \\ I & Y \end{bmatrix} \geq 0, \tag{3.40}$$

$$LJ = I. \tag{3.41}$$

See Apkarian and Gahinet (1995).

Inequalities (3.38)–(3.40) are LMIs in R, S, L, J and the structure constraints $L \in L_\Delta$ and $J \in J_\Delta$ are convex constraints. However, constraint (3.41) is strongly nonconvex and thus its numerical tractability is unclear. Fortunately, in the gain-scheduled $\mathscr{H}_\infty$ control problem the nonconvex constraint $LJ = I$ disappears. As a result, a sufficient condition can be obtained that is pure LMI and is therefore tractable. The theorem, which is used in the gain-scheduled control design, is the following.

Theorem 3.7 (Solution of the scaled $\mathscr{H}_\infty$ controller problem) *Consider an LPV plant given by the LFT interconnection structure in which P is a proper LTI plant and Θ is the parameter operator. Let Δ denotes the structure set associated with Θ and L_Δ denote the corresponding set of scaling matrices. Let N_X and N_Y denote orthonormal bases of the null spaces $(B_2^T, D_{\theta 2}^T, D_{12}^T, 0)$, and $(C_2, D_{2\theta}, D_{21}, 0)$, respectively. The gain-scheduled $\mathscr{H}_\infty$ control problem is solvable if and only if there exist pairs of symmetric matrices $X, Y \in \mathscr{R}^{n\times n}$ and $L, J \in \mathscr{R}^{r\times r}$ with $L \in L_\Delta$, $J \in J_\Delta$ satisfying the following system of LMIs:*

$$N_X^T \begin{bmatrix} AX + XA^T & \begin{bmatrix} XC_\theta & XC_1 \end{bmatrix} & \begin{bmatrix} B_\theta & B_1 \end{bmatrix} \\ \begin{bmatrix} C_\theta X \\ C_1 X \end{bmatrix} & -\gamma \begin{bmatrix} J & 0 \\ 0 & I \end{bmatrix} & \begin{bmatrix} 0 & 0 \\ 0 & 0 \end{bmatrix} \\ \begin{bmatrix} B_\theta \\ B_1 \end{bmatrix} & \begin{bmatrix} 0 & 0 \\ 0 & 0 \end{bmatrix} & -\gamma \begin{bmatrix} L & 0 \\ 0 & I \end{bmatrix} \end{bmatrix} N_X < 0, \tag{3.42}$$

$$N_Y^T \begin{bmatrix} A^T Y + YA & \begin{bmatrix} YB_\theta & YB_1 \end{bmatrix} & \begin{bmatrix} C_\theta & C_1 \end{bmatrix} \\ \begin{bmatrix} B_\theta Y \\ B_1 Y \end{bmatrix} & -\gamma \begin{bmatrix} L & 0 \\ 0 & I \end{bmatrix} & \begin{bmatrix} 0 & 0 \\ 0 & 0 \end{bmatrix} \\ \begin{bmatrix} C_\theta \\ C_1 \end{bmatrix} & \begin{bmatrix} 0 & 0 \\ 0 & 0 \end{bmatrix} & -\gamma \begin{bmatrix} J & 0 \\ 0 & I \end{bmatrix} \end{bmatrix} N_Y < 0, \tag{3.43}$$

$$\begin{bmatrix} X & I \\ I & Y \end{bmatrix} \geq 0, \tag{3.44}$$

$$\begin{bmatrix} L & I \\ I & J \end{bmatrix} \geq I. \tag{3.45}$$

See Apkarian and Gahinet (1995).

Theorem 3.7 provides sufficient conditions for the existence of gain-scheduled $\mathscr{H}_\infty$ controllers. An algorithm for the computation of the components of the controller is proposed by Apkarian and Gahinet (1995). The design of gain-scheduled $\mathscr{H}_\infty$ controllers is also found in Apkarian et al. (1995), Gahinet and Apkarian (1996), Apkarian and Adams (1998), Apkarian and Tuan (2000). Pairs (X, Y) are called feasible for the LMI system and computing feasible pairs is a convex optimization problem. Efficient polynomial-time algorithms are available to solve this LMI feasibility problem, see Nesterov and Nemirovsky (1993), Nemirovsky and Gahinet (1994).

3.4 Control Design Based on PDLF Methods

3.4.1 The Analysis of LPV Systems

In what follows, we would like to apply parameter varying Lyapunov functions. Thus, the parameter variation rate will also be involved and it is appropriate to introduce the following parameter ν-variation sets: let a compact set $\mathscr{P} \subset \mathscr{R}^S$ and finite non-negative numbers $\{\nu_i\}_{i=1}^s$ with $\nu = [\nu_1, \ldots, \nu_s]^T$ are given. The parameter ν-variation set $\mathscr{F}_{\mathscr{P}}^{\nu}$ denotes the following:

$$\mathscr{F}_{\mathscr{P}}^{\nu} = \{\rho \in C^1(R, R^s) : \rho(t) \in \mathscr{P}, |\dot{\rho}_i| \leq \nu_i, i = 1, \ldots, s\}, \tag{3.46}$$

where C^1 stands for the class of piecewise continuously differentiable functions.

Accordingly, we consider an nth order LPV system $G(\rho)$ system with bounded parameter variation rates. i.e., a system

$$\begin{bmatrix} \dot{x}(t) \\ z(t) \end{bmatrix} = \begin{bmatrix} A(\rho(t), \dot{\rho}(t)) & B(\rho(t), \dot{\rho}(t)) \\ C(\rho(t), \dot{\rho}(t)) & D(\rho(t), \dot{\rho}(t)) \end{bmatrix} \begin{bmatrix} x(t) \\ d(t) \end{bmatrix}, \tag{3.47}$$

where $\rho \in \mathscr{F}_{\mathscr{P}}^{\nu}$, $\dot{\rho} \in \bar{\mathscr{F}}$, $x \in \mathscr{R}^n$, $d \in \mathscr{R}^{n_d}$ and $z \in \mathscr{R}^{n_z}$, while $A : \mathscr{R}^S \to \mathscr{R}^{n \times n}$, $B : \mathscr{R}^S \to \mathscr{R}^{n \times n_u}$, $C : \mathscr{R}^S \to \mathscr{R}^{n_y \times n}$, $D : \mathscr{R}^S \to \mathscr{R}^{n_y \times n_u}$ are given continuous functions.

First parameter-dependent stability, which is the generalization of quadratic stability, is defined.

Definition 3.1 (*Parameter-dependent stability*) Given a compact set $\mathscr{P} \subset \mathscr{R}^S$, finite non-negative numbers $\{\nu_i\}_{i=1}^s$ and a function $A : \mathscr{R}^S \times \mathscr{R}^S \to \mathscr{R}^{n \times n}$, the function A is parametrically dependent stable over $\mathscr{P}$ if there exists a continuously differentiable function $P : \mathscr{R}^S \to \mathscr{S}^{n \times n}$ such that $P(\rho) > 0$ and

$$A^T(\rho, \beta)P(\rho) + P(\rho)A(\rho, \beta) + \sum_{i=1}^{s} \left(\beta_i \frac{\partial P}{\partial \rho_i} \right) < 0, \tag{3.48}$$

for all $\rho \in \mathscr{P}$ and $|\beta_i| \leq \nu_i$, $i = 1, 2, \ldots, s$.

If there are no bounds for parameter variations, i.e., $\nu_i \to \infty$, $i = 1, \ldots, s$ by restricting $\mathscr{P}$ to be a constant matrix, the notation for parameter-dependent stability goes back to quadratic stability. In Eq. (3.48) the left-hand side of the inequality is strictly less than zero.

Theorem 3.8 *Given a compact set $\mathscr{P}$, and the LPV system*

$$\dot{x}(t) = A(\rho(t), \dot{\rho}(t))x(t), \tag{3.49}$$

where $\rho \in \mathscr{F}_{\mathscr{P}}^{v}$. If a function A is parametrically dependent stable over $\mathscr{P}$, then there exists some $\delta > 0$, such that

$$A^T(\rho, \dot{\rho})P(\rho) + P(\rho)A(\rho, \dot{\rho}) + \frac{dP}{dt} < -\delta I_n, \tag{3.50}$$

for all trajectory $\rho \in \mathscr{F}_{\mathscr{P}}^{v}$.

For an LPV system, if function A is parametrically dependent stable, then the system is a parametrically dependent stable LPV system.

In what follows, the induced $\mathscr{L}_2$-norm performance will be analyzed. For a parametrically dependent stable LPV system with zero initial conditions $x(0) = 0$ the induced $\mathscr{L}_2$-norm is defined as

$$\|G_{\mathscr{F}_{\mathscr{P}}}\|_{i,2} = \sup_{\rho \in \mathscr{F}_{\mathscr{P}}} \sup_{\|d\|_2 \neq 0, d \in \mathscr{L}_2} \frac{\|z\|_2}{\|d\|_2}. \tag{3.51}$$

The $\mathscr{L}_2$-norm level for an LPV system represents the largest ratio of disturbance norm to performance norm over the set of all causal linear operators described by the LPV system. The following theorem formulates a sufficient condition to test whether the induced $\mathscr{L}_2$-norm of an LPV system is less than a prescribed performance level $\gamma > 0$.

Theorem 3.9 *Given a compact set $\mathscr{P} \subset \mathscr{R}^S$, finite non-negative numbers $\{v_i\}_{i=1}^s$ and the LPV system. If there exists a function $P : \mathscr{R}^S \to \mathscr{R}^{n \times n}$ such that $P(\rho) > 0$ and*

$$\begin{bmatrix} A^T(\rho,\beta)P(\rho) + P(\rho)A(\rho,\beta) + \sum_{i=1}^{s}\left(\beta_i \frac{\partial P}{\partial \rho_i}\right) & P(\rho)B(\rho,\beta) & \gamma^{-1}C^T(\rho,\beta) \\ B^T(\rho,\beta)P(\rho) & -I_{n_d} & \gamma^{-1}D^T(\rho,\beta) \\ \gamma^{-1}C(\rho,\beta) & \gamma^{-1}D(\rho,\beta) & -I_{n_c} \end{bmatrix} < 0, \tag{3.52}$$

for all $\rho \in \mathscr{P}$ and $|\beta_i| \leq v_i$, $i = 1, 2, \ldots, s$, then the function A is parametrically dependent stable over $\mathscr{P}$ and there exists a scalar δ with $0 \leq \delta < \gamma$ such that $\|G_{\mathscr{F}_{\mathscr{P}}^{v}}\|_{i,2} \leq \delta$

This theorem is the generalization of the Scaled Bounded Real Lemma. When constant matrix P is restricted, this theorem recovers the result of Becker et al. (1993), which is an analysis test for LPV systems with arbitrarily fast varying parameters. The theorem given by Wu (1995) is less conservative because of its exploitation of parameter variation rates information.

The condition of Theorem 3.9 is an infinite dimensional convex problem. By approximating the function space with finite basis functions, we can simplify the condition to a finite dimensional convex problem and solve the analysis problem using efficient convex optimization techniques. The following test includes 2^s LMIs of some positive definite functions, and only requires the gridding of parameter space thus it is computationally less expensive than the previous theorem.

Theorem 3.10 *Given is the LPV system without state space data dependence on parameter derivative. If there exists a function* $P : \mathscr{R}^S \to \mathscr{S}^{n\times n}$ *such that* $P(\rho) > 0$ *and*

$$\begin{bmatrix} A^T(\rho)P(\rho) + P(\rho)A(\rho) + \sum_{i=1}^{s} \pm\left(\nu_i \frac{\partial P}{\partial \rho_i}\right) & P(\rho)B(\rho) & \gamma^{-1}C^T(\rho) \\ B^T(\rho)P(\rho) & -I_{n_d} & \gamma^{-1}D^T(\rho) \\ \gamma^{-1}C(\rho) & \gamma^{-1}D(\rho) & -I_{n_z} \end{bmatrix} < 0, \tag{3.53}$$

for all $\rho \in \mathscr{P}$*, then the function A is parametrically dependent stable over* $\mathscr{P}$ *and there exists a scalar* δ *with* $0 \le \delta < \gamma$ *such that* $\|G_{\mathscr{F}^v_{\mathscr{P}}}\|_{i,2} \le \delta$

It is noted that the notation $\sum_{i=1}^{s} \pm(\cdot)$ in (3.53) indicates every combination of $+(\cdot)$ and $-(\cdot)$ should be included in the inequality.

3.4.2 The Control of LPV Systems With Induced $\mathscr{L}_2$-Norm Performance

In this section, the parameter-dependent output-feedback control problem for LPV systems with bounded parameter variation rates is studied. This problem determines the existence of a parameter-dependent controller which parametrically dependent stabilizes the closed-loop LPV system and guarantees that the induced $\mathscr{L}_2$-norm of the closed-loop system less than γ. The derivative of parameter is assumed to be achievable (or measurable) in real-time to construct such a controller.

For a given compact set $\mathscr{P} \subset \mathscr{R}^S$ let us consider the open-loop LPV system in the following way:

$$\dot{x} = A(\rho)x + B_1(\rho)d + B_2(\rho)u, \tag{3.54}$$
$$z = C_1(\rho)x + D_{11}(\rho)d + D_{12}(\rho)u, \tag{3.55}$$
$$y = C_2(\rho)x + D_{21}(\rho)d + D_{22}(\rho)u, \tag{3.56}$$

where $\rho \in \mathscr{F}^v_{\mathscr{P}}$, $x \in \mathscr{R}^n$, $d \in \mathscr{R}^{n_d}$, $z \in \mathscr{R}^{n_z}$, $u \in \mathscr{R}^{n_u}$, $y \in \mathscr{R}^{n_y}$.

Then the parametrically dependent m-dimensional linear feedback controller with the continuous functions $A_k : \mathscr{R}^S \to \mathscr{R}^{m\times m}$, $B_k : \mathscr{R}^S \to \mathscr{R}^{m\times n_y}$,$C : \mathscr{R}^S \to \mathscr{R}^{n_u\times m}$, $D : \mathscr{R}^S \to \mathscr{R}^{n_u\times n_y}$ are given. The controller depends on the parameter and its derivative according to the following equation:

$$\dot{x}_k = A_k(\rho, \dot{\rho})x_k + B_k(\rho, \dot{\rho})y, \tag{3.57}$$
$$u_k = C_k(\rho, \dot{\rho})x_k + D_k(\rho, \dot{\rho})y, \tag{3.58}$$

where $\rho \in \mathscr{F}^v_{\mathscr{P}}$, x_k is the m-dimensional controller states.

The following assumptions for the generalized plant are made:

- $D_{22}(\rho) = 0$. This assumption can be relaxed by including a feed through term to the controller for the modified plant.
- $D_{12}(\rho)$ is full column rank for all $\rho \in \mathscr{P}$ and $D_{21}(\rho)$ is full row rank for all $\rho \in \mathscr{P}$. The relaxation of these assumptions leads to singular $\mathscr{H}_\infty$ problem.

In the following, the parameter-dependent output-feedback controller synthesis is presented. In order to achieve simple formulas, $D_{11} = 0$ is assumed. However, the results can be generalized to $D_{11} \neq 0$ case. The following simplifications are also made: $D_{12} = \begin{bmatrix} 0 & I_{nz_2} \end{bmatrix}$ and $D_{21} = \begin{bmatrix} I_{nd_2} & 0 \end{bmatrix}$

The open-loop system is modified in the following form:

$$\left[\begin{array}{c} \dot{x}(t) \\ \hline z_1(t) \\ z_2(t) \\ y(t) \end{array}\right] = \left[\begin{array}{c|ccc} A(\rho(t)) & B_{11} & B_{12} & B_2 \\ \hline C_{11} & 0 & 0 & 0 \\ C_{12} & 0 & 0 & I_{nz_2} \\ C_2 & 0 & I_{nd_2} & 0 \end{array}\right] \left[\begin{array}{c} x(t) \\ \hline d_1(t) \\ d_2(t) \\ u_c(t) \end{array}\right], \tag{3.59}$$

where $\rho \in \mathscr{F}^v_{\mathscr{P}}$, $d_1 \in \mathscr{R}^{n_{d1}}$, $d_2 \in \mathscr{R}^{n_{d2}}$, $z_1 \in \mathscr{R}^{n_{e1}}$, $z_2 \in \mathscr{R}^{n_{e2}}$.

The closed-loop system with $\dot{x}_c^T(t) = \begin{bmatrix} x^T(t) & x_k^T(t) \end{bmatrix}$, $z^T(t) = \begin{bmatrix} z_1^T(t) & z_2^T(t) \end{bmatrix}$, $d^T(t) = \begin{bmatrix} d_1^T(t) & d_2^T(t) \end{bmatrix}$ is given by

$$\dot{x}_c = A_c(\rho, \dot{\rho})x_c + B_c(\rho, \dot{\rho})d, \tag{3.60}$$
$$z = C_c(\rho, \dot{\rho})x_c + D_c(\rho, \dot{\rho})d, \tag{3.61}$$

where

$$A_c(\rho, \dot{\rho}) = \begin{bmatrix} A(\rho) + B_2(\rho)D_K(\rho, \dot{\rho})C_2(\rho) & B_2(\rho)C_K(\rho, \dot{\rho}) \\ B_K(\rho, \dot{\rho})C_2(\rho) & A_K(\rho, \dot{\rho}) \end{bmatrix}, \tag{3.62}$$

$$B_c(\rho, \dot{\rho}) = \begin{bmatrix} B_{11}(\rho) & B_{12}(\rho) + B_2(\rho)D_K(\rho, \dot{\rho}) \\ 0 & B_K(\rho, \dot{\rho}) \end{bmatrix}, \tag{3.63}$$

$$C_c(\rho, \dot{\rho}) = \begin{bmatrix} C_{11}(\rho) & 0 \\ C_{12}(\rho) + D_K(\rho, \dot{\rho})C_2(\rho) & C_K(\rho, \dot{\rho}) \end{bmatrix}, \tag{3.64}$$

$$D_c(\rho, \dot{\rho}) = \begin{bmatrix} 0 & 0 \\ 0 & D_K(\rho, \dot{\rho}) \end{bmatrix}. \tag{3.65}$$

For a given performance level $\gamma > 0$ the parameter-dependent γ performance problem is solvable if there exists an integer $m \geq 0$, a function $P : \mathscr{R}^S \to S^{(n+m)\times(m+n)}$ and continuous matrix functions $A_k : \mathscr{R}^S \to \mathscr{R}^{m\times m}$, $B_k : \mathscr{R}^S \to \mathscr{R}^{m\times n_y}$, $C_k : \mathscr{R}^S \to \mathscr{R}^{n_u\times m}$, $D_k : \mathscr{R}^S \to \mathscr{R}^{n_u\times n_y}$ such that $P(\rho) > 0$ and

$$\begin{bmatrix} A_c^T(\rho,\beta)P(\rho) + P(\rho)A_c(\rho,\beta) + \sum_{i=1}^{s} \beta_i \frac{\partial P}{\partial \rho_i} & P(\rho)B_c(\rho,\beta) & \gamma^{-1}C_c^T(\rho,\beta) \\ B_c^T(\rho,\beta)P(\rho) & -I_{n_d} & \gamma^{-1}D_c^T(\rho,\beta) \\ \gamma^{-1}C_c^T(\rho,\beta) & \gamma^{-1}D_c^T(\rho,\beta) & -I_{n_z} \end{bmatrix} < 0, \tag{3.66}$$

for all $\rho \in \mathscr{P}$ and $|\beta_i| \leq \nu_i$, $i = 1, 2, \ldots, s$. The closed-loop matrices are defined in (3.62).

This problem is a generalization of the standard suboptimal $\mathscr{H}_\infty$ control problem. The output-feedback controller synthesis is based on the following theorem:

Theorem 3.11 *A compact set $\mathscr{P}$, the performance level $\gamma > 0$ and the LPV system are given. The parameter-dependent γ-performance problem is solvable if and only if there exist matrix functions $X : \mathscr{R}^S \to \mathscr{R}^{n\times n}$, and $Y : \mathscr{R}^S \to \mathscr{R}^{n\times n}$, such that for all $\rho \in \mathscr{P}$, $X(\rho) > 0$, $Y(\rho) > 0$ and*

$$\begin{bmatrix} Ric(X,\rho,\dot{\rho}) & X(\rho)C_{11}^T(\rho) & \gamma^{-1}B_1(\rho) \\ C_{11}(\rho)X(\rho) & -I_{n_{z1}} & 0 \\ \gamma^{-1}B_1^T(\rho) & 0 & -I_{n_d} \end{bmatrix} < 0, \tag{3.67}$$

$$\begin{bmatrix} Ric(Y,\rho,\dot{\rho}) & Y(\rho)B_{11}(\rho) & \gamma^{-1}C_1^T(\rho) \\ B_{11}^T(\rho)Y(\rho) & -I_{n_{d1}} & 0 \\ \gamma^{-1}C_1(\rho) & 0 & -I_{n_z} \end{bmatrix} < 0, \tag{3.68}$$

$$\begin{bmatrix} X(\rho) & \gamma^{-1}I_n \\ \gamma^{-1}I_n & Y(\rho) \end{bmatrix} \geq 0. \tag{3.69}$$

where

$$Ric(X,\rho,\dot{\rho}) = X(\rho)\hat{A}^T(\rho) + \hat{A}(\rho)X(\rho) - \sum_{i=1}^{s} \pm\left(\nu_i \frac{\partial X}{\partial \rho_i}\right) - B_2(\rho)B_2^T(\rho), \tag{3.70}$$

$$Ric(Y,\rho,\dot{\rho}) = \tilde{A}^T(\rho)Y(\rho) + Y(\rho)\tilde{A}(\rho) + \sum_{i=1}^{s} \pm\left(\nu_i \frac{\partial Y}{\partial \rho_i}\right) - C_2^T(\rho)C_2(\rho), \tag{3.71}$$

and

$$\hat{A}(\rho) = A(\rho) - B_2(\rho)C_{12}(\rho), \tag{3.72}$$

$$\tilde{A}(\rho) = A(\rho) - B_{12}(\rho)C_2(\rho). \tag{3.73}$$

If the conditions are satisfied, it is possible—by continuity and compactness—to perturb $X(\rho)$ such that the two LMIs (3.67) and (3.68) still hold and $Q(\rho) = Y(\rho) - \gamma^{-2}X^{-1}(\rho) > 0$ uniformly on $\mathscr{P}$. Define now the following variables

$$F(\rho) = -[B_2(\rho)X^{-1}(\rho) + D_{12}^T C_1(\rho)], \tag{3.74}$$

$$L(\rho) = -[Y^{-1}(\rho)C_2^T(\rho) + B_1(\rho)D_{21}^T], \tag{3.75}$$

$$H(\rho, \dot{\rho}) = -[X^{-1}(\rho)A_F(\rho) + A_F^T(\rho)X^{-1}(\rho) + \sum_{i=1}^{s}\left(\dot{\rho}\frac{\partial X^{-1}}{\partial \rho_i}\right) + \\ + C_F^T(\rho)C_F(\rho) + \gamma^{-2}X^{-1}(\rho)B_1(\rho)B_1^T(\rho)X^{-1}(\rho)], \tag{3.76}$$

with

$$A_F(\rho) = A(\rho) + B_2(\rho)F(\rho), \tag{3.77}$$

$$C_F(\rho) = C_1(\rho) + D_{12}(\rho)F(\rho). \tag{3.78}$$

Furthermore,

$$M(\rho, \dot{\rho}) = H(\rho, \dot{\rho}) + \gamma^2 Q(\rho)[-Q^{-1}(\rho)Y(\rho)L(\rho)D_{21} - B_1(\rho)]B_1^T(\rho)X^{-1}(\rho). \tag{3.79}$$

The strictly proper controller that solves the feedback problem is given by

$$A_k(\rho, \dot{\rho}) = A(\rho) + B_2(\rho)F(\rho) + Q^{-1}(\rho)Y(\rho)L(\rho)C_2(\rho) - \gamma^{-2}Q^{-1}(\rho)M(\rho, \dot{\rho}), \tag{3.80}$$

$$B_k(\rho) = -Q^{-1}Y(\rho)L(\rho), \tag{3.81}$$

$$C_k(\rho) = F(\rho), \tag{3.82}$$

$$D_k(\rho) = 0. \tag{3.83}$$

The proof of this theorem and the discussion of the general case $D_{11}(\rho) \neq 0$ are also in Wu (1995). Equation (3.67) is for the state feedback, (3.68) is for the output estimation, and (3.69) is the coupling condition. The LMIs in Theorem 3.11 lead to an infinite dimensional convex feasibility problem.

Note that the controller dynamics matrix $A_k(\rho, \dot{\rho})$ depends explicitly on $\dot{\rho}$. In order to construct a parameter-dependent controller, both ρ and $\dot{\rho}$ must be measured or available. In case of a single scheduling variable, i.e., when $\dot{\rho}$ is not measured, it is possible to perform a ρ-dependent change of variables to remove $\dot{\rho}$ dependence as follows.

In the scalar parameter case, the controller dynamics from Theorem 3.11 take the form

$$\dot{x}_k = A_1(\rho)x_k + \dot{\rho}A_2(\rho)x_k + B_k(\rho). \tag{3.84}$$

Now consider the change of variables

$$x_{k,new} = T(\rho)x_k + \dot{\rho}A_2(\rho)x_k + B_k(\rho), \tag{3.85}$$

where $T(\rho)$ is invertible. It is easy to show that if $T(\rho)$ satisfies the linear matrix differential equation

$$\frac{dT(\rho)}{d\rho} = -T(\rho)A_2(\rho), \tag{3.86}$$

then the resulting controller dynamics in the new coordinates $x_{k,new}$ will be independent of $\dot{\rho}$. In case of multiple scheduling variables, a similar method can be applied. However, the analytical solvability is more difficult. For more details, see Balas et al. (1997).

An alternative solution is to simply restrict the choice X to be independent of $\dot{\rho}$ in Eq. (3.76). However, this approach may be conservative, since the rate of change of the parameters is not bounded. Another possible solution is to apply a suitable extrapolation algorithm in order to achieve an estimation of the parameter $\dot{\rho}$. The disadvantage of this approach is that the sources of the scheduling variables are not independent.

In the following, the infinite convex feasibility conditions in Theorem 3.11 will be converted to finite-dimensional LMIs. In the solution a finite number of basis functions are selected to parameterize infinite-dimensional function space.

Theorem 3.12 *Given a finite number of scalar, continuously differentiable functions* $\{f_i\}_{i=1}^N$ *and* $\{g_i\}_{i=1}^N$ *with the parametrization*

$$X(\rho) = \sum_{i=1}^{N} f_i(\rho)X_i, \tag{3.87}$$

$$Y(\rho) = \sum_{i=1}^{N} g_i(\rho)Y_i. \tag{3.88}$$

The parameter-dependent γ*-performance problem is solvable if there exist matrices* $\{X_i\}_{i=1}^N$, $X_i \in \mathscr{S}^{n\times n}$ *and* $\{Y_i\}_{i=1}^N$, $Y_i \in \mathscr{S}^{n\times n}$ *such that for all* $\rho \in \mathscr{P}$, $X(\rho) > 0$, $Y(\rho) > 0$ *and*

$$\begin{bmatrix} Ric(X(\rho)) & \sum_{i=1}^{N} f_i(\rho)X_i C_{11}^T(\rho) & \gamma^{-1}B_1(\rho) \\ C_{11}(\rho)\sum_{i=1}^{N} f_i(\rho)X_i & -I_{n_{z1}} & 0 \\ \gamma^{-1}B_1^T(\rho) & 0 & -I_{n_d} \end{bmatrix} < 0, \tag{3.89}$$

$$\begin{bmatrix} Ric(Y(\rho)) & \sum_{i=1}^{N} g_i(\rho) Y_i B_{11}(\rho) & \gamma^{-1} C_1^T(\rho) \\ B_{11}^T(\rho) \sum_{i=1}^{N} g_i(\rho) Y_i & -I_{n_{d1}} & 0 \\ \gamma^{-1} C_1(\rho) & 0 & -I_{n_z} \end{bmatrix} < 0, \tag{3.90}$$

$$\begin{bmatrix} \sum_{i=1}^{N} f_i(\rho) X_i & \gamma^{-1} I_n \\ \gamma^{-1} I_n & \sum_{i=1}^{N} g_i(\rho) Y_i \end{bmatrix} \geq 0. \tag{3.91}$$

where

$$Ric(X(\rho)) = \sum_{i=1}^{N} f_i(\rho) \left(X_i \hat{A}^T(\rho) + \hat{A}(\rho) X_i \right) - \sum_{j=1}^{s} \pm \left(v_j \sum_{i=1}^{N} \frac{\partial f_i}{\partial \rho_i} X_i \right) - B_2(\rho) B_2^T(\rho) \tag{3.92}$$

$$Ric(Y(\rho)) = \sum_{i=1}^{N} g_i(\rho) \left(\tilde{A}^T(\rho) Y_i + Y_i \tilde{A}(\rho) \right) + \sum_{j=1}^{s} \pm \left(v_j \sum_{i=1}^{N} \frac{\partial g_i}{\partial \rho_i} Y_i \right) - C_2^T(\rho) C_2(\rho), \tag{3.93}$$

and the matrices $\hat{A}(\rho)$ *and* $\tilde{A}(\rho)$ *are defined in Eq. (3.72).*

The other problem is that the inequalities must hold for all $\rho \in \mathscr{P}$, which entails that an infinite number of constraints must be checked. In order to solve this infinite constraints convex problem, the compact set $\mathscr{P}$ must be gridded. For example, if a hyper rectangle $\mathscr{P} \subset \mathscr{R}^S$ is gridded with L points in each dimension, then the convex problem to determine appropriate $\{X_i\}_{i=1}^N$ and $\{Y_i\}_{i=1}^N$ includes approximately $L^s(2^{s+1} + 1)$ LMIs. Another problem is the complete lack of guidance provided by the theory to pick the basis functions, namely f_i and g_i. Thus, usually intuitive solutions for basis functions are applied.

3.4.3 Inexact LPV Control Design

We conclude this chapter with a design example for a polytopic LPV system when the measured varying parameters do not exactly fit the real ones, see Daafouz et al. (2008). In this example the plant and the desired controller are considered in the form

$$\dot{x} = A(\rho)x + B_1 w + B_2 u, \tag{3.94}$$

$$z = C_1 x + D_{12} u, \tag{3.95}$$

$$y = C_2 x + D_{21} w, \tag{3.96}$$

having

$$A(\rho) = \sum_{i=1}^{p} \rho_i A_i, \quad \rho_i \geq 0, \quad \sum_{i=1}^{p} \rho_i = 1,$$

and

$$\dot{x}_c = A_c(\hat{\rho})x + B_c y, \quad A_c(\hat{\rho}) = \sum_{i=1}^{p} \hat{\rho}_i A_{ci}, \tag{3.97}$$

$$u = C_c x, \tag{3.98}$$

respectively. We assume that $\hat{\rho} \in \Omega(\rho)$ with

$$\Omega(\rho) = \{\, \hat{\rho} \,|\, |\rho_i - \hat{\rho}_i| \leq \theta \rho_i \,\}, \tag{3.99}$$

where $\theta \geq 0$ is a given scalar.

Theorem 3.13 *Let us introduce the following LMIs:*

$$\begin{bmatrix} W & B_1^T & B_1^T X + D_{21}^T F^T \\ B_1 & Y & I \\ XB_1 + FD_{21} & I & X \end{bmatrix} > 0, \tag{3.100}$$

$$\begin{bmatrix} L_i^T + L_i + \theta R_i & A_i + M_i & YC_1^T + L^T D_{12}^T \\ A_i^T + M_i^T & H_i^T + H_i + \theta Q_i & C_1^T \\ C_1 Y + D_{12} L & C_1 & -I \end{bmatrix} < 0, \tag{3.101}$$

$$\begin{bmatrix} -R_i & M_i & YA_i^T \\ M_i^T & -Q_i & -X \\ A_i Y & -X & -I \end{bmatrix} < 0, \tag{3.102}$$

where

$$L_i = A_i Y + B_2 L, \quad H_i = XA_i + FC_2.$$

Then, the controller

$$A_{ci} = U^{-1}(M_i^T - XA_i Y - XB_2 L - FC_2 Y)V^{-1}, \tag{3.103}$$

$$B_c = U^{-1}F, \quad C_c = LV^{-1} \tag{3.104}$$

guarantees the performance index $\gamma < \mathrm{tr}(W)$ *for all* $\hat{\rho} \in \Omega(\rho)$, *where* $XY + UV = I$.

Part II
Vertical and Longitudinal Control

Chapter 4
Suspension Systems in Vertical Dynamics

Introduction

This section is concerned with designing the dynamic properties of vehicle suspension systems to improve the dynamic properties of vehicles. The performance of suspension systems can be assessed quantitatively in terms of four parameters: passenger comfort, suspension deflection, tire load variation, and energy consumption, see Gillespie (1992), Cole (2001). Vehicle vibrations excited by road irregularities might lead to the fatigue of the driver and passengers, as well as damage to the vehicle and the payload. It is widely accepted that there is a correlation between passenger comfort (or ride comfort) and the heave, pitch, and roll accelerations of the sprung mass. The suspension working space, which is defined as the relative displacement between the sprung and unsprung masses and also called suspension deflection, may affect directional stability because of particular suspension geometries. It is required that suspension deflection be minimized. The suspension system must guarantee that the vehicle remains on the track in all maneuvers. The wheel load is made up of a static component due to gravity and a dynamic component due to road unevenness. In order to reduce variations of the side force during a vehicle maneuver, it is necessary that the dynamic tire load component be kept as small as possible. The control force limitation is incorporated into the design procedure in order to avoid large control forces.

In order to improve passenger comfort, it is important to keep the effect of the road disturbance w on the heave acceleration z_{az} as well as on the pitch z_θ and roll z_ϕ accelerations small. Structural features of the vehicle place a hard limit on the amount of suspension deflection available for reducing the vertical, pitch, and roll accelerations of the car body. Hence it is also important to keep the effect of the disturbance on the suspension deflection z_s sufficiently small. In order to reduce the dynamic tire load deflection, the effect of the disturbance on tire deflection z_t should also be kept small.

One of the difficulties in the control design is that the different control goals are usually in conflict and a trade-off must be achieved between them. The variance of body acceleration decreases when the variance of suspension or tire deflections

P. Gáspár et al., *Robust Control Design for Active Driver Assistance Systems*,
Advances in Industrial Control, DOI 10.1007/978-3-319-46126-7_4

increases, thus its minimization implies maximal admissible deflections. The result also indicates that generally the constraints imposed on the suspension deflection limit the tire deflection simultaneously and vice versa, see Hac (1987).

4.1 Modeling of Performances in the Vertical Dynamics

4.1.1 Performance Specifications

It is well known that the vertical, pitch, and roll acceleration transfer functions have an invariant point at the tirehop frequency $\omega_{1i} = \sqrt{k_{ti}/m_{ui}}, i = f, r$. From the control design point of view this means that the transfer function from disturbance to heave acceleration has a zero at ω_{1i}. Similarly, the suspension deflection transfer function has an invariant point at the frequency $\omega_{2i} = \sqrt{k_{ti}/(m_{ui} + m_s)}$. This means that the transfer function from disturbance to suspension deflections has a zero at ω_{2i}. Frequency responses to the control force, i.e., the heave, pitch, roll accelerations, and suspension deflection, are illustrated in Fig. 4.1. The necessity of a trade-off between passenger comfort and suspension deflection is due to the fact that is not possible to simultaneously keep both the above transfer function small around the tirehop frequency and in the low frequency range. The small reduction in vertical, pitch, and roll accelerations at low frequency and in the vicinity of the tirehop frequency results in a large increase in suspension deflection at these frequencies and vice versa.

4.1.2 Weighting Functions in the Control Design

The weighting function for performances W_p contains weights for several performance components. The purpose of weighting functions $W_{p,az}$, $W_{p,\theta}$, and $W_{p,\phi}$ is to keep heave, pitch, and roll accelerations small over the desired frequency range. The purpose of weighting functions $W_{p,sd}$ and $W_{p,td}$ is to keep suspension and tire deflections small. At the same time, the magnitude of the control force is limited by the weighting function $W_{p,us}$. The weighting function for heave acceleration of the body can be set as follows:

$$W_{p,az} = 0.5 \frac{\frac{s}{350} + 1}{\frac{s}{10} + 1}. \tag{4.1}$$

In the design, the same weights are selected for the heave, pitch, and roll accelerations $W_{p,az} = W_{p,\theta} = W_{p,\phi}$. The weighting functions for suspension deflection and tire deflection are as follows:

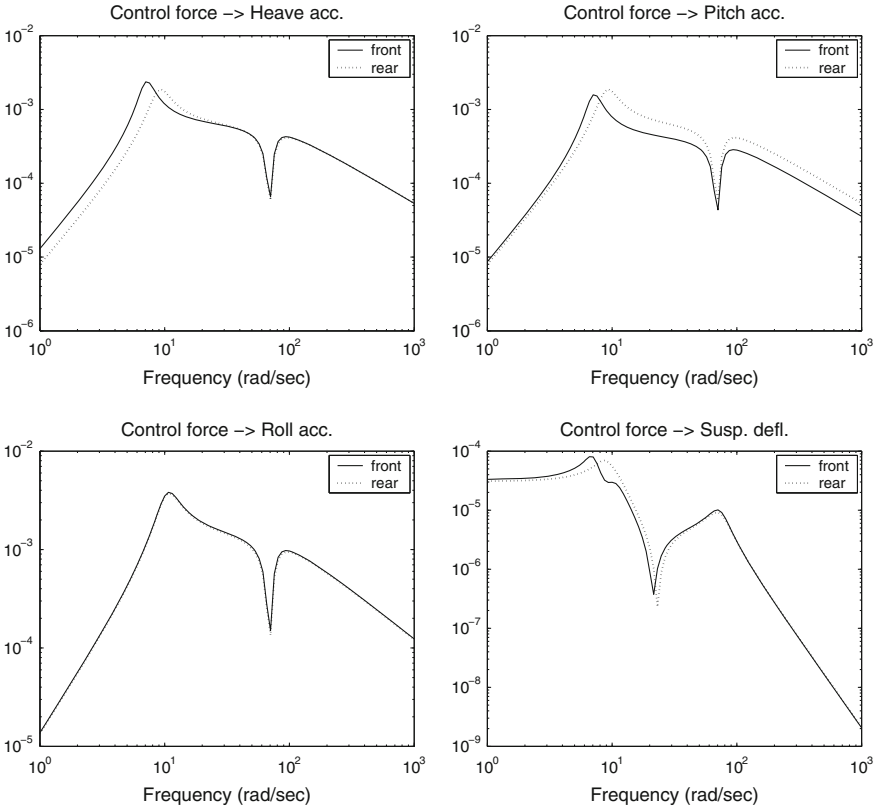

Fig. 4.1 Frequency responses of the full-car model to the control forces

$$W_{p,sd} = \frac{\frac{s}{350} + 1}{\frac{s}{10} + 1}, \tag{4.2}$$

$$W_{p,td} = 1. \tag{4.3}$$

The same performance weights are used for both the front and rear suspensions. It is assumed that in the low frequency domain disturbances at the heave, pitch, and roll accelerations of the body should be rejected by a factor of 0.5 and at the suspension and tire deflections by a factor of 1. These weighting functions are illustrated in Fig. 4.2. The weighting function for the control force is selected $W_{p,us} = 4 \times 10^{-3}$. The weight for disturbance is selected $W_w = 0.1$ to scale the magnitude of the road disturbance, i.e., the maximum road disturbance is assumed to be 10 cm. The weight for the sensor noise is selected $W_n = 0.001$, thus essentially it is assumed that the sensor noise is 0.001 m/s^2 at the front and rear body accelerations on the left and right-hand sides as well in the whole frequency domain.

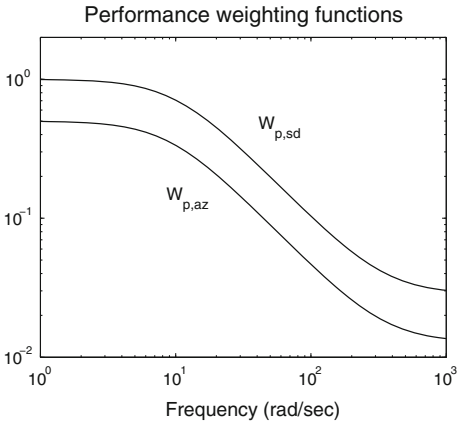

Fig. 4.2 Weighting functions for performance specifications

In order to guarantee a trade-off between passenger comfort and suspension deflection, the possibility of the LPV constructions is exploited. Two gains, ϕ_{az} and ϕ_{sd}, which reflect the relative importance of the acceleration and suspension deflection, respectively, are applied in the weighting functions.

$$W_{p,az}(\rho_k) = \phi_{az}(\rho_k) \cdot 0.5 \frac{\frac{s}{350} + 1}{\frac{s}{10} + 1}, \tag{4.4}$$

$$W_{p,sd}(\rho_k) = \phi_{sd}(\rho_k) \cdot \frac{\frac{s}{350} + 1}{\frac{s}{10} + 1}. \tag{4.5}$$

A large gain ϕ_{az} and a small gain ϕ_{sd} correspond to a design that emphasizes passenger comfort. On the other hand, choosing ϕ_{az} small and ϕ_{sd} large corresponds to a design that focuses on suspension deflection. In the *LPV* controller ρ_k is the relative displacement between the sprung and the unsprung masses: $\rho_k = x_1 - x_2$. ρ_k is used to focus on minimizing either the vertical acceleration or the suspension deflection response, depending on the magnitude of the vertical suspension deflection. In order to achieve the shift in focus from vertical acceleration to suspension deflection the weights associated with these signals, i.e., ϕ_{az} and ϕ_{sd}, are chosen to be parameter-dependent, i.e., the function of ρ_k.

The parameter-dependent gains ϕ_{az} and ϕ_{sd} capture the relative importance of the acceleration and deflection responses. When ρ_k is small, i.e., when suspension deflection is well away from its limits, $\phi_{az}(\rho_k)$ is large and $\phi_{sd}(\rho_k)$ is small, indicating that the LPV controller should focus on minimizing acceleration regardless of suspension deflection. On the other hand, when ρ_k is approaching the limit, $\phi_{sd}(\rho_k)$ is large and $\phi_{az}(\rho_k)$ is small, indicating that the controller should focus on preventing the suspension deflection from reaching its limit. The parameter dependence of the gains is characterized by the constants ρ_1 and ρ_2. The parameter dependent gains $\phi_{az}(\rho_k)$ and $\phi_{sd}(\rho_k)$ in contrast to the constant ϕ_{az} and ϕ_{sd} in Eq. (4.4) are selected in the following way:

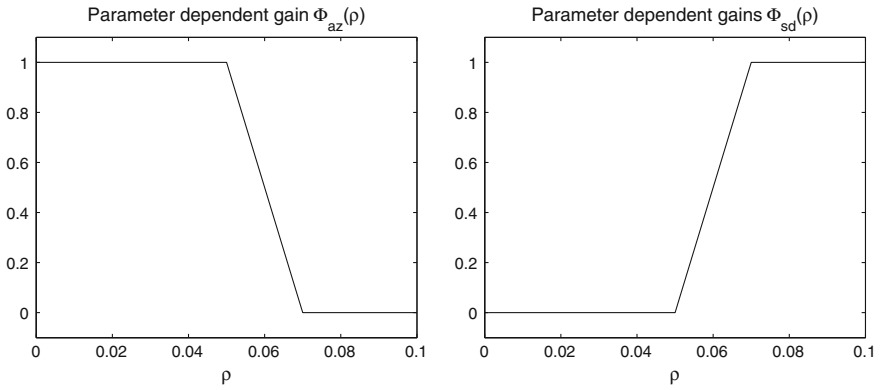

Fig. 4.3 Parameter-dependent gains in the performance specification

$$\phi_{az}(\rho_k) = \begin{cases} 1 & \text{if} \quad |\rho_k| < \rho_1 \\ \frac{1}{\rho_1 - \rho_2}(|\rho_k| - \rho_2) & \text{if} \quad \rho_1 \leq |\rho_k| \leq \rho_2 \\ 0 & \text{otherwise} \end{cases}, \tag{4.6}$$

$$\phi_{sd}(\rho_k) = \begin{cases} 0 & \text{if} \quad |\rho_k| < \rho_1 \\ \frac{1}{\rho_2 - \rho_1}(|\rho_k| - \rho_1) & \text{if} \quad \rho_1 \leq |\rho_k| \leq \rho_2 \\ 1 & \text{otherwise} \end{cases}. \tag{4.7}$$

In these gains, a scheduling variable relating to the relative displacement is used to guarantee a trade-off between passenger comfort and suspension deflection. The illustration of the parameter-dependent weights is in Fig. 4.3. Here, ρ_1 and ρ_2 are selected as 0.05 and 0.07, respectively. This corresponds to an LPV controller that minimizes only the vertical acceleration when the suspension travel is less than 5 cm, and which gradually begins focusing on the suspension deflection when the travel is greater than 5 cm. Over 7 cm, it minimizes only the suspension deflection.

4.2 Modeling of Vertical Dynamics by Using Uncertainties

4.2.1 Parameter Uncertainties

In this section, the modeling of uncertain components of vertical dynamics is considered. The parameters are assumed to be uncertain, with a nominal value and a range of possible variations $m_s = \bar{m}_s(1 + d_{ms}\delta_{ms})$, $k_i = \bar{k}_i(1 + d_{ki}\delta_{ki})$, $b_j = \bar{b}_j(1 + d_{bj}\delta_{bj})$, with d_{ms}, d_{ki}, d_{bj} scalars, and $-1 \leq \delta_{ms},\ \delta_{ki},\ \delta_{bj} \leq 1$, $i \in (sf, sr, tf, tr)$ and $j \in (sf, sr)$. The scalar d indicates the percentage of variation that is allowed for a given parameter around its nominal value. The changing of the δ parameters in the interval $\left[-1\ 1\right]$ determines the actual parameter deviation. All uncertainties can be

written in the lower Linear Fractional Transformation (LFT) form. The m_s parameter occurs in the denominator of the differential equation of the suspension dynamics. The other uncertainties, such as k_i and b_i, occur in the numerator. Their LFT representations are as follows:

$$\frac{1}{m_s} = \frac{1}{\bar{m}_s} - \frac{d_{ms}}{\bar{m}_s}\delta_{ms}(1 + d_{ms}\delta_{ms})^{-1} = \mathscr{F}_l\left(\begin{bmatrix} \frac{1}{\bar{m}_s} & -\frac{d_{ms}}{\bar{m}_s} \\ 1 & -d_{ms} \end{bmatrix}, \delta_{ms}\right) = \mathscr{F}_l(M_{ms}, \delta_{ms}), \tag{4.8}$$

$$k_i = \bar{k}_i + \bar{k}_i d_{ki}\delta_{ki} = \mathscr{F}_l\left(\begin{bmatrix} \bar{k}_i & 1 \\ d_{ki}\bar{k}_i & 0 \end{bmatrix}, \delta_{ki}\right) = \mathscr{F}_l(M_{ki}, \delta_{ki}), \quad i \in (sf,\ sr,\ tf,\ tr), \tag{4.9}$$

$$b_j = \bar{b}_j + \bar{b}_j d_{b_j}\delta_{b_j} = \mathscr{F}_l\left(\begin{bmatrix} \bar{b}_j & 1 \\ d_{b_j}\bar{b}_j & 0 \end{bmatrix}, \delta_{b_j}\right) = \mathscr{F}_l(M_{b_j}, \delta_{b_j}), \quad j \in (sf,\ sr). \tag{4.10}$$

The δ uncertainty blocks must be pulled out of the motion equations. Thus, let the input and output of δ_{ms} be y_{ms} and u_{ms}, δ_{ki} be y_{ki} and u_{ki}, and δ_{b_j} be y_{b_j} and u_{b_j}, respectively. The LFT structures of uncertain parameters are shown in Fig. 4.4. The outputs of M_{ms}, M_{ki} and M_{b_i} are expressed in the following forms: $\tilde{y}_{ms} = \frac{1}{\bar{m}_s}(\tilde{u}_{ms} - d_{ms}u_{ms})$, $\tilde{y}_{ki} = \bar{k}_i\tilde{u}_{ki} + u_{ki}$, $\tilde{y}_{bj} = \bar{b}_j\tilde{u}_{bj} + u_{bj}$, respectively.

In the differential equations, the suspension stiffness and tire stiffness occur in several places, and in these cases the uncertain parameters can be represented by repeated scalar blocks. It means that different uncertain parameters must be handled by the same uncertain coefficients (d, δ). The inputs and the outputs of these scalar blocks are distinguished by using upper indexes. Let y_{ki}^k and u_{ki}^k be the output and input of δ_{ki}, and let y_{bj}^k and u_{bj}^k be the output and input of δ_{bi}. From equations of uncertain components follow that some expressions can be given in full-car motion equations as

$$\frac{1}{m_s}\alpha = \frac{1}{\bar{m}_s}(\alpha - d_{ms}u_{ms}), \tag{4.11}$$

$$k_i^k(-x_{1i} + x_{2i}) = \bar{k}_i^k(-x_{1i} + x_{2i}) + u_{ki}^k, \tag{4.12}$$

$$b_j^k(-\dot{x}_{1j} + \dot{x}_{2j}) = \bar{b}_j^k(-\dot{x}_{1j} + \dot{x}_{2j}) + u_{bj}^k. \tag{4.13}$$

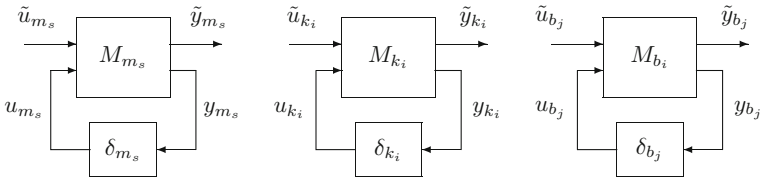

Fig. 4.4 The LFT structures of uncertain parameters

with $i \in (sf,\ sr,\ tf,\ tr), j \in (sf,\ sr), k \in 1, 2$ and

$$\alpha = \Big[k_{sf}\left(-x_{1fl} - x_{1fr} + x_{2fl} + x_{2fr}\right) + k_{sr}\left(-x_{1rl} - x_{1rr} + x_{2rl} + x_{2rr}\right) + b_{sf}\left(-\dot{x}_{1fl} - \dot{x}_{1fr} + \dot{x}_{2fl} + \dot{x}_{2fr}\right) + b_{sr}\left(-\dot{x}_{1rl} - \dot{x}_{1rr} + \dot{x}_{2rl} + \dot{x}_{2rr}\right) - - f_{fl} - f_{fr} - f_{rl} - f_{rr} \Big].$$

The motion equations of the full-car model changes since the parametric uncertainties are taken into consideration. The modified motion equations can be formalized as follows:

$$M_s\ddot{q} = LB_s(\dot{x}_u - \dot{x}_s) + LK_s(x_u - x_s) - Lf + F_1 u_\delta, \tag{4.14}$$

$$M_u\ddot{x}_u = B_s(\dot{x}_s - \dot{x}_u) + K_s(x_s - x_u) + K_t(w - x_u) + f + F_2 u_\delta, \tag{4.15}$$

where we have $u_\delta = \left[u_{ms}\ u_{ks}\ u_{kt}\right]^T$, $u_{ks} = \left[u^1_{ksf}\ u^2_{ksf}\ u^1_{ksr}\ u^2_{ksr}\ u^1_{b_{sr}}\ u^2_{b_{sr}}\right]^T$, $u_{kt} = \left[u^1_{ktf}\ u^2_{ktf}\ u^1_{ktr}\ u^2_{ktr}\right]^T$ and $F_1 = \left[\begin{bmatrix} -d_{ms} \\ 0 \\ 0 \end{bmatrix} L\ 0\right]$, $F_2 = \left[0\ I\ I\right]$, respectively.

Using $z = \left[q^T\ x_u^T\right]^T$, the motion equation is the following:

$$M\ddot{z} + B\dot{z} + Kz = Fu_\delta + K_r w + L_a f, \tag{4.16}$$

with $F = \left[F_1\ F_2\right]^T$. The state-space representation of the uncertain full-car model is

$$\dot{x} = Ax + B_1\tilde{w} + B_2 u, \tag{4.17}$$

where $\tilde{w} = \left[u_\delta^T\ w^T\right]$, $u = f$ and

$$A = \begin{bmatrix} 0 & I \\ -M^{-1}K & -M^{-1}B \end{bmatrix}, \quad B_1 = \begin{bmatrix} 0 & 0 \\ M^{-1}F & M^{-1}K_r \end{bmatrix}, \quad B_2 = \begin{bmatrix} 0 \\ M^{-1}L_a \end{bmatrix}.$$

4.2.2 Weighting Functions

In the control design, it is assumed that there is 20 % uncertainty in m_s, 15 % uncertainty in k_{sf}, k_{sr}, b_{sf} and b_{sr}, and 25 % uncertainty in k_{tf} and k_{tr}. In preparation for the control design, the uncertainty weighting function W_r must be selected. In the complex μ synthesis uncertainties are modeled as a complex full block with multiplicative uncertainty at the plant input. The weighting function of the unmodelled dynamics is selected

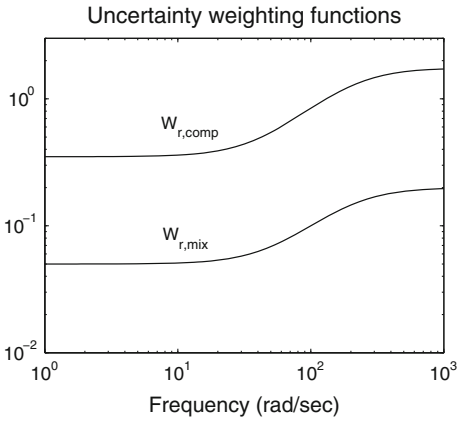

Fig. 4.5 Weighting functions for unstructured model uncertainties

$$W_{r,comp} = 0.35 \frac{\frac{s}{40} + 1}{\frac{s}{200} + 1}, \tag{4.18}$$

which is illustrated in Fig. 4.5. It means that in the low-frequency domain, uncertainties are about 35 % and, in the upper frequency domain they are up to 100 %. In the mixed μ synthesis, in which mixed uncertainty is applied, information about the model uncertainties between the model and the plant must be used in the control design, and the magnitude of the unmodeled dynamics must be reduced. The uncertainty structure contains a full complex uncertainty block, which represents the ignored actuator dynamics and real uncertainty blocks, which come from the variations of nominal parameters. Thus, it is possible to select weighting function significantly smaller than in the previous case. It means that in the low frequency domain, the modeling error is about 5 % and in the upper frequency domain it is up to 100 %.

$$W_{r,mix} = 0.05 \frac{\frac{s}{50} + 1}{\frac{s}{200} + 1} \tag{4.19}$$

If parametric uncertainties of mechanical components are known, it is possible to reduce the uncertainties for unmodeled dynamics. The magnitude of the unmodeled dynamics between the model and the plant is reduced and the weighting function for uncertainties is also reduced. In the case of mixed μ synthesis, information about the real parametric uncertainties can be used in the control design. This method yields a less conservative compensator than other robust control design methods.

4.3 Active Suspension Design Based on $\mathscr{H}_\infty$ Control

Active suspension design for linear models is based on the $\mathscr{H}_\infty$ method. The performance specifications are the sprung mass acceleration, the roll and pitch angle accelerations, suspension deflections, tire deflections, and control forces (Fig. 4.6):

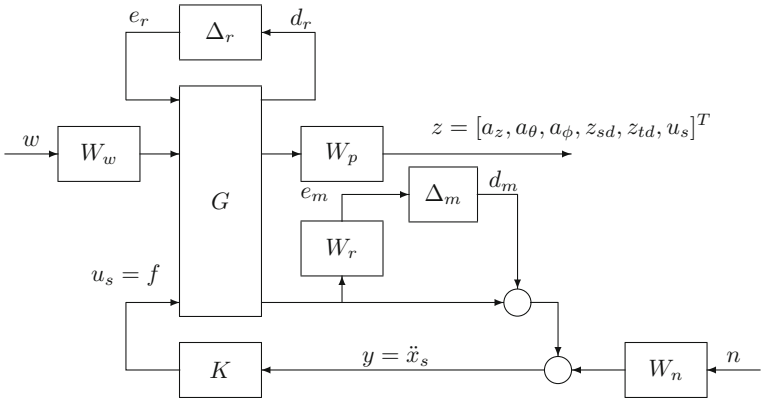

Fig. 4.6 The closed-loop interconnection structure in the $\mathscr{H}_\infty$ method

$$z = \left[a_z \; a_\theta \; a_\phi \; z_{sd} \; z_{td} \; u_s\right]^T. \tag{4.20}$$

The purpose of the weighting functions is to keep the heave, pitch and roll accelerations, suspension deflection, and tire deflection small over the desired frequency range and minimize the control input to avoid actuator saturation. Since there is a trade-off between performance specifications, weighting functions are selected in the frequency domain. The weighting functions for performance specifications, i.e., for accelerations, suspension deflections and tire deflections, are the following:

$$W_{p,az} = W_{p,\theta} = W_{p,\phi} = 0.5\frac{\frac{s}{350}+1}{\frac{s}{10}+1}, \tag{4.21}$$

$$W_{p,sd} = \frac{\frac{s}{350}+1}{\frac{s}{10}+1}, \tag{4.22}$$

$$W_{p,td} = 1. \tag{4.23}$$

The weighting functions for performances are illustrated in Fig. 4.2. The other weighting functions for the control force $W_{p,us} = 4 \times 10^{-3}$, for the road disturbance $W_w = 0.1$, and for the sensor noise $W_n = 0.001$ are selected in Sect. 4.1. In the control design it is assumed that there are 20 % uncertainty in m_s, 15 % uncertainty in k_{sf}, k_{sr}, b_{sf}, b_{sr}, and 25 % uncertainty in k_{tf} and k_{tr}. The weighting function for unmodeled dynamics is selected

$$W_{r,mix} = 0.05\frac{\frac{s}{50}+1}{\frac{s}{200}+1}, \tag{4.24}$$

which is illustrated in Fig. 4.5. The modelling of uncertainties is presented in Sect. 4.2.

Table 4.1 Summary of the D-K iteration

Iteration	#1	#2	#3
Controller order	29	37	77
D-scale order	0	8	48
Gamma achieved	13.281	2.443	0.996
Peak μ value	3.935	1.039	0.842

Table 4.2 Summary of the D, G-K iteration

Iteration	#1	#2	#3
Controller order	29	109	123
D-scale order	0	80	74
G-scale order	0	0	20
Gamma achieved	7661.89	3.929	1.233
Peak μ value	9.788	1.248	0.979

In the complex μ case, the weighting function for unmodeled dynamics is selected

$$W_{r,comp} = 0.35 \frac{\frac{s}{40} + 1}{\frac{s}{200} + 1}. \tag{4.25}$$

In the case of complex μ synthesis, in which the model uncertainties are treated with full or scalar complex blocks, the magnitude of uncertainties must be assumed larger than in the mixed μ synthesis because of the worst case principle, or the designed compensator may not be robust against uncertainties.

The nominal parameters, which are used in the design procedure, are in Table 2.1. In the case of the complex μ synthesis, the control design is performed by using the *D-K* iteration. The important values of the steps of the iteration are shown in Table 4.1. As a result of Step 3, the compensator order is selected 77, and all the nominal performance, robust stability, and robust performance are achieved. In the case of the mixed μ synthesis, control design is performed by using the *D*, *G-K* iteration method. The values of the steps of iteration are shown in Table 4.2.

Because of Step 3, the compensator order is selected 123, and all nominal performance, robust stability, and robust performance are achieved. The price of the mixed $\mathscr{H}_\infty$ synthesis is usually a controller of a larger order. It is possible to reduce the order of the controller effectively by using a model reduction method, which usually causes deterioration in the performance of the control system. The Hankel model reduction method has been applied to the controller, see Anderson and Liu (1989). The order of the controller is selected 30. The result of the μ test in Fig. 4.7 shows that robust performance properties are achieved. Thus, the controller ensures both robust stability and robust performance while the controller takes the parametric uncertainties into account.

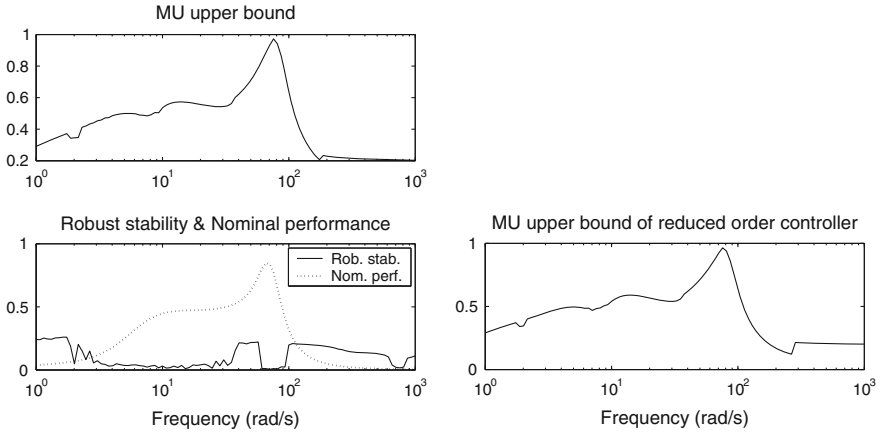

Fig. 4.7 Results of the μ test for robust performance

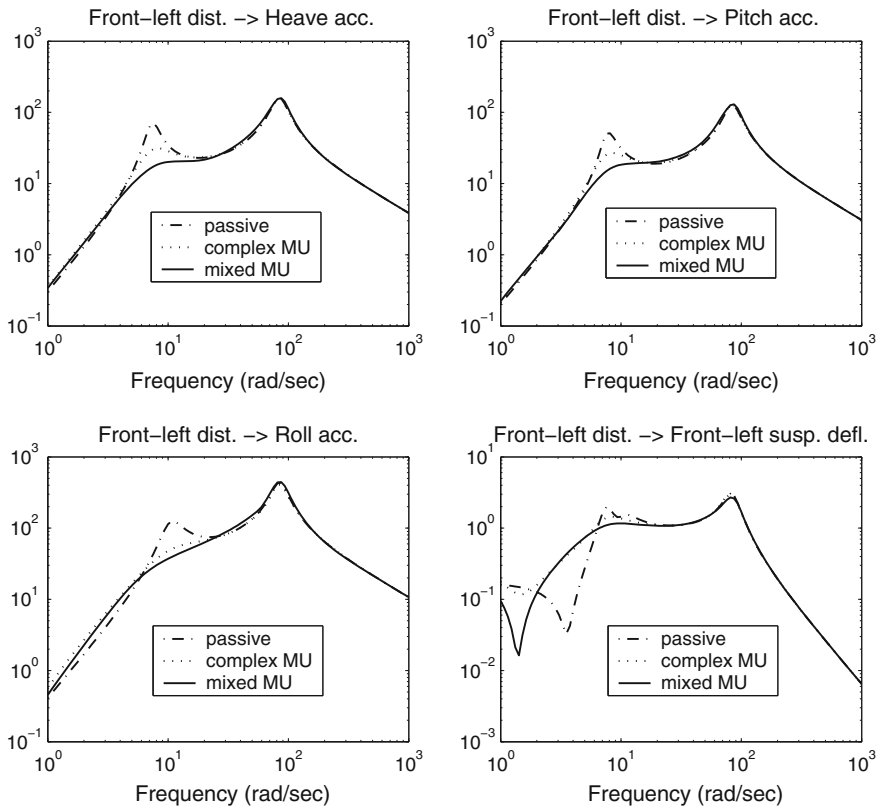

Fig. 4.8 Frequency responses of the controlled system based on the $\mathscr{H}_\infty$ method

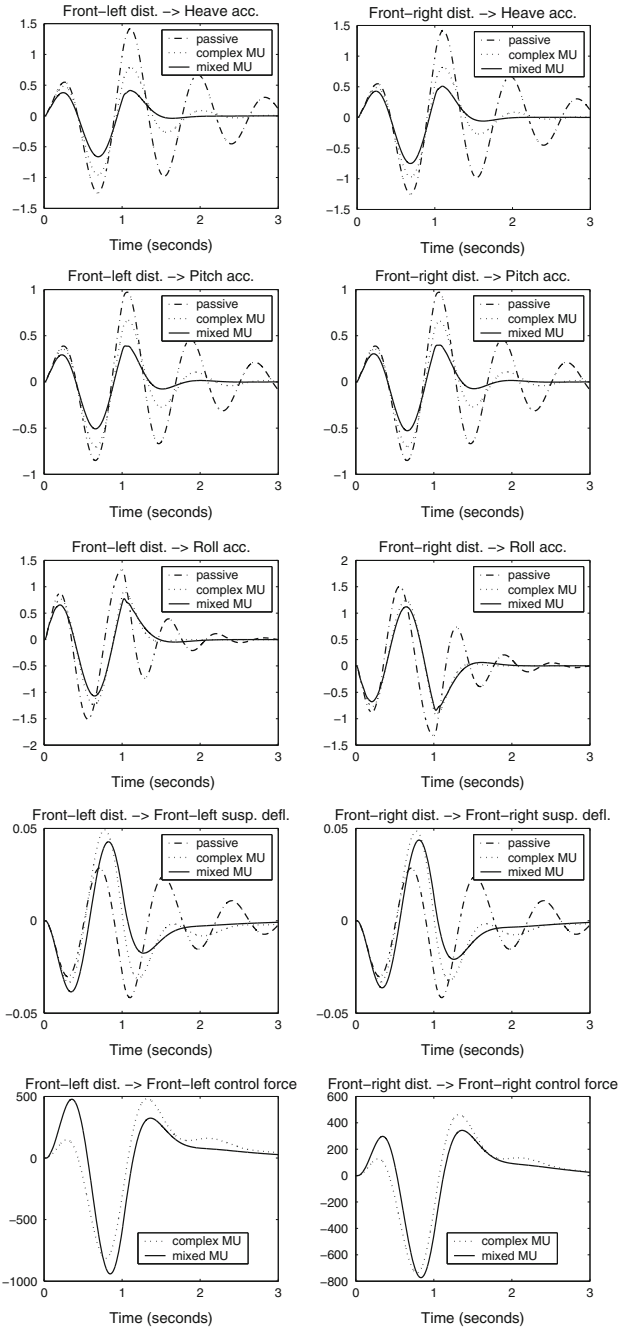

Fig. 4.9 Time responses of the system based on the $\mathscr{H}_\infty$ method to the step function

The frequency responses of the sprung mass accelerations and suspension deflections are illustrated in Fig. 4.8. The solid line corresponds to the mixed μ synthesis, the dashed line to the complex μ synthesis, the dashed-dotted line to the passive system. We can observe the reduction in vertical, pitch and roll acceleration in the low frequency range. The first amplitude peak, which corresponds to the eigen-frequency of the body mass, is larger in the case of the complex μ design, and it practically disappears in the mixed μ design. The acceleration responses are close to the passive responses in the vicinity of the tirehop frequency. This is due to the fact that the tirehop frequency is an invariant point and hence the magnitude of the responses at this point cannot be reduced by feedback.

The effects of the disturbance on accelerations, suspension deflections, and the control forces are illustrated in the time domain in Fig. 4.9. In the example, the input signal is simulated as a 5 cm high bump. The effects of the disturbance on the sprung mass acceleration are seen as large oscillations with long duration in the case of the complex μ control. The mixed μ control shows better properties in terms of both the value and the duration of the oscillation. The effects of the disturbance on suspension deflection are larger in the controlled case than in passive case due to the trade-off between passenger comfort and suspension deflection. In the mixed μ case, suspension deflection achieves its steady state value within a short time. With respect to the control force the mixed μ control requires the largest input force, however it achieves its steady state value without any oscillation.

4.4 Active Suspension Design Based on LPV Control

In this section, the design of an active suspension is based on a nonlinear model, i.e., the model contains suspension components with nonlinear behavior and actuator dynamics. The aim is to design an active suspension system based on the LPV method. In the LPV model, three parameters are selected, which are linked to the relative displacement, the relative velocity, and the load pressure of the actuator: $\rho = \begin{bmatrix} \rho_{ks} & \rho_b & \rho_Q \end{bmatrix}^T$.

The control design is based on a closed-loop interconnection structure. The measured signal is the suspension deflection. The performances are the sprung mass acceleration, suspension deflection, tire deflection, and the control force

$$z = \begin{bmatrix} a_z & z_{sd} & z_{td} & u_s \end{bmatrix}^T. \tag{4.26}$$

The augmented plant includes the parameter-dependent vehicle dynamics and the weighting functions, which are defined in the following form:

$$\begin{bmatrix} \tilde{z} \\ y \end{bmatrix} = P(\rho) \begin{bmatrix} \tilde{w} \\ u \end{bmatrix}, \tag{4.27}$$

where $\tilde{w} = \begin{bmatrix} d_m & w & n \end{bmatrix}^T$, $\tilde{z} = \begin{bmatrix} e_m & z \end{bmatrix}^T$. In the LPV model ρ denotes the scheduling variable.

The closed-loop system $M_r(\rho)$ is given by a lower LFT structure:

$$M(\rho) = \mathscr{F}_\ell(P(\rho), K(\rho)), \tag{4.28}$$

where $K(\rho)$ also depends on the scheduling variable ρ. The goal of the control design is to minimize the induced $\mathscr{L}_2$ norm of an LPV system $M(\rho)$, with zero initial conditions, which is given by

$$\|M(\rho)\|_\infty = \sup_{\rho \in \mathscr{F}_\mathscr{P}} \sup_{\|\tilde{w}\|_2 \neq 0, \tilde{w} \in \mathscr{L}_2} \frac{\|\tilde{z}\|_2}{\|\tilde{w}\|_2}. \tag{4.29}$$

The weighting functions for performance specifications are the following:

$$W_{p,az} = \phi_{az}(\rho_k) \cdot \frac{0.5(\frac{s}{350} + 1)}{\frac{s}{10} + 1}, \tag{4.30}$$

$$W_{p,sd} = \phi_{sd}(\rho_k) \cdot \frac{\frac{s}{350} + 1}{\frac{s}{10} + 1}, \tag{4.31}$$

$$W_{p,td} = 1, \tag{4.32}$$

where $\rho_k = x_2 - x_1$ is the relative displacement between the sprung and the unsprung masses. Here, the gains $\phi_{az}(\rho_k)$ and $\phi_{sd}(\rho_k)$ are selected in a parameter-dependent way. The selection of these gains is presented in Sect. 4.1 and illustrated in Fig. 4.3.

$$\phi_{az}(\rho_k) = \begin{cases} 1 & \text{if} \quad |\rho_k| < \rho_1 \\ \frac{1}{\rho_1 - \rho_2}(|\rho_k| - \rho_2) & \text{if} \quad \rho_1 \leq |\rho_k| \leq \rho_2 \\ 0 & \text{otherwise} \end{cases}, \tag{4.33}$$

$$\phi_{sd}(\rho_k) = \begin{cases} 0 & \text{if} \quad |\rho_k| < \rho_1 \\ \frac{1}{\rho_2 - \rho_1}(|\rho_k| - \rho_1) & \text{if} \quad \rho_1 \leq |\rho_k| \leq \rho_2 \\ 1 & \text{otherwise} \end{cases}. \tag{4.34}$$

The purpose of the suspension controller is to emphasize different performance objectives depending on the magnitude of suspension deflection. When suspension deflection is small, the controller should focus on passenger comfort. As the deflection limit is approached, the controller should focus on preventing suspension deflection from exceeding this limit. The other weighting functions selected for the control force $W_{p,us} = 4 \times 10^{-3}$, for the road disturbance $W_w = 0.1$, and for the sensor noise $W_n = 0.001$ are selected in Sect. 4.1. In control design model, uncertainties are also taken into consideration as unmodeled dynamics. The weighting function for unmodeled dynamics is selected

$$W_r = 0.35 \frac{\frac{s}{40} + 1}{\frac{s}{200} + 1} \tag{4.35}$$

In the design of the LPV control, three signals are used to calculate the parameters in the scheduling vector $\rho = \begin{bmatrix} \rho_k & \rho_{ks} & \rho_b & \rho_Q \end{bmatrix}^T$. Parameter ρ_k is equal to the relative displacement, then its square ρ_{ks} is calculated. Parameter ρ_b depends on the signum of the relative velocity. In practice, the relative displacement is a measured signal. The relative velocity is usually determined by numerical differentiation from the measured relative displacement. Parameter ρ_Q is linked to the load pressure of the actuator, which is assumed to be calculated directly from Eq. (2.57). For the interconnection structure, an LPV controller is synthesized for six values of each scheduling variable. Weighting functions for both the performance and robustness specifications are defined in all of the grid points. With respect to the robustness requirement, the same frequency weighting functions are applied in the whole parameter space and the effect of the scheduling variable is neglected. It is a reasonable engineering assumption, since unmodeled dynamics does not depend on the forward velocity. Note that although weighting functions are formalized in the frequency domain, their state-space representation forms are applied in the weighting strategy and in the control design.

The nominal parameters of the quarter-car model are in Table 2.3. In the first demonstration example the *LPV* controller, in which a balance between the minimization of the heave acceleration and suspension deflection are taken into consideration, is analyzed. The controlled systems are tested by using bumps of different heights, i.e., 3, 5, 8, and 10 cm. The time responses of the heave acceleration, suspension deflection, tire deflection, and the control force are illustrated in Fig. 4.10.

In the second example, the *LPV* synthesis is performed in three different approaches. They differ in the weighting strategy applied. In the first case, the focus of the control design is passenger comfort, i.e., $\Phi_{az} = 1$ is constant. In the second case, the focus is the suspension deflection, i.e., $\Phi_{sd} = 1$ is constant. Finally, in the

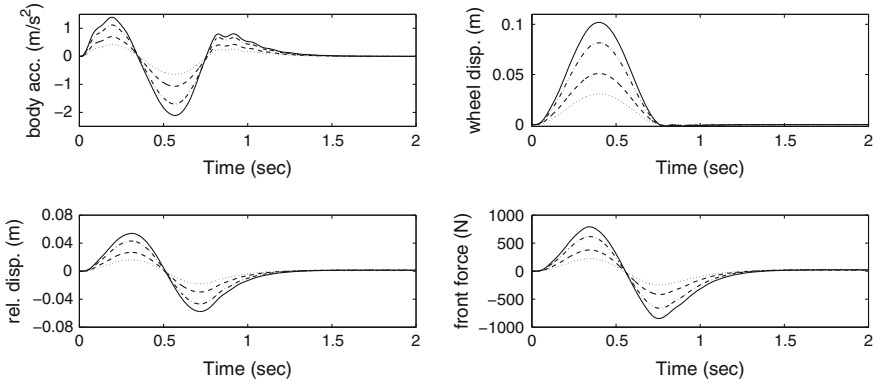

Fig. 4.10 Time responses of the controlled system using an *LPV* controller to different bumps

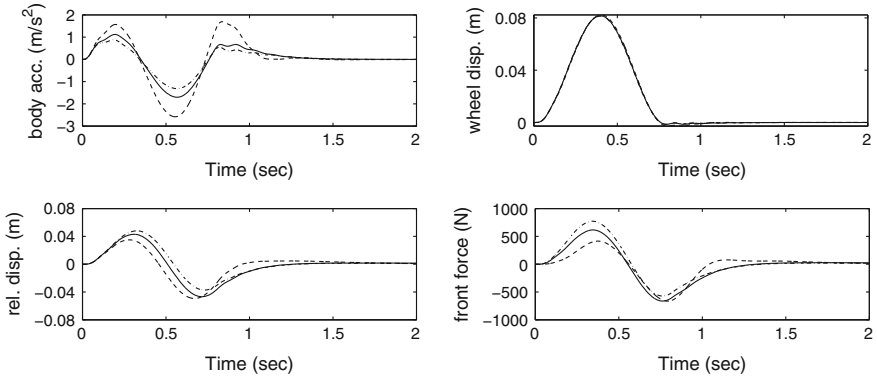

Fig. 4.11 Time responses of the controlled system using LPV controllers to a bump

third case both Φ_{az} and Φ_{sd} are scheduled, i.e., if either of them decreases the other increases and vice versa. In this way, the third solution guarantees a trade-off between passenger comfort and suspension deflection.

The controlled systems are tested by using an 8 cm high bump. The time responses of the heave accelerations, suspension deflections, tire deflections and the control forces are illustrated in Fig. 4.11. The solid line corresponds to the *LPV* synthesis in which a balance between the minimization of the vertical acceleration and suspension deflection are taken into consideration. The dashed line illustrates the result of the synthesis, in which the control design focuses only on the minimization of the vertical acceleration, while the dashed-dotted line illustrates the case when only suspension deflection is minimized.

In the case of the *LPV*-based controlled system, in which a balance between the different optimization criteria is taken into consideration, the effects of the disturbance both on the sprung mass acceleration and suspension deflection are seen as relatively small oscillations with short duration. The control system minimizes only the vertical acceleration when suspension deflection is less than 5 cm. It gradually begins focusing on suspension deflection when it is greater than 5 cm. Over 8 cm it minimizes only suspension deflection. In the case of the *LPV* control which only takes the body mass acceleration into consideration, the effects of the disturbance on suspension deflection generate larger values than the physical limit of the working space. In the case of the *LPV* control which minimizes only suspension deflection, the effects of the disturbance on the sprung mass acceleration are seen as large oscillations with long duration.

Note that in practice semi-active suspension systems are applied. An important book was published in the analysis and control of semi-active suspension control, see Savaresi et al. (2010), Poussot-Vassal et al. (2008, 2011).

4.5 Design of a Hierarchical Controller for an Active Suspension System

In the suspension designs, the highly nonlinear actuator can be considered in an additional step by imposing a tracking problem of the nonlinear dynamics for the given suspension force, see Alleyne and Hedrick (1995), Alleyne and Liu (2000), Zhang and Alleyne (2002). In these schemes, the additional delay introduced in the control loop might yield a serious performance degradation. A robust state feedback solution for this problem was proposed in Du and Zhang (2007) and an output feedback solution in Briat et al. (2009).

A different approach was proposed in Fialho and Balas (2002) where the separating layer was moved into the actuator by adding a linear equation for the pressure through the hydraulic piston to the quarter-car model. The remaining part from the actuator, i.e., the dynamic equations for the valve is related to this system through a fictitious input that contains all the nonlinearities of the actuator as a static expression. While both models are LTI by introducing scheduled performance weights the overall design is an LPV one. In contrast to these two-level approaches in Gáspár et al. (2003b) a joint scheme was proposed for a LPV quarter-car model and a hydraulic actuator where all the nonlinearities were handled using certain scheduling variables in a single LPV model.

Global vehicle control is now an important issue in the future of vehicle control technology. The aim of the integrated control methodologies is to combine and supervise all controllable subsystems affecting vehicle dynamic responses in order to ensure the management of resources. The solution might be the integration of the control logic of subsystems which assumes a more complex modeling technique, i.e., a full-car model.

The approach followed in Gáspár et al. (2003b) cannot be applied directly for a full-car model due to the increased complexity of the resulting control problem. In this paper, the design of a two-level controller is proposed for integrated active suspension systems which contain nonlinear suspension components and actuator dynamics. LPV design presented in the paper is proposed for active suspensions.

In the design of a high-level controller a full-car LPV model containing the suspension dynamics is considered where passenger comfort, road holding, and tire deflection are taken into consideration as performance outputs and the control input designed is the control force. In this step, the uncertainties of the model are also considered. A weighting strategy is applied to meet performance specifications, i.e., passenger comfort and road holding, guarantee a trade-off between performances that are in conflict with each other and consider the model uncertainties.

The designed control force is a required force, which must be created by the hydraulic actuator. The required force is tracked by a low-level controller by setting the valve of the actuator. The backstepping-based nonlinear method is presented for the design of the low-level controller. This approach explores the possibilities of the application of classical nonlinear control techniques for the output tracking control of an actuator subsystem used in active suspensions.

The advantage of the two-level method proposed in this paper is that the actuator dynamics and the suspension dynamics are handled in two independent control design steps. The proposed separation layers met the intuitive structure of the different subsystems, i.e., chassis and actuators while keeping the complexity of resulting control problems between reasonable bounds. In contrast to Fialho and Balas (2002) this approach allows a modular design—changes in the actuator do not affect the upper level design.

4.5.1 Modeling of the Actuator Dynamics

The required force designed by the high-level controller must be tracked by a low-level controller by setting the valve of the actuator. In order to provide a formal test of the achieved control configuration at a global level, one has to formulate the problem globally. Once the local controllers are designed, it is possible, in principle, to perform an analysis step in the same robust control framework at a global level, for details see Langbort et al. (2004). This might be an unreliable and highly computational-intensive procedure. Therefore in practice this step is omitted and the quality of the overall control scheme is assessed through simulation experiments.

The control forces designed by the high-level control are the required forces in the front and the rear at the right and the left-hand sides of the vehicle. These required forces must be tracked by the low-level controllers by setting the valve of the corresponding actuators. The hydraulic actuator which generates the necessary force for the suspension system is a four-way valve-piston system. In this paper, a nonlinear model of an electrical hydraulic actuator is used, e.g., Alleyne and Hedrick (1995), Fialho and Balas (2002), Merritt (1967).

The force of the actuator is expressed in the following way:

$$f_{ij} = A_P P_{Lij}, \tag{4.36}$$

where A_P is the area of the piston and P_{Lij} $(i \in f, r, j \in l, r)$ is the pressure drop across the piston, Merritt (1967). The derivative of P_{Lij} is given by

$$\dot{P}_{Lij} = -\beta P_{Lij} + \alpha A_P z_{ij} + \gamma Q_{ij}, \tag{4.37}$$

in which Q_{ij} is the hydraulic load flow, $z_{ij} = \dot{x}_{2ij} - \dot{x}_{1ij}$ is the damper velocity and α, β, γ are constants. The hydraulic load flow can be expressed using (2.57).

The displacement of the spool valve is controlled by the input to the servo-valve u_{ij}

$$\dot{x}_{vij} = \frac{1}{\tau_{ij}} \left(-x_{vij} + u_{ij} \right). \tag{4.38}$$

where τ_{ij} is a time constant.

Each of the four actuator models are formalized separately based on the generic model which is used for the design of the low-level control as

$$\dot{\xi}_1 = -\beta\xi_1 + \gamma Q_0(\xi_1, \xi_2)\xi_2 + \alpha A_P z, \tag{4.39}$$

$$\dot{\xi}_2 = -\frac{1}{\tau}\xi_2 + \frac{1}{\tau}u. \tag{4.40}$$

for the ijth actuator with ξ_1 and ξ_2 denote P_{Lij} and x_{vij}, respectively, while $Q_0 = Q_{0ij}$ $z = z_{ij}$ and $\tau = \tau_{ij}$.

It is assumed that the reference for the force demand (which is a linear function of ξ_1) is given by the LPV controller. The goal is to asymptotically track this reference with the actuator dynamics. Since the actuator subsystem and the suspension subsystem form a cascade of a nonlinear and a LPV system, the backstepping methodology, or an approach based on the exact linearization of the actuator dynamics, is an appropriate choice for our control goal. In what follows for the sake of completeness both methods will be presented.

Remark 4.1 Note that the control design in the actuator level can also be performed by using LPV methods. In order to reduce the complexity of the control design the actuator dynamics is built into the quarter-car model, illustrated in Fig. 2.9. The equations of the quarter-car model are

$$m_s\ddot{x}_1 = F_{kf} + F_{bf} - f_f \tag{4.41}$$

$$m_u\ddot{x}_2 = -F_{kf} - F_{bf} - F_{tf} + f_f \tag{4.42}$$

$$\dot{P}_L = -\beta P_L + \alpha A_P(\dot{x}_2 - \dot{x}_1) + \gamma Q \tag{4.43}$$

$$\dot{x}_v = -\frac{1}{\tau}x_v + \frac{1}{\tau}u. \tag{4.44}$$

where $f_f = A_P P_L$, $Q = sgn(P_S - sgn(x_v)P_L)Q_0 x_v$.

The state-space representation of vertical dynamics

$$\dot{x} = A(\rho)x + B(\rho)u, \tag{4.45}$$

The components of the state vector are the vertical displacement of the sprung mass x_1, the vertical displacement of the unsprung mass x_2, their derivatives $x_3 = \dot{x}_1$, $x_4 = \dot{x}_2$, the pressure drop $x_5(= P_L)$, and the servo-valve displacement $x_6(= x_v)$. The input signal is the input to the servo-valve. Scheduling vector is selected as $\rho_s = \begin{bmatrix}\rho_Q & \rho_b & \rho_k\end{bmatrix}$ where the scheduling variables are assumed to be available

$$\rho_Q = sgn(P_S - sgn(x_v)P_L)Q_0,$$
$$\rho_b = \dot{x}_2 - \dot{x}_1,$$
$$\rho_k = x_2 - x_1.$$

The advantages of this approach are that in the control-oriented model the nonlinear behavior of suspension components, the actuator dynamics and the performance specifications are taken into consideration. Moreover, the control design is based on LPV methods. However, the disadvantage is that the solution does not provide modularity in the design. The details can be seen in Gáspár et al. (2003b).

4.5.2 Tracking Control Based on Backstepping Design

The LPV system augmented by four times the dynamics of (4.39) and (4.40) is a cascaded system

$$\dot{\zeta} = A(\zeta)\zeta + B(\zeta)[\xi_1^{ij}], \tag{4.46}$$

$$\dot{\xi}_1^{ij} = a_1(\zeta, \xi_1^{ij}) + b_1(\xi_1^{ij}, \xi_2^{ij})\xi_2^{ij}, \tag{4.47}$$

$$\dot{\xi}_2^{ij} = a_2(\xi_2^{ij}) + b_2 u, \tag{4.48}$$

that can be put in the strict feedback form, see Chap. 6. of Sepulchre et al. (1997),

$$\dot{\zeta} = A(\zeta)\zeta + B(\zeta)[\xi_1^{ij}], \tag{4.49}$$

$$\dot{\xi}_1^{ij} = a_1(\zeta, \xi_1^{ij}) + \tilde{\xi}_2^{ij}, \tag{4.50}$$

$$\dot{\tilde{\xi}}_2^{ij} = \tilde{a}_2(\xi_1^{ij}, \tilde{\xi}_2^{ij}) + \tilde{b}_2(\xi_1^{ij}, \tilde{\xi}_2^{ij})u, \tag{4.51}$$

by using the state transform $\tilde{\xi}_2^{ij} = b_1(\xi_1^{ij}, \xi_2^{ij})\xi_2^{ij}$. For the resulting system a standard recursive backstepping method can be applied according to Sepulchre et al. (1997), van der Schaft (2000). Since the nominal system (4.49) is globally asymptotically stable by construction the resulting closed-loop system containing the tracking controllers will be stable, see e.g., Chap. 5 in van der Schaft (2000).

In what follows, the main steps that lead to the tracking control on each of the actuators will be presented. In order to show the principle of the method, the notations of van der Schaft (2000) are used. The pressure demand $P_{L,dem}$ required by the high-level control and given by the feedback $K(\zeta)$ will be denoted by $\xi_{1,dem}$ while $\xi_{2,dem}$ denotes the demand of the spool valve displacement $x_{v,dem}$. The state transform that leads to the strict feedback form is needed only to relate the original system to the already developed passivity-based framework of cascaded systems. The actual computations can be done on the original system.

The backstepping design for the actuator subsystem can be performed in two steps. In the first step, let us consider $\xi_{2,dem}$ as a virtual input and $y_1 = \xi_1 - K(\zeta)$ as a virtual output. Since ξ_1 is not a manipulable input, we would like to construct a feedback that guarantees the tracking of $K(\zeta)$ with ξ_1. It is reasonable therefore to define the tracking error to be linear and stable, i.e., $\dot{y}_1 = -k_1 y_1$, $k_1 > 0$. Using (4.46) and (4.47) the desired time-function for $\xi_{2,dem}$ can be computed as a nonlinear feedback of the form

$$\xi_{2,dem} = \frac{1}{b_1(\xi_1, \xi_{2,dem})}[-a_1(\zeta, \xi_1) + \dot{K}(\zeta) - \\ - k_1(\xi_1 - K(\zeta))]. \tag{4.52}$$

In the second step, the desired input is u while the (virtual) output is defined as $y_2 = \xi_2 - \xi_{2,dem}$. For the tracking error, a stable linear dynamics is prescribed: $\dot{y}_2 = -k_2 y_2$, $k_2 > 0$. Using (4.46)–(4.48), we can now express the physically manipulable actuator input u as a function of ζ, ξ_1, and ξ_2 in the following form:

$$u = \frac{1}{b_2}[-a_2(\xi_2) + \dot{\xi}_{2,dem}]. \tag{4.53}$$

By applying the above design, the closed-loop system will be asymptotically stable with Lyapunov function $S(\zeta, y_1, y_2) = V(\zeta) + \frac{1}{2}y_1^2 + \frac{1}{2}y_2^2$ (see Sepulchre et al. 1997), where $V(\zeta)$ is the Lyapunov function resulting from the high-level LPV design.

Since $a_1(\zeta, \xi_1) = -\beta\xi_1 + \alpha A_P z$ and $b_1(\xi_1, \xi_2) = \gamma Q_0(\xi_1, \xi_2)$ one has

$$\xi_{2,dem} = \frac{-\beta\xi_1 + \alpha A_P z + \dot{\xi}_{1,dem} - k_1(\xi_1 - \xi_{1,dem})}{\gamma Q_0(\xi_1, \xi_{2,dem})}.$$

The tracking error dynamics for $\xi_{2,dem}$ is written as

$$\dot{\xi}_2 - \dot{\xi}_{2,dem} = -k_2(\xi_2 - \xi_{2,dem}). \tag{4.54}$$

with a chosen positive constant parameter k_2. This gives

$$-\frac{1}{\tau}\xi_2 + \frac{1}{\tau}u - \dot{\xi}_{2,dem} = -k_2(\xi_2 - \xi_{2,dem}), \tag{4.55}$$

from which the following expression for the physical input u_{ij} is deduced:

$$u = \xi_2 + \tau\dot{\xi}_{2,dem} - \tau k_2(\xi_2 - \xi_{2,dem}). \tag{4.56}$$

In this method, the controller parameters k_1 and k_2 determine the convergence speed of the virtual outputs y_1 and y_2, respectively. As a conclusion in the backstepping method two parameters, k_1 and k_2, are chosen to handle the dynamics of the tracking. By selecting suitable parameters the accuracy of tracking can be improved but the physical limits of the actuator must be taken into consideration. Failing to do so may result in discrepancy between the planned and the realized forces, i.e., tracking error.

The algorithm uses both $\dot{\xi}_{1,dem}$ and $\dot{\xi}_{2,dem}$, which are not measured. In order to practically implement the control law, we need to compute the time derivatives of $\xi_{1,dem}$ and $\xi_{2,dem}$, which can be done in a number of ways depending on the measurement noise conditions and the required precision. Possible strategies for numerical

differentiation are contained in Diop et al. (2000), Levant (2003), Vasiljevic and Khalil (2006).

We conclude this section by showing that the choice of σ in the regularization of the sign function does not influence the practical implementation. In the second step of the backstepping algorithm, one has to compute the derivative of $\xi_{2,dem}$, i.e.,

$$\begin{aligned}\frac{d}{dt}(\Psi) &= \frac{d}{dt}\left(\xi_{2,dem}\gamma Q_0(\xi_1, \xi_{2,dem})\right) = \\ &= \frac{d}{dt}\left(-\beta\xi_1 + \alpha A_P z + +\dot{\xi}_{1,dem} - k_1(\xi_1 - \xi_{1,dem})\right). \end{aligned} \tag{4.57}$$

By performing the computations one has

$$\dot{\xi}_{2,dem}\left(1 + \frac{\gamma}{2Q_0^2}\frac{\xi_{2,dem}/\sigma}{\cosh^2(\xi_{2,dem}/\sigma)}\right) = \frac{1}{Q_0}\left(\dot{\Psi} - \xi_{2,dem}\gamma\frac{\dot{\xi}_1\tanh(\xi_{2,dem}/\sigma)}{2Q_0}\right) \tag{4.58}$$

Since the function $\max\{\|\frac{x/\sigma}{\cosh^2(x/\sigma)}\|\} \to 0$ very fast as $\sigma \to 0$ one has that for sufficiently small σ

$$\dot{\xi}_{2,dem} = \frac{1}{Q_0}\left(\dot{\Psi} - \xi_{2,dem}\gamma\frac{\dot{\xi}_1 \text{sign}(\xi_{2,dem})}{2Q_0}\right), \tag{4.59}$$

i.e., $\dot{\xi}_{2,dem}$ can be computed as if the non-smoothness of the sign function were ignored.

The algorithm of the backstepping method is illustrated in Fig. 4.12. The measured signals required by the algorithm are $\xi = P_L$, $x_2 = x_v$ and z. The implementation of the backstepping method requires the computation of the time derivatives of $\dot{\xi}_1 = \dot{P}_L$, $\ddot{\xi}_1 = \ddot{P}_L$, $\xi_{1,dem} = P_{L,dem}$ and $\dot{z}$ which can be done in a number of ways depending on the measurement noise conditions and the required precision. In this method, the

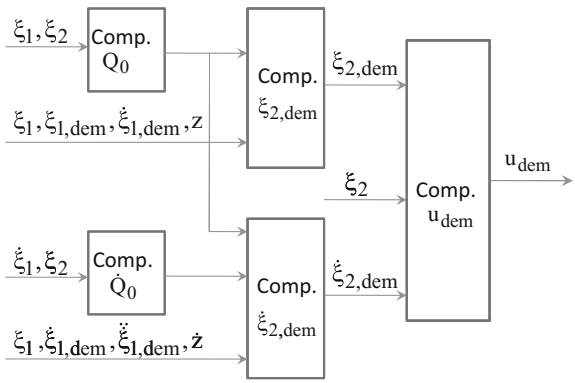

Fig. 4.12 Illustration of the backstepping method

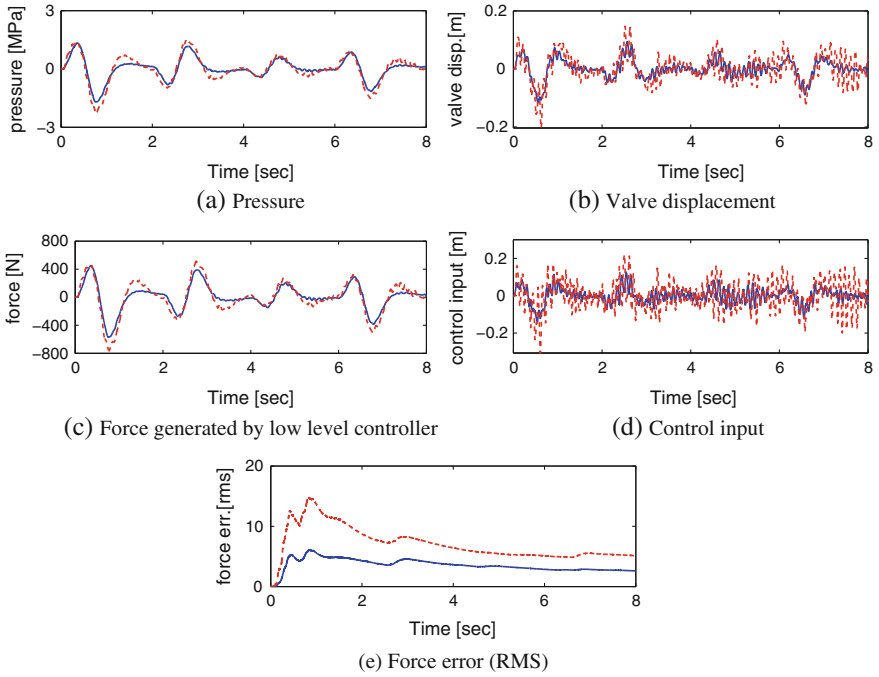

Fig. 4.13 Analysis of the tracking properties using the nonlinear control design methods (*solid* backstepping method, *dashed* feedback-linearization method)

controller parameters k_1 and k_2 determine the convergence speed of the tracking errors e_1 and e_2, respectively. As a conclusion in the backstepping method two parameters, k_1 and k_2 are chosen to handle the dynamics of the tracking. By selecting suitable parameters the accuracy of tracking can be improved but the physical limits of the actuator must be taken into consideration. Failing to do so may result in discrepancy between the planned and the realized forces, i.e., tracking error. Possible strategies for numerical differentiation are contained in Levant (2003), Vasiljevic and Khalil (2006).

4.5.3 Simulation Examples

The operation of the low-level force-tracking controllers is illustrated in Fig. 4.13. In the control design the parameters are selected as $k_i = 20$ for the backstepping method. In the simulation example the sampling time of the measured signals is selected $T_s = 0.01$ s, which corresponds to practice. The illustrated signals are the pressure drop across the piston, the displacement of the spool valve, the control input, the achieved force and the RMS of the force error. In both cases, the achieved force

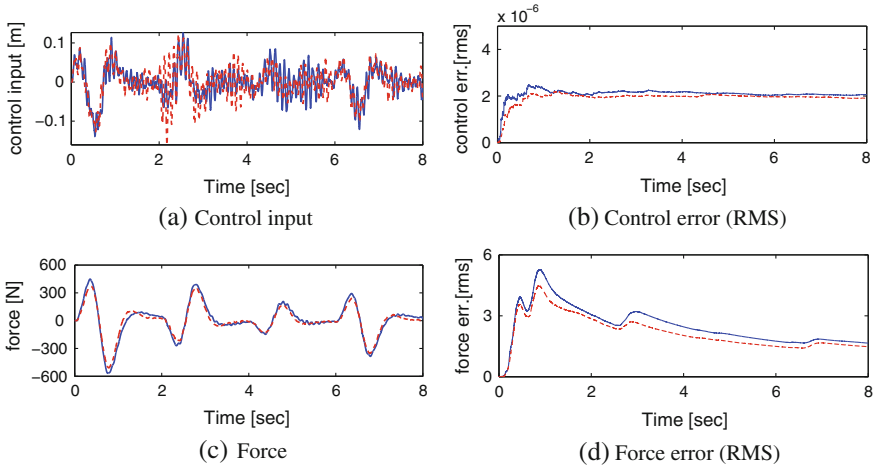

(a) Control input (b) Control error (RMS)

(c) Force (d) Force error (RMS)

Fig. 4.14 The effect of the actuator parameter τ in the backstepping method (*solid* $\tau = 1/30\,\mathrm{s}$, *dashed* $\tau = 1/27\,\mathrm{s}$)

generated by the actuator follows the required force with high precision. However, the simulations indicate that the backstepping method performs slightly better. The hairy plot for the generated input of the feedback design is due to the repeated numerical differentiation.

The tracking properties of the backstepping scheme are also tested in an uncertain case. The low-level controller is based on a nominal nonlinear system, hence its robustness against uncertainties—in contrast to the high-level controller—is not guaranteed by the design procedure. Here, the uncertainty of the parameter τ is taken into consideration. τ defines the dynamics between the control input and the displacement of the spool valve according to the Eq. (4.40). In the analysis besides the nominal value of $\tau_{nom} = 1/30\,\mathrm{s}$ the uncertain $\tau_{act} = 1/27\,\mathrm{s}$ is considered. The control input, the RMS of the control error, the achieved force and the RMS of the force are illustrated in Fig. 4.14. The results show robustness of the control scheme against this parametric uncertainty.

The nominal parameters which are used in the design procedure are listed in Table 2.1. The controllers are designed and implemented by using the MATLAB®/Simulink® software. The verification of the designed controller is performed by using the CarSim simulation software, in which the vehicle is represented with high accuracy.

Chapter 5
Anti-roll Bars for Rollover Prevention

Introduction

The aim of rollover prevention is to provide the vehicle with an ability to resist overturning moments generated during cornering. The problem with heavy vehicles in terms of roll stability is a relatively high mass center and narrow track width. When the vehicle is changing lanes or trying to go round obstacles, the vehicle body rolls out of the bend and the center of mass shifts out of the centerline, and a destabilizing moment is created. The lateral load transfer ratio has an important role in the prediction of the rollover Larish et al. (2013). In the literature there are several papers on the active control of heavy vehicles with different approaches to reducing rollover risk. Three main schemes concerned with the possible active intervention into the vehicle dynamics have been proposed: active anti-roll bars, active steering, and an active brake.

One of the methods proposed in the literature employs active anti-roll bars by using a pair of hydraulic actuators in order to improve the roll stability of heavy vehicles, Németh et al. (2015b). The lateral acceleration makes vehicles with conventional passive suspensions tilt out of the bend. The center of the sprung mass shifts out of the vehicle centerline and this creates a destabilizing moment that reduces roll stability. The lateral load response is reduced by active anti-roll bars, which generate a stabilizing moment to balance the overturning moment in such a way that the control torque leans the vehicle into the bend, see Lin et al. (1996), Sampson and Cebon (1998), Sampson (2000), Sampson and Cebon (2003). The ride and roll performances for an active anti-roll bar system are analyzed in Zulkarnain et al. (2012). In another case, the combined roll moment of the front and rear suspensions is designed to reduce body roll and distribute the roll moment, see Abe (1994), Hwang and Park (1995), Kim and Park (2004).

In the second method, an enhanced roll stability control system focusing on rollover prevention by active steering is presented. An actuator sets a small auxiliary front wheel steering angle in addition to the steering angle commanded by the driver. The aim is to reduce the rollover risk due to the transient roll overshoot of the vehicle when changing lanes or going round obstacles. The advantage of the active

P. Gáspár et al., *Robust Control Design for Active Driver Assistance Systems*,
Advances in Industrial Control, DOI 10.1007/978-3-319-46126-7_5

steering control is that it affects the lateral acceleration directly, see Mammar and Koenig (2002). However the active steering control has an effect on not only the roll dynamics of the vehicle, but it also modifies the desired path of the vehicle, so it affects the yaw motion. In this control, a proportional feedback of both the roll rate and the roll acceleration is used, see Ackermann and Bünte (1998). One extension of this method is the gain scheduling method, which takes into account the change in velocity of the vehicle and the height of the center of gravity, see Ackermann and Odenthal (1999). This control concept is also extended by a nonlinear steering control loop to prevent rollovers, see Ackermann et al. (1995), Odenthal et al. (1999).

In the third method, an electronic brake mechanism which enhances rollover stability is proposed. In this method a small brake force is applied to each of the wheels and the slip response is monitored. In this way, it is possible to establish whether a given wheel is lightly loaded and the lift-off is imminent. When an emergency is detected, unilateral brake forces are activated to reduce the lateral tire forces acting on outside wheels, see Palkovics et al. (1999), Frank et al. (2000), Chen and Peng (2001), Gáspár et al. (1998), Alberding et al. (2014). The brake system directly reduces the lateral tire force, which is responsible for the rollover. Additional reasons for using the brake system of a vehicle are the use of the most appropriate actuator and the low cost of the solution.

It should be noted that the disadvantage of the active anti-roll bars is that the maximum stabilizing moment is limited physically by the relative roll angle between the body and the axle. The active anti-roll bars do not effect the yaw motion of the vehicle directly, while the steering control and the brake control do. Both with active steering and an active brake control the only physical limit is the saturation of the actuator. These compensators, however, have effects not only on the roll dynamics of the vehicle but they also modify the desired path of the vehicle, so they affect the yaw motion. Thus, the different control structures should be combined in one control mechanism. In Odenthal et al. (1999) the linear steering control is extended by nonlinear emergency steering and braking control. As far as autonomous vehicle control is concerned, a combination of the brake and throttle are proposed, see Hedrick et al. (1997), Hedrick and Uchanski (2001).

Several solutions have been proposed to prevent the rollover of heavy vehicles by using the LPV method. Active anti-roll bars, an active brake, an active steering, and an active suspension system have been proposed in Gáspár et al. (2003c, e, 2004a, b, 2006), Gáspár and Bokor (2005). A combination of the active brake and active anti-roll bars has been proposed in Gáspár et al. (2003d). A combination of an active brake and an active suspension has been proposed in Gáspár et al. (2004a). A fault-tolerant control structure with active control mechanisms, i.e., an active suspension, active anti-roll bars and an active brake mechanism, has been proposed in Gáspár and Bokor (2006), Gáspár et al. (2005a). The purpose of this control structure is to improve rollover prevention and passenger comfort and guarantee the suspension working space. The benefits of the integration of anti- roll bars and the lateral control are presented in Yim et al. (2012). Further methods, such as self-tuning fuzzy and switching LQ-type anti-roll bar controllers are proposed in Muniandy et al. (2015), Varga et al. (2015).

Several researchers have focused on the integration of control systems. Kiencke (1995) focused on the combined use of brakes and rear-steer to augment the driver's front-steer input in controlling the yaw dynamics. Hirano et al. (1993) proposed a four-wheel steer and four-wheel drive ($4WS/4WD$) controller via feedforward and feedback compensators. Nagai et al. (1998) designed an integrated control system with RWS and integrated yaw moment control. Trachtler (2004a) constructed an integrated vehicle control of active chassis systems, see also Trachtler (2004b). Mastinu et al. (1994) created an integrated control by using steering and suspension systems. Zin et al. (2005) proposed a global chassis control involving an active suspension and ABS to improve road holding and passenger comfort. Several control solutions have also been suggested as a result of the PATH project, see Maciuca (1996), Hedrick et al. (1997), Prohaska and Devlin (1997), Hedrick and Uchanski (2001). Rajamani and Piyabongkarn (2013) focuses on an integrated control wherein the objectives of yaw stability and rollover prevention are addressed simultaneously. Thus, a tradeoff between yaw stability, speed, and rollover prevention performance through steer-by-wire is achieved.

5.1 Modelling of Performances in the Yaw–Roll Dynamics

5.1.1 Rollover Threshold

The objective of the roll control system is to enhance the roll stability of the vehicle. The rollover of the vehicle starts when, in a bend, the tire contact force on the inner wheels has become zero. The rollover is caused by the high lateral inertial force generated by lateral acceleration. If the position of the center of gravity (CG) is high or the forward velocity of the vehicle is larger than allowed at a given steering angle, the resulting lateral acceleration is also large and might cause a rollover.

Definition 5.1 (*Rollover threshold*) Sampson (2000) The rollover threshold is the limit of steady-state lateral acceleration that a vehicle can sustain without losing roll stability

The lateral tire forces generated at the ground during cornering produce a steady-state lateral acceleration of the vehicle, see Fig. 5.1. Three moments act on the vehicle: the overturning moment arising from the lateral acceleration ($ma_y h$), the restoring moment arising from the lateral load transfer from the inside tires to the outside tires ($\Delta F_z \ell_w$), and the lateral displacement moment arising from the roll motion which displaces the center of mass laterally from the nominal center line ($mgh\phi$). Here, it is assumed that the cross-slope angles are normally quite small, thus small angle approximations are used. A steady-state moment balance yields the following equation:

$$ma_y h = \Delta F_z \ell_w - mgh\phi. \tag{5.1}$$

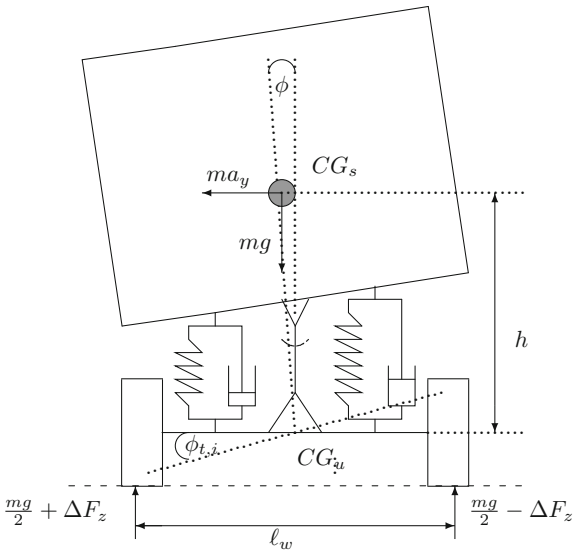

Fig. 5.1 A vehicle model for rollovers

Roll stability is achieved by limiting the lateral load transfers for both axles, $\Delta F_{z,l}$ and $\Delta F_{z,r}$, to below the levels for wheel lift-off. The lateral load transfer is calculated:

$$\Delta F_{z,i} = \frac{k_{t,i}\phi_{t,i}}{l_w}, \tag{5.2}$$

where $k_{t,i}$ is the stiffness of tires at the front and rear axles, $\phi_{t,i}$ is the roll angle of the unsprung mass and l_w is the vehicle's width, and $i = f, r$ denotes the front and rear of the vehicle. While attempting to minimize load transfers, it is also necessary to constrain the roll angles between the sprung and the unsprung masses $(\phi - \phi_t)$ to be within the limits of the travel of the suspensions. A maximum suspension roll angle of $6-7^\circ$ is typical.

The tire contact force is guaranteed if $\frac{mg}{2} \pm \Delta F_z > 0$ for both sides of the vehicle. This requirement leads to the definition of the normalized lateral load transfer, which is the ratio of the lateral load transfers at the front and rear axles

$$R_i = \frac{\Delta F_{z,i}}{m_i g}. \tag{5.3}$$

The normalized lateral load transfer R_i value corresponds to the largest possible lateral load transfer. If R_i takes on the value ± 1 then the inner wheels in the bend lift off. The limit of cornering is reduced when the load on the inside wheels has become zero and all the load has been transferred to the outside wheels. The lateral

acceleration at which rollover begins is the rollover threshold. Using $R_i = 1$ and assuming $m_i = \frac{m}{2}$ on the state moment balance (5.3), the rollover threshold is

$$a_y^* = \frac{\ell_w g}{2h} - \phi^* g, \tag{5.4}$$

where ϕ^* is the critical roll angle at the wheel lift-off.

Note that vehicles in real life often experience rollovers even with lateral acceleration much lower than the value of (5.4). The value is a result of a static analysis and does not take the dynamics of factors such as suspension compliance or tire deformation into account. Most rollover accidents occur when the driver reacts to sudden, unforeseen circumstances such as an obstacle on the road or unexpected behavior of other vehicles or pedestrians with abrupt steering.

In the calculation of the normalized lateral load transfer, the roll angles of the unsprung masses both at the front and rear axles must be applied. This performance has been applied in Sampson (2000), Gáspár et al. (2003c, d). The method requires the measurement of the roll angle of the unsprung masses. However, this is not a cheap measurement to make. It would therefore be more useful if roll rate or roll acceleration could be measured and fed back into the controller. The roll rate could be measured using a rate gyro, and roll acceleration by accelerometers. These measurements would be cheaper and simpler, see Dorling (1996). In this dissertation, a new method is proposed for the estimation of the roll angles of the unsprung masses.

Note that there are other solutions to monitor the rollover coefficient, which is the basis of the stability problem. Odenthal et al. (1999) proposed a method for calculating the rollover coefficient, see also Ackermann and Odenthal (1999). However, it ignores the roll angle of the unsprung masses, and it assumes that all the wheels have road contact. Takano and Nagai (2001) analyzed the critical threshold value for the lateral acceleration. Palkovics et al. (1999) proposed a heuristic method in which a small effect was generated by the brake or throttle system, see also Frank et al. (2000).

5.1.2 Design of Weighting Functions

The roll stability of the vehicle can be improved by two means. By varying the control torques between the sprung and unsprung masses the active roll control system can manipulate the axle load transfers and the body roll angles. Using the brake system of the vehicle a yaw moment can be generated by unilateral brake forces, which can reduce the lateral acceleration directly.

In the control design in terms of rollover risk, W_p represents weighting functions for the lateral acceleration, lateral load transfers and control inputs of active anti-roll bars and an active brake, $W_{p,ay}$, $W_{p,Fz}$, $W_{p,ua}$, $W_{p,uF}$, respectively. The purpose of the weighting functions is to keep the lateral acceleration, lateral load transfers and

control inputs small over the desired frequency range. The weighting function $W_{p,ay}$ is selected as:

$$W_{p,ay} = \phi_{ay} \frac{\frac{s}{2000} + 1}{\frac{s}{12} + 1}. \tag{5.5}$$

Here, it is assumed that in the low frequency domain the steering angle at the lateral accelerations of the body should be rejected by a factor of ϕ_{ay}. The weighting function for lateral load transfers is

$$W_{p,Fz} = \text{diag}(1/10^2, 1/10^3), \tag{5.6}$$

which means that the weight is 10^2 for the front axle and 10^3 for the rear axle. The weighting functions for control inputs correspond to the front and rear control torques $W_{p,ua} = 1/20$, and to the brake force $W_{p,uF} = 1/10$. The input scaling weight $W_w = W_\delta$ normalizes the steering angle to the maximum expected command. It is selected $5\pi/180$, which corresponds to a 5 deg steering angle command. W_n is selected as a diagonal matrix, which accounts for sensor noise models in the control design. For example, the noise weights are chosen 0.01 m/s^2 for the lateral acceleration and 0.01 deg/sec for the derivative of roll angle $\dot{\phi}$.

The goal is to design a controller that is only activated when the vehicle comes close to rolling over, i.e., the normalized load transfer has reached the critical value. In a normal driving situation the controller should not be activated. Consequently, when the situation is not critical the weighting function should be small and when the acceleration has reached the critical value the weight should be large to avoid the rollover. ϕ_{ay} is a gain, which reflects the relative importance of the normalized lateral load transfer in the LPV controller design. A large gain ϕ_{ay} corresponds to a design that reduces rollover risk. When the vehicle is in a normal cruising ϕ_{ay} is small and the minimization of lateral acceleration is not needed. In order to take into consideration a nonlinear function of the controller with respect to the operating domain a parameter-dependent weighting function must be used.

The weight should be scheduled by the normalized lateral load transfer at the rear side R, which can be deduced from the rollover situation. The rollover of a vehicle is affected by the suspension stiffness to load ratio, which is greater at the rear axle than at the front one. Thus, in case of emergency, the rear wheels lift off first. In this dissertation R denotes the normalized lateral load transfer at the rear axle R_r. When R is small, i.e., when the vehicle is not in an emergency, $\phi_{ay}(R)$ is small, indicating that the LPV controller should not focus on minimizing acceleration. On the other hand, when R is approaching the critical value, $\phi_{ay}(R)$ is large, indicating that the controller should focus on preventing the rollover. The parameter dependence of the gain is characterized by the constants R_1 and R_2. The parameter-dependent gain $\phi_{ay}(R)$ in Equation (5.5) is as follows:

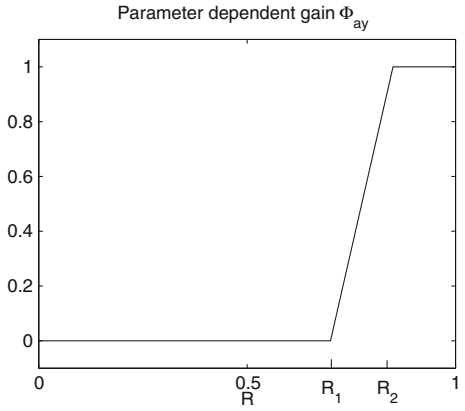

Fig. 5.2 Parameter-dependent gain $\Phi_a(R)$ in the performance specification

$$\phi_{ay}(R) = \begin{cases} 0 & \text{if} \quad |R| < R_1 \\ \frac{1}{R_2 - R_1}(|R| - R_1) & \text{if} \quad R_1 \leq |R| \leq R_2 \\ 1 & \text{otherwise} \end{cases}. \tag{5.7}$$

Thus, the normalized lateral load transfer is defined to monitor the rolling over of the vehicle, thus it is applied as a scheduling variable. R_1 defines the critical status when the vehicle is close to rolling over, i.e., all wheels are on the ground but the lateral tire force of the inner wheels is approaching zero or the suspension has reached its physical limit and the active anti-roll bars are not capable of generating more stabilizing moment. The closer R_1 is to 1 the later the control will be activated. Parameter R_2 shows how fast the control should focus on minimizing the lateral acceleration. The smaller the difference between R_1 and R_2 is the more quickly the performance weight punishes the lateral acceleration. In the control design, the constants are selected as $R_1 = 0.85$ and $R_2 = 0.95$. The function $\phi_{ay}(R)$ is illustrated in Fig. 5.2.

Since the brake is activated only in emergencies, the control structure can be considered a switching system. In practice, when such switching is used, chattering may occur. Chattering causes small amplitude oscillations with high frequency around the switching point, which may degrade the performance properties of the vehicle. In our case the switching point is the critical normalized lateral load transfer defined as R_1, and the brake system is switched on and off at this value. In order to eliminate chattering, a hysteresis characteristic is applied with respect to the critical value of the normalized lateral load transfer R_1. It means that the value of R_1 must be larger when the brake system is switched on than when it is switched off. Such a normalized lateral load transfer hysteresis is defined as

$$R_1 = R_{1n} + \frac{\text{sgn}(\dot{R})}{w_h}, \tag{5.8}$$

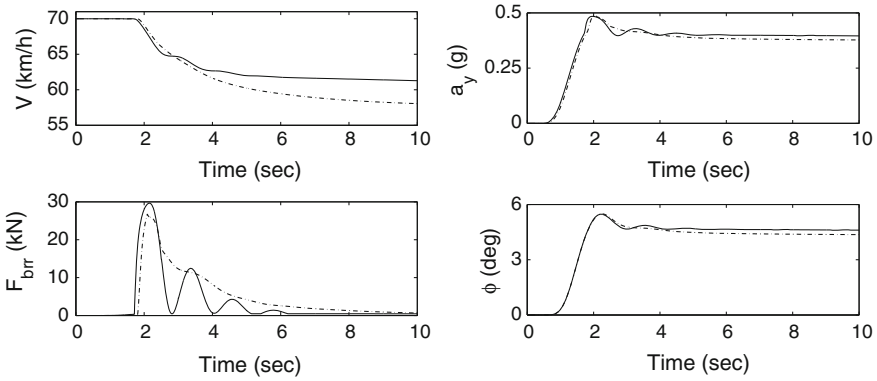

Fig. 5.3 Time responses to cornering with and without chattering elimination

where R_{1n} is a nominal value of the switching point and w_h is the parameter with the width of hysteresis window. In Equation (5.8), it is assumed that the signum of the derivative of the normalized lateral load transfer, which is denoted by $\text{sgn}(\dot{R})$ is also computed in real time. $\text{sgn}(\dot{R})$ is used to deduce the direction of the load transfer change. If it is positive the load transfer is increasing and the brake system is switched on above R_{1n}. However, when it is negative, i.e., the normalized lateral load transfer is decreasing, the brake system is switched off at a smaller value than its nominal value. $\text{sgn}(\dot{R})$ is used as an additional scheduling variable in the control design and its possible values are selected $\{-1,\ 0,\ 1\}$.

In the LPV model of the combined yaw and roll motion three parameters are selected: the forward velocity v, the normalized lateral load transfer at the rear side R, and the signum of its derivative $\text{sgn}(\dot{R})$. The value v is measured directly, the parameter R can be calculated by using the measured (or estimated) roll angle of the unsprung mass $\phi_{t,r}$, while $\text{sgn}(\dot{R})$ is also a calculated signal.

In this example, the effect of the chattering phenomenon is illustrated. Time responses to cornering when chattering elimination is not included in the control design are illustrated by solid line in Fig. 5.3. Note that chattering in the brake force occurs while the vehicle is being decelerated. This small oscillation causes the brake system to be switched on and off around the critical value R_1, and this degrades the roll stability of the vehicle. The chattering is eliminated by applying a hysteresis characteristic with respect to the critical value of the normalized lateral load transfer. Due to the hysteresis characteristic the oscillation of the brake force ceases. It is illustrated by dashed line in Fig. 5.3.

5.2 LPV Control Methods for Rollover Prevention Systems

In this section, a method using a combination of active anti-roll bars and an active brake mechanism is proposed to prevent the rollover of heavy vehicles. In the LPV model, the forward velocity is used to calculate the parameters in the scheduling vector, see in Eq. (2.84). The measured signals are the lateral acceleration and the roll rate of the sprung mass.

The combined controller uses active anti-roll bars all the time to prevent rollovers. The brake mechanism is only activated when the vehicle comes close to rolling over. In normal cruising the brake part of the control should not be activated. However, if the normalized lateral load transfer reaches a critical value the brake system must minimize the lateral acceleration to prevent the rollover. The critical value of the normalized lateral load transfer is determined when the lateral load transfer of one of the curve-inner wheels has reached zero. The advantage of this solution is that the controller guarantees performance specifications with smaller control energy.

The control design is based on a closed-loop interconnection structure, which is illustrated in Fig. 5.4. The control input is the difference between the brake forces ΔF_b, which generates a yaw moment, which affects the lateral tire forces directly. The active anti-roll bars generate a stabilizing roll moment between the sprung and unsprung masses u_{af} and u_{ar}.

The performance outputs in the control design are the lateral acceleration, lateral load transfers and control inputs:

$$z_r = \left[a_y \ \Delta F_{zf} \ \Delta F_{zr} \ u_r^T\right]^T , \tag{5.9}$$

where $u_r = \left[u_{af} \ u_{ar} \ \Delta F_b\right]^T$. In the design of the LPV control two signals are used to calculate the parameters in the scheduling vector, i.e., the forward velocity and the normalized lateral load transfer. The scheduling vector is $\rho = \left[\frac{1}{v} \ \frac{1}{v^2} \ v \ R \ \text{sgn}(\dot{R})\right]^T$.

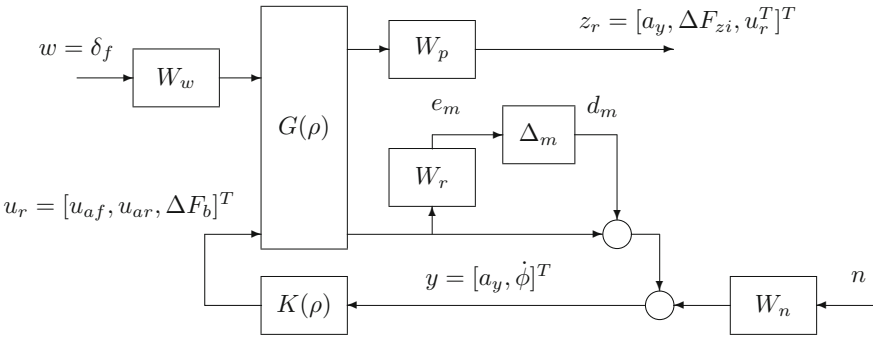

Fig. 5.4 The closed-loop interconnection structure for the design of a combined control

In this section, the operation of the combined control mechanism, which is based on the LPV control is illustrated. The results of the combined control are compared with the controlled systems which only use active anti-roll bars and which only use an active brake mechanism. The values of the vehicle parameters are found in Table 2.4.

In the example a double lane change maneuver is performed. The maneuver has a 2 m path deviation over 100 m. The size of the path deviation is chosen to model a real obstacle evasion in an emergency on a road. The velocity of the vehicle is 75 kph. The steering angle input is generated in such a way that the vehicle with no roll control will come close to rolling over during the maneuver and its normalized lateral load transfers are above the value ± 1. The steering angle applied in the simulation is a ramp signal. The forward velocity is not constant during the maneuver because in the case of brake and combined control the brake force provided by the compensator decelerates the vehicle. In simulation, the driver does not push down on the brake pedal, hence the only change in forward velocity is caused by the compensator. Figure 5.5 shows the time responses in cases when active anti-roll bars (dash-dot), an active brake mechanism (dash) and a combined roll control system (solid) are used.

In the case of the combined control, the lateral acceleration is similar to that when using active anti-roll bars. The reason is that only the active anti-roll bars reduce the acceleration and the brake control will not work until the normalized lateral load transfer has reached the critical value R_1. Hence, the combined control can be considered as simple active anti-roll bars when the normalized lateral load transfer is less than R_1. However, the required control action with respect to the brake force is less than in the case of the active brake control. In the case of the combined roll control, only the active anti-roll bars work and generate a stabilizing lateral displacement moment when the normalized lateral load transfer does not reach the critical value and the brake system is not activated. Hence, the brake force required to prevent the rollover of the vehicle is less than when using only the brake system. When the combined control and the brake mechanism are applied the roll angle of the sprung mass is in the same phase as in the uncontrolled case and the physical limit of the suspension travel is not exceeded. It can be observed that the critical value of the lateral acceleration is the second peak from the rollover point of view. The engineering interpretation of this phenomenon is that the vehicle generates larger lateral acceleration when it starts returning into the lane because the driver must set a double steering angle with -180 phase shifting to steer back the vehicle into its original position. As far as all of the three control structures are concerned, the roll angles of the unsprung masses at the front and rear axle are slightly different due to the different suspension parameters and the stiffness to load ratio.

The path of the vehicle for all controls can be seen in Fig. 5.5. In case of the active anti-roll bars the vehicle keeps the desired path. In the case of the brake control, the real path is significantly different from the desired path due to the brake moment, which affects the yaw motion. The only limit to using the active brake mechanism is the saturation of the brake actuators. This means that the minimization of the lateral acceleration is restricted by the physical limit of the actuator. However, the only problem is that if too much unilateral brake force is applied the stability of the yaw motion is degraded. In order to avoid the degradation of yaw dynamics the combined

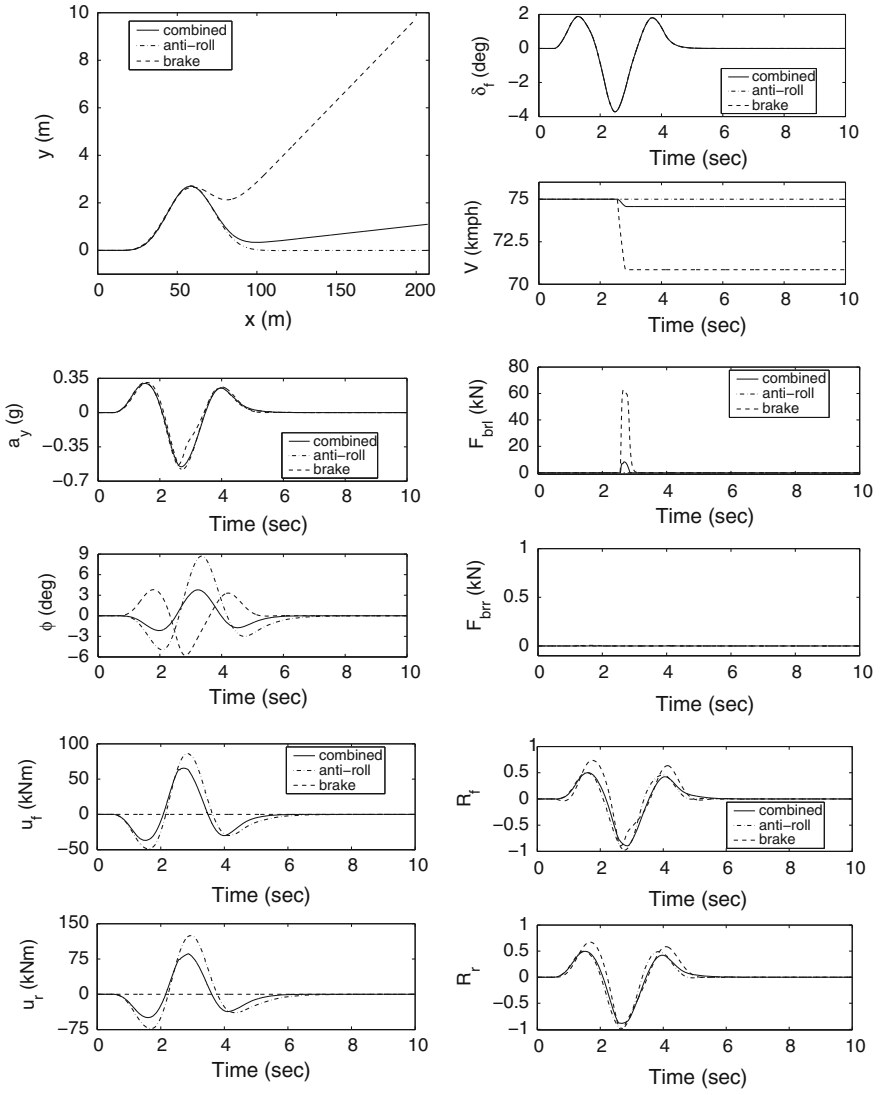

Fig. 5.5 Time responses to a double lane change steering input when the combined control is compared with other controllers

control is used, in which case the real path is only slightly different from the desired path because the brake force is less than in the case of the active brake control. In the case of braking control or in the case of combined control, the deviation in path can be corrected by changing the steering angle. In the case of combined control, the deviation between the real and the desired path can be corrected by a small change in the steering angle. It is noted that changing the steering angle has negative effects on

the roll movement. The greater the difference between the desired path and the real path is, the larger steering angle is needed, which in turn increases the overturning moment. As in the case of combined control mechanism the real path is only slightly different from the desired path and a small correction is needed. Thus, the effect of the steering angle does not result in overturning.

5.3 Design of a Fault-Tolerant Rollover Prevention System

In practice, three fault scenarios are considered for a hydraulic actuator. First is a lock failure, in which case the piston of the hydraulic actuator remains locked in a particular position. In this case, the hydraulic actuator does not work after the fault and the actuator resists the motion of the vehicle in the roll plane. The physical characteristic of this phenomenon is that the piston of the hydraulic actuator is clutched and it is not moving any longer. Second is a floating failure, in which case the relative displacement of the hydraulic actuator changes the suspension travel instantaneously. This means that the active anti-roll bars cannot generate lateral displacement moment to balance an overturning moment and the piston of the hydraulic actuator can move freely in the cylinder. This situation may arise when the power supply is cut off and sufficient oil pressure is not maintained. The third type of failure is the loss in effectiveness. This means that the effectiveness of the actuator is reduced. When this failure occurs the actuator goes on working but with reduced power. This is the case for example when the leakage coefficient of the piston is too high, hence the actuator cannot generate the torque required by the control valve.

Falult information provided by a fault detection filter is given by $\rho_f = \frac{\hat{f}}{f_{max}}$, where f_{max} is an estimation of the maximum value of the potential failure (fatal error). Fault information ρ_f is used as a scheduling variable. Using this parameter the controller is adjusted when different types of actuator failures occur. Note that ρ_f is normalized fault information whose value is taken from interval $\left[0\ 1\right]$. The zero value of normalized fault information means a fault-free actuator and value 1 is the total fault of the active anti-roll bars. In other words in case of value 1 the actuator is not able to generate control torque. This situation is classified as a float failure because the anti-roll bars have broken down but the actuators do not resist the displacement of the suspension. In this case, the only control input which can prevent the rollover of vehicle is the brake system. If ρ_f takes the value between 0 and 1 there is a loss in effectiveness, i.e., the active anti-roll bars can be used to generate stabilizing moment but with reduced power.

Fault information is taken into consideration in the performance weighting for lateral acceleration, since an active brake affects this signal directly. The weighting function for lateral acceleration $W_{p,ay}(R)$ is selected, where gain $\phi_{ay}(R)$ depends on the normalized lateral load transfer R. Here, R_1 defines the critical status when the vehicle is close to rolling over.

On the event of a fault the range of operation of the brake system must be extended in such a way that critical value of the normalized lateral load transfer which starts

the activation of the brake mechanism is smaller than in the fault-free case. A small value of R_1 corresponds to activating the brake system early and gradually, whereas a large value of R_1 corresponds to activating the brake system rapidly. Thus, the design parameter R_1 is chosen to be scheduled on fault information ρ_f.

$$R_1 = R_1 - \frac{\rho_f}{10}. \tag{5.10}$$

If a fault occurs, the critical value R_1 is reduced, which causes the brake mechanism to be activated even at a smaller value of R.

In the design of the LPV control, three signals are used to calculate the parameters in the scheduling vector, i.e., the forward velocity v, the normalized lateral load transfer R and the parameter of the normalized fault information ρ_f: The scheduling vector is $\rho = \left[\frac{1}{v} \ \frac{1}{v^2} \ v \ R \ \text{sgn}(\dot{R}) \ \rho_f\right]^T$. Here v is measured directly, ρ_f is provided by the FDI filter, while parameter R is calculated by using the measured roll angle of the unsprung mass $\phi_{t,r}$.

Based on the fictitious control inputs, the actual control forces at the front and rear, on both sides, generated in the suspension points can be calculated in simple matrix manipulations. The implementation of the reconfigurable control strategy is illustrated in Fig. 5.6.

The FDI filter is tested during a cornering maneuver. Figure 5.7 shows the time responses of the controlled system which uses active anti-roll bars. The steering angle applied in the simulation is a ramp signal. The forward velocity is not constant during the cornering maneuver. Braking input is used to decelerate the vehicle during the maneuver. This example illustrates that the FDI filter works reliably in the entire velocity region. The initial forward velocity is 80 kph and the vehicle is decelerated to approximately 68 kph.

The fault scenario used in the closed-loop simulations is a 10 kNm anti-roll bar failure starting from 2 s and 0.1 rad/sec sensor failure occurring at 5 s. In our case, the step failure represents a loss in effectiveness. The step sensor failure means that the $\dot{\phi}$ sensor measures a signal with a constant additive failure. Figure 5.7 also shows the

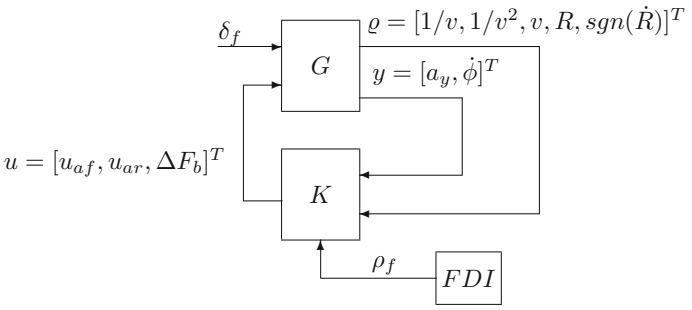

Fig. 5.6 The implementation of a fault-tolerant control strategy

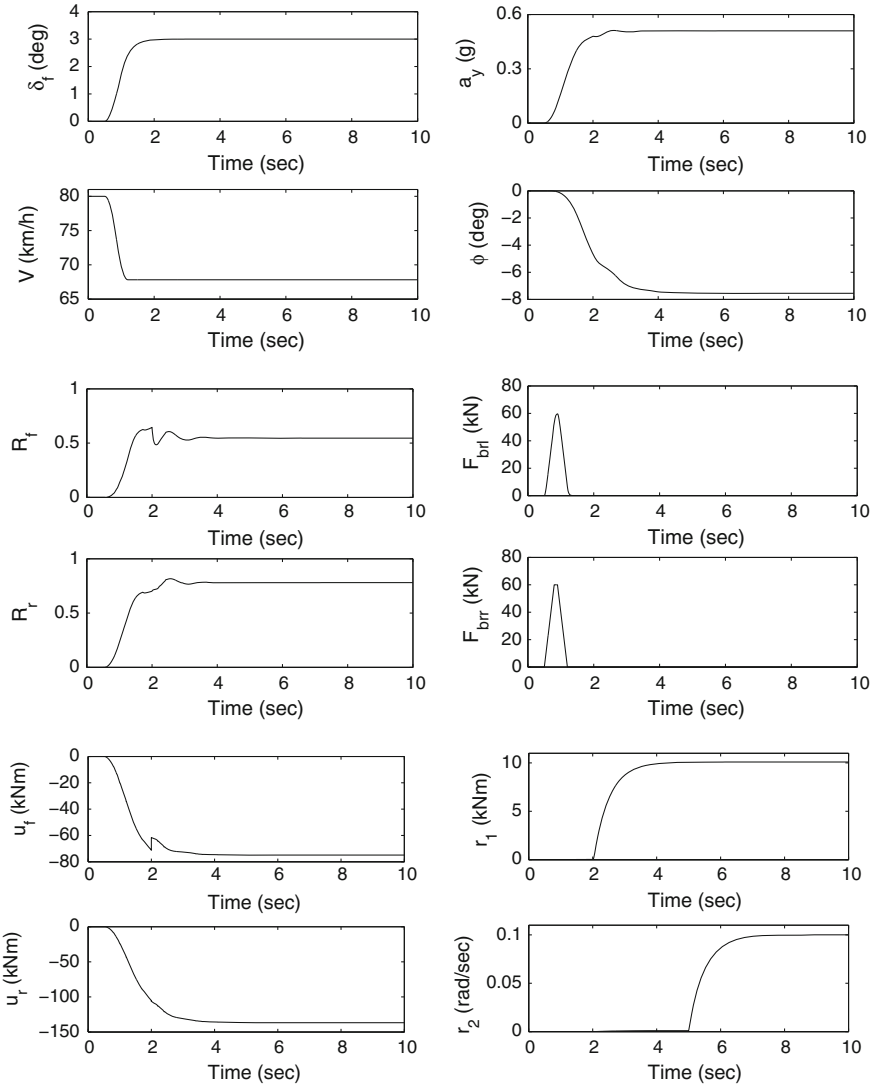

Fig. 5.7 Time responses to a cornering when an actuator fault is detected by an FDI filter

lateral acceleration and the roll angle of the sprung mass. The controller is not able to reduce the lateral acceleration, with the help of the anti roll bars, i.e., it does not have a direct effect on changing the acceleration. In the case of the anti-roll control, the vehicle rolls into the bend. Hence, this motion of the vehicle generates a stabilizing lateral displacement moment, which balances the destabilizing overturning moment caused by lateral acceleration. The roll angle of the unsprung masses is slightly different due to the different suspension parameters and the stiffness to load ratio.

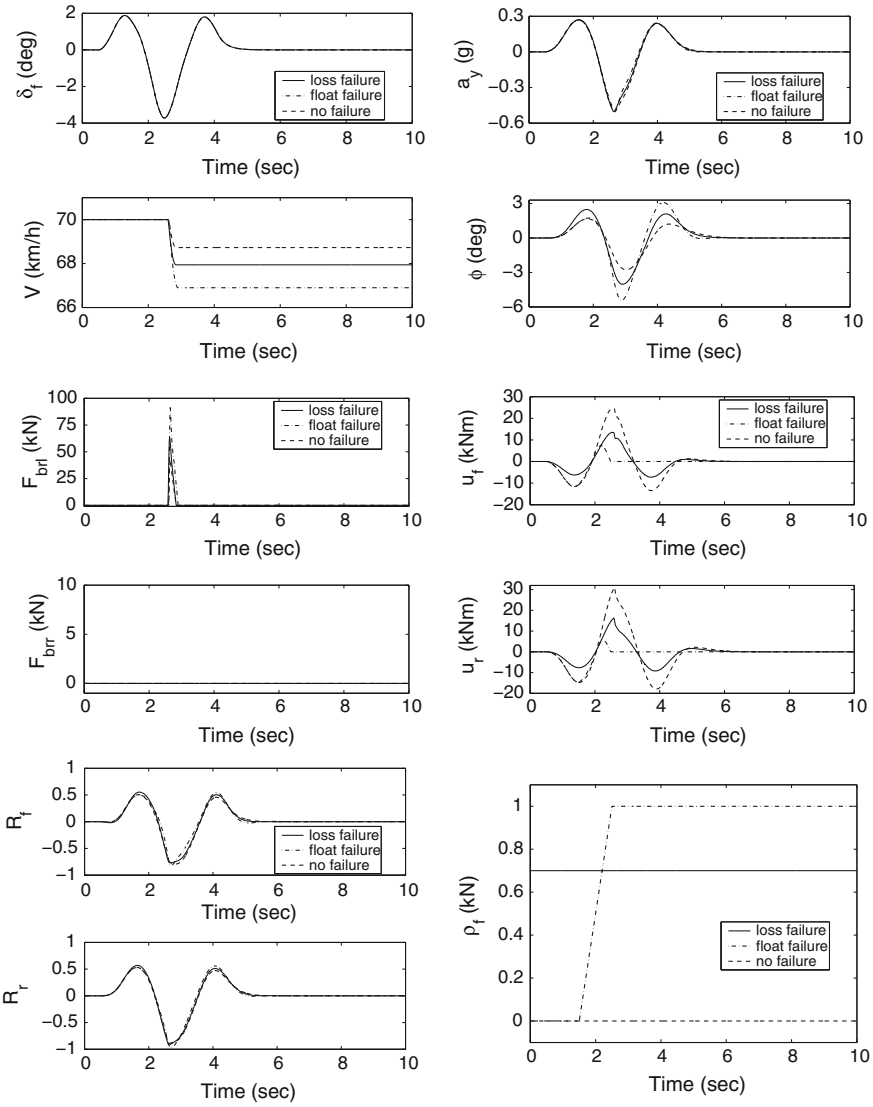

Fig. 5.8 Time responses to a double lane change steering input in different failures

The control torque is approximately -70 kNm at the front axle and -140 kNm at the rear axle. As the lateral acceleration is increasing, the normalized lateral load transfer lifts up the rear axle faster than the front one since the ratio of effective roll stiffness to axle load is greater at the driven axle. The simulation results of the FDI filter in a closed-loop are seen in Fig. 5.7. The first residual shows the actuator fault r_1 and the second one the sensor fault r_2. The effects of the two failures are decoupled

and the residuals give a close estimation of faults in the active anti-roll bars and the sensor fault, the time of their occurrence and their values.

The operation of the fault-tolerant combined control structure is demonstrated in a double lane change maneuver. In the first scenario, ρ_f is set at the constant value 0.7. In this case, actuator effectiveness is reduced by 70 %. The second fault scenario is when the ρ_f is a ramp signal with unity slope starting from 1.5 to 2.5 s. Here, the fault is that actuator effectiveness gradually drops to zero. Using different fault scenarios the responses of yaw roll dynamics are compared. Figure 5.8 shows the responses in case of a float type failure (dash-dot), loss in effectiveness failure (solid) and the fault-free situation (dashed). The velocity of the vehicle is 70 kph.

The lateral acceleration in each case is slightly different. The reason for this fact is that where the normalized lateral load transfers do not reach the critical value R_1 only the active anti-roll bars are activated and the brake system is not used. However, the active anti-roll bars are not able to reduce the lateral acceleration because they do not have a direct effect on changing acceleration. So, the effect of a fault in the actuator does not appear in the lateral acceleration. It can be observed that, when faults occur, the roll angle increases due to the reduced power of the actuators. In the absence of a fault the actuator can generate higher control torque than when a fault is present, so it can balance the primary overturning moment more effectively. It can be seen that the control torque is smaller in the case of loss failure than in a fault-free situation. In the case of a float type failure its effectiveness decreases gradually and becomes zero when the normalized fault information has reached value 1. The required brake force is the largest in the case of a float failure. This is because the active anti-roll bars are not able to generate control torque over 2.5 s, so the reconfigured controller structure is identical to the controller in which only the brake system is used to prevent the rollover of the vehicle. In the fault-free case the active anti-roll system is working and generates stabilizing lateral displacement moment. Hence, the brake force required to prevent the rollover of the vehicle is less than in the faulty cases.

Chapter 6
Adaptive Cruise Control in Longitudinal Dynamics

6.1 Adaptive Cruise Control

In the last decade, the longitudinal vehicle control based on the look-ahead approach has been in the focus of the automotive research centers. It is widespread in the cruise control, which is able to guarantee an energy-efficient driving, see Sciarretta et al. (2015). Since adaptive cruise control (ACC) allows to maintain a desired travel speed set by the driver by acting on the throttle and brakes, the combination of look-ahead control and ACC is a novel trend in the vehicle control design.

Several methods in the topic of cruise control systems have been proposed. Model Predictive Control (MPC) algorithm is largely employed for cruise control purposes. In Borrelli et al. (2001), a vehicle model with an affine approximation of the frictional torque is proposed. In the robust MPC problem, the constraints on the torque, on its variation, and on the slip are considered. Li et al. (2011) presented a two-level MPC architecture, in which the nonlinearities in the vehicle dynamics and the minimum tracking error, fuel consumption, and the car-following requirements are incorporated in different layers. Using nonlinear MPC methods further results can be achieved. In Sakai et al. (2010), nonlinear MPC method is used for torque tracking control for the desired torque, which attains velocity tracking control by calculating desired torque from desired car speed.

Sliding-mode and adaptive controls are widely used techniques in the longitudinal control. The aim of the sliding-mode control is generally the computation of the desired vehicle motion, such as acceleration, speed, see Gerdes and Hedrick (1997), Lu and Hedrick (2005). These signals in another layer are converted to the input of engine, transmissions, retarders, and brakes. Xu and Ioannu (1994) presents an adaptive control-based design method for the throttle input, in which the adaptation to the parameter variations is handled. The uncertainties of the tire-road contact based on adaptive control law is considered in Chen and Wang (2011). In the paper, a complex vehicle formulation using the LuGre tire model is applied.

Martinez and Canudas-de-Wit (2007) focuses on stop-and-go scenario using a combined feedforward and feedback PD controller. The reference model is non-

P. Gáspár et al., *Robust Control Design for Active Driver Assistance Systems*,
Advances in Industrial Control, DOI 10.1007/978-3-319-46126-7_6

linear and provides dynamic solutions consistent with safety constraints and comfort specifications. A composite Lyapunov function-based vehicle following control using Bilinear Matrix Inequalities optimization is found in Enache et al. (2009) Kolmanovsky and Filev (2010) focuses on the longitudinal control in such a way as to achieve optimal trade-off between expected average fuel economy and expected average travel speed using Bellman's principle.

Robust control technics are also used in the longitudinal control design. A combined $\mathscr{H}_\infty$ feedback and feedforward control is employed to damp out longitudinal oscillations using μ analysis in Lefebvre et al. (2003). The robust $\mathscr{H}_\infty$ method is compared to the Linear Quadratic Regulator design in Junaid et al. (2005). In the paper a third-order linear system is applied, which describes the dynamics of the vehicle and the power-train. The controlled system is robust against exogenous disturbances and the parameter uncertainty of power-train time is constant. A LPV control design has been presented in Németh and Gáspár (2013b), in which the differences of driving and braking dynamics are considered in the velocity tracking problem. The designed system is robust against longitudinal disturbances, such as rolling resistances, road inclinations, and aerodynamic forces.

In some papers, the longitudinal control is a part of an integrated framework, see, e.g., Katriniok et al. (2013). Recently, a cruise control strategy using a nonlinear Lyapunov control method is designed in Attia et al. (2014b). The control strategy is based on a cascade control architecture where an outer-loop ensures the reference speed tracking and computes the torque to be applied on the wheels. An inner-loop provides the throttle opening and the brake pressure to generate the required control torque.

Several publications and patents deal with the topics of driveline control implementation and look-ahead strategies. Hellström et al. (2009) present the design and the implementation of a predictive speed controller. The intervention of the look-ahead control is connected to the reference signal of the PID-based speed controller, which modifies the fuel injection of the engine. Kiencke and Nielsen (2000) uses a dynamic longitudinal model for the design of the speed controller. It influences the engine torque based on the engine rpm and the fuel injection, which are control inputs in the architecture.

A test platform for the implementation of look-ahead control is introduced in Gustafsson (2006). The platform contains the user interface, the controller structure together with the look-ahead optimization, CAN softwares, and interfaces. The proposed device is in connection with the CAN bus of the vehicle. The look-ahead method of the platform considers the engine torque, the gear position, and road geometry information. The implementation of an optimal ACC for passenger cars is presented in Li et al. (2013), Németh et al. (2015a). The system uses radar and acceleration sensor measurements, from which the acceleration of the preceding vehicle are derived. The optimization algorithm yields a reference acceleration signal, which is the input of the vehicle dynamic controller together with the estimated preceding vehicle acceleration.

Further automotive industrial patents on the predictive speed control algorithms are presented in Lattemann et al. (2004). The method of Eriksson and Steén (2003) is based on the forthcoming terrain characteristics to select gear position, according to the required driver's performance (fuel consumption, emission, traveling time). Takahashi et al. (1998) introduce an algorithm which computes the optimal driveline torque considering the road inclinations.

6.2 Model-Based Robust Control Design

6.2.1 Modeling Longitudinal Dynamics

First, the modeling of longitudinal dynamics is presented. Since the cruise control method must be easily adaptable to a vehicle, a small number of vehicle parameters are involved. Thus, the longitudinal dynamics is described in the approach by the following simplified model:

$$m\ddot{\xi}_0 = F_{l1} - F_{d1} \tag{6.1}$$

where m is the mass of the vehicle, ξ_0 is the vehicle position, F_{l1} is the realized longitudinal force on the wheels. F_{d1} includes the longitudinal disturbances, such as the aerodynamic forces, rolling resistance and road slope

$$F_{d1} = C_a\dot{\xi}_0^2 + C_r gm\cos\vartheta + mg\sin\vartheta \tag{6.2}$$

where ϑ is road slope and C_a, C_r are vehicle parameters related to aerodynamic and resistances forces.

In the following, the transformation of the vehicle model has two focuses. First, the mass of the vehicle is an uncertain parameter of the vehicle. The mass has a nominal value m_0, which is known, but the variation of the mass m_v is unknown. However, the variation is assumed to be a bounded parameter, e.g., $m_v/m_0 = \pm 15\,\%$. Second, the road inclination is assumed to be known. In practice, the slope of the road can be obtained in two ways: either a contour map which contains the level lines is used or an estimation method is applied. In the former case, a map used in other navigation tasks can be extended with slope information. Several methods have been proposed for slope estimation. Cameras, laser/inertial profilometers, differential GPS, or a GPS/INS systems are used, for example, see Bae et al. (2001), Labayrade et al. (2002), Hahn et al. (2004). An estimation method based on a vehicle model and Kalman filters has been proposed by Lingman and Schmidtbauer (2002).

Since the handling of vehicle mass uncertainty is a requirement for the control system, it is necessary to define the actual mass m of the vehicle such as

$$m = m_0 + m_v. \tag{6.3}$$

Substituting (6.3) in (6.1), the longitudinal motion equation is reformulated in the following way:

$$(m_0 + m_v)\ddot{\xi}_0 = F_{l1} - F_{d1} \tag{6.4}$$

$$m_0\ddot{\xi}_0 = F_{l1} - F_{d1} - m_v\ddot{\xi}_0 \tag{6.5}$$

Considering that $\ddot{\xi}_0$, the actual longitudinal acceleration, is a measurable and bounded signal of the vehicle, $m_v\ddot{\xi}_0$ is handled as a disturbance of the vehicle. Combining it with F_d, the next expression is yielded:

$$\begin{aligned} F_{d1} + m_v\ddot{\xi}_0 &= C_a\dot{\xi}_0^2 + C_r g(m_0 + m_v)\cos\vartheta \\ &\quad + (m_0 + m_v)g\sin\vartheta + m_v\ddot{\xi}_0 \\ &= \left(C_a\dot{\xi}_0^2 + C_r g m_0\cos\vartheta + m_0 g\sin\vartheta\right) \\ &\quad + m_v\left(C_r g\cos\vartheta + g\sin\vartheta + \ddot{\xi}_0\right) \\ &= F_{d1,1} + m_v f_{d,2} \end{aligned} \tag{6.6}$$

Note that the expression (6.6) contains two different elements. $F_{d1,1}$ and $f_{d,2}$ incorporate measurable signals, such as velocity, road slope, and longitudinal acceleration. Thus, $F_{d1,1}$ is handled in this approach as a measured disturbance. Since there is no information about the mass variation m_v, the term $m_v f_{d,2}$ is considered as an unknown disturbance—where actually $f_{d,2}$ is a measurable part of the disturbance expression.

6.2.2 Robust Control Strategy

In the following section, the control design for the longitudinal velocity tracking control problem is proposed. The controlled system must guarantee precise tracking, robustness against mass variation, road slope, and further disturbances. The conservativeness of the control algorithm can be reduced through the consideration of the measurements on disturbances. In the proposed control scheme, $F_{d1,1}$ is considered as a measured disturbance. Thus, it is recommended to derive a feedforward term in the control strategy for the direct elimination of F_{d1}. In the following, a robust control design method is presented, which combines the advantages of the feedforward and feedback control design.

The realized total longitudinal control force on the wheels F_{l1} is divided into two elements

$$F_{l1} = F_{l1,0} + F_{l1,1} \tag{6.7}$$

where the purpose of $F_{l1,1}$ is to compensate for the measured disturbance $F_{d1,1}$, while $F_{l1,0}$ guarantees the unknown disturbance rejection and the performances.

If $F_{d1,1}$ is fully compensated for, then the feedforward control input is

$$F_{l1,1} = F_{d1,1} = C_a \dot{\xi}_0^2 + C_r g m_0 \cos\vartheta + m_0 g \sin\vartheta \tag{6.8}$$

where $\dot{\xi}_0$, ϑ are measured and estimated parameters, see Vahidi et al. (2005). Thus, the efficiency of the feedforward disturbance compensation is based on the accuracy of $\dot{\xi}_0$, ϑ. Since the measurement of the speed and the estimation of the road slope are inaccurate, the feedforward compensation has an error $F_{d,11}$. The longitudinal motion of the vehicle is formed using (6.4), (6.6), (6.7) and (6.8), which is described as

$$m_0 \ddot{\xi}_0 = F_{l1,0} + F_{l1,1} - F_{d1,1} - F_{d1,11} - f_{d,2} m_v \tag{6.9}$$

$$= F_{l1,0} - F_{d1,11} - f_{d,2} m_v \tag{6.10}$$

In the next step a feedback control input $F_{l1,0}$ is designed, which is able to handle the disturbances $F_{d1,11}$, $f_{d,2} m_v$ in (6.9).

6.2.3 Modeling Actuator Dynamics

In the real intervention of the driveline/brake system, the physical construction of the actuator has an important role. Generally, the actuators delay the controlled action and provide additional dynamic motion. Therefore, it is necessary to consider the dynamics of the actuator in the design of the controller to improve the tracking capability of the Advanced Driver Assistance System. In the following, a simplified formulation of the actuator dynamics which generates the longitudinal force F_{l1}, is considered as

$$\dot{F}_{l1} = -\frac{1}{\tau} F_{l1} + \frac{1}{\tau} u \tag{6.11}$$

where u is the control input computed by the control algorithm. The robust control design is based on the relation (6.11) between u_0 and $F_{l1,0}$. The considered actuator dynamics (6.11) for the feedback design can be reformulated as a transfer function

$$G(s) = \frac{1}{\tau s + 1} = 1 - \frac{\tau s}{\tau s + 1} \tag{6.12}$$

The reformulation of the actuator dynamics can be handled as an input multiplicative uncertainty of the system, where $W_u = -\tau s/(\tau s + 1)$ is the uncertainty of the system. In this case, the robustness of the system requires the consideration of the highest bound of W_u in the control design. The Bode amplitude diagram of W_u depends on τ. Since the maximum bound W_u is defined by the highest τ value, the robust control must be designed with it. The maximum τ value is related to the slowest actuation of the driveline/braking systems. This τ value must be considered in the robust control design.

6.2.4 Design of Feedback Controller

The feedback control input $F_{l1,0}$ has three main goals in the control strategy: the rejection of unknown disturbances ($F_{d1,11}$, $f_{d,2}m_v$), the handling of the unmodelled actuator dynamics and the guarantee of the performance. The state-space representation of the system is the following:

$$\begin{bmatrix}\ddot{\xi}_0\end{bmatrix} = \begin{bmatrix}0\end{bmatrix}\begin{bmatrix}\dot{\xi}_0\end{bmatrix} + \begin{bmatrix}-\frac{1}{m_0} & -\frac{1}{m_0}\end{bmatrix}\begin{bmatrix}F_{d1,11}\\ F_{d1,2}\end{bmatrix} + \begin{bmatrix}\frac{1}{m_0}\end{bmatrix} F_{l,0} \tag{6.13}$$

where the disturbances are compressed to a vector $F_{d,fb} = \begin{bmatrix}F_{d1,11} & F_{d1,2}\end{bmatrix}^T$, where $F_{d1,2} = f_{d,2}m_v$. The measured output of the system is the velocity $\dot{\xi}_0$, which is also the state in the formulation.

The performance of the system is expressed by the tracking of the reference velocity λ and the minimization of the control input u_0. Note that the influence on the control input is necessary to avoid the extremely high actuation of the longitudinal control. The performance signals are

$$|z_1| = |\lambda - \dot{\xi}_0| \rightarrow \min \tag{6.14}$$

$$|z_2| = |u_0| \rightarrow \min \tag{6.15}$$

The state-space representation of the system for the control design, which incorporates the performance and the measurement, is the following:

$$\dot{x} = Ax + B_1 F_{d,fb} + B_2 u_0 \tag{6.16}$$

$$z = C_1 x + D_{1,2}(\rho) u_0 \tag{6.17}$$

$$y = C_2 x \tag{6.18}$$

The weighting functions for the performance considering z_1 and z_2, are parameter-dependent, formulated as follows:

$$W_{p,1} = \frac{1}{1-\rho} G_{p,1} \tag{6.19}$$

$$W_{p,2} = \frac{1}{\rho} G_{p,2} \tag{6.20}$$

where the transfer functions $G_{p,1}$ and $G_{p,2}$ are employed to introduce some performance in the control design. $F_{d,s}$ is a sensor noise on the velocity measurement and ($F_{d,11}$ an unknown disturbances. The augmented plant for the LPV design is illustrated in Fig. 6.1. In the example, the following weighting functions are applied for the performance signals, control input, and the disturbances:

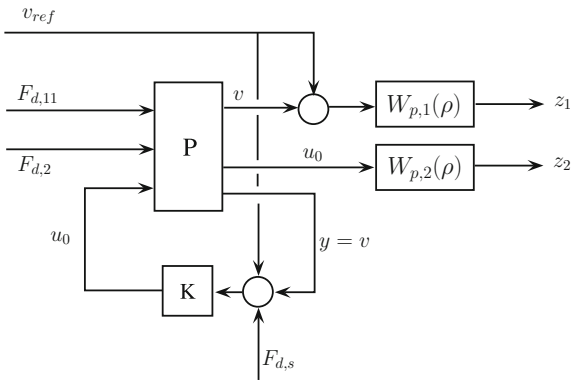

Fig. 6.1 Closed-loop interconnection

$$W_{p,1} = \frac{1428.57}{1-\rho}\frac{0.0049s + 0.07}{0.05s^2 + 0.6s + 1},$$
$$W_{p,2} = \frac{1}{7000\rho^2}\frac{0.01s + 1}{10s + 1},$$
$$W_u = \frac{0.025s}{0.025s + 1},$$

$$W_{d,11} = \frac{0.5s^2 + 1.667s + 1.389}{0.01s^2 + 0.2s + 1},$$
$$W_{d,2} = \frac{6.107s^2 + 20.36s + 16.96}{0.01s^2 + 0.2s + 1},$$
$$W_{d,s} = \frac{0.1}{0.0011 + 1}.$$

The aim of parameter dependency is to guarantee the limitation of the control input. In this way, the saturation of the actuator can be avoided. The defined scheduling variable ρ is computed based on the rule illustrated in Fig. 6.2. Note that in this rule the feedforward control input u_1 must also be considered. The transfer function $G_{p,1}$ in (6.19) has an additional role in the control design. Since the overshoot of the

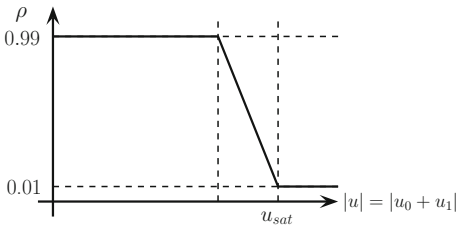

Fig. 6.2 Computation rule of ρ

velocity must be minimized as much as possible, this criterion is considered in the appropriate selection of $G_{p,1}$ characteristics.

Finally, a parameter-dependent $K(\rho)$ controller is yielded. The feedback control input is formally computed as $u_0 = K(\rho) \cdot (v_{ref} - v)$. As a result of the combined feedforward-feedback strategy, the control law of the system, using (6.8), is yielded as

$$\begin{aligned} u &= K(\rho)(v_{ref} - v) + C_a v^2 + C_r g m_0 \cos\theta + m_0 g \sin\theta \\ u &= u_0 + u_1 \end{aligned} \tag{6.21}$$

Thus, the control input u is given by the sum of two different components u_0 and u_1. The goal of u_1, i.e., the feedforward control, is to compensate for the resistance of road slope (slope is considered as a measured signal). The other component u_0, i.e., the feedback control, is computed by the LPV controller. Its role is to guarantee accurate velocity tracking and robustness against further disturbances (velocity sensor noise, feedforward imprecision, actuator time lag) and mass variation.

6.3 Speed Design Based on Multiobjective Optimization

In the previous sections, the control design of the longitudinal dynamics is presented. Although the tracking control is an important element of an advanced intelligent cruise control, the computation of the reference speed trajectory is also a crucial point of the cruise control system. In the following, a multiobjective optimization-based look-ahead speed design method is presented.

6.3.1 Motivation of the Speed Design

The purpose of energy-efficient control strategy is to design the speed of road vehicles, in which several factors are taken into consideration such as energy requirement, fuel consumption, road slopes, speed limits, emissions, and traveling time. The multiobjective optimization criteria are handled by the so-called look-ahead control methods. In the paper traffic, information such as the speed of the current traffic flow and the speeds of vehicles in the lanes is also considered. Consequently, the look-ahead control can be considered as an extension of the adaptive cruise control with road and traffic information.

The optimization problem of the energy-efficient look-ahead control was formed using the receding (sliding) horizon control in Hellström et al. (2010), Passenberg et al. (2009) and evaluated in real experiments in Hellström et al. (2009). The look-ahead control based on road inclinations, speed limits, a preceding vehicle in the lane and traveling time was proposed by Németh and Gáspár (2013b). The optimization criterion between journey time and fuel consumption was converted into a

constrained fuel optimization task in Saerens et al. (2013). A predictive cruise control with upcoming traffic signal information to improve fuel economy was proposed by Asadi and Vahidi (2011). In hybrid electric vehicles road prediction is important to optimize battery recovery. The predictive reference signal generator method to maximize recuperated energy using the topographic profile of the future road segments was proposed by Ambuhl and Guzzella (2009). The shape of the speed profile at a road segment was estimated in a nonlinear constrained optimization process in van Keulen et al. (2010). The look-ahead control is also motivated by the design of a platoon control system. A cooperative control strategy based on preview information, which initiates the change in speed for all vehicles in the platoon, was proposed by Alam et al. (2013). The method of the look-ahead control was extended to the design of the common speed of the vehicles in the platoon in Németh and Gáspár (2014).

In the optimization methods proposed by the publications environmental conditions such as topographic data and speed limits along the road are exploited. However, in the methods less emphasis is placed on traffic information such as speed of the current traffic flow and speeds of the vehicles in the lanes. This is a critical point in speed design. For example, a vehicle using the look-ahead control is able to create a balance between energy/fuel saving and journey time according to its own priorities. However, other vehicles on the road have different priorities, which can lead to conflict, e.g., fast vehicles are held up by vehicles traveling in a fuel efficient fashion, see e.g., Gáspár and Németh (2015).

6.3.2 Design of Speed Profile

It is assumed that the energy-efficient optimal speed v_{opt} is calculated by using a multi-criterion optimization method in the look-ahead control. In the design, the control energy, traveling time and, moreover, environmental conditions such as topographic data and speed limits along the road are exploited. However, the vehicle preferring energy saving travels in traffic. Since the vehicle may catch up with a preceding vehicle, it is necessary to consider its speed, which is denoted by v_{lead}. Moreover, since the vehicle may be in conflict with other vehicles preferring cruising at the speed limit v_{lim}.

The purpose is that the look-ahead control will be applied both as a part of driver assistance systems or in the autonomous vehicle control. Consequently, the control is extended by traffic information. However, traffic modifies the result of the multi-criterion optimization and results in a less energy efficient speed. The combination of the look-ahead concept and the congestion problem leads to a complex multi-criterion optimization task. The paper focuses on the development of this task.

The structure of the proposed computation algorithm is illustrated in Fig. 6.3. The road inclinations α and speed limits v_{lim} data ahead of the vehicle are established using the current position and a navigation map. Moreover, the vehicle receives information about the motion of preceding and follower vehicles through V2V communication.

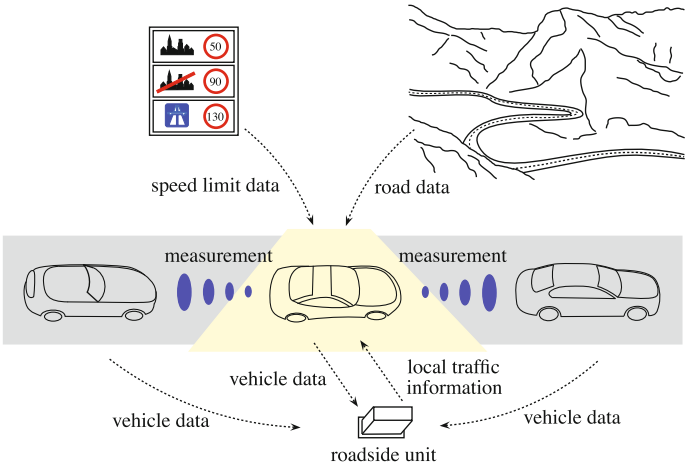

Fig. 6.3 Communication and information flow

A survey of the future communication possibilities in automotive and traffic control was provided by Ebnre and Hermann (2001). In order to detect potentially hazardous situations a computer vision-based approach to tracking surrounding vehicles and estimating their trajectories was presented by Nuevo et al. (2010). An extension of adaptive cruise control with traffic information considering vehicle-to-roadside and vehicle-to-vehicle communication was proposed in Kesting et al. (2007). In order to prevent emergencies and accidents vehicle-to-vehicle communication and vehicle-to-roadside sensor communication were combined by Festag et al. (2008).

6.3.3 *Principles of the Optimization of the Look-Ahead Control*

In the following section, the principles of the look-ahead control are presented briefly. The road ahead of the vehicle is divided into several sections, which may be of different lengths consistently with the topography of the road. The rates of the slopes of the road and the speed limits are assumed to be known at the endpoint of each section. There are n number of segments and $n + 1$ number of points as Fig. 6.4 shows. Then reference speeds at the section points are defined using road information: $v_{ref,0}, v_{ref,1}, \ldots, v_{ref,n}$. It is assumed that the acceleration of the vehicle may change in the different intervals, but within a single interval it is approximately constant. The aim is to calculate the speed of the vehicle at which the reference speeds at the section points can be reached while both energy reduction and traveling time are considered.

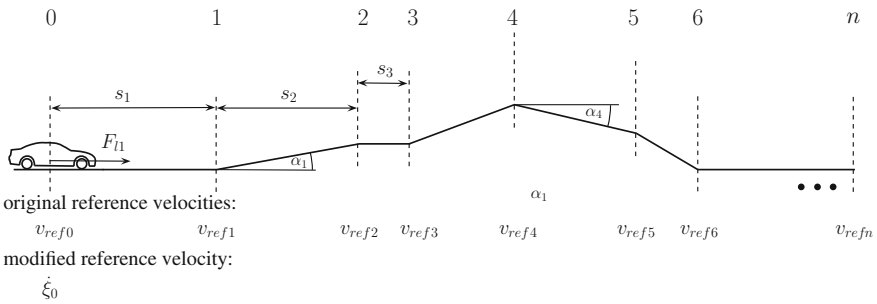

Fig. 6.4 Division of road

The speed of the vehicle at point $i \in (1, n)$ is written as:

$$\dot{\xi}_i^2 = \dot{\xi}_0^2 + \frac{2}{m} \sum_{j=1}^{i} s_j \left(F_{lj} - F_{dj} \right), \quad i \in \{1, 2, \ldots, n\}, \tag{6.22}$$

where $\dot{\xi}_0$ is the speed of the vehicle at the initial point, $\dot{\xi}_i$ is the speed of vehicle at the i^{th} point and s_j is the distance of the interval $[j-1, j]$. F_{lj} is the longitudinal force. At the calculation of the control force, it is assumed that the current control force F_{l1} affects the vehicle, however, the effects of the additional longitudinal forces are not considered, i.e., $F_{li} = 0, i > 1$. Thus, in the method the current longitudinal drive force acting on the vehicle in the first road section is calculated. F_{dj} is the disturbance force resulting from the road slopes, rolling resistance, aerodynamic forces, etc. The disturbance force originating from the road slopes and aerodynamic forces is estimated in every section

$$F_{dj,r} = mg \sin \alpha_j + \frac{1}{2} c_w \rho A \dot{\xi}_j^2, \quad j \in [1, n], \tag{6.23}$$

where m is the vehicle mass, α_j is the angle of the road slope, c_w is the drag coefficient, ρ is the density of the air, A is the contact surface size of the vehicle front, K is the road surface resistance. The rest of the disturbances $F_{d1,o}$ can be considered unknown.

The aim of the control design is that at every section point the speed $\dot{\xi}_i$ of the vehicle must reach the predefined reference speed $\dot{\xi}_i^2 \to v_{ref,i}^2$. This defined condition is rearranged using the kinematic relationship and the form of disturbance. Consequently, the equations of the vehicle speeds at the section points are calculated in the following way:

$$\dot{\xi}_i^2 = \dot{\xi}_0^2 + \frac{2}{m} s_1 F_{l1} - \frac{2}{m} s_1 F_{d1,o} - \frac{2}{m} \sum_{j=1}^{i} s_j F_{dj,r}. \tag{6.24}$$

In the next step, prediction weights $Q, \gamma_1, \gamma_2, \ldots, \gamma_n$ are applied to the section points. They represent the priority of the i^{th} condition. The weights must sum up to one, i.e.,

$$\gamma_1 + \gamma_2 + \cdots + \gamma_n + Q = 1. \tag{6.25}$$

While the prediction weights γ_i represent the rate of the road conditions, weight Q has a crucial role: it determines the tracking requirement of the current reference speed $v_{ref,0}$. By increasing Q the momentary speed becomes more important while road conditions become less important. For example when $Q = 1$ the control task is simplified to a cruise control problem.

Applying the weights in (6.24) the following formula is yielded:

$$\dot{\xi}_0^2 + \frac{2}{m} s_1 (1 - Q) F_{l1} - \frac{2}{m} s_1 (1 - Q) F_{d1,o} = \vartheta \tag{6.26}$$

where value ϑ depends on the road slopes, the reference speeds and the weights

$$\vartheta = Q v_{ref,0}^2 + \sum_{i=1}^{n} \gamma_i v_{ref,i}^2 + \frac{2}{m} \sum_{i=1}^{n} s_i F_{di,r} \sum_{j=i}^{n} \gamma_j. \tag{6.27}$$

In order to take the road information (road slopes, speed limits) into consideration in the speed design, Eq. (6.26) is applied. The momentary acceleration of the vehicle is expressed in the following way: $\ddot{\xi}_0 = (F_l - F_{d1,o} - F_{d1,r})/m$ where $F_{d1,r} = mg \sin \alpha$. It yields the predicted speed, which is considered as a reference signal in the control design

$$\dot{\xi}_0 \to \lambda \tag{6.28}$$

where parameter λ is calculated in the following way based on the designed ϑ:

$$\lambda = \sqrt{\vartheta - 2 s_1 (1 - Q)(\ddot{\xi}_0 + g sin\alpha)}. \tag{6.29}$$

Equation (6.26) shows that the predicted speed $\dot{\xi}_0$ depends on the weights (Q and γ_i). A detailed description of the speed profile design is found in Németh and Gáspár (2013b).

6.4 Optimization of the Vehicle Cruise Control

The design of the vehicle speed poses two optimization problems: the longitudinal force must be minimized and the deviation from the reference velocity must be minimized. The minimization of the longitudinal control force $F_{l1}^2 \to \min$ leads

to the first quadratic optimization problem (*Optimization 1*), which is solved by selecting the weights using (6.26)

$$\bar{F}_{l1}^2 = (\beta_0(\bar{Q}) + \beta_1(\bar{Q})\bar{\gamma}_1 + \ldots + \beta_n(\bar{Q})\bar{\gamma}_n)^2 \rightarrow \min \tag{6.30}$$

with the following constrains $0 \leq \bar{Q}, \bar{\gamma}_i \leq 1$ and $\bar{Q} + \sum \bar{\gamma}_i = 1$. The minimization of the difference between the current velocity and the reference velocity leads to the second optimization problem (*Optimization 2*)

$$|v_{ref,0} - \dot{\xi}_0| \rightarrow \min \tag{6.31}$$

leads to the optimal solution, which is achieved by selecting the weights: $\breve{Q} = 1$ and $\breve{\gamma}_i = 0, i \in [1, n]$, since in this case the vehicle tracks the predefined speed.

The two optimization criteria lead to different optimal solutions and a balance between the performances must be achieved. Thus, two performance weights are introduced. Performance weight R_1 is related to the importance of (6.30) in the first optimization while performance weight R_2 is related to (6.31) in the second optimization. There is a constraint on the performance weights: $R_1 + R_2 = 1$, in which $0 \leq R_1 \leq 1$ and $0 \leq R_2 \leq 1$. Thus a balance between the optimizations tasks can be achieved by selecting the following performance weights:

$$Q = R_1\bar{Q} + R_2\breve{Q} = 1 - R_1(1 - \bar{Q}) \tag{6.32a}$$

$$\gamma_i = R_1\bar{\gamma}_i + R_2\breve{\gamma}_i = R_1\bar{\gamma}_i, \quad i \in \{1, \ldots, n\} \tag{6.32b}$$

The equations show that the prediction weights depend on R_1. Normally drivers set weight R_1 based on their goals and requirements, thus they create a balance between energy saving and traveling time. The optimal momentary speed of the vehicle is approximated by

$$v_{opt} = \bar{\lambda}, \tag{6.33}$$

in which

$$\bar{\lambda} = \sqrt{\bar{\vartheta} - 2s_1R_1(1 - \bar{Q})(\ddot{\xi}_0 + gsin\alpha)}, \tag{6.34}$$

and

$$\bar{\vartheta} = v_{ref,0}^2 - R_1(1 - \bar{Q})v_{ref,0}^2 + R_1\sum_{i=1}^{n}\bar{\gamma}_i v_{ref,i}^2 + R_1\frac{2}{m}\sum_{i=1}^{n}s_i F_{di,r}\sum_{j=i}^{n}\bar{\gamma}_j. \tag{6.35}$$

6.4.1 Handling the Preceding Vehicle in the Speed Design

Since the vehicle may catch up with a preceding vehicle, it is necessary to consider the speed of the latter v_{lead}. This task is handled by the performance weight R_1 since the control must focus on speed rather than energy saving in order to avoid a collision, thus it leads to a conventional cruise control solution.

The safe stopping distance between the vehicles is calculated according to the 91/422/EEC, 71/320/EEC UN and EU directives (the velocity in km/h): $d_{safe} = 0.1\dot{\xi} + \dot{\xi}^2/150$, in which $\dot{\xi}$ is the current speed. When the distance between vehicles is below d_{safe}, the current speed must be v_{lead}. In order to avoid the abrupt braking the speed reduction starts at a longer distance $(1+c)\cdot d_{safe}$ with constant $0 < c < 1$. Considering d_{safe} weight $R_{1,p}$ is selected in the following structure:

$$R_{1,p} = \begin{cases} 0 & \text{if} \quad d < d_{safe} \\ R_1 \frac{d - d_{safe}}{(1+c)d_{safe}} & \text{if } d_{safe} \leqq d \leqq (1+c)\cdot d_{safe} \\ R_1 & \text{if} \quad d > (1+c)\cdot d_{safe} \end{cases} \tag{6.36}$$

Moreover, $v_{ref,0} = v_{lead}$ if $d < (1+c)\cdot d_{safe}$.

The optimal speed of the vehicle during the journey is calculated by applying $R_1 = R_{1,p}$ in the expression (6.33). Note when $R_{1,p} = 0$ and $v_{ref,0} = v_{lead}$ the look-ahead control is a conventional cruise control and only the tracking of the preceding vehicle will be carried out. If a preceding vehicle does not disturb the motion of the vehicle using a look-ahead control, the weight is set $R_{1,p} = 1$.

6.4.2 Motion of the Follower Vehicle in the Speed Design

The vehicle controlled by an energy-efficient method overtakes slower preceding vehicles on the highway. At the same time, another vehicle accelerates to reach the speed limit and also begins an overtaking maneuver. Since the vehicle preferring energy saving travels in traffic, it may be in conflict with other vehicles preferring cruising at the speed limit. Preferring the weight R_1 leads to a nonoptimal motion for the traffic. A balance between the energy-efficient speed and the flow of the local traffic is proposed by the modification of the value R_1. The motion of follower vehicles is considered in a three-step procedure. In the first step, the speed and the motion of the vehicle using the look-ahead control is predicted (*Step 1*). In the second step, the motion of the follower vehicle is predicted (*Step 2*). In the third step, the safe distance is calculated, which is the basis of the R_1 selection *Step 3*.

Step 1: The optimal speed of the vehicle using the look-ahead control is based on (6.33). Based on (6.35) the expression of $\bar{\vartheta}$ can be rewritten as

$$\begin{aligned}\bar{\vartheta} &= v_{ref,0}^2 - R_1 v_{ref,0}^2 + R_1 \bar{Q} v_{ref,0}^2 + \\ &+ R_1 \sum_{i=1}^{n} \bar{\gamma}_i v_{ref,i}^2 + R_1 \frac{2}{m} \sum_{i=1}^{n} s_i F_{di,r} \sum_{j=i}^{n} \bar{\gamma}_j = \\ &= v_{ref,0}^2 (1 - R_1) + R_1 \tilde{\vartheta} \end{aligned} \tag{6.37}$$

where $\tilde{\vartheta}$ contains the expression of ϑ according to Eq. (6.27), in which energy-efficient prediction weights $\bar{Q}, \bar{\gamma}_i$ are used.

From (6.34) the optimal speed $\bar{\lambda}$ is calculated based on the predicted road information. Through prediction weights $\bar{Q}, \bar{\gamma}_i$ the optimal speed is calculated in the following form:

$$\begin{aligned}\bar{\lambda}^2 &= v_{ref,0}^2 (1 - R_1) + R_1 \tilde{\vartheta} - 2 s_1 R_1 (1 - \bar{Q})(\ddot{\xi}_0 + g \sin\alpha) \\ &= v_{ref,0}^2 (1 - R_1) + R_1 \tilde{\lambda}^2 \end{aligned} \tag{6.38}$$

where $\tilde{\lambda}$ contains the expression of λ according to Eq. (6.29), in which energy-efficient prediction weights $\bar{Q}, \bar{\gamma}_i$ are used.

From (6.24) and (6.38) the predicted estimated speed of the vehicle at section point n is

$$\begin{aligned}\dot{\xi}_n^2 &= v_{ref,0}^2 (1 - R_1) + R_1 \tilde{\lambda}^2 \\ &+ \frac{2}{m} s_1 F_{l1} - \frac{2}{m} s_1 F_{d1,o} - \frac{2}{m} \sum_{i=1}^{n} s_i F_{di,r} = \\ &= R_1 \mathscr{N}_1 + \mathscr{N}_2 \end{aligned} \tag{6.39}$$

According to (6.39) the predicted speed $\dot{\xi}_n$ at point n is based on the momentary speed, the longitudinal force, and the disturbances. Consequently, the predicted speed at point n is independent of $v_{ref,n}$. However, it may be misleading, since when $R_1 = 0$ the predicted speed at point n must be $v_{ref,n}$. In order to meet this requirement, the predicted speed must be modified using the reference speed and the weighting factor in the following way:

$$\dot{\xi}_n^2 = (R_1 \mathscr{N}_1 + \mathscr{N}_2) R_1 + (1 - R_1) v_{ref,n}^2 \tag{6.40}$$

The advantage of this equation is that the reference speed is built into the predicted speed, thus the numerical procedure is more reliable.

Step 2: In the second step, the motion of the follower vehicle is predicted. It is assumed that the controlled vehicle has information about the speed and acceleration of the follower vehicle ($\dot{\eta}_0$, $\ddot{\eta}_0$) and the momentary distance between the vehicles e_0. It is also assumed that the follower vehicle accelerates evenly until it reaches the speed limit, i.e., $i < j$. Then it does not accelerate further, thus in the oncoming sections the predicted speeds of the vehicle are $v_{ref,j}, \ldots, v_{ref,n}$, i.e., $i \geqq j$.

Based on the information $(\dot{\eta}_0, \ddot{\eta}_0, e_0)$ the motion of the vehicle must be calculated in every section in which the traveling time is $\Delta t_i, i = \{1 \dots n\}$. During acceleration the displacements of the follower vehicle are

$$\eta_k = \frac{\ddot{\eta}_0}{2}\left(\sum_{i=1}^{k} \Delta t_i\right)^2 + \dot{\eta}_0 \sum_{i=1}^{k} (\Delta t_i), \quad k \in [1, j-1] \tag{6.41}$$

in which traveling time in a section is Δt_i. When the follower vehicle reaches the speed limit, it does not accelerate further. Moreover, its speeds do not exceed the predefined reference speeds $v_{ref,j}, \dots, v_{ref,n}$. The displacements of the vehicle are

$$\eta_l = \eta_{j-1} + \sum_{i=j}^{l} (v_{ref,i} \Delta t_i), \quad l \in [j, n] \tag{6.42}$$

Step 3: Finally, in the third step, the safe distance is calculated. Now the safe distance between the controlled vehicle and the follower one must be guaranteed. The safe distance d_{safe} is assumed to be predefined.

The controlled vehicle intends to use the energy-efficient predicted cruise control, while the follower vehicle aims to keep the speed limit. Thus, the look-ahead control strategy is modified in such a way that the motion of the follower vehicle is taken into consideration. A possible method is to modify performance weight R_1 during the journey and create a balance between the designed speed and the required speed of the follower vehicle. The aim of this section is to develop a method for the redesign of weight $R_{1,f}$.

The criterion of the safe distance is based on the motion of the vehicles. During the journey in every section the distance between the two vehicles must be guaranteed by the following inequalities:

$$\xi_i + e_0 - \eta_i \geq d_{safe}, \quad i \in \{1, 2, \dots, n\} \tag{6.43}$$

where ξ_i is the predicted displacement of the controlled vehicle, e_0 is the momentary distance between the vehicles $(t = 0)$ and η_i is the predicted displacement of the follower vehicle. It is necessary to find the maximum of performance weight R_1, which satisfies the inequality constraints (6.43). Note that an increase in R_1 induces longer journey time. Therefore R_1 can be limited by the driver using a predefined bound $R_{1,max}$.

The optimization criterion for safe cruising is formulated as follows:

$$R_{1,f} = \max_{[0; R_{1,max}]} R_1 \tag{6.44}$$

such that the following conditions are satisfied:

$$\sum_{i=1}^{j} \xi_i + e_0 - \eta_j - d_{safe} \geq 0, \quad j \in \{1, \ldots, n\} \tag{6.45}$$

The result of the optimization $R_{1,f}$ is used in the calculation of the prediction weights Q and γ_i. Based on the prediction weights the reference speed of the controlled vehicle λ is computed. The optimization procedure (6.44) is performed in each step, thus performance weight $R_{1,f}$ is rewritten continuously according to the current local traffic information. If a follower vehicle does not disturb the motion of the vehicle using a look-ahead control, the weight is set $R_{1,f} = 0$.

In practice the solution of the optimization procedure (6.44) requires a great deal of computation effort. However, in solution (6.44) the result of the previous computation step $R_{1,old}$ can be applied as initial value. If the new solution $R_{1,new}$ is searched for in the interval

$$[\max(R_{1,old} - \alpha, 0), \min(R_{1,old} + \alpha, R_{1,max})]$$

with for example $n = 10$ points and $\alpha = 0.1$, the computation time is reduced significantly. Note that $R_{1,max}$ is set by the driver within the interval $R_{1,max} = [0; 1]$.

6.4.3 A Decision Method of the Lane Change

In this section, the decision algorithm of the lane change is proposed. During the lane change safe operation must be guaranteed and the conflicts between vehicles and tailbacks must be prevented. First of all, the safe distance from both the preceding vehicle and the follower one in the new lane must be ensured. Consequently, the safe distance must be examined before the lane change is carried out. Second, conflicts between the vehicle preferring energy saving and the following vehicle preferring cruising at the speed limit must be avoided. Thus, handling the preceding vehicle and considering the motion of the follower vehicle must be incorporated into the decision method.

Essentially, the lane change is preferred if the vehicle using energy-efficient speed control is not able to keep the designed speed in the current lane and at the same time the designed speed can be ensured and the maneuver is safe in the adjacent lane. The speed profile is influenced by two weighting factors in the look-ahead control. Weight $R_{1,f}$ is used to consider the follower vehicle while weight $R_{1,p}$ is used to handle the preceding vehicle. Besides the calculation of the optimal speed, during the journey the acceptable speed is computed for both the current lane and the adjacent lane. Since the weighting factors $R_{1,f}$ and $R_{1,p}$ influence the acceptable speed, they are also computed and considered. In the decision method of the lane change, these two factors must be analyzed.

Scenario 1: The controlled vehicle catches up with a preceding vehicle.

In this scenario $R_{1,p}$ tends to zero and the vehicle adapts to the velocity of the preceding vehicle. Since the preceding vehicle is traveling slower, the current speed may differ significantly from the designed velocity, thus the lane change must be analyzed. $R^a_{1,p}$ must be computed for the adjacent lane.

Scenario 2: The follower vehicle catches up with the controlled vehicle.

Since $R_{1,f}$ is reduced, the vehicle adapts to the velocity of the follower vehicle. Since the follower vehicle is traveling faster, the current speed may differ significantly from the designed velocity, thus the lane change must be analyzed. $R^a_{1,f}$ must be computed for the adjacent lane.

Two basic inequalities must be checked. $R^a_{1,p}$ and $R^a_{1,f}$ are computed for the adjacent lane and they are compared to the current $R_{1,p}$ and $R_{1,f}$. The lane change must be carried out if the following two inequalities persist. $R^a_{1,p}$ is significantly greater than $R_{1,p}$, which means that in the adjacent lane there is not a preceding vehicle and at the same time $R^a_{1,f}$ is larger than $R_{1,f}$, which means that the follower vehicles are not hindered and the energy-efficient velocity can be ensured. Moreover, the safe distances from the preceding vehicle and the follower one in the new lane can also be guaranteed. d_p and d_f are the distances from the preceding vehicle and the follower one in the new lane, respectively.

Summarizing the above thoughts, the following logic-based decision method can be formed:

$$\text{If} \quad R^a_{1,p} - R_{1,p} > \varepsilon_p \quad \text{and} \quad R^a_{1,f} - R_{1,f} > \varepsilon_f, \tag{6.46}$$

and, moreover,

$$\text{if} \quad d_p \geq d_{safe} \quad \text{and} \quad d_f \geq d_{safe}, \tag{6.47}$$

where ε_p and ε_f are predefined values, then the lane change should be performed.

In this case, the lane-change maneuver should be realized in an autonomous system or this suggestion should be made to the driver in a driver assistance system.

6.5 Implementation of the Method in the Driving/Braking Systems

The command variable of the robust control design is the longitudinal force input $u = F_{l1}$. However, the real physical system has two inputs, such as driveline and brake inputs. In the following section, the transformation of F_{l1} to the real physical inputs is presented.

In the conventional engine-powered driveline system, the gear positioning and the throttle are the intervention possibilities. The proposed method considers an automatic transmission, where the positioning of the gear is determined by the engine speed and the throttle $\varepsilon \in [0 \ldots 1]$. Thus, it is necessary to find an appropriate ε,

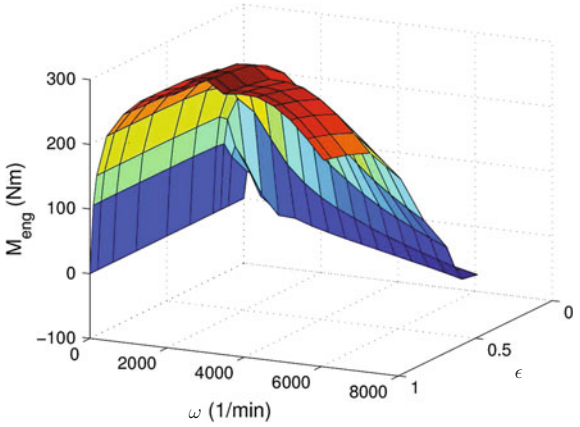

Fig. 6.5 Typical engine characteristics

which guarantees the realization of F_{l1}. Since the driveline dynamics (6.11) is faster than the longitudinal dynamics, the transients of the driveline are ignored in the computations. The conversion between F_{l1} and α is based on static relations.

The required torque of the engine is computed with the following expression as:

$$M_{eng} = \frac{F_{l1} R_w}{k_0 k_g} \tag{6.48}$$

where R_w is wheel radius, k_0 and k_g are the ratio of the driven axle and the transmission. The value of k_g depends on the current gear position. The conversion between M_{eng} and ε is performed through the engine characteristics, see, e.g., Fig. 6.5. This computation requires the measurement of the engine speed ω, and the inversion of the characteristics based on M_{eng} and ω.

The braking system in the paper is a conventional hydraulic construction. The dynamics of the braking hydraulics τ is faster than the longitudinal motion, therefore the relationship between F_l and brake cylinder pressures is described by static equations. First, the longitudinal force is divided between the front and the rear axles, using the following expression, see Zomotor (1991):

$$F_r = -F_{fr} - \frac{mg\ l_2}{2h} + \sqrt{\frac{F_{fr}(l_1 + l_2)\ mg}{h} + \left(\frac{mg\ l_2}{2h}\right)^2} \tag{6.49}$$

where F_r and F_{fr} are the wheel forces at the rear and at the front, respectively. h represents the height of the center of gravity height, l_1, l_2 are the distances between the axles and the center of gravity. F_{fr} and F_r are divided equally between the left and the right sides. Second, the wheel longitudinal forces are converted into the cylinder braking pressures, such as

$$p_i = \frac{F_i R_w}{C_{pM,i}} \tag{6.50}$$

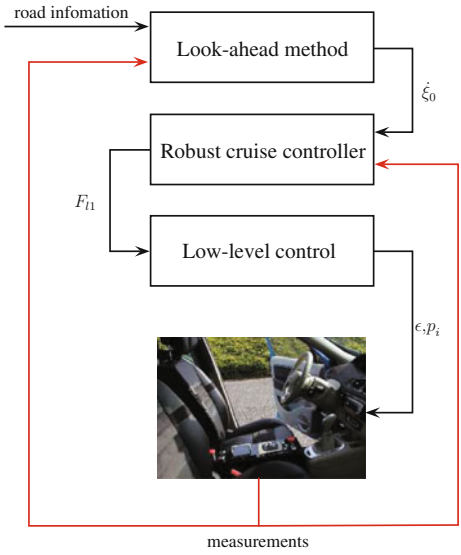

Fig. 6.6 Architecture of the cruise control

where F_i is the longitudinal force of the wheel, and $C_{pM,i}$ is the constant, which depends on the wheel brake construction.

The decision between the actuation of the driveline and the braking system depends on the control force F_{l1}. If $F_{l1} > 0$ then throttle is activated, otherwise the braking pressures of the cylinders are increased.

6.5.1 SIL Implementation of the Controller

In the following section, the implementation of the proposed system in a SIL environment is presented. The control algorithm has three layers, which are illustrated in Fig. 6.6.

- The high layer contains the look-ahead control strategy, which generates the reference velocity signal of the cruise control. It is based on the information about the forthcoming road intersections, e.g., the road slopes. It guarantees the fuel-efficiency of the vehicle cruising.
- The middle layer is the feedforward-feedback $\mathscr{H}_\infty$ controller. It guarantees the velocity tracking and the robustness against mass variation and longitudinal disturbances. The output of the controller is the F_{l1} signal.
- The low layer incorporates the transformation of the control force F_{l1} to the engine throttle ε. Moreover, it realizes the distribution of the driving and braking forces on the wheels of the vehicle.

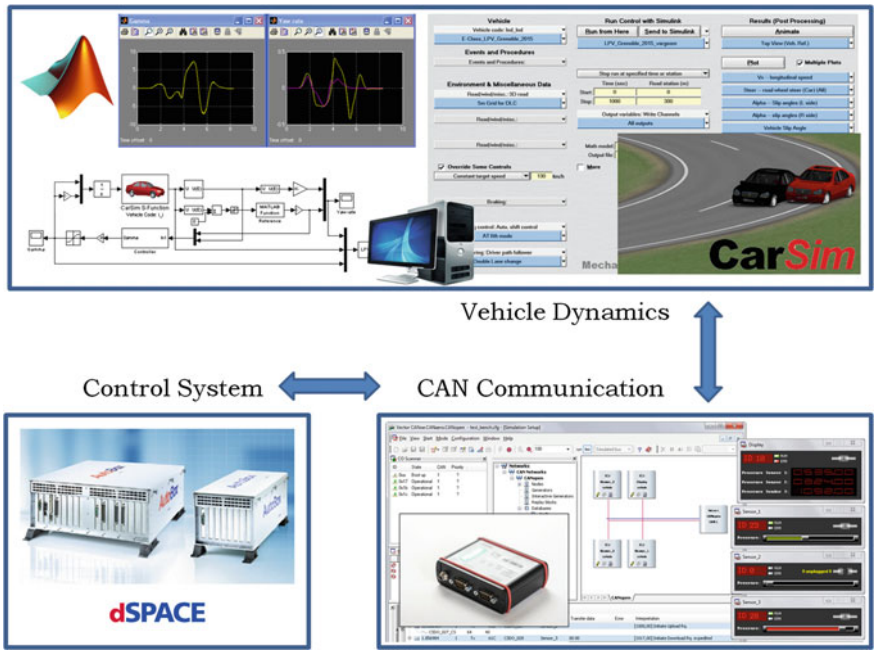

Fig. 6.7 Software-in-the-loop simulation

The scheme of the SIL environment is illustrated in Fig. 6.7. The SIL consists of a workstation with the CarSim vehicle simulator, the dSPACE environment, in which the controller is implemented. In the workstation, the CarSim works together with MATLAB®/Simulink®. The CarSim simulator with the MATLAB/Simulink software, which are standard industrial tools, simulate the vehicle dynamics with high accuracy. The communication between the workstation and the dSPACE is realized through the CAN bus. Before the SIL simulation, the designed control system is set on the real-time equipment. The control signal is computed in dSPACE by the discrete-time solver of the differential equations with $0.01s$ sampling time.

6.5.2 Simulation Examples

In the simulation a transportational route with real data is analyzed. The terrain characteristics and geographical information are those of a French highway between Mulhouse and Belfort in a 35 km-long section. In the simulation, a conventional compact SUV passenger car is used. The regulated maximal velocity is 130 km/h, but the road section contains other speed limits, and the road section also contains hilly parts. The data of the highway (altitude, speed limitations) from up-to-date geographical/navigational databases, such as Google Earth and Google Maps are reached.

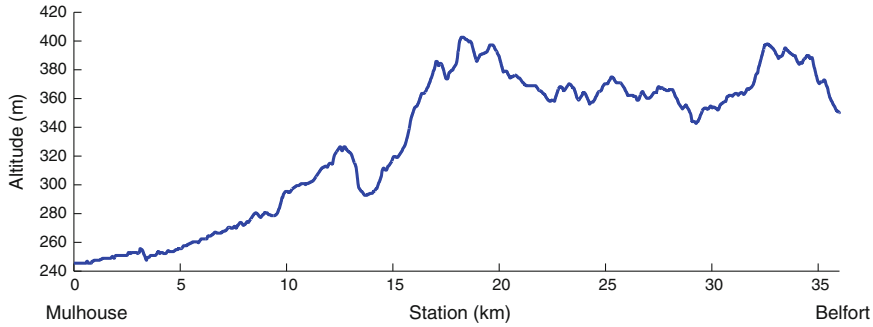

(a) Road altitude

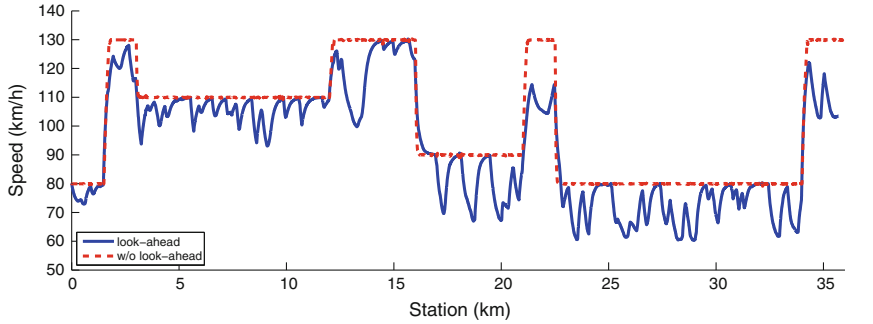

(b) Velocity of vehicle

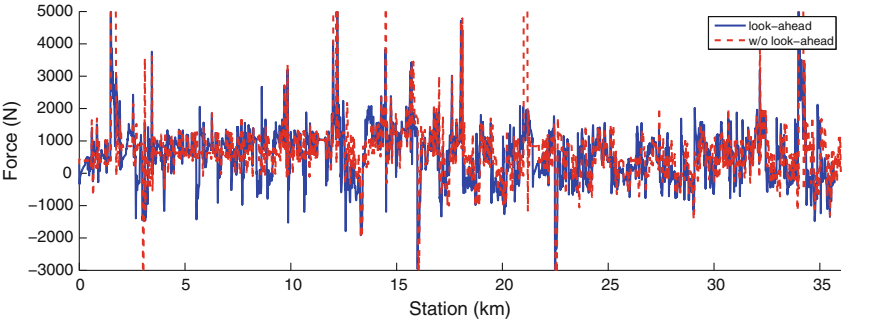

(c) Actuated force of vehicle

Fig. 6.8 Simulation of the cruise control

The goals of the simulations are to demonstrate the efficiencies of the combined feedforward-feedback cruise control and the look-ahead strategy. Thus, in the simulations two scenarios are shown, such as with or without look-ahead control. In the look-ahead simulation, the information about the upcoming terrain characteristics and speed regulations are considered, which influences the speed profile of the vehicle.

Figure 6.8a shows the altitude of the highway, which contains several uphill and downhill sections. During the road several speed limitations (80, 90, 110 km/h) are

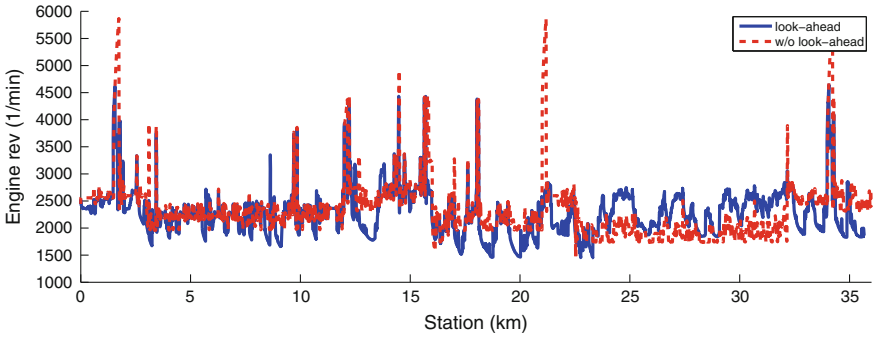

(a) Engine rev

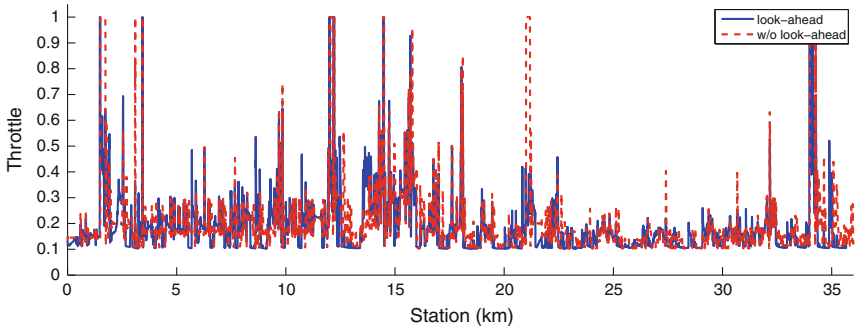

(b) Throttle

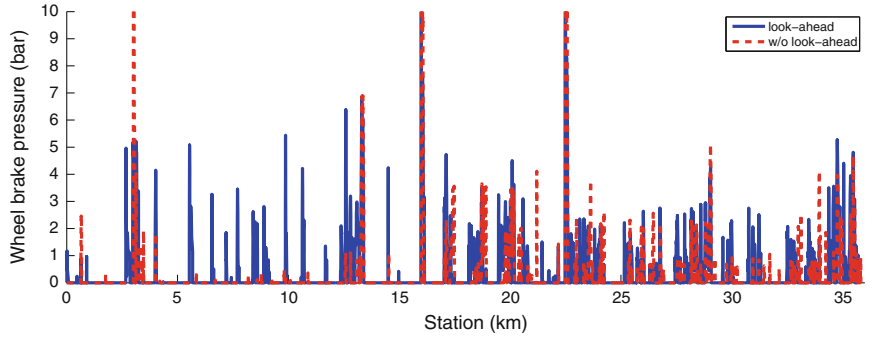

(c) Brake pressure on front wheels

Fig. 6.9 Actuation in the cruise control

found, as can be seen in Fig. 6.8b. The results show that the designed feedforward-feedback controller is able to track the change of the limitations. In case of the look-ahead cruise control the desired speed is significantly varied to consider the effects of the hills and speed limits. For example, between the section points 12 . . . 14 km there is a valley in the highway. Thus, the traction force of the vehicle is reduced in front of the valley (see Fig. 6.8c), which results in the reduction of the vehicle speed.

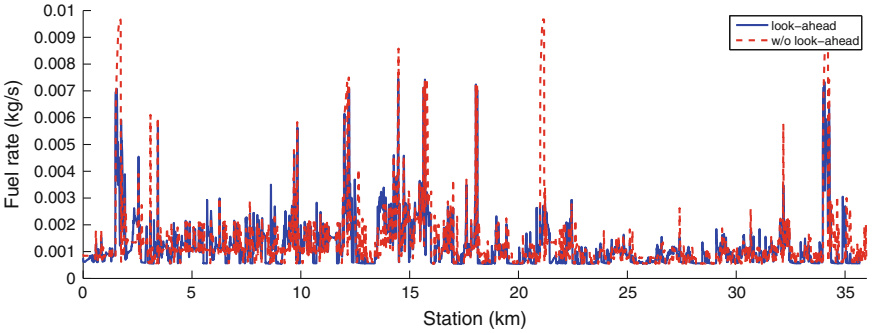

(a) Fuel rate during theroad

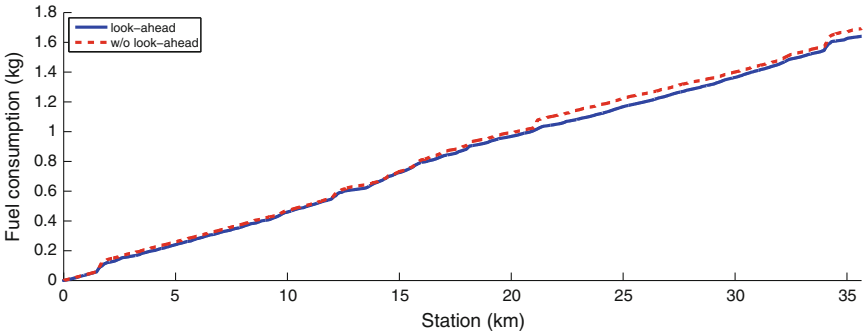

(b) Total fuel consumption

Fig. 6.10 Data of the fuel consumptions

However, the vehicle in the downhill section of the valley is accelerated, which leads to energy sparing.

The actuation of the longitudinal control elements are found in Fig. 6.9. Figure 6.9a shows that the rev of the engine on the cruising is generally reduced. It is resulted by the smaller actuation of the throttle angle, see Fig. 6.9b. It leads to the sparing of the fuel consumption due to the less engine actuation. The brake pressures are illustrated through the example of the front wheels, see Fig. 6.9c.

Finally, the fuel consumption of the cruise controls are presented in Fig. 6.10. The proposed look-ahead method requires less fuel consumption than the cruise control method without look-ahead control. The saving of the total fuel is 3 %, which is resulted by the adaptation to the actual terrain characteristics and speed limitations. Since in the look-ahead method, the speed of the vehicle may be below the permitted maximum for the given section and accelerations/decelerations are carried out more slowly and gradually than in the conventional method, the duration of the journey is expected to be longer. However, the difference in the traveling time is only 2 minutes.

Part III
Lateral and Integrated Control

Chapter 7
Design of Integrated Vehicle Control

7.1 Motivation of the Integrated Vehicle Control

Conventionally, the control systems of vehicle functions to be controlled are designed separately by the suppliers and the vehicle companies. One of the problems of independent design is that the performance demands, which are met by independent controllers, are sometimes in conflict with each other in terms of the full vehicle. The braking action affects the longitudinal dynamics of the vehicle, the velocity, and the pitch angle. However, due to the geometry of the vehicle, the braking action causes changes in both the yaw and roll dynamics, see Fig. 7.1. Similarly, the steering angle also modifies the yaw angle of the vehicle. Since the center of gravity is high the consequence of the steering maneuver is that the roll angle and the pitch angle of the sprung mass will also change, see Fig. 7.2. Moreover, the second problem in the independent control design is that control hardware can be grouped into discrete subsets with sensor information and control demands operating in parallel processes and these solutions can lead to unnecessary hardware redundancy.

The purpose of the integrated vehicle control is to combine and supervise all controllable subsystems affecting vehicle dynamic responses. In more details it means that multiple-objective performance from available actuators must be improved, sensors must be used in several control tasks, the number of independent control systems must be reduced, at the same time the flexibility of control systems must be enhanced. An integrated control system is designed in such a way that the effects of a control system on other vehicle functions are taken into consideration in the design process by selecting the various performance specifications. In line with the requirements of the vehicle industry several performance specifications are in the focus of the research, e.g., improving road holding, enhancing passenger comfort and improving roll and pitch stability, proposing fault-tolerant solutions, see e.g., Gordon et al. (2003), Yu et al. (2008).

The demand for vehicle control methodologies including several control components arises at several research centers and automotive suppliers. Here are a few examples for illustration. A vehicle control with four-wheel-distributed steering and

P. Gáspár et al., *Robust Control Design for Active Driver Assistance Systems*,
Advances in Industrial Control, DOI 10.1007/978-3-319-46126-7_7

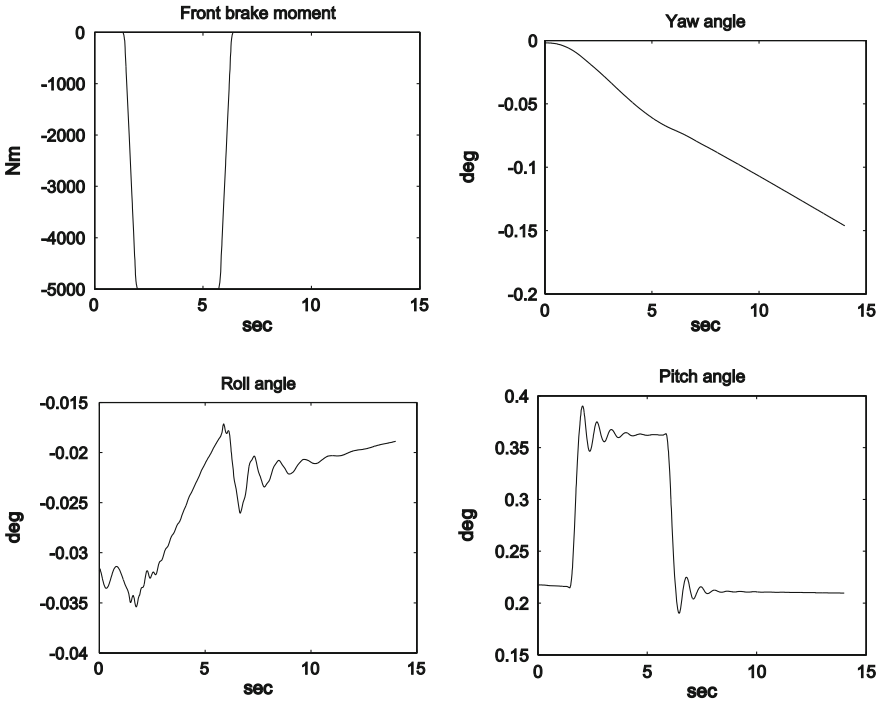

Fig. 7.1 The effect of braking on vehicle dynamics

four-wheel-distributed traction/braking systems is proposed by Ono et al. (2006). A process to design the control strategy for a vehicle with throttle control and automatic transmission is proposed by Kim et al. (2007). A yaw stability control system in which an active torque distribution and differential braking systems are used is proposed by Zhang et al. (2009). An integrated control that involves both four-wheel steering and yaw moment control is proposed by Jianyong et al. (2007), Wang and Nagai (1996). An integrated control that involves both steering and differential braking is proposed by Bardawil et al. (2014). The integration of differential braking and the steering angle using model predictive control based on the piecewise affine approximation of the tire force characteristic is proposed by Cairano et al. (2013). Active steering and suspension controllers are also integrated to improve yaw and roll stability Mastinu et al. (1994). A global chassis control involving an active suspension and ABS is proposed by Poussot-Vassal et al. (2008), Zin et al. (2008), Fergani et al. (2015). The driveline system and the brake are integrated in Rajamani et al. (2000). An important solution to the roll stability control is based on the ESC brake control, see Lu et al. (2007), Palkovics and Fries (2001). A possible integration of the brake, steering and suspension system is presented by Burgio and Zegelaar (2006), Gáspár et al. (2010), Trachtler (2004a). An LPV-based integrated control design, in which the performances are guaranteed through the optimal selection of the schedul-

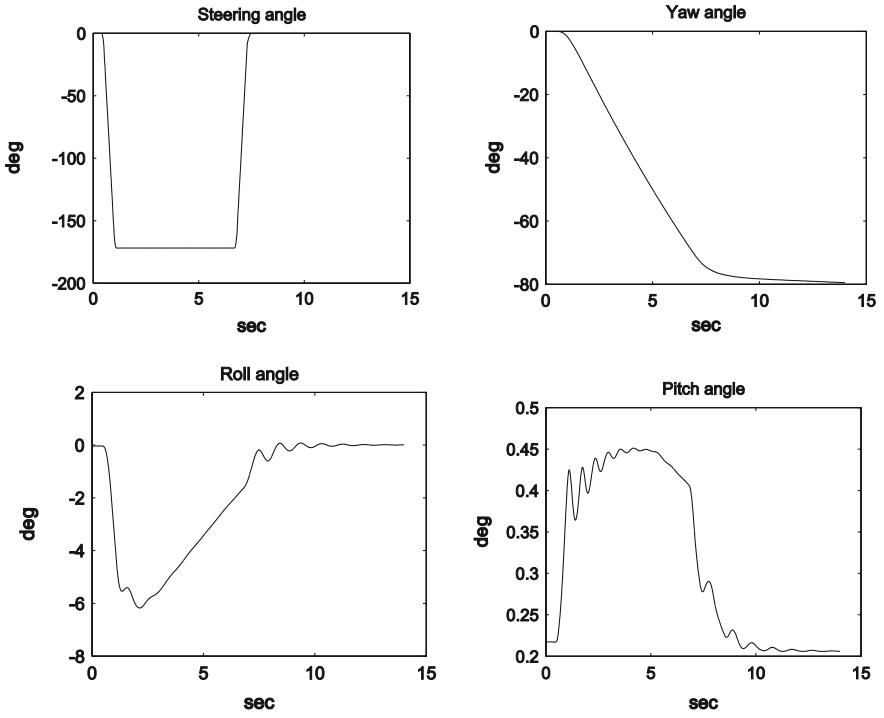

Fig. 7.2 The effect of steering on vehicle dynamics

ing variables is proposed in Gáspár and Németh (2016). In Doumiati et al. (2013) a gain scheduled LPV-based method for the coordination of steering and braking is presented. In Song et al. (2015) a hierarchical method for the design of integrated chassis controller is adopted for a full drive-by-wire vehicle. Automated guidance system design using nonlinear model predictive control based steering coupled with the longitudinal control is presented in Attia et al. (2014a).

A centralized controller has several advantages: the designed controller guarantees performance specifications and robustness against uncertainties; the solution reduces the number of necessary sensors; it improves the flexibility of the actuators and avoids unnecessary duplications. The high-complexity control problem, however, is often difficult to handle, i.e., the more complex the vehicle model is the more numerical problems must be handled. Moreover, this centralized approach is not suitable for the partial design tasks carried out by vehicle component suppliers. Furthermore, if a new component is added to the system the entire system must be redesigned (Fig. 7.3).

Thus, decentralized controllers which operate simultaneously are applied for the vehicle. The advantage of this architecture is that the complexity of the vehicle model can be divided into several parts. In this decentralized control structure there is a logical relationship between the supervisor and the local control components.

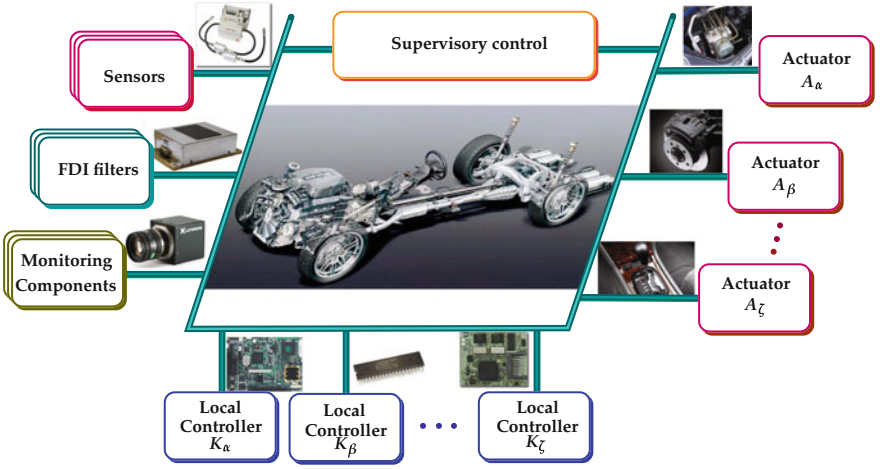

Fig. 7.3 The architecture of integrated vehicle control

The communication within local controls is performed by using the CAN bus. The role of the supervisor is to meet performance specifications, create a cooperation between components, and prevent the interference and conflict between them. The supervisor has information about the current operational mode of the vehicle, i.e., the various vehicle maneuvers or the different fault operations gathered from monitoring components and fault detection and identification (FDI) filters. The supervisor is able to make decisions about the necessary interventions into the vehicle components and guarantee the reconfigurable and fault-tolerant operation of the vehicle. These decisions are propagated to the lower layers through predefined interfaces encoded as suitable scheduling signals. As some examples for the topic of fault detection methods in industrial mechatronic products, see Muenchhof et al. (2009).

7.2 LPV-Based Concept of the Integrated Control

The objective of the control design is to track a predefined path, guarantee road holding and increase yaw, roll, and pitch stability. Several control components are applied in the system: the active brake, steering, and the suspension system, see Fig. 7.4. The tracking problem is solved by using active steering. In this system the control input is the steering angle: $u_d = \delta_f$. Road holding and passenger comfort are improved by applying an active suspension system. The suspension system is also able to improve pitch and roll stability by generating pitch moment during abrupt braking and roll moments during emergency maneuver. The control inputs are generated by the suspension actuators: $u_s = \left[f_{fl}, f_{fr}, f_{rl}, f_{rr}\right]^T$. In the control system the brake is able to modify the yaw angle of the vehicle during a cornering

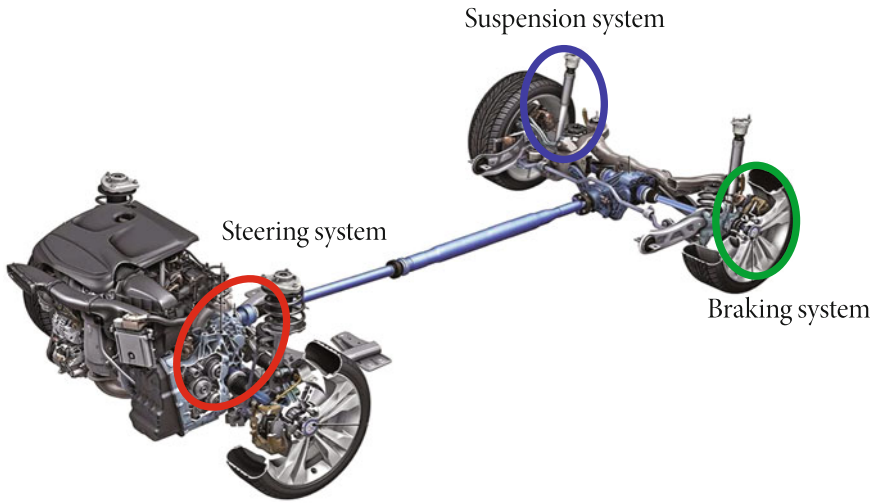

Fig. 7.4 Integrated system with three control components

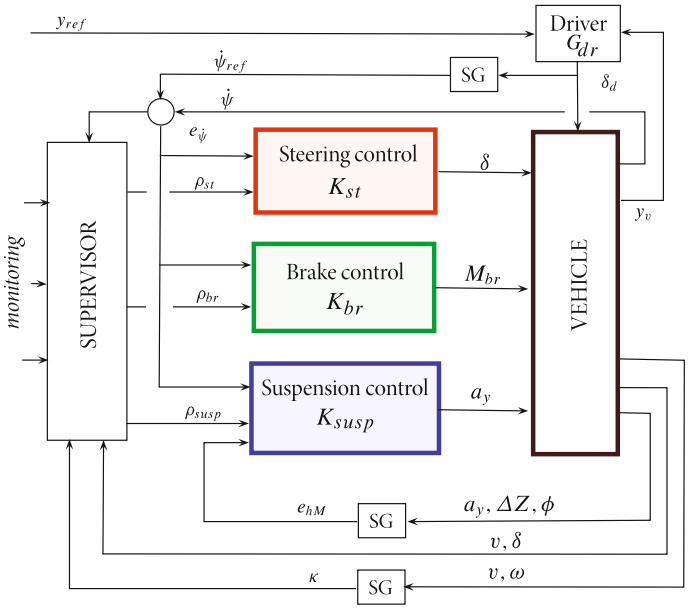

Fig. 7.5 Closed-loop structure of the integrated control

and reduce the effect of lateral acceleration. When a rollover is imminent and this emergency persists the brake system is activated to reduce the rollover risk. It is also able to generate unilateral brake forces at the front and the rear wheels at either of the two sides $u_b = \Delta F_b$.

The structure of the supervisory control, in which three active control systems are integrated is shown in Fig. 7.5. In the following parts of the chapter the principle of the integrated control is presented.

7.3 Design of the Local and Reconfigurable Control Systems

The local controllers are designed based on vehicle models with different complexity. Their design is based on state space representation form

$$\dot{x} = A(\rho)x + B_1(\rho)w + B_2(\rho)u, \tag{7.1}$$

where x, w and u are the state, disturbance and input, respectively, vector ρ includes the scheduling variables and $A(\rho) = A_0 + \sum_{i=1}^{n} \rho_i A_i$, $B_1(\rho) = B_{10} + \sum_{i=1}^{n} \rho_i B_{1i}$, $B_2(\rho) = B_{20} + \sum_{i=1}^{n} \rho_i B_{2i}$, in which n is the number of the scheduling variables ρ_i. First the state equation is defined and then the performances and measured output are selected considering the control tasks.

The nonlinear effects of the forward velocity v, the adhesion coefficient of the vehicle in the lateral direction μ, or the nonlinear characteristics in the suspension damper components ρ_{bij} are taken into consideration $\rho = [v, \mu, \rho_{bij}]^T$ in the design. For example the adhesion coefficients depend on the type of road surface. It is difficult to accurately quantify and measure the effect of all of the external factors on μ, which is a nonlinear and time-varying function. An adaptive observer-based gray-box identification method has been proposed for its estimation, Gáspár et al. (2005b). It is assumed that with suitably selected scheduling variables ρ these nonlinear components can be transformed into affine parameter-dependent forms. Then the nonlinear models are transformed into LPV models in which nonlinear terms are hidden with suitably selected scheduling variables.

The local components also include units for monitoring vehicle operations. These components are able to detect emergency vehicle operations, various fault operations, or performance degradations in controllers. They also send messages to the supervisor. In the reconfigurable and fault-tolerant control of the local controller several signals must be monitored and scheduling variables are added to the scheduling vector in order to improve the safety of the vehicle, e.g., variables are needed to encode the rollover risk, represent the harmful effects of abrupt braking and take a detected failure of an active component into consideration.

The efficient operation of the supervisor and the local controllers require reliable and highly accurate signals from the system. To meet this requirement redundant sensors, diverse calculations, and fault detection filters are needed. To achieve the efficient and optimal intervention the detections of faulty sensors are important since they must be substituted in operations based on these sensors. Low-cost solutions are

preferred in the vehicle industry, thus simple sensors and software-based redundancy must be applied.

The closed-loop system applied in the design of a local control includes the feedback structure of the model $G(\rho)$, the compensator and elements associated with the performance objectives:

$$z = C(\rho)x + D_1(\rho)w + D_2(\rho)u, \tag{7.2}$$

where $w = [d \ n]^T$ includes both the external disturbances and the sensor noise.

In the interconnection structure performance requirements z are imposed by a suitable choice of the weighting functions W_p. Usually, the purpose of weighting functions W_p is to define penalty functions, i.e., weights should be large where small signals are desired and small where large performance outputs can be tolerated. The proposed approach realizes the reconfiguration of the performance objectives by an appropriate scheduling of these weighting functions. Δ_m block contains the uncertainties of the system, such as unmodelled dynamics and parameter uncertainty. In this augmented plant unmodelled dynamics is represented by a weighting function W_r and a block Δ_m. The purpose of the weighting functions W_d and W_n is to reflect the disturbance and sensor noises.

In the proposed solution the design of local control components is based on LPV methods. LPV methods are well elaborated and successfully applied to various industrial problems. The LPV approaches allow us to take into consideration the highly nonlinear effects in the state space description. The main point of the approach is that in the control design of the local components scheduling variables received from the supervisor are used as a key of integration. In this way the operation of a local controller can be extended to reconfigurable and fault-tolerant functions.

If parameter-dependent Lyapunov functions are used, the designed controller depends explicitly on $\dot{\varrho}$. Thus, in order to construct a parameter-dependent controller, both ϱ and $\dot{\varrho}$ must be measured or available. When $\dot{\varrho}$ is not measured in practice, a suitable extrapolation algorithm must be used to achieve an estimation of the parameter $\dot{\varrho}$. To remove $\dot{\varrho}$ dependence a ϱ-dependent change of variables was proposed in Balas et al. (1997).

The quadratic LPV performance problem is to choose the parameter-varying controller $K(\varrho)$ in such a way that the resultant closed-loop system $M(\varrho)$ is quadratically stable and the induced $\mathscr{L}_2$ norm from w to z is less than γ, i.e.,

$$\|M(\rho)\|_\infty = \inf_K \sup_\Delta \sup_{\|w\|_2 \neq 0, w \in \mathscr{L}_2} \frac{\|z\|_2}{\|w\|_2}. \tag{7.3}$$

By assuming an unstructured uncertainty and by applying a weighted small gain approach the existence of a controller that solves the quadratic LPV γ-performance problem can be expressed as the feasibility of a set of LMIs, which can be solved numerically, see Wu (2001).

The existence of a controller that solves the quadratic LPV γ-performance problem can be expressed as the feasibility of a set of Linear Matrix Inequalities (LMIs),

which can be solved numerically. Stability and performance are guaranteed by the design procedure, see Balas et al. (1997), Wu et al. (1996). When the LPV controller has been synthesized, the relation between the state, or output, and the parameter $\rho = \sigma(x)$ is used in the LPV controller, such that a nonlinear controller is obtained.

7.3.1 Design of the Brake System

Roll stability is achieved by limiting the lateral load transfers on both axles to below the levels for wheel liftoff during various vehicle maneuvers. The lateral load transfers are calculated at both axles: $\Delta F_{z,i} = C_i \phi_{t,i}$. The tire contact force is guaranteed if $\frac{mg}{2} \pm \Delta F_z > 0$ for both sides of the vehicle. The normalized values of the lateral load transfers are the ratio of $\Delta F_{z,i}$ and the masses of the vehicle on the axles: $\rho_R = \Delta F_{z,i}/m_i g$. The aim of the control design is to reduce the maximum value of the normalized lateral load transfer if it exceeds a predefined critical value (Fig. 7.6).

In the design of the brake system the command signal is the difference in brake forces while the performance signal is the lateral acceleration: $z_b = \left[a_y, u_r\right]^T$. The weighting function of the lateral acceleration is selected as:

$$W_{p,ay} = \gamma_a \frac{T_{b1}s + 1}{T_{b2}s + 1}. \tag{7.4}$$

where T_{bi} are time constants. Here γ_a is a gain, which reflects the relative importance of the lateral acceleration and it is chosen to be parameter-dependent, i.e., the function of ρ_R.

$$\gamma_a = \begin{cases} 1 & \text{if} \quad |\rho_R| > R_b \\ \frac{|\rho_R| - R_a}{R_b - R_a} & \text{if} \quad R_a \le |\rho_R| \le R_b \\ 0 & \text{if} \quad |\rho_R| < R_a \end{cases}$$

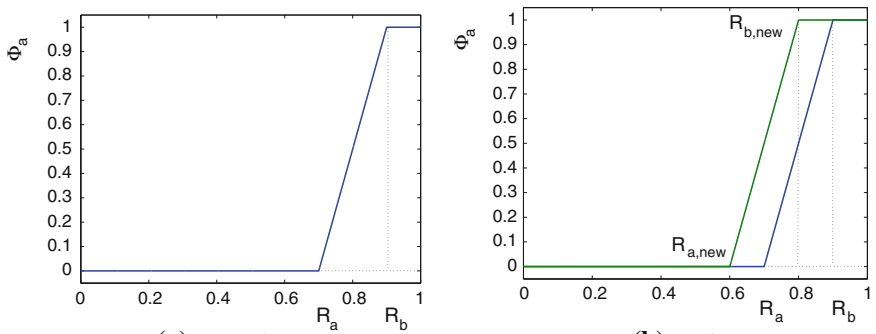

(a) Normal case **(b)** Fault case

Fig. 7.6 Parameter-dependent gain in the brake control

When ρ_R is small ($|\rho_R| < R_b$), i.e., when the vehicle is not in an emergency, γ_a is small, indicating that the LPV control should not focus on minimizing acceleration. When ρ_R is approaching the critical value, i.e., when $|\rho_R| \geqq R_b$, γ_a is large, it indicates that the control should focus on preventing the rollover. Here R_b defines the critical status when the vehicle is close to the rollover. Note that the weights used in the chapter are proportional–differential components. Their time constants and gains reflect the required steady state and transient behavior of the different signals that describe the performance specifications.

Remark 7.1 If a fault concerning roll stability is detected in the suspension system its role is substituted by the brake system. The brake system is activated at a smaller critical value than in a fault-free case, i.e., when $|\rho_{Da}| > 0$. Consequently, the brake is activated in a modified way and the brake moment is able to assume the role of the suspension actuator in which the fault has occurred. The modified critical value is

$$R_{a,new} = R_a - \alpha \cdot \rho_{Da}, \tag{7.5}$$

where α is a predefined constant factor.

7.3.2 Design of the Steering System

Yaw stability is achieved by limiting the effects of the lateral load transfers. The purpose of the control design is to minimize the lateral acceleration, which is monitored by a performance signal: $z_a = a_y$. Unilateral braking is one of the solutions, in which brake forces are generated in order to achieve a stabilizing yaw moment. In the second solution additional steering angle is generated in order to reduce the effect of the lateral loads. These solutions, however, require active driver intervention into the motion of the vehicle to keep the vehicle on the road.

Another control task is to follow a road by using a predefined yaw rate (angle). In this case the current yaw rate must be monitored and the difference between the reference and the current yaw rate is calculated. The purpose of the control is to minimize the tracking error: $z_{\dot{\psi}} = \dot{\psi}_{cmd} - \dot{\psi}_{ref}$.

In order to solve the yaw rate tracking problem in the design of the steering system, the command signal must be fed forward to the controller ($\dot{\psi}_{\text{cmd}}$). The command signal is a predefined reference displacement and the performance signal is the tracking error: $z_{\dot{\psi}} = e_{\dot{\psi}}$, which is the difference between the actual yaw rate and the yaw rate command. The weighting function of the tracking error is selected as:

$$W_{pe} = \gamma_e \frac{T_{d1}s + 1}{T_{d2}s + 1}, \tag{7.6}$$

where T_{di} are time constants. Here, it is required that the steady state value of the tracking error should be below $1/\gamma_e$ in steady state.

Remark 7.2 If a fault is detected in the steering system ($|\rho_{Ds}| > 0$), the brake must focus on yaw dynamics in order to reduce the tracking error. Thus, in the control design of the brake the performance specification concerning the steering system is also built in:

$$W_{pe} = \gamma_{be} \frac{T_{b3}s + 1}{T_{b4}s + 1}, \tag{7.7}$$

where γ_{be} depends on $|\rho_{Ds}|$

$$\gamma_{be} = \begin{cases} 1 & \text{if} \quad |\rho_{Ds}| > \rho_{crit} \\ \frac{|\rho_R| - \rho_{tol}}{\rho_{crit} - \rho_{tol}} & \text{if} \quad \rho_{tol} \leq |\rho_{Ds}| \leq \rho_{crit} \\ 0 & \text{if} \quad |\rho_{Ds}| < \rho_{tol} \end{cases}$$

In this weighting the critical value of the brake intervention is used together with a tolerance value.

Remark 7.3 When there is a performance degradation in the operation of the brake system, it is not able to create sufficient yaw moment to improve roll stability. In this sense the brake system is substituted by the steering system. The steering system receives the fault message from the supervisor and it modifies its operation in such a way that the effects of the lateral loads are also reduced. The difficulty in this solution is that a performance degradation concerning the tracking task also occurs, since the steering system must create a balance between tracking and roll stability.

7.3.3 Design of the Suspension System

Road holding is achieved by reducing the normalized suspension deflections ρ_k between the sprung and unsprung masses at the four corner points of the vehicle. Since increasing road holding reduces the passenger comfort in the design of the suspension system its desired level is subject to a design decision.

The performance signals in the suspension design are: $z_s = \left[a_z \; s_d \; t_d \; u_s\right]^T$. The goals are to keep the heave accelerations $a_z = \ddot{q}$, suspension deflections $s_d = x_{1ij} - x_{2ij}$, wheel travels $t_d = x_{2ij} - w_{ij}$, and control inputs small over the desired operation range. The performance weighting functions for heave acceleration, suspension deflections, and tire deflections are selected as

$$W_{p,az} = \gamma_{az} \frac{T_{s1}s + 1}{T_{s2}s + 1}, \tag{7.8}$$

$$W_{p,sd} = \gamma_{sd} \frac{T_{s3}s + 1}{T_{s4}s + 1}, \tag{7.9}$$

$$W_{p,td} = \gamma_{td} \frac{T_{s5}s + 1}{T_{s6}s + 1}, \tag{7.10}$$

where T_{si} are time constants while γ_{td} are parameter-dependent gains, which depend on the suspension deflection ρ_{kij}.

In normal cruising the suspension system focuses on the conventional performances based on the parameter-dependent gain, which is a function of the suspension deflection ρ_{kij}. The trade-off between passenger comfort and suspension deflection is due to the fact that it is not possible to guarantee them together simultaneously. A large gain γ_{az} and a small gain γ_{sd} correspond to a design that emphasizes passenger comfort while choosing γ_{az} small and γ_{sd} large corresponds to a design that focuses on suspension deflection. The parameter dependence of the gains, which is illustrated in Fig. 7.7, is characterized by the constants ρ_1 and ρ_2 in the following way:

$$\gamma_{az} = \begin{cases} 1 & \text{if} \quad |\rho_{kij}| < \rho_1, \\ \frac{|\rho_{kij}|-\rho_2}{\rho_1-\rho_2} & \text{if} \quad \rho_1 \le |\rho_{kij}| \le \rho_2, \\ 0 & \text{if} \quad R \ge R_s \ \text{ or } \ |\rho_{kij}| > \rho_2. \end{cases}$$

$$\gamma_{sd} = \begin{cases} 0 & \text{if} \quad |\rho_{kij}| < \rho_1, \\ \frac{|\rho_{kij}|-\rho_1}{\rho_2-\rho_1} & \text{if} \quad \rho_1 \le |\rho_{kij}| \le \rho_2, \\ 1 & \text{if} \quad R \ge R_s \ \text{ or } \ |\rho_{kij}| > \rho_2. \end{cases}$$

Remark 7.4 The idea of the reconfigurable suspension system is based on the fact that active suspension systems are used not only to eliminate the effects of road irregularities but also to generate roll moments to improve roll stability or generate pitch moment to improve pitch stability.

$$W_{p,\theta} = \gamma_P \frac{T_{s7}s + 1}{T_{s8}s + 1},$$
$$W_{p,\gamma} = \gamma_R \frac{T_{s9}s + 1}{T_{s2}s + 10}.$$

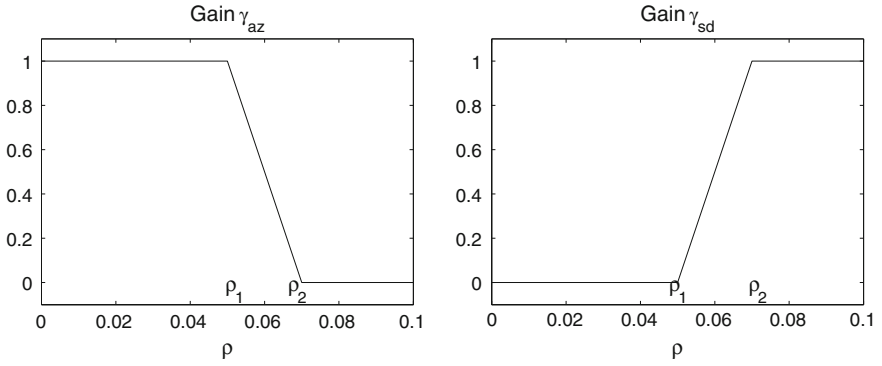

Fig. 7.7 Parameter-dependent gains in the suspension control

For a reconfigurable suspension system the parameter-dependent gains are selected as functions of the normalized lateral load transfer ρ_R and the normalized value of the pitch angle ρ_P. If ρ_P exceeds a predefined critical value, i.e., when $|\rho_P| \geqq R_P$, the controller must focus on pitch stability. In an emergency, however, i.e., when $|\rho_R| \geq R_s$, the suspension system must reduce the rollover risk and guaranteeing passenger comfort (and pitch angle) is no longer a priority.

7.3.4 Actuator Selection Procedure

In this section the selection of the weighting functions applied to the control design is based on the effects of the actuators on vehicle dynamics.

The maximal control input of the steering is determined by its physical construction limits, while in the case of the braking system the constraints are the tire road adhesion conditions.

In the control design the distribution of the wheel forces must also be taken into consideration. In a front-wheel-driven vehicle the traction force is distributed between the front wheels by using a differential gear. The steering angle is limited by construction (δ_{crit}), therefore when the maximal steering angle is reached the desired lateral dynamics of the vehicle must be achieved by the brake moment. During braking the load of wheels is modified due to the pitch dynamics of the vehicle. The braking of the front wheels must be stronger while the braking of the rear wheels must be reduced. It is necessary to avoid the skidding of tires, thus in such a case the generation of differential braking must be reduced. The skidding of tires can be monitored by the estimation of the longitudinal slips of the tires κ; a possible method is found in Gustafsson (1997), de Wit et al. (2003). These constraints must also be taken into consideration in the control design and must be guaranteed by the supervisor.

Moreover, the activation of the different components have an energy requirement. By using differential braking the velocity of the vehicle is reduced, which must be compensated for by the driveline with additional energy. Therefore the use of differential braking must be avoided during acceleration and front-wheel steering is preferred. During deceleration the brake is already being used, thus the lateral dynamics is handled by the braking for practical reasons. Thus differential braking is preferred, but close to the limit of skidding, front-wheel steering must also be generated. The actuation of differential braking causes increased strain on the tires. When the vehicle moves in the lateral direction the position of each tire is longitudinal and they are not rotating. This also shows that using front-wheel steering is more efficient.

The bandwidth of the different actuators must also be taken into consideration in the weighting functions. In the case of front-wheel steering and the variable-geometry suspension, the inertia of the systems effects a slower operation of the actuators than the bandwidth of differential braking. In the following, the bandwidths of the actuation are compared.

The dynamics of steering is determined by the moment which rotates the wheels $M_{st} = 2\vartheta_{st}\ddot{\delta} + M_{res,st}$, where ϑ_{st} is the inertia of the wheel on the axle of steering, δ is the steering angle. M_{st} is controlled by a servo power system according to the rack, where $M_{res,st} = M_{gy,st} + M_{ch,st}$ is the sum of the steering resistances. In order to the steer the rotating wheels it is necessary to generate energy against the gyroscopic effect. It is formulated by using the following assumption: $M_{gy,st} = 2J_w v\dot{\delta}/r_w$, where J_w is the inertia of the wheel on the axle of rotation and r_w is the wheel radius. During steering the positions of wheels are modified. Since the axle of a steered wheel is skew the vertical position of the entire chassis also moves. Thus, it is necessary to generate energy to improve the lateral dynamics of the chassis: $M_{ch,st} = B\pi s_{susp}(\sin n)\ \delta$, where B is the wheel track, s_{susp} is the suspension stiffness and n is the angle between the road and the axis of wheel steering. The transfer function of the steering system between the steering angle δ and the moment M_{st} is

$$G_{st} = (\vartheta_{st}s^2 + \frac{2J_w v}{r_w}s + B\pi s_{susp}\sin n)^{-1}$$

The bandwidth of the actuation rate is analyzed as a function of velocity. Figure 7.11 shows that the bandwidth values change significantly with the change of velocity (Fig. 7.8).

The maximal longitudinal force of the wheels ($F_{i,max}$) is calculated and compared to the momentary longitudinal wheel forces (F_i). Note that the maximum longitudinal force depends on the maximum adhesion coefficient and the static and dynamic components of the vertical force at the wheel, i.e., the lateral and pitch dynamics.

$$F_{i,max} = \mu_{max}\{F_{z,stat} \pm ma_y h/2/L \pm m\dot{\psi}vh/b\}.$$

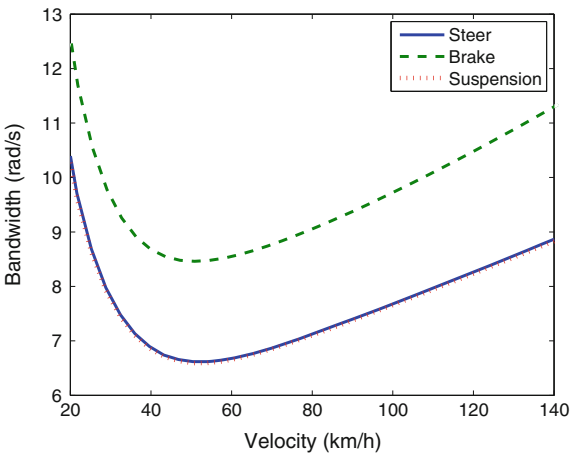

Fig. 7.8 Bandwidth values of actuators

This calculation must be performed at all wheels and the highest rate of $\nu = F_i/F_{i,max}$ is selected. If a skidding incident is imminent the actuation of the brake moment must be reduced and it is replaced by the actuation of front-wheel steering. The variable $\nu = max\{F_i/F_{i,max}\}$ is the maximal value between the force ratios considering all the wheels and ν_{crit} is a design parameter.

According to the inertia of steering, the bandwidths of steering and suspension are lower at each velocity than the bandwidth of differential braking. The fast operation of actuators is an important feature mainly at high velocities. At higher velocities it is recommended to use differential braking, while at lower velocities steering actuation is preferred for practical reasons. The weighting functions for the front-wheel steering, brake yaw moment and suspension moment are selected in the following form:

$$W_{act,\delta} = \rho_\delta/\delta_{max} \tag{7.11}$$

$$W_{act,Mbr} = \rho_{br}/M_{brmax} \tag{7.12}$$

respectively, where δ_{max} and γ_{max} are determined by the constructional maximum of the steering and the camber angle, while M_{brmax} is the maximum of the brake yaw moment. Weighting factors ρ_{st}, ρ_{br} are chosen to influence the priority of the actuators. Figure 7.9 shows the characteristics of the weighting factors.

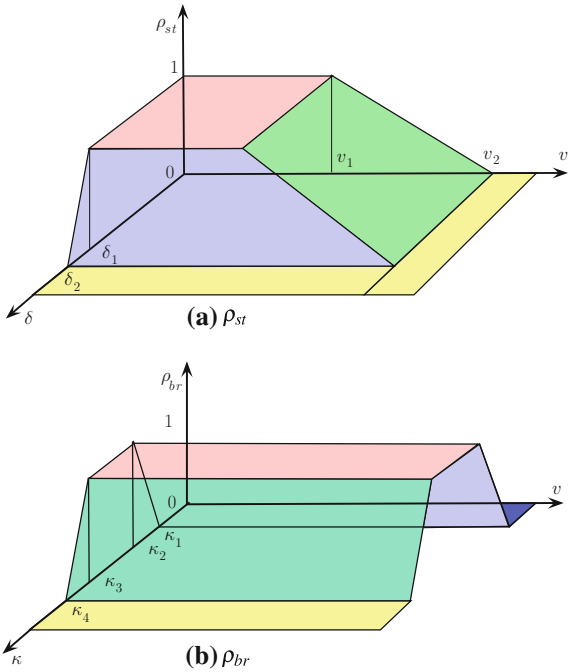

Fig. 7.9 Selection of parameters ρ_{st} and ρ_{br}

When the vehicle is being driven the front-wheel steering is actuated, which is determined by factor ρ_{st}, see Fig. 7.9a. The value is reduced between δ_1 and δ_2, which represents the constructional criterion of the steering system. In this interval differential braking is preferred for practical reasons. The values of ρ_{st} also depend on the velocity of the vehicle. The effect of velocity on the weighting factors is the consequence of the difference between the bandwidth values of the actuators. According to the inertia of steering, the bandwidth of steering is lower at each frequency than the bandwidth of differential braking. At higher velocities it is recommended to use differential braking, while at lower velocities the steering actuation is preferred for practical reasons. Consequently, two additional design parameters (v_1 and v_2) are also introduced. In the case of braking the tire longitudinal slip angle κ affects ρ_{br}, see Fig. 7.9b. It requires an interval to reduce tire skidding (κ_1, κ_2) and it also requires an interval to prevent chattering between steering and differential braking (κ_3, κ_4).

7.3.5 *Fault Information in the Decentralized Control*

The fault-tolerant local controllers also require components for monitoring fault information. Here the normalized fault information provided by an FDI filter is given by

$$\rho_D = \frac{f_{act}}{f_{max}}, \tag{7.13}$$

where f_{act} is an estimation of the failure (output of the FDI filter) and f_{max} is an estimation of the maximum value of the potential failure (fatal error). The estimated value f_{act} means the measure of the performance degradation of an active component.

The interconnection structure includes the vehicle model $G(\rho)$, the FDI filter $F(\rho)$, and elements associated with performance objectives, see Fig. 7.10. The weight W_{p_f} reflects the relative importance of the fault signal. This weight should be large when small errors are desired and small when large errors can be tolerated. The

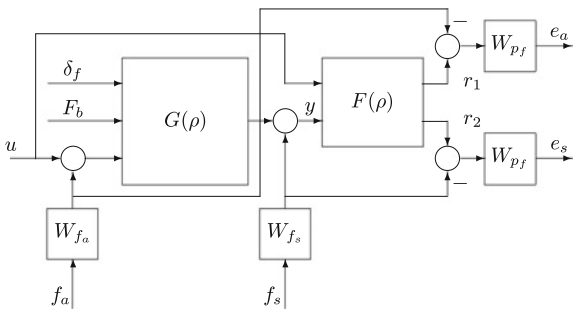

Fig. 7.10 Design of an FDI filter

weight W_{f_a} defines the size of the possible fault in the actuator channel. The weight W_{f_s} defines the size of the possible fault in the sensor channel.

The design requirement for $\mathscr{H}_\infty$ residual generation is to maximize the effect of the fault (f) on the residual and simultaneously minimize the effect of exogenous signals ($d,\ u$) on the residual.

$$||T_{rd}||_\infty = \sup_{||f||_2=1, \rho \in \mathscr{P}} ||r||_2, \tag{7.14}$$

where the residual can be expressed as $r = T_{ru}u + T_{rd}d + T_{rf}f$. The FDI filter designed in the open-loop system can be implemented in the closed-loop system. The filter receives the measured outputs, the control inputs and the filter provides the fault residuals. For more details on the main steps of the FDI filter design see Gáspár et al. (2005c).

The fault-tolerant control requires fault information in order to guarantee performances and modify its operation. Thus, FDI filters are also designed for the operation of the actuators. As an example the fault information provided by a fault detection filter is given by $\rho_D = f_{act}/f_{max}$, where f_{act} is an estimation of the failure (output of the FDI filter) and f_{max} is an estimation of the maximum value of the potential failure (fatal error). The value of a possible fault is normalized into the interval $\rho_D = [0,\ 1]$. The estimated value f_{act} means the rate of the performance degradation of an active component.

The detection of a sensor failure as accurately as possible is crucial since the controller may generate fault actuator intervention as a result of fault sensor information. Sensor failures may also prevent certain actuators from being used; then handling the sensor failure leads to an actuator reconfiguration problem. Thus complex vehicle systems require various FDI filters both for actuator and sensor failures.

7.4 Control Design of Trajectory Tracking

7.4.1 Modeling of Trajectory Tracking

The control system of the lateral vehicle dynamics assists the driver in tracking road geometry. It has advantages in critical situations, in which the driver is not able to ensure vehicle stability. In trajectory tracking the vehicle is moving in the road and both the longitudinal and the lateral dynamics must be taken into consideration. In the design of trajectory tracking assistance systems it is necessary to guarantee that the vehicle must perform the desired lateral motion of the driver. The nonlinear dynamics of the tire and the velocity of the vehicle influence the sideslip angles on the front and rear axles of the vehicle. The balance of these two angles determines the steering motion of the vehicle, which changes depending on velocity. Unfortunately

the driver does not have information about this motion during the journey, which may cause emergencies.

Three actuators are used in the system, i.e., the front-wheel steering angle δ, the differential brake torque M_{br}, and the wheel camber angle γ. In the vehicle system a variable-geometry suspension system which changes the camber angle of the rear wheels is applied. Various solutions for the variable-geometry suspension system have already been proposed, see Watanabe and Sharp (1999), Evers et al. (2008). A rear suspension active toe control to enhance driving stability is proposed by Lee et al. (2008), Goodarzia et al. (2010).

The lateral force of the tire F_y via the tire sideslip α is approximated as $F_y = C\alpha + C_\gamma \gamma$, where C is cornering stiffness, α is the tire sideslip angle, C_γ is a coefficient, which represents the degree of offset and γ is the camber angle of the rear wheels. Here, the linearized tire model in the direction of the wheel-ground contact velocity is extended with the effect of the wheel camber. Using this equation the lateral dynamics of the vehicle is formulated as:

$$J\ddot{\psi} = C_1 l_1 \alpha_f - C_2 l_2 \alpha_r + M_{br} - C_{2,\gamma} l_2 \gamma \tag{7.15}$$

$$mv(\dot{\psi} + \dot{\beta}) = C_1 \alpha_f + C_2 \alpha_r + C_{2,\gamma} \gamma \tag{7.16}$$

where m is the mass, J is the yaw inertia of the vehicle, l_1 and l_2 are geometric parameters, C_1, C_2 and $C_{2,\gamma}$ are cornering stiffnesses, $\dot{\psi}$ is the yaw rate of the vehicle, β is the sideslip angle. Moreover, $\alpha_f = -\beta + \delta - l_1 \cdot \dot{\psi}/v$ and $\alpha_r = -\beta + l_2 \cdot \dot{\psi}/v$ are the tire sideslip angles at the front and rear, respectively.

The lateral assistance controller must estimate the steering intention of the driver. For this estimation it is required to measure the velocity of the vehicle and the steering wheel angle. The reference yaw rate of the controller, which is desired by the driver, is calculated using the following expression:

$$G_{\dot{\psi}_{ref},\delta_d} = \frac{v}{l_1 + l_2 + \eta v^2/g} \cdot \frac{1}{\tau s + 1} \tag{7.17}$$

with an understeer gradient η and the time constant τ, see Pacejka (2004). In trajectory tracking both the longitudinal and lateral dynamics must be taken into consideration, i.e., the vehicle must track two reference signals. It is required to measure the yaw rate signal of the vehicle, and the driver assistance controller must perform the next minimization criterion:

$$|\dot{\psi}_{ref} - \dot{\psi}| \to 0. \tag{7.18}$$

Moreover, the difference between the lateral position of the vehicle and the reference lateral position must be minimized:

$$|y_{v,ref} - y_v| \to 0. \tag{7.19}$$

which is the deviation of the vehicle from the lateral position of the reference road geometry in the coordinate system of the vehicle.

The designs of the three control systems are based on the state space representation form of the vehicle:

$$\dot{x} = A(\rho)x + B(\rho)u \tag{7.20}$$

where the state vector of the system $x = \left[\dot{\psi}\ \beta\right]^T$ contains the yaw rate and the sideslip angle of the vehicle. In the case of the brake control the input of the system is $u = M_{br}$, in the steering control the input is $u = \delta$, while in the variable-geometry suspension the control input is $u = \gamma$. Using a scheduling variable $\rho = v$ the vehicle model is transformed into an LPV model. The measured output of the system is the yaw rate $y = \dot{\psi}$.

7.4.2 Weighting Functions in the Control Design

In this section the selection of the weighting functions applied to the control design is based on the effects of the actuators on vehicle dynamics.

The maximal control input of the steering and variable-geometry suspension systems are determined by their physical construction limits, while in the case of the braking system the constraints are the tire road adhesion conditions. It is necessary to avoid the skidding of tires, thus in such a case the generation of differential braking must be reduced. The skidding of tires can be monitored by the estimation of the longitudinal slips of the tires κ; a possible method is found in Gustafsson (1997). These constraints must also be taken into consideration in the control design and must be guaranteed by the supervisor.

Moreover, the activation of the different components have an energy requirement. By using differential braking the velocity of the vehicle is reduced, which must be compensated by the driveline with additional energy. Therefore the use of differential braking must be avoided during acceleration and front-wheel steering is preferred. During deceleration the brake is already being used, thus the lateral dynamics is handled by the braking for practical reasons. Thus differential braking is preferred, but close to the limit of skidding, front-wheel steering must also be generated. The actuation of differential braking causes increased strain on the tires. When the vehicle moves in the lateral direction the position of each tire is longitudinal and they are not rotating. This also shows that using front-wheel steering is more efficient.

The bandwidth of the different actuators must also be taken into consideration in the weighting functions. In the case of front-wheel steering and the variable-geometry suspension, the inertia of the systems effects a slower operation of the actuators than the bandwidth of differential braking. In the following, the bandwidths of the actuation are compared.

The dynamics of steering is determined by the moment which rotates the wheels $M_{st} = 2\vartheta_{st}\ddot{\delta} + M_{res,st}$, where ϑ_{st} is the inertia of the wheel on the axle of steering, δ is the steering angle. M_{st} is controlled by a servo power system according to the rack, where $M_{res,st} = M_{gy,st} + M_{ch,st}$ is the sum of the steering resistances. In order to the steer the rotating wheels it is necessary to generate energy against the gyroscopic effect. It is formulated by using the following assumption: $M_{gy,st} = 2J_w v\dot{\delta}/r_w$, where J_w is the inertia of the wheel on the axle of rotation and r_w is the wheel radius. During steering the positions of wheels are modified. Since the axle of a steered wheel is skew the vertical position of the entire chassis also moves. Thus, it is necessary to generate energy to improve the lateral dynamics of the chassis: $M_{ch,st} = B\pi s_{susp}(\sin n)\ \delta$, where B is the wheel track, s_{susp} is the suspension stiffness and n is the angle between the road and the axis of wheel steering. The transfer function of the steering system between the steering angle δ and the moment M_{st} is

$$G_{st} = (\vartheta_{st}s^2 + \frac{2J_w v}{r_w}s + B\pi s_{susp}\sin n)^{-1}$$

The moment of the suspension system is controlled by a hydraulic system. $M_{susp} = \vartheta_{susp}\ddot{\gamma} + M_{res,susp}$, where ϑ_{susp} is the inertia of the wheel on the axle of wheel camber rotation and $M_{res,susp} = M_{gy,susp} + M_{ch,susp}$. The gyroscopic torque component is similar to the steering moment: $M_{gy,susp} = J_w v\dot{\gamma}/r_w$. During the modification of the wheel camber angle, the position of the chassis also changes. The moment, which must be compensated for by the actuator of the variable-geometry suspension, is approximated as: $M_{ch,susp} = Bs_{susp}r_w(1-\gamma)$. The transfer function of the suspension system between the wheel camber angle γ and the moment M_{susp} is

$$G_{susp} = (\vartheta_{susp}s^2 + \frac{J_w v}{r_w}s - Bs_{susp}r_w)^{-1}$$

In the case of differential braking the input of the model is the brake yaw moment, the output is the yaw rate. In the case of steering system it is necessary to combine the bicycle model with the second-order steering model in order to transform the steering angle into a steering moment. Similarly, in the case of suspension system it is necessary to combine the bicycle model with the suspension model. Then the three models can be compared. The bandwidth of the actuation rate is analyzed as a function of velocity. Figure 7.11 shows that the bandwidth values change significantly with the change of velocity.

According to the inertia of steering, the bandwidths of steering and suspension are lower at each velocity than the bandwidth of differential braking. The fast operation of actuators is an important feature mainly at high velocities. At higher velocities it is recommended to use differential braking, while at lower velocities steering actuation is preferred for practical reasons. The weighting functions for the front-wheel steering, brake yaw moment, and suspension moment are selected in the following form:

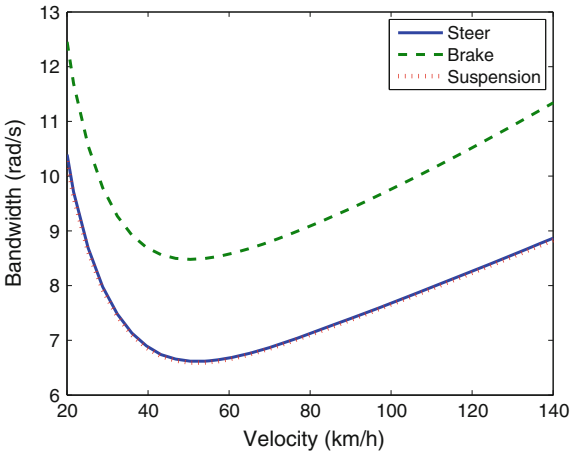

Fig. 7.11 Bandwidth values of actuators

$$W_{act,\delta} = \rho_{\delta}/\delta_{max} \tag{7.21}$$

$$W_{act,Mbr} = \rho_{br}/M_{brmax} \tag{7.22}$$

$$W_{act,susp} = \rho_{susp}/\gamma_{max} \tag{7.23}$$

respectively, where δ_{max} and γ_{max} are determined by the constructional maximum of the steering and the camber angle, while M_{brmax} is the maximum of the brake yaw moment. Weighting factors ρ_{st}, ρ_{br}, ρ_{susp} are chosen to influence the priority of the actuators. Figure 7.9 shows the characteristics of the weighting factors.

When the vehicle is being driven the front-wheel steering is actuated, which is determined by factor ρ_{st}, see Fig. 7.9a. The value is reduced between δ_1 and δ_2, which represents the constructional criterion of the steering system. When the brakes are being applied the tire longitudinal slip angle affects factor ρ_{br}, see Fig. 7.9b. In this interval differential braking is preferred for practical reasons. It requires an interval to reduce tire skidding and it also requires an interval to prevent chattering between steering and differential braking. Therefore four parameters are designed: κ_1 and κ_2 are used to prevent chattering between steering and braking and κ_3 and κ_4 are applied to prevent the skidding of tires. The weights also depend on the velocity of the vehicle. The effect of the velocity on the weighting factors is the consequence of the interaction between the bandwidth values of the actuators.

Note that at the construction or adhesion limits the actuations of the steering and the brake are reduced. In this case it is necessary to compensate for the actuator reduction by another actuator. It means that if $\sum \rho (= \rho_{br} + \rho_{st}) < 1$ then the variable-geometry suspension system is activated $\rho_{susp} = 1 - (\rho_{br} + \rho_{st})$.

7.4.3 Design of the Integrated Control

In the design of the control system the advantages of the LPV methods are exploited. These methods allow us to take into consideration the highly nonlinear effects in the state space description in such a way that the model structure is nonlinear in the parameters, but linear in the states. The designed controller meets robust stability and performance demands in the entire operational region, see Bokor and Balas (2005), Balas et al. (1997), Wu et al. (1996). The control design is based on a weighting strategy, which is formulated through a closed-loop interconnection structure. In the supervisory integrated control scheme each controlled subsystem has its own LPV controller, and the scheduling variables of these LPV controllers are selected by a supervisory logic. The selection of input and output weighting functions is typically based on the specifications of disturbances and the performances.

In the trajectory tracking problem two reference signals are introduced in order to guarantee the tracking of the road geometry. They are the reference velocity and the reference lateral displacement $R = [v_{ref} \;\; y_{v,ref}]^T$. Performances of the control system are the minimization of the tracking error of the yaw rate tracking error and the minimization of the deviation from the reference lateral position

$$z_1 = [\dot{\psi}_{ref} - \dot{\psi};\;\; y_{v,ref} - y_v]^T \rightarrow min! \tag{7.24}$$

The weighting function for performance specification is selected as a second-order proportional form: W_p where $\varepsilon_1, \varepsilon_2, T_1, T_2$ are designed parameters. The purpose of the weighting functions W_w and W_n is to reflect the disturbance and sensor noises, respectively, and they are selected in a first-order proportional form. The magnitude of the neglected dynamics is handled by a weighting W_u. The role of W_{act} is to guarantee the desired actuation of controlled systems. Three weighting functions are applied according to (7.21). Since these weighting functions must be built into the performance of the actuators, $\rho_{st}, \rho_{br}, \rho_{susp}$ are selected as scheduling variables of the controlled systems in the LPV design. Therefore another performance of the system is formulated as

$$z_2 = |u| \rightarrow min! \tag{7.25}$$

In the design of local controllers the quadratic LPV performance problem is to choose the parameter-varying controller in such a way that the resulting closed-loop system is quadratically stable and the induced $\mathscr{L}_2$ norm from w to z is less than γ. The existence of a controller that solves the quadratic LPV γ-performance problem can be expressed as the feasibility of a set of LMIs.

The architecture of the controlled supervisory system is shown in Fig. 7.12. The stability of the individual LPV controllers is guaranteed by the quadratic stability of the integrated system. When several controllers are used simultaneously it is necessary to guarantee the stability of the global closed-loop system. The global

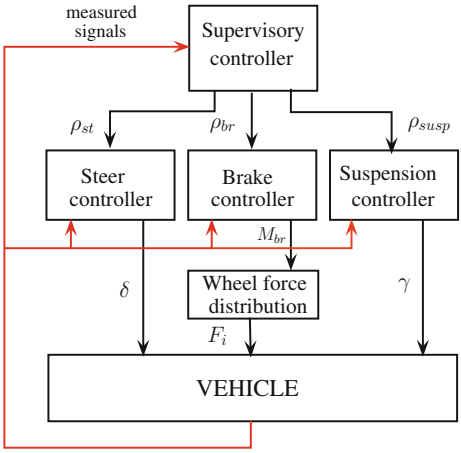

Fig. 7.12 Architecture of the supervisory system

control system contains three controllers, such as the brake, the steering, and the suspension.

Since each LPV controller contains one scheduling variable, the global system uses three additional scheduling variables $[\rho_{br}, \rho_{st}, \rho_{susp}]$. Consider that the convex polytopic set depends on the scheduling variables. A common Lyapunov function for the polytopic set of closed-loop systems must exist. The next polytopic set of closed-loop systems is given

$$\dot{x}(t) = A\, x(t);\;\; A \in \mathbf{Co}\{A_1, \ldots A_n\} \tag{7.26}$$

For the stability of the LTI system it is necessary to guarantee that all trajectories of system A converge to zero as $t \to \infty$. A sufficient condition for this is the existence of a quadratic function $V(\xi) = \xi^T P \xi$, $P > 0$, which decreases along every nonzero trajectory of (7.26). If there exists such a P, then (7.26) is said to be quadratically stable and V is called a quadratic Lyapunov function. The necessary and sufficient condition for quadratic stability of system (7.26) for all of A_i is

$$A_{cl,i}^T P + P A_{cl,i} < 0;\;\; P > 0;\;\; i = 1, \ldots n \tag{7.27}$$

Therefore it is necessary to find a V common Ljapunov function for the closed-loop systems, which can guarantee the global stability of the systems in every scheduling variable. The aim is to find a solution $P > 0$. To analyze the global stability of the LTI systems, $\mathbf{Co}\{A_1, \ldots A_n\}$ is covered by the convex hull of finitely many matrices $A_{cl,i}$ Scherer (2000). For the analysis of global stability this convex hull can be used.

7.4.4 Simulation Results

In the example the efficiency of the integrated control is compared to the individual actuated control systems. In the analysis of the individual actuator controllers and in the analysis of the supervisory case, the same brake, steering and suspension controllers are used. The vehicle is traveling along a predefined road, while the suspension system supports the driver to guarantee trajectory tracking. A typical E-Class automobile is applied in the simulation. The mass of the 6-gear car is 2023 kg, its engine power is 300 kW (402 hp), and independent McPherson suspensions are applied. The width of the track is 1605 mm and the wheel base is 3165 mm.

In the simulation example the vehicle is traveling along a section of Waterford Michigan Race Track, which is shown in Fig. 7.13a. In Fig. 7.13 the vehicle using a supervisory control (dashed line) is compared to the vehicle without any control (solid line). The aim is to track the centerline of the road. The velocity of the vehicle changes along its route as Fig. 7.13b shows. The course has two dangerous curves. Figure 7.13c, d show that the uncontrolled vehicle is not able to track the trajectory,

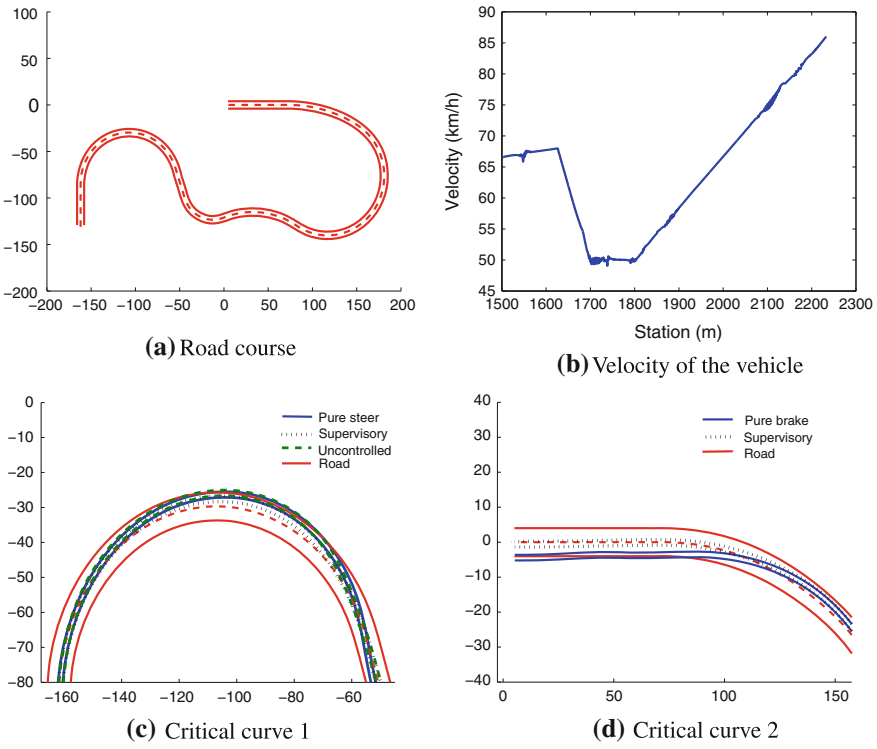

(a) Road course **(b)** Velocity of the vehicle **(c)** Critical curve 1 **(d)** Critical curve 2

Fig. 7.13 Trajectories of vehicles

i.e., the driver is not able to keep the vehicle on the track without a driver assistance system.

In the figure the supervisory control is compared to systems which use only one controller. When a steering system is used only, it is not able to guarantee trajectory tracking in the first critical curve. The individual steering actuator is not able to prevent the skidding of the vehicle on the road. In this curve the supervisory integration of the steering and the brake ensures trajectory tracking with an acceptable threshold. When a brake system is used only, it generates increased braking pressures to keep the vehicle in the centerline. However, during braking the slip of the rear tires increases, which leads to loss of stability. In the supervisory integrated system the brake control is able to consider the slips of tires and avoid the saturation of the differential braking.

The lateral errors of the trajectories are shown in Fig. 7.14a. This figure illustrates that at the beginning of the course when a steering control is used only the lateral error is the highest, while in the last section during the traveling the lateral error increases significantly when a brake is used only. The supervisory integrated control gives the smallest lateral error during the operation. In Fig. 7.14b the yaw rate tracking of

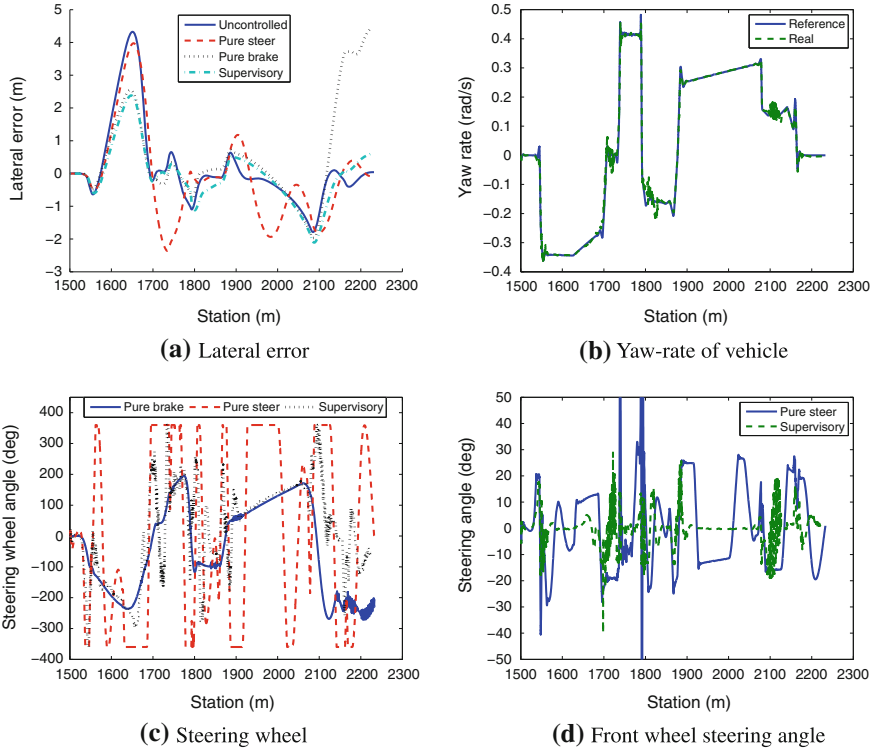

(a) Lateral error

(b) Yaw-rate of vehicle

(c) Steering wheel

(d) Front wheel steering angle

Fig. 7.14 Operation of the supervisory control

the supervisory integrated control is shown. Thus, the integrated control provides an acceptable z_1 performance. Figure 7.14c illustrates the angle of steering wheel turned by the driver. When a steering system is used only, the driver needs to turn the steering wheel in the entire steering range, which is uncomfortable and dangerous. When a brake system is used only, the driver turns the steering wheel relatively smoothly. In

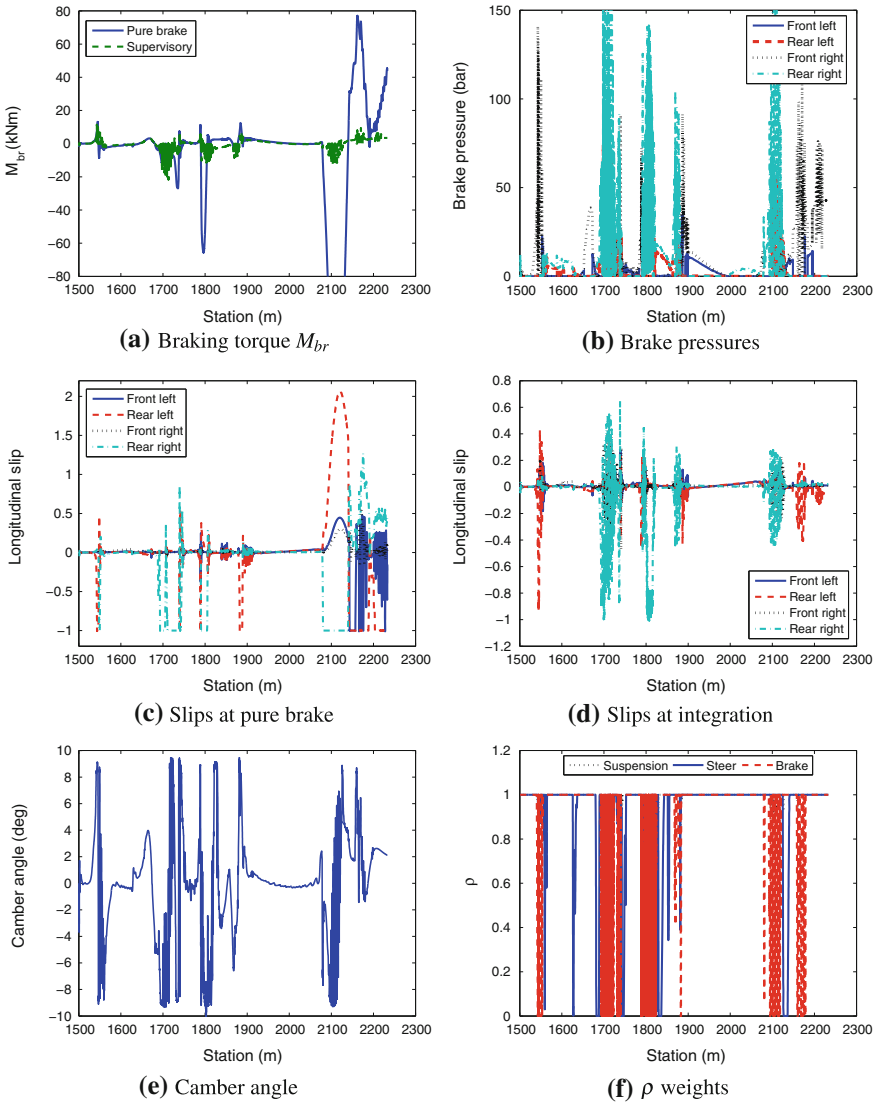

(a) Braking torque M_{br} **(b)** Brake pressures

(c) Slips at pure brake **(d)** Slips at integration

(e) Camber angle **(f)** ρ weights

Fig. 7.15 Operation of the supervisory control (Continued)

the supervisory integrated control case the driver must increase the steering angle slightly compared to the pure braking.

Figure 7.14d shows the difference between the front-wheel steering angles at the steering only and the integrated case. When a steering system is used only, the steering angle is significantly larger than the integrated system, since the turning of the steering wheel affects the front steering angles. When a brake system is used only, the differential braking torque is larger than the integrated system. Note that from 2080 m the torque M_{br} sharply increased due to the skidding effect, see Fig. 7.15a. This characteristic is shown in the longitudinal slip, see Fig. 7.15c. When a brake system is used only the longitudinal slip of rear right wheel exceeds -1, which leads to skidding. In the integrated case the longitudinal slip does not exceed -1, see Fig. 7.15d. It is also shown at the end of the course, where the increased longitudinal slips cause the loss of stability in case of brake actuation only.

In Fig. 7.15e the camber angle of the variable-geometry suspension is shown. This figure illustrates that the rear wheel camber angle is increased at the critical situations. In the second critical curve the brake torque M_{br} must be reduced in the integrated supervisory system in order to avoid skidding. From that point the variable-geometry suspension system must generate the required control input. The interaction between the steering and the brake is shown in Fig. 7.15f. The figure shows that according to the example, ρ_{st} is reduced when the front-wheel steering angle reaches its construction limit. The value of ρ_{br} depends on the maximum value of longitudinal slip of tires. It is critical when control input M_{br} is high, which may cause skidding. Consequently, ρ_{br} is reduced and ρ_{susp} is increased, while the variable-geometry suspension system compensates for the differential brake torque.

Chapter 8
Control of the Variable-Geometry Suspension

8.1 Lateral Dynamics of the Vehicle Model

A variable-geometry suspension system is applied as a driver assistance system in vehicles. While the driver performs a maneuver using the steering wheel, an autonomous control system modifies the camber angle of the front wheels in order to improve road stability. Since various safety and economy properties of the vehicle are determined by the suspension geometry it has significant influence on the control design. The advantages of the variable-geometry system are the simple structure, low energy consumption, and low cost compared to other mechatronic solutions, such as an active front wheel steering, see Evers et al. (2008).

The height of the roll center has an important role in the roll dynamics of the vehicle. A possible way to minimize the chassis roll angle is the minimization of the height of the roll center. The roll center depends on the camber angle of the front wheels, which can be modified by the variable-geometry suspension system. The lateral movement of the contact point of the variable-geometry system is also relevant from the aspect of tire wear, when the suspension moves up and down while the vehicle moves forward, see Gough and Shearer (1956). Using an appropriately designed variable-geometry control, these unnecessary movements can be eliminated. In summary, in normal cruising maneuvers the steering system focuses on trajectory tracking and the variable-geometry suspension system guarantees various performances which are related to the chassis roll angle and half-track change.

Moreover, by changing the camber angles of the front wheels, the yaw rate of the vehicle is modified, which can be used to reduce the tracking error from the reference yaw rate. Thus, with the reconfiguration of the camber angles, the variable-geometry system is able to focus on trajectory tracking and assist the driver to carry out various vehicle maneuvers. Thus, in an emergency such as a sharp cornering the variable-geometry system focuses on trajectory tracking instead of the conventional performances. In this way, the variable-geometry system can also be used as a driver assistance system. However, one of the properties might only be improved to the detriment of other properties. For example, if the tracking ability is enhanced at the

P. Gáspár et al., *Robust Control Design for Active Driver Assistance Systems*,
Advances in Industrial Control, DOI 10.1007/978-3-319-46126-7_8

same time, the performances in terms of roll dynamics and half-track change are degraded. The conflict between different performance demands must be resolved in such a way that a balance between the performances is achieved. In the control design a parameter-dependent weighting strategy is applied.

Several papers for various kinematic models of suspension systems have been published. A review of the first variable-geometry suspensions was presented by Sharp (1998). The selection of the suspension components and the influence of the distribution of vertical forces were analyzed in Braghin et al. (2008b). A nonlinear model of the McPherson strut suspension system was published by Fallah et al. (2009), Németh and Gáspár (2012). Using this model the kinematic parameters such as camber, caster, and king-pin angles were examined. The kinematic design of a double-wishbone suspension system was examined by Sancibrian et al. (2010). The vehicle-handling characteristics based on a variable roll center suspension was proposed by Lee et al. (2008). A rear-suspension active toe control for the enhancement of driving stability was proposed by Goodarzia et al. (2010). Another field of variable-geometry suspension is the steering of narrow vehicles. These vehicles require the design of an innovative active wheel tilt and steer control strategies in order to perform steering as if for a car on straight roads and leaning in the bends as a motorcycle, see Daniel and Cabrera (2010). The active tilt control system, which assists the driver in balancing the vehicle and performs tilting in the bend, is an essential part of a narrow vehicle system, see Piyabongkarn et al. (2004). In Németh and Gáspár (2011, 2013a) the simultaneous design of robust control and the construction of a variable-geometry suspension system for the enhancement of vehicle stability was analyzed.

The bicycle model illustrated in Fig. 8.1 is used in the control design. Although the Magic form gives a highly accurate description of the lateral tire force, see e.g., Pacejka (2004), a simplified form is constructed for numerical reasons. The lateral tire forces in the direction of the wheel ground contact are approximated linearly to the tire side-slip angles α_f, α_r and the wheel camber angle γ.

$$F_{yf} = C_1\alpha_f + C_\gamma\gamma, \tag{8.1}$$

$$F_{yr} = C_2\alpha_r, \tag{8.2}$$

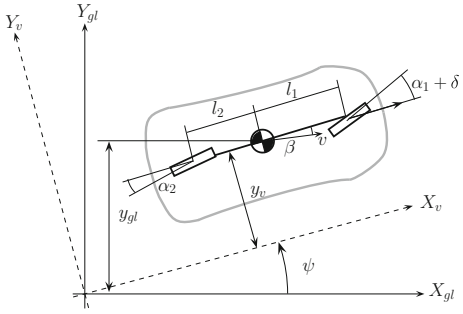

Fig. 8.1 Lateral model of the vehicle

where C_1, C_2 are cornering stiffnesses, C_γ is a coefficient which represents the degree of offset.

Using the bicycle model the lateral dynamics of the vehicle is formalized. The first equation considers forces for the lateral dynamics, while the second one is the torque balance equation for yaw moments.

$$mv(\dot{\psi} + \dot{\beta}) = F_{yf} + F_{yr} = C_1\alpha_f + C_2\alpha_r + C_{1,\gamma}\gamma, \tag{8.3}$$

$$J\ddot{\psi} = F_{yf}l_1 - F_{yr}l_2 = C_1l_1\alpha_f - C_2l_2\alpha_r + C_{1,\gamma}l_1\gamma, \tag{8.4}$$

where J is the yaw inertia of the vehicle, l_1 and l_2 are geometric parameters, ψ is the yaw of the vehicle, β is the side-slip angle of the vehicle. Moreover, $\alpha_f = -\beta + \delta - l_1 \cdot \dot{\psi}/v$ and $\alpha_r = -\beta + l_2 \cdot \dot{\psi}/v$ are the tire side-slip angles at the front and rear, respectively, in which v denotes the longitudinal velocity. In the design of trajectory tracking control it is necessary to guarantee that the lateral position of the vehicle tracks the geometry of the road.

The required lateral motion is controlled by the difference between the actual yaw rate of the vehicle and the yaw rate desired by the driver. The desired yaw rate, which is the reference signal of the system, can be computed using the following formula Rajamani (2005):

$$\dot{\psi}_{ref} = \frac{v}{l_1 + l_2}\delta \tag{8.5}$$

where δ is the steering angle actuated by the driver. The side-slip angles of the tires influence the actual yaw rate, which differs from the reference yaw rate. Thus, the cornering maneuver might lead to understeering or oversteering. The control goal is to compensate for the effects of side-slip angles on the vehicle.

8.2 Modeling of a Variable-Geometry Suspension System

The kinematic model of the variable-geometry mechanism is presented using the double-wishbone suspension system (see Fig. 8.2). The kinematic model contains the geometry of the actuator and shows the suspension displacements.

The suspension system is analyzed in a local coordinate system, whose center point is C. Point A in the variable-geometry suspension system is able to move only in a horizontal direction. In the variable-geometry system the change of point A in the direction y is the real input of the mechanism, which is denoted by a_y. Two further points B and D are marked on the tire, which move both in directions y and z. Their movements are denoted by b_y, b_z, d_y, d_z. T is the road-wheel contact point, which moves as a function of the road irregularities, i.e., t_y, t_z. The aim is to formalize the relationship between the input a_y and the wheel camber output γ. In the following

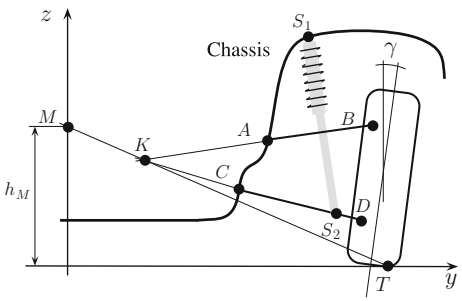

Fig. 8.2 Kinematic model of the suspension system

only the main results are summarized. More details are found in Németh and Gáspár (2011, 2013a).

Let us introduce the following vector of variables: $\eta = \begin{bmatrix} b_y & b_z & d_y & d_z & t_y \end{bmatrix}^T$. The relationship between η and a_y is formalized in the following form:

$$A_\eta(\eta)\ \eta = K(t_z) + B_\eta(a_y)\ a_y \tag{8.6}$$

where t_z can be considered as the disturbance. In the equation η is unknown, the variables A_η and $K(t_z)$ change as a function of η and t_z, and B_η depends on a_y. The vector η is expressed from (8.6)

$$\eta = A_\eta(\eta)^{-1}[K(t_z) + B_\eta(a_y)a_y] \tag{8.7}$$

where $A_\eta(\eta)$ is invertible. The output of the system is the camber of the wheel $\gamma = \arccos\{(B_z - D_z)/L_{BD}\}$. Thus, the output equation is expressed $C_\eta \eta = D_\eta$, where $C_\eta = \begin{bmatrix} 0 & 1 & 0 & -1 & 0 \end{bmatrix}^T$ and $D_\eta = L_{BD}\cos(\gamma) + D_z - B_z$. Consequently, the input of the mechanism a_y is expressed in the following form:

$$a_y = [C_\eta A_\eta(\eta)^{-1} B_\eta(a_y)]^{-1}[D_\eta - C_\eta A_\eta(\eta)^{-1} K(t_z)] \tag{8.8}$$

Equation (8.8) gives the relationship between γ and a_y. It is a parameter-varying expression, which depends on η, t_z and a_y (Fig. 8.3).

The relationship between a_y and γ as a function of t_z based on the numerical solution of (8.8) is shown in Fig. 8.4a. An analysis shows that it is possible to approximate it with linear functions in the following form:

$$\gamma = \kappa + \xi_1 t_z + \varepsilon_1 a_y \tag{8.9}$$

The static components of the lateral forces are approximately equal, thus in the next computations constant κ is omitted from (8.9).

In normal cruising maneuvers, the steering control assists the driver in following the trajectory, while the variable-geometry suspension control focuses on two performances. It minimizes the chassis roll angle by modifying the roll center of the

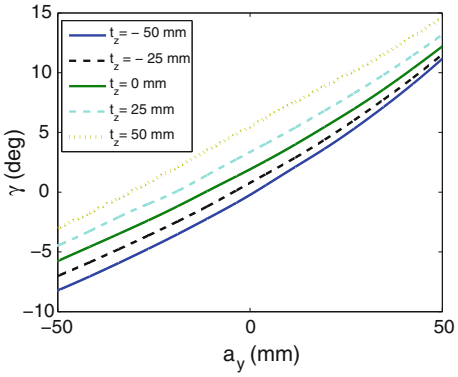

Fig. 8.3 a_y—γ characteristics

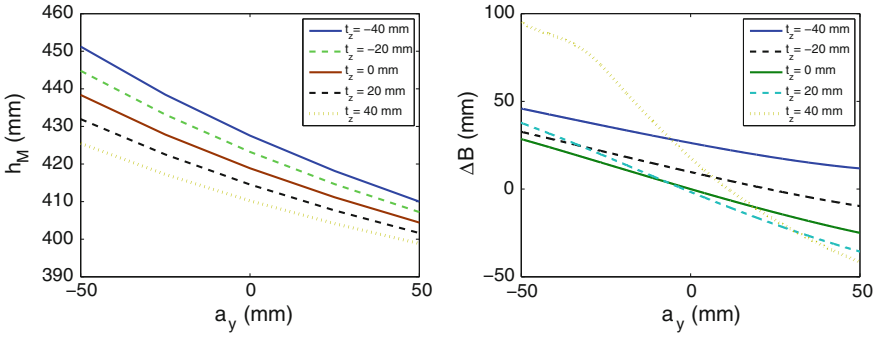

(a) Height of roll center (b) Half track change

Fig. 8.4 Properties of the variable-geometry suspension system

vehicle. Moreover, the half-track change can also be minimized using the variable-geometry suspension system. In the driver assistance system an additional performance requirement is also applied. The variable-geometry system is able to focus on trajectory tracking and assist the driver in carrying out various vehicle maneuvers. Thus, in an emergency, the variable-geometry suspension control also focuses on trajectory tracking. Consequently, the performance requirements are related to the yaw-rate tracking, the roll angle and the half-track change.

In the trajectory tracking control the vehicle must follow the reference yaw rate, which is approximated by (8.5). The difference between the yaw rate of the vehicle and the reference yaw rate must be minimized

$$z_1 = |\dot{\psi}_{ref} - \dot{\psi}| \tag{8.10}$$

It has been shown that the roll center depends on both a_y and t_z. The height of the roll center has an important role in the roll dynamics of the vehicle Rajamani (2005):

$$(I_{xx} + m\Delta h^2)\ddot{\phi} = mg\Delta h\phi + mv\Delta h(\dot{\beta} + \dot{\psi}) - \\ - B_i \sum F_{susp,i} \tag{8.11}$$

where Δh is the difference between the height of the center of gravity and the height of the roll center ($\Delta h = h_{CG} - h_M$), ϕ is the chassis roll angle, I_{xx} is the inertia of the chassis, B_i is the half track and $F_{susp,i}$ are the vertical forces of suspension.

In order to minimize the chassis roll angle, the dynamic displacement of the height of the roll center based on (8.13) must be minimized

$$z_2 = |\Delta h_M| \tag{8.12}$$

The construction of suspension determines the height of the roll center of the chassis, h_M. The intersection of the arms (A, B) and (C, D) is marked by K. The intersection of the line (T, K) and the vertical centerline of the chassis is the roll center itself. The relationship between a_y and h_M as a function of t_z based on the numerical solution of (8.8) is shown in Fig. 8.4b. The height of the roll center can be divided into static and dynamic components as follows: $h_M = h_{M,st} + \Delta h_M$. Component $h_{M,st}$ represents the height of the roll center of a stationary vehicle, while Δh_M represents the change of height during traveling. The dynamic component is expressed in the following linear form:

$$\Delta h_M = \xi_2 t_z + \varepsilon_2 a_y \tag{8.13}$$

Thus, the performance criterion is formalized in the following form: $z_2 = |\zeta_2 t_z + \varepsilon_2 a_y| \rightarrow min$.

The fulfillment of this performance can be reached by increasing actuation a_y. However, in practice Δh_M has a physical limit since actuation a_y also has a limitation. Therefore, a signal $h_{ref} (< h_{CG} - h_{M,ST})$ is introduced instead of Δh_M and applied as a reference signal for the tracking task.

An additional important economy parameter is the half-track change. Using a linear approximation and based on (8.15) the performance criterion is formalized in the following form:

$$z_3 = |\Delta B| \tag{8.14}$$

During traveling the half-track change ΔB is also an important economical dynamic parameter of the suspension system, since it is related to tire wear. The relationship between a_y and ΔB as a function of t_z based on the numerical solution of (8.8) is shown in Fig. 8.4c. The figure shows that the relationship between a_y and ΔB can be expressed linearly in the following form:

$$\Delta B = \xi_3 t_z + \varepsilon_3 a_y \tag{8.15}$$

Thus, the performance criterion is formalized in the following form: $z_3 = |\xi_2 t_z + \varepsilon_3 a_y| \rightarrow min$.

Note that the performance requirements are in conflict, thus a balance must be achieved between them. The aim of the control design is to achieve a balance between performances.

8.3 Robust Control of the Variable-Geometry Suspension System

The control design of the variable-geometry suspension system is based on the control-oriented bicycle model

$$\dot{x} = Ax + B_1 w + B_2 u \tag{8.16}$$

$$z = C_1(\rho)x + D_{11}(\rho)w + D_{12}(\rho)u \tag{8.17}$$

$$y = C_2 x \tag{8.18}$$

where the state vector of the system contains the yaw rate and the side-slip angle $x = \left[\dot{\psi},\ \beta\right]^T$. The control input of the system is $u = a_y$, the disturbances are $w = \left[\delta,\ t_z\right]^T$, while the performances are $z = \left[z_1,\ z_2,\ z_3\right]^T$.

The control design is formalized through a closed-loop interconnection structure, see Fig. 8.5. Input and output weighting functions are selected to the specifications of disturbances, inputs, and outputs.

The crucial point of the control design is the selection of the weighting functions for performances. In the control design parameter-dependent weighting functions

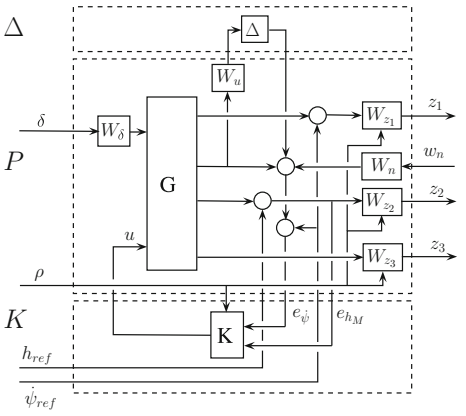

Fig. 8.5 Closed-loop interconnection structure

are applied to the performances, i.e., the yaw-rate tracking, the roll angle and the half-track change:

$$W_{z_1} = \frac{\rho}{e_{\dot{\psi}_{max}}} \tag{8.19}$$

$$W_{z_2} = \frac{1-\rho}{\phi_{max}} \tag{8.20}$$

$$W_{z_3} = \frac{1-\rho}{\Delta B_{max}} \tag{8.21}$$

where $\rho \in [0; 1]$ is a scheduling variable, $e_{\dot{\psi}_{max}}$ is the possible maximum of the yaw-rate error, ϕ_{max} is the maximum of the chassis roll angle and ΔB_{max} is a maximum of the half-track change.

The role of parameter ρ in the weighting functions is to create a balance between the different performances. For example, in the case of $\rho = 1$ the control system prefers the yaw-rate tracking, while in the case of $\rho = 0$ the control system focuses on both the roll angle and half-track change. Note that the reference height of the roll moment h_{ref} is also used in the control design.

In normal cruising maneuvers, the control of the variable-geometry suspension system guarantees two performances which are related to the chassis roll angle and the half-track change. In an emergency, the variable-geometry system must focus on trajectory tracking and assist the driver in carrying out various vehicle maneuvers. Thus the control design must be extended with a reconfigurable structure.

Figure 8.6 illustrates the architecture of the reconfigurable control system. It contains several components besides the vehicle model and the driver model, such as the

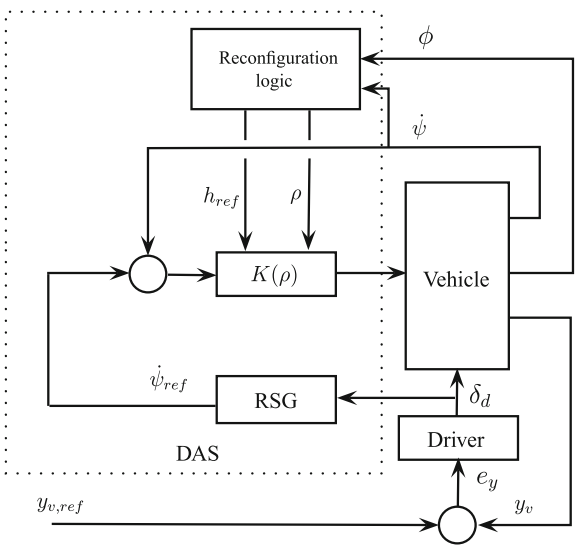

Fig. 8.6 Architecture of control systems

suspension control $K(\rho)$, the generator of the reference yaw-rate signal (RSG), and the block of the reconfiguration logic. The role of the variable-geometry suspension control $K(\rho)$ is to minimize the chassis roll angle and the half-track change and, in an emergency, to reduce the yaw-rate error. Since these performances are in conflict, a reconfiguration logic is applied. The variable-geometry suspension control is activated using two signals, ρ and h_{ref}.

In the following various vehicle scenarios are distinguished:

- Half-track change minimization: In normal cruising, the goal of the variable-geometry suspension control is to minimize half-track change ΔB. This configuration is achieved by the selection $\rho = 0, h_{ref} = h_M$.
- Roll angle minimization: When the roll angle ϕ increases significantly, the variable-geometry suspension control must minimize the roll angle. This configuration is achieved by the selection $\rho = 0, h_{ref} = h_{ref,max}$.
- Balance between half-track change and roll angle minimization It is possible to achieve vehicle maneuvers in which there is a balance between the two performances, i.e., the reduction of the half-track change and that of the roll angle. In these configurations $\rho = 0$ and h_{ref} is selected in an interval $h_M < h_{ref} < h_{ref,max}$.
- Yaw-rate tracking: When the suspension system must focus on trajectory tracking the scheduling variable ρ is selected greater than 0.
- In an emergency maneuver, when there has been an extreme increase in the yaw-rate error, the suspension system must focus on the tracking error $e_{\dot{\psi}}$ instead of the conventional two performances. This configuration is achieved by the selection $\rho = 1$ and $h_{ref} = h_M$.

In the simulation examples, the vehicle is traveling along a predefined road, while the variable-geometry suspension system assists the driver in carrying out maneuvers. The control design is performed using the MATLAB®/Simulink® while the verification of the designed controller is performed using the CarSim simulation software. The efficiency of the proposed driver assistance system is illustrated using the CarSim simulation software.

In the first simulation example, the interaction between performance specifications is presented. The solid line illustrates the case $\rho = 1$, dashed: $\rho = 0, h_{ref} = h_M$, while the dashed-dotted line illustrate the case $\rho = 0, h_{ref} = h_{ref,max}$. The vehicle is traveling along a course, which is depicted in Fig. 8.7a.

Figure 8.7b shows the tracking of the yaw-rate error of the control systems with different configurations and without any control. In the uncontrolled vehicle the driver is not able to compensate for either the understeering or the oversteering motion, therefore the tracking error of the yaw rate significantly increases. In the controlled vehicles the tracking of the reference yaw rate with an acceptable threshold is guaranteed.

When the suspension system focuses on the tracking task, i.e., $\rho = 1$, the yaw-rate error is significantly reduced, which is shown in Fig. 8.7c. In the default case, when the suspension system focuses on the half-track change, i.e., $\rho = 0, h_{ref} = h_M$, the half-track change is minimized, see Fig. 8.7c. However, in this case the roll angle increases. When the suspension system focuses on the roll angle minimization, i.e.,

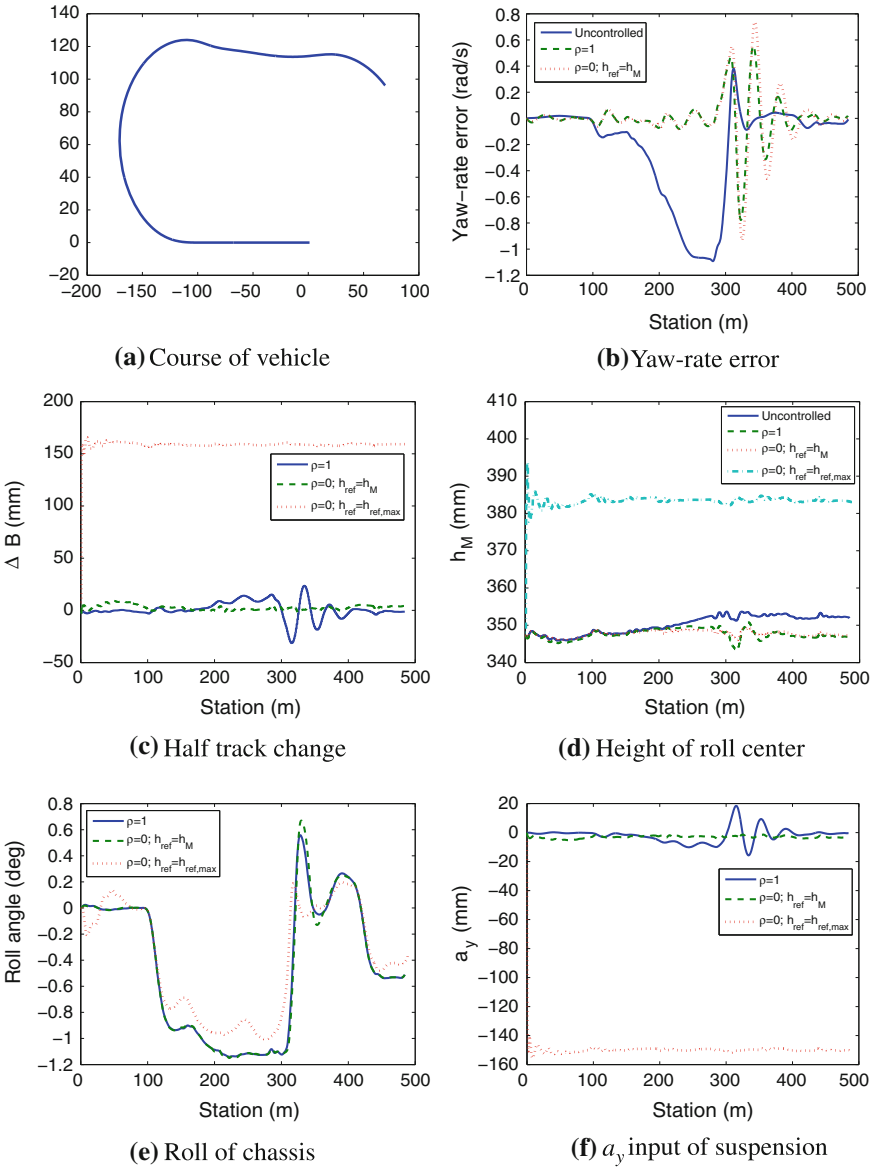

(a) Course of vehicle **(b)** Yaw-rate error

(c) Half track change **(d)** Height of roll center

(e) Roll of chassis **(f)** a_y input of suspension

Fig. 8.7 Performances in the driver assistance system

$\rho = 0, h_{ref} = h_{ref,max}$, the half-track change significantly increases since lifting up the height of the roll center requires significant control input a_y, see Fig. 8.7d, f. Figure 8.7d, e illustrate the relationship between the increased roll center and the

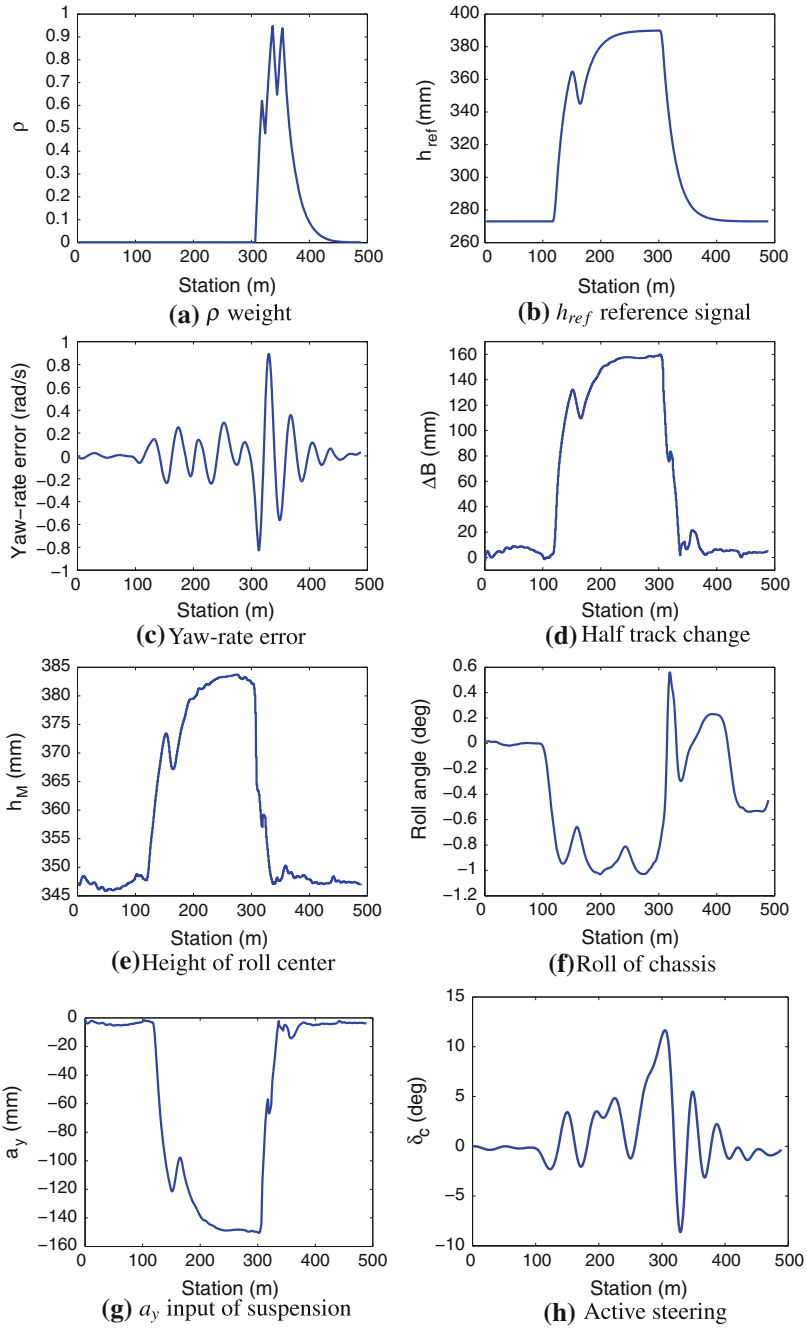

Fig. 8.8 Operation of the driver assistance system

reduced roll angle. Figure 8.7f shows the control inputs of the variable-geometry suspension a_y.

In the second example, the efficiency of the driver assistance system during the same cornering maneuver is presented. Figure 8.8a, b show scheduling variable ρ and reference signal h_{ref}, respectively. The reconfigurable control of the variable-geometry suspension system is based on these variables.

In Fig. 8.8c the yaw-rate error of the vehicle is shown. The scheduling variable ρ shows the relationship between the variable ρ and the yaw-rate error. When the control focuses on the half-track change and it decreases, the control action requires significant control input and at the same time the yaw-rate error increases, see Fig. 8.8d, g. Figure 8.8e, f show the height of roll center and roll angle of the chassis. The change of h_{ref}, which is also shown in Fig. 8.8b, induces the modification of h_M. The change of the reference height modifies the roll angle of the chassis ϕ, thus the roll dynamics.

Chapter 9
Control Design of In-Wheel Motors

Introduction

The growing need of economical and environmentally sound road vehicles enhances the attention of researchers and car makers towards electric vehicles. Within this segment of alternative transportation tools in-wheel electric vehicles using hub motors integrated inside the wheels have several advantages compared to conventional electric vehicles.

The lack of heavy and space-consuming powertrain components enables engineers to create roomy cabins for small size city vehicles, while at the same time the total mass of the vehicle can be reduced. Although the increased mass of the wheel may affect the ride and stability of the vehicle adversely, using semi-active or active suspension can address these effects, see Wang et al. (2014b). From vehicle dynamic control perspective-independent maneuverability of each wheels along with the fast and accurate torque generation of the hub motors are the most attractive features, making possible to design highly effective stabilizing and anti-slip control systems, see Castro et al. (2012), Ringdorfer and Horn (2011). Additionally, with the independent electric motors of each wheels efficiency of regenerative braking can be improved, as proposed by Wang et al. (2014a). Most of the recent researches concentrate on utilizing the specific advantages of the in-wheel motors. Methods have been designed to avoid rollover of the vehicle (see Kawashima et al. (2009)), while several authors focus on lateral trajectory control of in-wheel vehicles, see Wu et al. (2013), Katsuyama (2013), Xiong et al. (2012), Shuai et al. (2013).

Although fault-tolerant and reconfigurable control strategies for road vehicles have been studied broadly by authors (see Németh and Gáspár (2012)), relatively few research address the issues related to in-wheel vehicles. The fault or performance degradation of an in-wheel hub motors due to overheating, mechanical failures, or motor control faults may lead to dangerous vehicle instability, thus there is and outstanding demand of fault-tolerant control design for such vehicles. Adequate handling of a faulty in-wheel motor after a failure have been studied by Ifedi et al. (2013),

P. Gáspár et al., *Robust Control Design for Active Driver Assistance Systems*,
Advances in Industrial Control, DOI 10.1007/978-3-319-46126-7_9

while Wang and Wang (2012) proposed a fault-tolerant method for reallocating wheel torques among the healthy hub motors after a fault event. The vehicle control system must also address steering system failure or performance degradation.

9.1 Design of In-Wheel Motor Vehicle Control

In this section, the aim of the trajectory tracking control design is to perform both velocity tracking and path following even under a fault event. Thus, longitudinal and lateral dynamics must be considered for the in-wheel vehicle, for which the well-known two-wheeled bicycle model is applied, see Fig. 9.1. The motion equations of the in-wheel vehicle considering the planar plane are formulated as follows:

$$J\ddot{\psi} = c_1 l_1 \alpha_1 - c_2 l_2 \alpha_2 + M_z \tag{9.1}$$

$$m\dot{\xi}(\dot{\psi} + \dot{\beta}) = c_1 \alpha_1 + c_2 \alpha_2 \tag{9.2}$$

$$m\ddot{\xi} = F_l - F_d \tag{9.3}$$

where m is the mass total mass of the vehicle, J is the yaw inertia, l_1 and l_2 are geometric parameters, c_1 and c_2 are cornering stiffness of the front and rear tires, while $\alpha_1 = \delta - \beta - \dot{\psi} l_1/\dot{\xi}, \alpha_2 = -\beta + \dot{\psi} l_2/\dot{\xi}$ are the front and rear side-slip angles. The yaw rate and side-slip angle of the in-wheel vehicle is noted with $\dot{\psi}$ and β, while ξ is the longitudinal displacement. Note, that the nonlinearity of the vehicle model is caused by the velocity $\dot{\xi}$. The high-level inputs of the proposed model are the longitudinal force F_l, the yaw moment M_z and the front steer angle δ.

The longitudinal disturbance force F_d contains the following components: The disturbance originating from the road slope: $F_{d1} = mgsin\alpha_s$, where α_s is the angle of the road slope. The aerodynamic drag disturbance $F_{d2} = c_w \eta A \dot{\xi}^2/2$, where c_w is the drag coefficient, η is the density of the air, A is the frontal area of the in-wheel

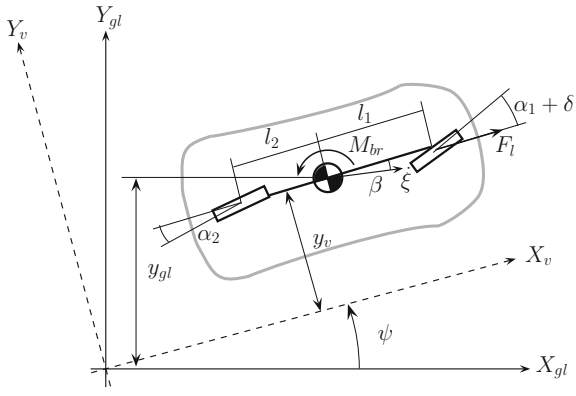

Fig. 9.1 Two-wheeled bicycle model

vehicle. Here, the rolling resistance $F_{d3} = mgf \cos \alpha_s$ is assumed to be a function of the vehicle mass m, the slope angle α_s and the road friction coefficient f. The sum of the above-described disturbances is the total disturbance force F_d.

Finally, the motion equations of the in-wheel vehicle detailed in (9.1) are transformed into state-space form as follows:

$$\dot{x} = A(\rho_1)x + B_1 w + B_2(\rho_2)u \tag{9.4}$$

where the state vector is $x = \left[\dot{\xi}\ \xi\ \dot{\psi}\ \beta\right]^T$, the control inputs are the drive/brake force F_l, the steer angle δ and the generated yaw moment M_z. These are also put in an input vector $u = \left[F_l\ \delta\ M_z\right]^T$. The measurements used in the control system are the velocity and the yaw rate of the vehicle, formulated in the output vector $y = \left[\dot{\xi}\ \dot{\psi}\right]^T$. Note, that the above defined disturbances are formalized with $w = \left[F_d\right]^T$, while ρ_1 and ρ_2 are scheduling variables of the vehicle system.

9.2 High-Level Control Design of the LPV Controller

The aim of the control design is to realize yaw rate and velocity tracking of the in-wheel vehicle, which has already been investigated by several authors, see Shibahata et al. (1993), Anwar (2005). Hence, in order for the in-wheel vehicle to achieve the required control goals, reference signals must be defined. Here, both the reference velocity and the yaw rate are set by the driver. Note, that the latter reference is given by the steering manipulation δ_d of the vehicle driver as follows Rajamani (2005): $\dot{\psi}_{ref} = v/d \cdot e^{-\frac{t}{\tau}} \cdot \delta_d$, where τ is a time constant and d parameter depends on the geometry and velocity of the in-wheel vehicle. Thus, the given references induced by the driver are put in a refernce vector $R = [\dot{\xi}_{ref}\ \dot{\psi}_{ref}]^T$.

Hence, the control goal is to track both reference signals given in vector R. For this purpose, both velocity error $z_{\dot{\xi}} = |\dot{\xi}_{ref} - \dot{\xi}|$ and yaw rate error $z_{\dot{\psi}} = |\dot{\psi}_{ref} - \dot{\psi}|$ must be minimized. Thus, optimization criterion $z_{\dot{\xi}} \to 0$ and $z_{\dot{\psi}} \to 0$ are defined and put in the performance vector $z_1 = \left[z_{\dot{\xi}}\ z_{\dot{\psi}}\right]^T$. Also, constraints of the control inputs related to the in-wheel electric motors and the electric steering system must also be considered in the design. These are formulated in another performance vector $z_2 = \left[F_l\ \delta\ M_z\right]^T$.

Since the system matrix A in (9.4) depends on vehicle velocity $\dot{\xi}$ nonlinearly, a gain scheduling LPV controller must be realized in order to gain a global solution. Hence, utilizing a scheduling variable $\rho_1 = \dot{\xi}$ the originally given nonlinear vehicle model is transformed into a LPV model.

The fault-tolerant design of the in-wheel vehicle is realized with high-level control reconfiguration, in order to handle critical driving situations or faulty actuators. For this reason, a second scheduling variable $\rho_2 \in [0.01, 1]$ is introduced, which corresponds to the allocation of steering and yaw moment generation.

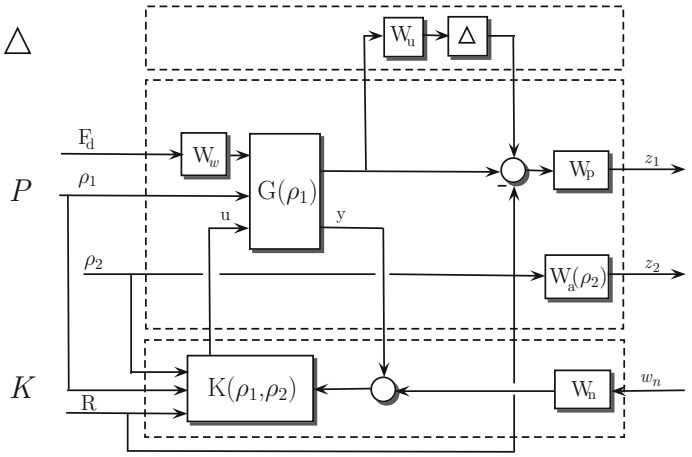

Fig. 9.2 Closed-loop interconnection structure

The proposed control system is based on a weighting strategy, realized with the closed-loop interconnection architecture depicted in Fig. 9.2.

Here, the role of weighting function W_p is to guarantee an optimal balance between the control performances formulated in vector z_1. Since they serve as penalty functions, large weights should be applied where small signals are expected and contrariwise. The aim of weighting functions W_w and W_n are to account the disturbances and sensor noises, while system uncertainties (unmodelled dynamics and uncertain parameters of the vehicle) handled by the Δ block are represented by the weighting function W_u The uncertainties of the system are handled by the Δ block, whereas the neglected dynamics are interpreted by weighting function W_u. These above detailed weighting functions are given in a second-order proportional form as follows:

$$W_p = \vartheta \frac{\kappa_2 s^2 + \kappa s + 1}{T_1 s^2 + T_2 s + 1} \tag{9.5}$$

where ϑ, $\kappa_{1,2}$ and $T_{1,2}$ are designed parameters.

In case of a fault event, control reconfiguration is handled with the weighting function W_a, which represents two different weighting functions. It is divided into the weighting function of the steering $W_{a\delta} = (\delta_{max}\chi_1)/(\rho_2)$ and the yaw moment $W_{aM_z} = (\rho_2)/(M_{zmax}\chi_2)$, where δ_{max} and M_{zmax} stands for the maximal value of steering angle and yaw moment, χ_1 and χ_2 are parameters adjusted to obtain a convenient control allocation. Thus, a small value of ρ_2 induces a big amount of yaw moment and small amount of steering angle, while the increasing value of ρ_2 generates more and more steering and less yaw moment for the in-wheel vehicle.

The fault-tolerant consideration is realized by further defining parameters $\rho_2^{M_z}$ and ρ_2^{δ}, which have the following relation with the scheduling variable ρ_2:

- In case of no steering fault detection by the FDI filter, $\rho_2 = \rho_2^{M_z}$ is applied for the above described weighting functions noted with W_a.
- In case of steering fault detection, $\rho_2^{\delta} = 0$ is set and $\rho_2 = \rho_2^{\delta}$ is applied.

The calculation of $\rho_2^{M_z}$ corresponding with a hub motor fault or wheel slip have already been introduced in Gáspár et al. (2015), thus here only a brief summary is given. Using the special ability of the in-wheel motors for fast and accurate torque generation, the transmitted wheel forces can be estimated precisely, see Hu and Yin (2011). Thus, the total amount of transmitted yaw moment can be expressed as

$$M_z^{trans} = \left(\frac{-T_{fL}^{trans} + T_{fR}^{trans}}{R_{eff}} \right) \frac{b_f}{2} + \left(\frac{-T_{rL}^{trans} + T_{rR}^{trans}}{R_{eff}} \right) \frac{b_r}{2} \tag{9.6}$$

where b_f and b_r are the front and rear track of the in-wheel vehicle, T_{ij}^{trans} $i \in [f = front, r = rear]$, $j \in [L = left, R = right]$ are the transmitted wheel torques. Thus, $\rho_2^{M_z}$ is calculated as

$$\rho_2 = \left| \frac{\left| M_z - M_z^{trans} \right|}{M_z} \right| \tag{9.7}$$

where M_z is the yaw moment given by the high-level controller. Equation (9.7) indicates that if the prescribed high-level yaw moment cannot be realized because of an electric in-wheel motor fault or performance degradation, the value of $\rho_2^{M_z}$ increases and the high-level LPV controller prescribes bigger steering angle and less yaw moment for the vehicle.

The design of the high-level controller is based on LPV framework. The design method is founded on applying parameter-dependent Lyapunov functions as described in Bokor and Balas (2005), Fen et al. (1996). The LPV performance problem is to find a parameter-varying controller such that the quadratic stability of the consequent closed-loop system is guaranteed, while the induced $\mathcal{L}_2$ norm from the disturbance to the performances is smaller than γ. Hence, the minimization problem can be written as

$$\inf_{K} \sup_{\varrho \in \mathcal{F}_{\mathcal{P}}} \sup_{\|w\|_2 \neq 0, w \in \mathcal{L}_2} \frac{\|z\|_2}{\|w\|_2} \leq \gamma. \tag{9.8}$$

where w is the disturbance of the system, Δ is the unmodelled dynamic of the in-wheel vehicle. The quadratic LPV γ-performance problem is solved using LMIs, calculating a feedback gain for every vertex. The LPV control $K(\varrho)$ is built in a manner that the global gain is a convex combination of the local gains.

9.3 Control Implementation

The fault-tolerant control system considering actuator reconfiguration is constructed in a multi-layer, hierarchical structure as depicted in Fig. 9.3.

The first layer consists the high-level LPV controller, with the aim to calculate the control inputs listed in Sect. 9.2 based on the driver reference signals, the measured velocity and yaw rate of the in-wheel vehicle and the value of the derived scheduling variable ρ_2.

The goal of the second layer is to distribute the resulting inputs of the first layer between the vehicle actuators, i.e., the longitudinal force F_l, the yaw moment M_z and the steering angle δ. The latter is limited by $\delta_{min} \leq \delta \leq \delta_{max}$ and sent directly to the third layer. Hence, the main task of the second layer is to calculate the in-wheel motor torques for the third layer. In this process, the high-level control signals of the first layer (longitudinal force and yaw moment) is distributed with the consideration of vehicle dynamics. Here, a dynamic allocation procedure is applied unifying methods listed in Zhao et al. (2014), Shuai et al. (2013). Measuring the longitudinal acceleration of the in-wheel vehicle using accelerometers, the pitch dynamics can be considered in the allocation process. Hence, the axle loads of the vehicle can be formulated as follows:

$$F_{zf} = \frac{mgl_2 - ma_x h}{(l_1 + l_2)}, F_{zr} = \frac{mgl_1 + ma_x h}{(l_1 + l_2)}, \tag{9.9}$$

where h is the center of gravity height, a_x is the longitudinal acceleration. Rearranging the previous equation the load distribution is given as

$$\frac{F_{zf}}{F_{zr}} = \frac{mgl_2 - ma_x h}{mgl_1 + ma_x h} = \kappa \tag{9.10}$$

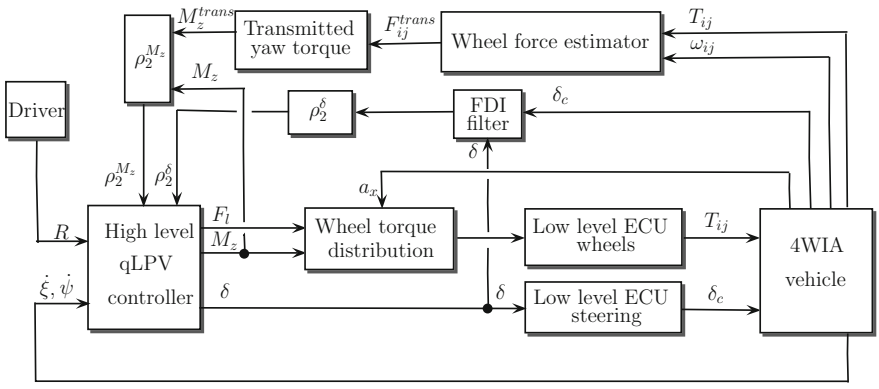

Fig. 9.3 Multi-layer reconfigurable control system

With a small angle assumption for δ, the longitudinal force F_l should fulfill the following equation:

$$F_l = F_{fL} + F_{fR} + F_{rL} + F_{rR} \tag{9.11}$$

where F_{ij} $i \in [f = front, r = rear]$, $j \in [L = left, R = right]$ are the longitudinal forces of each wheel. Moreover, the generated yaw moment M_z can be expressed as follows:

$$\Delta M_z = (-F_{fL} + F_{fR}) \cdot \frac{b_f}{2} + (-F_{rL} + F_{rR}) \cdot \frac{b_r}{2} \tag{9.12}$$

Since $F_i = \mu F_{zi}$, the following relationship holds: $F_f / F_r = \kappa$. Hence, the longitudinal force and yaw moment can be given as follows:

$$F_l = (F_{fL} + F_{fR}) \left(1 + \frac{1}{\kappa}\right) \tag{9.13}$$

$$M_z = (-F_{fL} + F_{fR}) \left(1 + \frac{1}{\kappa}\right) \frac{b}{2} \tag{9.14}$$

Finally, by rearranging above equations each wheel forces can be expressed as:

$$F_{fL} = \frac{F_l}{2\left(1 + \frac{1}{\kappa}\right)} - \frac{M_z}{b\left(1 + \frac{1}{\kappa}\right)}, \quad F_{rL} = \left(\frac{1}{\kappa}\right) F_{fL}, \tag{9.15}$$

$$F_{fR} = \frac{F_l}{2\left(1 + \frac{1}{\kappa}\right)} + \frac{M_z}{b(\left(1 + \frac{1}{\kappa}\right)}, \quad F_{rR} = \left(\frac{1}{\kappa}\right) F_{fR} \tag{9.16}$$

Note that the desired in-wheel motor torques sent to the third layer are given with $T_{ij} = R_{eff} F_{ij}$.

Finally, the third layer contains the low-level controllers responsible for generating the actual physical inputs for the steer-by-wire steering system and the in-wheel motors. The current control of the electric motors are not detailed here, but it has been studied broadly, see Wu et al. (2013), Yang and Lo (2008). For this purpose, a simple first order model is used to relate the torque signal of the second layer with the actually generated torque of the in-wheel hub motor, written as follows:

$$T_{motor}(s) = \frac{1}{1 + (L_m / R_m)s} T \tag{9.17}$$

where T_{motor} is the actual motor torque, T is the reference torque given by the second layer, while L_m and R_m are motor parameters related to inductance and resistance.

9.4 Simulation Results

Simulation has been performed in CarSim with a small 4WIA vehicle equipped with four in-wheel motors and a steer-by-wire steering system. The physical parameters of the electric hub motors based on specifications given by Watts et al. (2010) are shown in Table 9.1.

Other physical parameters of the 4WIA vehicle including mass, aerodynamic coefficient, suspension geometry, and wheel cornering stiffness are those of a conventional A-Class vehicle, see Table 9.2.

In the two simulation cases, the in-wheel vehicle is driven by a driver who must follow the trajectory of an S-turn, as shown in Fig. 9.4a. The vehicle velocity is set to a constant 54 km/h (see Fig. 9.4b), while the reference yaw rate for the vehicle to follow shown in Fig. 9.4c is generated by the driver operating the steering wheel.

It is assumed that the yaw rate, longitudinal, and lateral accelerations of the 4WIA vehicle can be measured with low-cost inertial sensors and accelerometers, as well

Table 9.1 Electric motor specifications

Parameter	Value	Unit
Total motor mass	34	kg
Peak output power	75	kW
Continuous output power	54	kW
Peak output torque	1000	Nm
Continuous output torque	650	Nm

Table 9.2 Parameters of the 4WIA vehicle

Parameter	Value	Unit
Vehicle mass (m)	830	kg
Yaw moment of inertia (J)	1110.9	kgm^2
Distance from C.G to front axle (l_1)	1.103	m
Distance from C.G to rear axle (l_2)	1.244	m
Tread front (b_f)	1.416	m
Tread rear (b_r)	1.375	m
Height of COG (h_{COG})	0.54	m
Cornering stiffness front (c_1)	22	kN/rad
Cornering stiffness rear (c_2)	85	kN/rad
Aerodynamic drag coefficient (c_w)	0.343	–
Front contact surface (A)	1.6	m^2

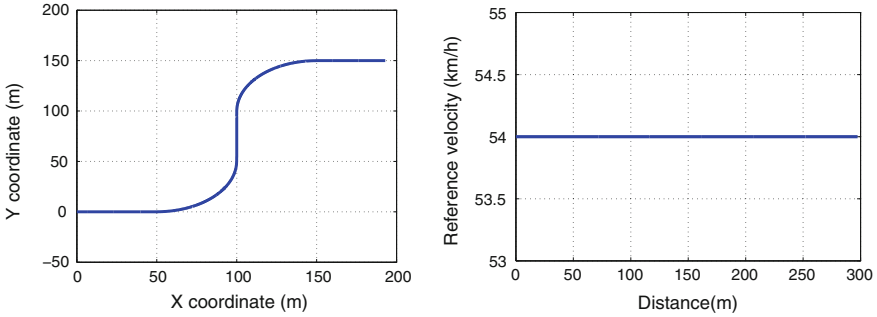

(a)Geometry of the S-turn (b)Reference velocity

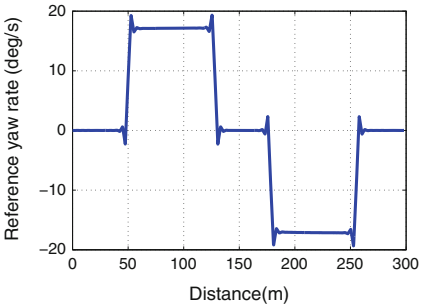

(c)Reference yaw rate

Fig. 9.4 Reference signals

as wheel speeds. Note that these measurements are essential to evaluate the reconfiguration control strategy described in the paper.

9.4.1 In-Wheel Motor Fault

In the first simulation case, the effect of an in-wheel motor fault is analyzed by comparing the results without any fault event. Here, the front left in-wheel motor is generated before the second corner.

The prescribed high-level control signals of the LPV controller for both cases are shown in Fig. 9.5. The operation of the high-level reconfiguration strategy is well demonstrated by observing Fig. 9.5b, c. In the first bend, an effective combination of steering and yaw moment generation is shown. During the second corner due to the faulty in-wheel motor and the increased value of ρ_2, the LPV controller of the 4WIA vehicle prescribed much bigger steering angle and reduced yaw moment for the vehicle compared to the normal case without a fault event.

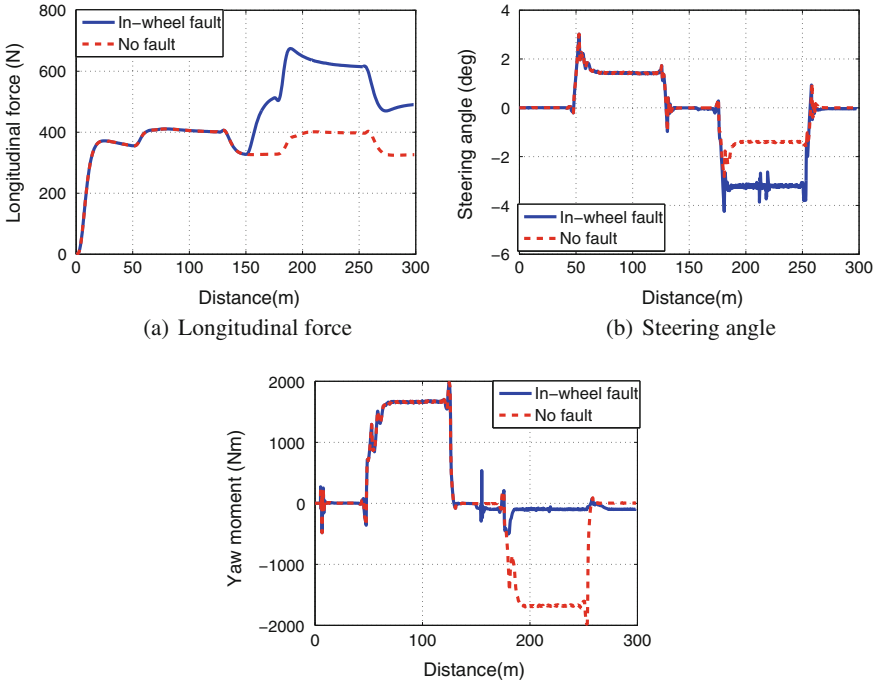

(a) Longitudinal force (b) Steering angle

(c) Yaw moment

Fig. 9.5 High-level control signals

As a result of the dynamic wheel-torque allocation method presented in Sect. 9.3, the in-wheel motors generate differential torque considering the vehicle pitch, as shown in Fig. 9.6. It is well-demonstrated by observing Fig. 9.6a, that without a fault event the left and right side motors generate the same amount of differential torque in both corners. Meanwhile, when the front left in-wheel motor fails before the second corner producing no torque as shown in Fig. 9.6, the differential torque generation of the healthy in-wheel motors are also reduced due to the high-level control reallocation represented by ρ_2.

The performances of the proposed method are shown in Fig. 9.7. The velocity error of the 4WIA vehicle does not exceed 1 km/h even under the fault event of the front left electric motor (see Fig. 9.7a), while the yaw rate error depicted in Fig. 9.7b also remains acceptably small due to the control reconfiguration. Although the lateral error from the lane center increases in case of an in-wheel motor failure as depicted in Fig. 9.7c, the vehicle is able to evaluate the cornering maneuver successfully.

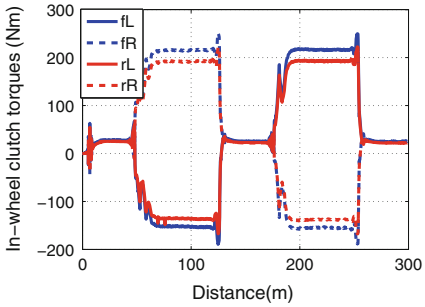

(a) Without fault event

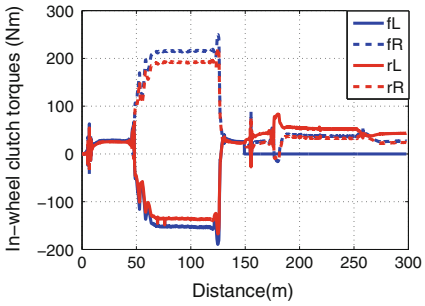

(b) With in-wheel fault

Fig. 9.6 Hub motor torques

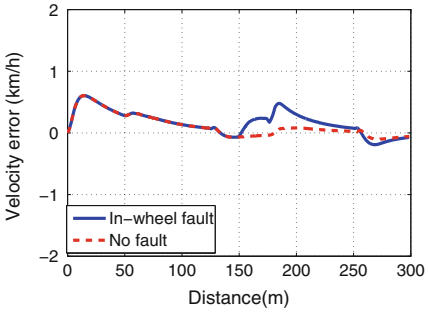

(a) Velocity error

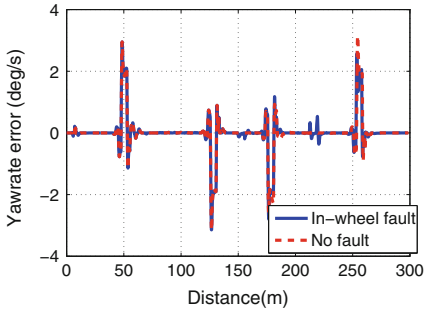

(b) Yawrate error

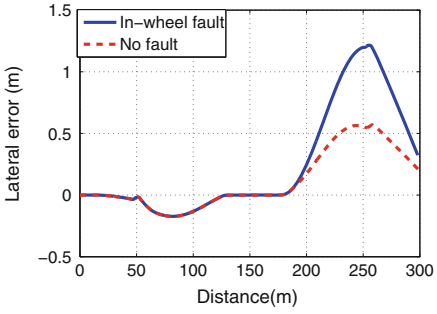

(c) Lateral error

Fig. 9.7 Performances of different methods

9.4.2 *Steering System Fault*

In the second simulation case, the steer-by-wire steering system is assumed to develop a serious failure before the second corner. Thus, the fault-tolerant reconfiguration method detailed in Sect. 9.2 sets ρ_2 to be equal with $\rho_2^{\delta} = 0$ when the fault event occurs.

Hence, after the fault in the steer-by-wire steering system is detected, the high-level control signals are reconfigured in such way that the vehicle evaluates the cornering solely by yaw moment generation, as shown in Fig. 9.8b, c. It is well-demonstrated by comparing with the faultless case that the effect of the steering is substituted with prescribing significantly more yaw moment.

As a result of the high-level control reconfiguration and the prescribed extra yaw moment, the differential in-wheel hub motor torques are more pronounced in the second corner compared to the normal case, as demonstrated by comparing Fig. 9.9a, b.

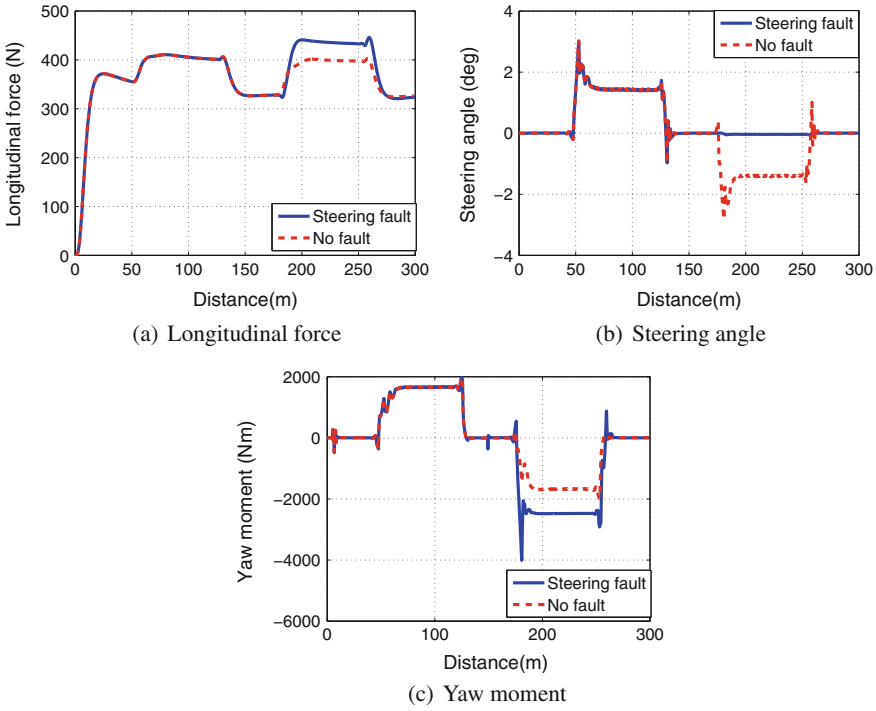

(a) Longitudinal force (b) Steering angle

(c) Yaw moment

Fig. 9.8 High-level control signals

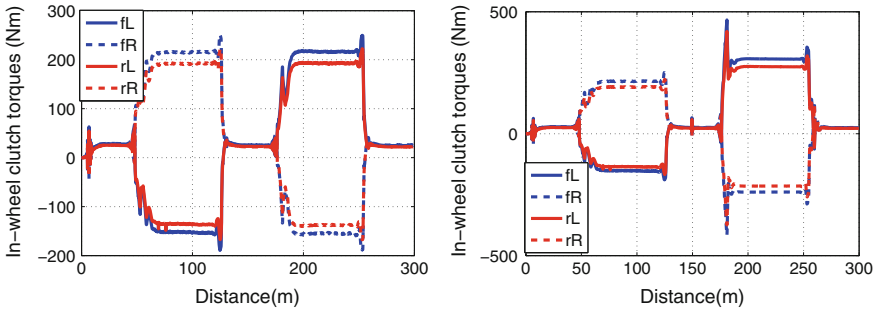

(a) Without fault event (b) With steering fault

Fig. 9.9 Hub motor torques

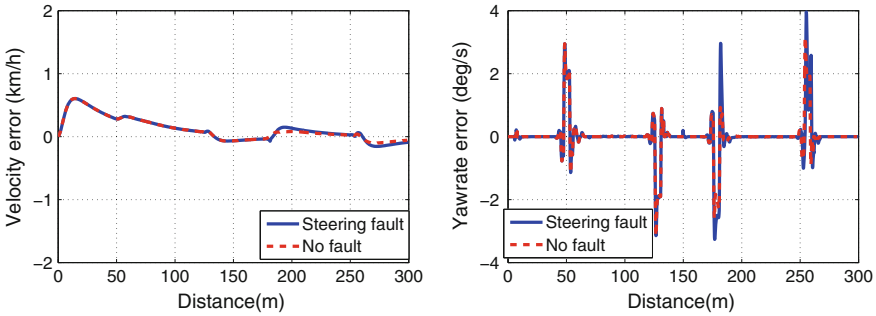

(a) Velocity error (b) Yawrate error

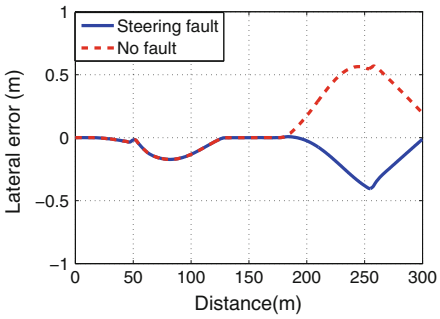

(c) Lateral error

Fig. 9.10 Performances of different methods

The performances of the control system in case of a steering system failure are shown in Fig. 9.10. The velocity and yaw rate errors shown in Fig. 9.10a, b remain small due to the effective reconfiguration. The lateral error of the vehicle shown in Fig. 9.10c is similar to that without a fault event.

Chapter 10
Driver Models in the Control Systems

Introduction

The integrated control proposed in this paper is based on a supervisory integrated structure in which the control components are designed independently. The role of the supervisor is to guarantee coordination between components and meet performance specifications. The supervisor has information about the current operational mode of the vehicle, i.e., the various vehicle maneuvers or the different fault operations gathered from monitoring components. Then it is able to make decisions about the necessary interventions into the vehicle components.

In integrated control systems the characteristics of the drivers' behavior should be taken into consideration in the control. The control solutions create a balance between driving (or road holding) and comfort and guarantee safety all the time. This balance often leads to compromises between vehicle functions, which may not be suitable for all the drivers. For example, a driver who wants to minimize the length of the trajectory in the bend selects the curvature radius as small as possible, while the driver who requires comfort selects a larger curvature radius. At the same time, however, the selection of different curvature radiuses is also related to the possible speed selection, e.g., the larger radius allows the driver to select larger speed. The control solutions in practice are based on the drivers' behavior, which is learnt by the system during traveling.

The driver input is not only a function of the planned trajectory but it also affects the vehicle dynamics. Thus, a driver model must be combined with the vehicle model. In this paper, the supervisory control is combined with a driver model in order that the driver behaviors and requirements are incorporated in the design of the control system. Consequently, in the driver assistance system the interaction between the vehicle and driver is taken into consideration. The control solutions in practice are based on the drivers' behavior, which is learnt by the system during traveling. In other solutions, the vehicle has a manual mode switch that ensures the vehicle dynamics according to the driver requirement. For example, the driver can make the suspension stiffen to achieve the sport mode or can make the suspension soft to improve the ride in outstanding comfort.

P. Gáspár et al., *Robust Control Design for Active Driver Assistance Systems*,
Advances in Industrial Control, DOI 10.1007/978-3-319-46126-7_10

In the specifications of the performance criteria, the driver behavior must be taken into consideration through various driver models. In the following, a brief survey is given before the driver model, which is used for control-oriented purposes, is presented. Kiencke et al. (1999) developed a hybrid driver model, in which the discrete event system theory is combined with the classical control theory. In the driver model, visual perception was divided into two classes, i.e., the traffic-relevant and the vehicle-relevant factors. The model handled both the lateral and longitudinal motions of the vehicle, see also Kiencke and Nielsen (2000). Based on the physical limitations, the prediction and adaptation capabilities of drivers Macadam (2003) set up driver models both in the longitudinal and the lateral directions. A method for the detection of driver lane changes is developed by Salvucci et al. (2007). The driver behavior in the context of the intelligent transportation system within the PATH project was analyzed by Delorme and Song (2001). Multiple driver models were constructed for the driver assistance systems by Fujiwara et al. (2004). Based on the inverse of the bicycle model and the proposed voting and switching rule the necessary steering operation was calculated. Neural network model, fuzzy logic, and genetic algorithm approaches of the driver models were also widely used, see e.g., Kageyama et al. (2000). Game theory-based approaches and noncooperative model predictive control are used for developing the driver steering control model in Na and Cole (2013). A learning-based driver model, by which it is able to identify manoeuvres on the highway and predict the future driver inputs is found in Lefevre et al. (2015).

A detailed analysis of a mathematical model for the driver steering control was formulated in Sharp et al. (2000). The driver model was linked to a nonlinear vehicle dynamics model so that the vehicle followed a prescribed path. In the longitudinal and lateral position of the center of gravity of vehicle approach, the vehicle yaw angle and the vehicle longitudinal velocity were taken into consideration. Various control scenarios were analyzed, such as steering control, speed control, and path following control. A driver model of the steering control operating in the closed-loop system was constructed by Hess and Modjtahedzadesh (1990). The driver model was divided into high- and low-frequency compensation elements. The high-frequency compensation refers to frequencies around the crossover frequency of the overall system. An analysis on the parameter dependency of driver steering model is presented in Pauwelussen (2012). In Rossa et al. (2014), a bifurcation analysis is adopted for analyzing the steady-state cornering and straight ahead motion of the interconnected car-driver model.

Menhour et al. (2009) constructed a two-level driver model for steering control. The goal of the anticipatory part, which was based on the lateral dynamics, was to generate the reference curvature of the road and the preview position. The compensatory part, which was based on a set of PID controllers, corrected both the yaw angle and the lateral displacement. The selection of the appropriate PID controller was based on a switching mechanism. On the basis of the two-level approach, the driver's steering model was extended to higher lateral accelerations by Edelmann et al. (2007). Ungoren and Peng (2005) focused on an adaptive lateral preview driver model. Although the template of the driver model had only a few parameters, they

were adjusted in such a way that they are tended to the steering actions of an average human driver as well as drivers with different driving styles. Different methods were proposed for a preview driver model, in which the future path information was directly concerned in the space-horizon model, see e.g., Jiang et al. (2011). Braghin et al. (2008a) developed a race driver model, in which the focus was the trajectory planning, since the goal of the race car driver is to obtain the lowest lap time. Thus, either the length of the course had to be minimized or the speed of the car had to be maximized. The consideration of the driver's neuromuscular dynamics is found in Cole (2012), Mehrabi et al. (2015).

A framework of controlling a system with multiple interactive control loops including a continuously activated primary loop and discretely activated secondary loops was proposed by Lu and Filev (2009). The primary loop included the driver while the secondary loops included electronic devices.

Weather conditions were also considered in the modeling of the driver, see Hoogendoorn (2010). Parameters of a driver model is estimated by using driving simulator experiences and measurements. An identification method for a human driving model based on measured car-following data was presented in Lee and Peng (2004). Here, a Gipps model was implemented in the simulator for verification purposes, and the proposed method was used for collision warning and avoidance systems. Finally, an evaluation of the different driver models under different critical situations is proposed in Markkula et al. (2014).

10.1 Driver Model for Control Design Purposes

10.1.1 Control-Oriented Driver Model

The driver models proposed by previous papers are suitable for human drivers and provide a complex description of driver behavior. In this section, a driver model is applied to control-oriented purposes. Since the driver operates in a closed-loop system together with the active components such as the active steering and the brake, the design of the driver assistance system requires the model of the driver. The model should be selected in such a way that the accuracy of the combined driver/vehicle model will be acceptable and the model can be easily used in the control design. The control-oriented driver model was selected as a work of Hess and Modjtahedzadesh (1990).

The input of the driver model is the difference between the lateral position of the vehicle realized by the driver y_v and the reference lateral position of the road $y_{v,ref}$:

$$e_y = y_{v,ref} - y_v. \tag{10.1}$$

The output is the steering wheel angle of the driver δ_d.

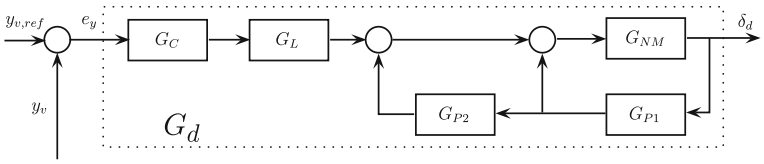

Fig. 10.1 Driver model for control design purposes

The driver model has been divided into high- and low-frequency compensation elements as Fig. 10.1 illustrates. The high-frequency driver compensation describes a decade range around the crossover frequency of the overall driver/vehicle open-loop return ratio. It is defined by three components with loops. The driver model G_{NM} is a second order transfer function of the neuromuscular system of the driver's arms: $G_{NM} = K_N/(T_{N1}s^2 + T_{N2}s + 1)$, where T_{N1}, T_{N2} are time constants. G_{P1} and G_{P2} represent feedback of variables derived from the motion of human limbs and muscle tissue. Their forms are $G_{P1} = K_1 s/(T_1 s + 1)$ and $G_{P2} = K_2/(T_2 s + 1)$.

The low-frequency driver compensation is defined by two components with a delay. Inherent human signal processing delay is represented by a time delay G_L. The time delay is approximated with a first order transfer function: $G_L = 1/(T_L s + 1)$. The low-frequency compensation of the driver model is represented by G_C, which is formalized as $G_C = K_C(T_C s + 1)$.

The driver model between the lateral error e_y and the steering output δ_d is formalized as follows:

$$G_d = (I + G_{NM}G_{P2}G_{P1} + G_{NM}G_{P1})^{-1}G_{NM}G_L G_C \tag{10.2}$$

Theoretically, the driver model can be approximated by a four-order proportional transfer function. Using (10.1), the driver model is transformed into a state-space representation form:

$$\dot{x}_{dr} = A_{dr}x_{dr} - B_{dr}y_v + B_{dr}y_{v,ref} \tag{10.3}$$

$$\delta_d = C_{dr}x_{dr}. \tag{10.4}$$

The differences between the various drivers depend on the pole configuration of the different transfer functions. In the following section, a preliminary identification is carried out to analyze driver behaviors.

10.2 Control-Oriented Model for Lateral Dynamics

The basic dynamics of the vehicle shown in Fig. 9.1 is determined by the driver, while lateral dynamics is assisted by the control systems. They have advantages mainly in crucial situations, when the driver himself is not able to guarantee trajectory tracking.

The vehicle lateral dynamics is based on the bicycle model, see e.g., Rajamani (2005). The lateral tyre forces are approximated linearly to the tire side-slip angles: $F_{yf} = C_f \alpha_f$ and $F_{yr} = C_r \alpha_r$, where C_f and C_r are cornering stiffnesses of the linearized tire model. The tire side-slip angles are expressed as $\alpha_f = -\beta + \delta - l_1 \cdot \dot{\psi}/v$, $\alpha_r = -\beta + l_2 \cdot \dot{\psi}/v$, where β is the side-slip angle, δ is the front-wheel steering angle, $\dot{\psi}$ is the yaw rate of the vehicle, l_1 and l_2 are geometric parameters, and v is longitudinal velocity.

The actuators in the system are the front-wheel steering angle δ_c and the brake yaw moment M_{br}. During maneuvers, the difference between the lateral direction of the vehicle and the reference lateral direction is minimized by the driver. He generates the steering angle δ_d by using the steering wheel. If it is necessary, this angle is corrected by the automatic steering system by using additional steering angle δ_c. Thus, the steering angle is divided into two components: $\delta = \delta_c + \delta_d$. The equations of the bicycle model are the following:

$$J\ddot{\psi} = C_1 l_1 \alpha_f - C_2 l_2 \alpha_r + M_{br} \tag{10.5}$$

$$mv(\dot{\psi} + \dot{\beta}) = C_1 \alpha_f + C_2 \alpha_r \tag{10.6}$$

$$\ddot{y}_v = v(\dot{\psi} + \dot{\beta}) \tag{10.7}$$

where m is the mass, J is the yaw inertia of the vehicle, and $\ddot{y}_v$ is lateral acceleration of the vehicle. The motion equation of the vehicle is transformed into a state-space representation form:

$$\dot{x}_{veh} = A_{veh} x_{veh} + B_{veh,1} \delta_d + B_{veh,2} u_{veh} \tag{10.8}$$

$$z_{veh} = C_{veh,2} x_{veh} \tag{10.9}$$

$$y_{veh} = C_{veh,1} x_{veh} \tag{10.10}$$

where the state vector of the vehicle $x_{veh} = \begin{bmatrix} \dot{\psi} & \beta & \dot{y}_v & y_v \end{bmatrix}^T$ contains the yaw rate, the side-slip angle, and the lateral velocity and position. The control input and the disturbance are $u_{veh} = \begin{bmatrix} \delta_c & M_{br} \end{bmatrix}^T$ and δ_d, respectively. The performance signal is the lateral position of the vehicle $z_{veh} = y_v$ and the measured signal is the yaw rate of the vehicle $y_{veh} = \dot{\psi}$.

10.3 Interconnection of the Driver-Vehicle System

The interconnection structure between the driver and the vehicle models in the architecture of the driver assistance system is illustrated in Fig. 10.2. The input of the driver model is the lateral position error e_y, while its output is the steering angle of the driver δ_d. The control inputs of the vehicle model are the brake yaw moment M_{br} and the front steering angle δ_c, while its outputs are the lateral position of the vehicle y_v and the yaw rate $\dot{\psi}$. The purpose of the system is to improve road holding and

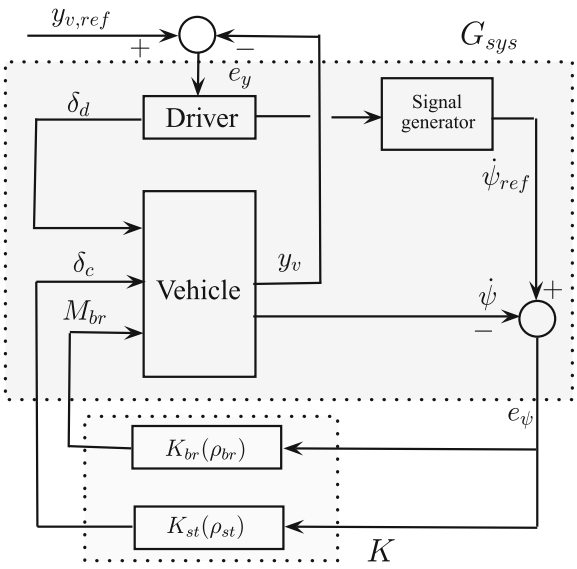

Fig. 10.2 Architecture of the driver assistance system

guarantee the balance between road stability and passenger comfort during vehicle maneuvers. Two control systems are used in the interconnection system, i.e., the steering system K_{st}, and the braking system K_{br}. Their operations are based on the yaw rate error, in which the reference yaw rate is generated by the steering angle of the driver δ_d.

In practice, the maneuvering requirements of the driver must be estimated from the steering wheel angle δ_d, in which the velocity v must be taken into consideration. This is formed by the reference yaw rate $\dot{\psi}_{ref}$, which must be tracked by the integrated control system. Based on δ_d, the reference yaw rate $\dot{\psi}_{ref}$ is calculated using a first order proportional transfer function, see Pacejka (2004).

$$G_{\dot{\psi}_{ref},\delta_d}(s) = \frac{v}{l_1 + l_2 + \frac{\eta}{g}v^2} \cdot \frac{1}{\tau s + 1} \tag{10.11}$$

with an understeer gradient η and the time constant τ. The block of the reference signal generator is inserted into the architecture of the driver assistance system. The state-space representation form of the signal generator is

$$\dot{x}_{SG} = A_{SG}x_{SG} + B_{SG}\delta_d \tag{10.12}$$

$$\dot{\psi}_{ref} = C_{SG}x_{SG} \tag{10.13}$$

Finally, the state-space representation of the entire complex system G_{sys} is formed by using the vehicle, the driver and the signal generator blocks (10.3), (10.8), and (10.12), respectively. The augmented state vector is introduced in the following

form: $x_{aug} = \left[x_{veh}\ x_{dr}\ x_{SG}\right]^T$. Since δ_d and y_v are expressed by (10.4) and (10.9), respectively, the state-space representation of the augmented system is the following:

$$\dot{x}_{aug} = \left[\begin{array}{c|c|c} A_{veh} & B_{veh,1}C_{dr} & 0 \\ \hline -B_{dr}C_{veh,2} & A_{dr} & 0 \\ \hline 0 & B_{SG}C_{dr} & A_{SG} \end{array}\right] x_{aug} + \tag{10.14}$$
$$+ \begin{bmatrix} B_{veh,2} \\ 0 \\ 0 \end{bmatrix} u_{veh} + \begin{bmatrix} 0 \\ B_{dr} \\ 0 \end{bmatrix} y_{v,ref}$$
$$y = \left[-C_{veh,1} \middle| 0 \middle| C_{SG}\right] x_{aug} \tag{10.15}$$

in which the output of the augmented system is the yaw rate error $y = e_{\dot{\psi}}$, which is used in the controllers.

Remark 10.1 Note that in the closed-loop interconnection structure $\dot{\psi}_{ref}$ is used instead of δ_d, which is compared to the measured yaw rate $\dot{\psi}$. Thus, from the control design aspect the signal δ_d is not a disturbance as in Eq. (10.8).

Remark 10.2 The actuator selection depends on several factors. They are the construction limit, the energy requirements, and the dynamics of the actuators. For example, to avoid the skidding of tires brake yaw moment must be reduced and, simultaneously, the yaw motion must be controlled by front-wheel steering. Similarly, to avoid reaching the steering limit differential braking must be increased. The actuator selection strategy is not within the scope of the paper.

10.4 Performance Specifications of the Driver Assistance System

Based on the interconnection structure of the driver assistance system both the vehicle-oriented and the driver-oriented performances are defined.

10.4.1 Formulation of Performances

In order to guarantee lane keeping during maneuvers, the lateral position of the vehicle y_v from the centerline of the lane $y_{v,ref}$ must be minimized. The lateral position is defined by the driver in its maneuvers. The role of the controllers is to assist the driver in reducing the lateral error. The trajectory tracking performance of the control system is the following:

$$z_1 = y_{ref} - y_v; \qquad |z_1| \to min! \tag{10.16}$$

Simultaneously, during control actuation actuator saturations must be avoided. The maximum values of the actuators during driving and braking are determined by their physical construction limits and the maneuvers, e.g., the tyre-road adhesion conditions. Thus, the control inputs are also formulated as performance criteria as given below:

$$z_2 = \begin{bmatrix} \delta_c & M_{br} \end{bmatrix}^T; \qquad |z_2| \rightarrow min! \tag{10.17}$$

The human driver performance of the system is the actuation of the driver. The driver's steering wheel angle δ_d has two aspects: the magnitude and the rate of the angle, which must be influenced by the control design.

- Magnitude of δ_d: During a vehicle maneuver the steering wheel must be rotated by the driver. Although usually the steering wheel is rotated with two hands, the angle of rotation should be as small as possible. Otherwise, steering is uncomfortable and might be dangerous. The goal is to limit the magnitude of δ_d to reduce the angle of rotation as given below:

$$z_{3,1} = \delta_d; \qquad |z_{3,1}| \rightarrow min! \tag{10.18}$$

- Rate of δ_d: Besides the magnitude of the steering wheel angle, the speed of the rotation is also a significant factor. The high speed requires concentration and it might also be dangerous. Therefore, the goal is to limit the rate of δ_d as given below:

$$z_{3,2} = \dot{\delta}_d; \qquad |z_{3,2}| \rightarrow min! \tag{10.19}$$

10.4.2 Weighting Strategy of Performances

In the control design, several performances must be taken into consideration. Since they are in conflict a balance must be achieved between them. In the following, weighting functions are introduced into the transfer functions with their magnitudes and frequencies for the performance specifications.

The weighting function of the lateral tracking error is selected in such a way that its steady state should be below a predefined value:

$$W_{z_1} = e_{y,max} \frac{T_{z_1} s + 1}{T_{z_2} s + 1}, \tag{10.20}$$

where $e_{y,max}$ is the design parameter and T_{z_1}, T_{z_2} are time constants.

The performance z_2 has an important role in the supervisory control design. The steering and braking controllers are designed independently in the distributed control system. Their integration is guaranteed by actuator selection parameters ρ_{st} and ρ_{br}. Thus, weighting function for z_2 is formulated for the steering and the braking separately by the following transfer functions.

The weighting function of the steering angle is selected as follows:

$$W_{z_{2,1}} = (1 - \rho_{st}) \frac{T_{d1}s + 1}{T_{d2}s + 1}, \tag{10.21}$$

where T_{di} is time constant and the parameter-dependent gain ρ_{st} focuses on the relative importance of the steering actuation. It depends on the steering angle δ and the velocity v. The weighting function of the differential brake torque is selected as follows:

$$W_{z_{2,2}} = (1 - \rho_{br}) \frac{T_{b1}s + 1}{T_{b2}s + 1}, \tag{10.22}$$

where T_{bi} is time constant and the parameter-dependent gain ρ_{br} focuses on the relative importance of the braking actuation. It depends on the longitudinal slips of the tires κ.

The human driver performances have importance in different frequency ranges, thus the following performance weight is selected as the following:

$$W_{z_{3,1}} = \delta_{d,max} \frac{(\varepsilon_{dr,1}s + 1)(\varepsilon_{dr,2}s + 1)^2}{(T_{dr,1}s + 1)(T_{dr,2}s + 1)^2}, \tag{10.23}$$

where $\delta_{d,max}$ is related to the maximum permitted driver steering wheel angle. The role of this part is to guarantee the limitation of δ_d according to performance $z_{3,1}$. $\varepsilon_{dr,1}$, $\varepsilon_{dr,2}$ $T_{dr,1}$, and $T_{dr,2}$ are design parameters, which have a role in the limitation of the steering wheel angle, see Fig. 10.3. The selection of the weighting function of $\dot{\delta}_d$ is the following:

$$W_{z_{3,2}} = \frac{\dot{\delta}_{d,max}}{T_{dr,3}s + 1}, \tag{10.24}$$

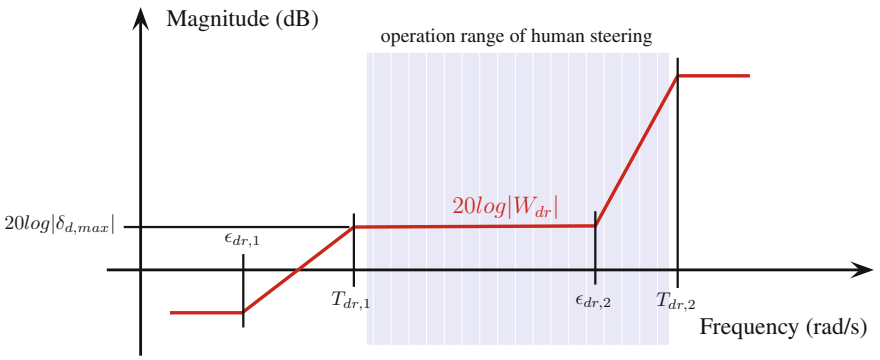

Fig. 10.3 Weighting of δ_d

10.5 Integrated Control Design of the Driver Assistance System

The closed-loop interconnection structure, which includes the feedback relationship of the augmented model G_{sys} and controller K, is shown in Fig. 10.4. This scheme is applied to the design of both the steering and the brake control. The external signals of the controllers are the reference of the lateral position $y_{v,ref}$, the sensor noise w_n, and the another control signal, which can be considered as disturbance u_{ext} while ρ is the scheduling variable used in the actuator selection.

The control design is based on a weighting strategy in the closed-loop interconnection structure. The purpose of weighting functions $W_{z_{i,j}}$, $i \in \{1, 2, 3\}$, $j \in \{1, 2\}$ is to define the performance specifications, see Sect. 10.4. The purpose of the weighting functions W_{ref} is to generate the reference of the lateral position, W_n reflects the sensor noise, while W_{ext} represents the external signals.

The control design leads to a quadratic LPV performance problem. The advantage of these methods is that the controller meets stability and performance demands by using affinely parametrized Lyapunov functions in the entire operational interval, since the controller is able to adapt to the current operational conditions, see Bokor and Balas (2005), Wu et al. (1996).

The quadratic LPV performance problem is to find a parameter-varying controller in such a way that the resulting closed-loop system is quadratically stable, and the induced $\mathscr{L}_2$ norm from the disturbance w and the performances z is less than a predefined value γ as follows:

$$\inf_{K} \sup_{\rho \in \mathscr{F}_{\mathscr{P}}} \sup_{\|w\|_2 \neq 0, w \in \mathscr{L}_2} \frac{\|z\|_2}{\|w\|_2} < \gamma \tag{10.25}$$

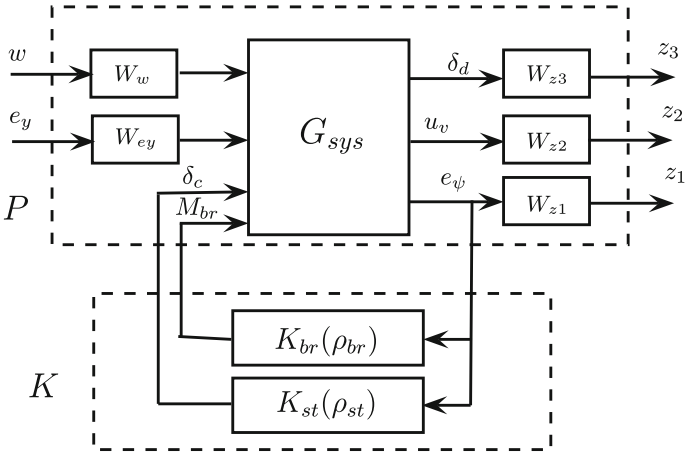

Fig. 10.4 Closed-loop interconnection structure

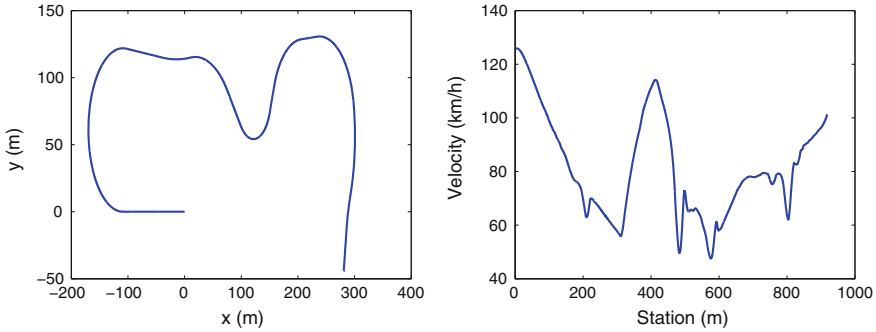

Fig. 10.5 Course of vehicles

The solution of an LPV problem is governed by the set of infinite dimensional LMIs being satisfied for all $\rho \in \mathscr{F}_{\mathscr{P}}$, thus it is a convex problem. In practice, this problem is set up by gridding the parameter space and solving the set of LMIs that hold on the subset of $\mathscr{F}_{\mathscr{P}}$. The control design is based on the LPV method that uses parameter-dependent Lyapunov functions.

10.5.1 Simulation Results

In the final section, the operation of the proposed control design is illustrated through a simulation example. The purpose of the driver is to travel along the course of the Waterford Michigan Race Track, see Fig. 10.5. The road trajectory contains several difficult and sharp bends. The data of the vehicle and the driver are found in Table 10.1.

In the simulation two scenarios are compared: in the uncontrolled case there is no driver assistance system in the vehicle, while in the controlled case the proposed integrated driver assistance system assists the driver.

Table 10.1 Data of vehicle and driver

m	1833 kg	K_C	10
J	2765 kgm^2	T_C	2
l_1	1.402 m	K_N	1
l_2	1.646 m	T_{N1}	0.01
C_1	70000 N/rad	T_{N2}	0.1414
C_2	105000 N/rad		
K_1	5	T_1	5
K_2	8	T_2	4

The driver changes the velocity along the road. The sharp bends of the track result in an increase of the lateral error of the vehicle $e_y = y_{ref} - y_v$. The driver without an assistance system is not able to follow the track, leaves the lane and the lateral error increases significantly. The proposed integrated control system is able to assist the driver in its operation and reduce the lateral error. The difference between the errors in the two cases $|e_{y,uncontrolled}| - |e_{y,controlled}|$ is illustrated in Fig. 10.6a. The proposed driver assistance system reduces the lateral trajectory error, significantly.

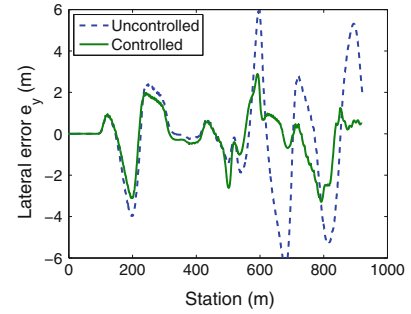

(a) Lateral error improvement e_y

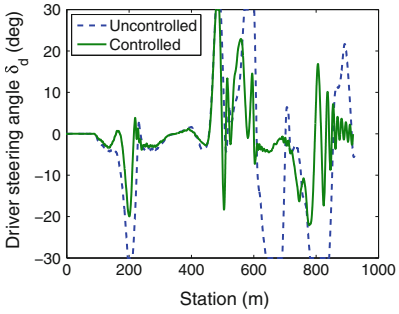

(b) Driver steering δ_d

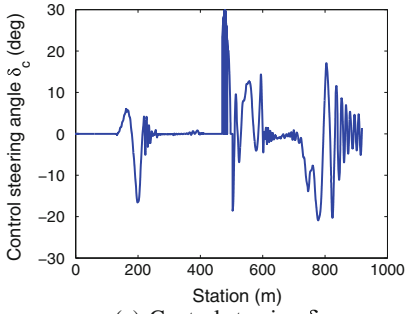

(c) Control steering δ_c

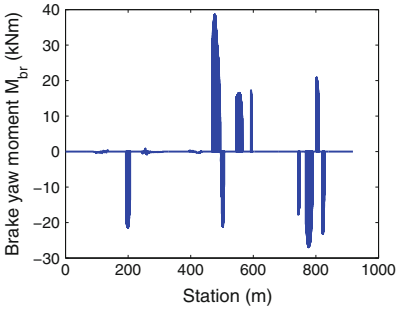

(d) Braking M_{br}

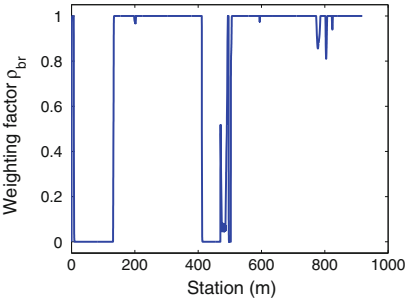

(e) Weighting factor in the braking selection

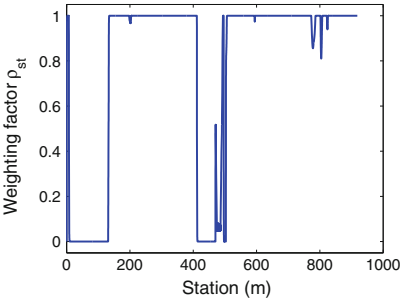

subfigure
[Weighting factor in the steering selection]

Fig. 10.6 Interactions between the driver and the control

Figure 10.6b shows that not only e_y is reduced by the driver assistance system but also the steering wheel angle δ_d. The appropriately designed weighting functions $W_{z_{3,1}}$ and $W_{z_{3,2}}$ make steering more comfortable. Their parameters are selected $\varepsilon_{dr,1} = 20$, $\varepsilon_{dr,2} = 0.2$, $T_{dr,1} = 10$, $T_{dr,2} = 0.1$, $T_{dr,3} = 10$, $\delta_{d,max} = 3.18$, and $\dot{\delta}_{d,max} = 0.16$.

However, it should be noted that there is a trade-off between the reduction of δ_d and the actuation of the inputs δ_c and M_{br}. Since δ_d is the source of the calculation $\dot{\psi}_{ref}$, see (10.11), it also affects the control inputs. The reduction of δ_d and $\dot{\psi}_{ref}$ requires larger and more frequent control interventions. The control inputs δ_c and M_{br} required by the maneuvers are illustrated in Fig. 10.6c, d, respectively. The interventions of actuators are controlled by the selection weights ρ_{st} and ρ_{br}, see Fig. 10.6e, f. The appropriate selection of ρ_{st} and ρ_{br} guarantees the priority between controllers in the driver assistance system. The simulation example shows that the proposed integrated driver assistance system is able to improve the maneuverability of the vehicle, while both the lateral error and the steering wheel angle are reduced. It results in safer and more comfortable maneuvers for the driver.

10.5.2 Simulation Environment of the Driver Model

Based on the analysis of the theoretical driver models, a system identification method is performed by using a real car. The internal signals of the model structure related to the neuromuscular system or the motion of human limbs illustrated in Fig. 10.1 are not measured; the identification leads to black-box identification between the input and output signals. In this section the identification results are presented.

The identification procedure is performed by using a real car in a simulation environment. The hardware-in-the-loop simulation environment is built in such a way that the simulator tends to the real vehicle functions as much as possible.

The challenge is to keep the original vehicle functions intact while implementing simulation functions. For this reason, the control of the vehicle's communication network has been taken over by the simulator unit, implementing full simulation for the instrument cluster in simulation mode. Although the vehicle is stationary during the simulations and only the wheels rotate on a bogie, the driver has a driving sensation similar to the real experience. The stationary vehicle can be driven exactly the same way as on a test track: there is engine sound and screech while skidding; the instrument panel displays the current speed and revolution and one can shift gears just like in real life.

The simulation environment contains several important components such as a HMI (human–machine interface): a high-accuracy validated simulation software operated on a PC and a visual system with real-time graphics. The specific signals (the positions of the accelerator and the brake pedal, and the steering angle) are read through the CAN network by using a standard communication interface. As vehicle simulations are carried out with the engine switched off, the missing internal signals are also generated in the vehicle to ensure the basic functions.

The driver can induce various vehicle maneuvers by using the steering wheel and the accelerator/brake pedals of the car. Based on the excitations, the validated simulation software generates the signals of the vehicle during simulation. The driving simulator of the CarSim shows the vehicle maneuvers by real-time graphics projected in front of the vehicle, and it provides the signals during the journey. While the car is traveling along a path, the driver reduces both the lateral position error and the heading error.

The driver experiences with a standing car and a projected path is shown in Fig. 10.7. Various journey scenarios can be generated by the simulation system. The advantage of the system is that besides measuring various signals, i.e., the steering angle, the positions of the accelerator, and the brake pedal or the gear level, in principle any signals can be monitored during the simulations. In this way, signals which are not measurable in practice can be achieved for identification purposes. In the later stage of the project, real measurements will also be carried out to enhance and validate the identification results.

In the identification procedure the ARX model structure, in which AR refers to the autoregressive part and X to the extra input (exogenous) part, is used. In the ARX structure, the relationship between input $u(t)$ and output $y(t)$ is obtained by describing it as a linear difference equation as follows:

$$y(t) = \frac{B(q)}{A(q)}u(t) + e(t) \tag{10.26}$$

Fig. 10.7 Illustration of the driver experience

where $A(q) = 1 + a_1 q^{-1} + ... + a_n q^{-n}$, $B(q) = b_1 q^{-1} + ... + b_m q^{-m}$, q is the delay operator, and $e(t)$ is the noise term. The orders of the operators n and m are related to the orders of the preliminary driver models. Since the identified model (10.26) is in discrete time, a discrete to continuous conversion is also applied to achieve the driver models.

Several drivers with different behaviors and abilities are traveling along a predefined road. The trajectory with the measured signals are illustrated in Fig. 10.8.

An identification procedure consists of the following main steps: structure estimation, parameter estimation, model validation, and model analysis. The structure, i.e., the orders of the operators, is determined by the preliminary theoretical approach. This structure has also been examined by using various criteria such as AIC (Akaike information criterion) and FPE (final prediction error), Khorshidi and Karim (2009). Then, the identification method is performed to identify the model $\hat{G}_d$. The result of an identification procedure is illustrated in Fig. 10.9.

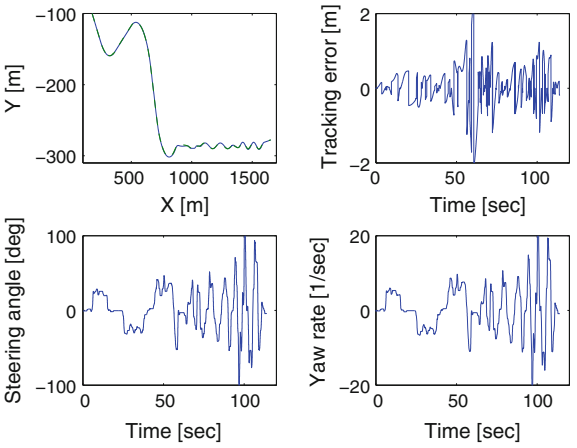

Fig. 10.8 Typical vehicle maneuvers

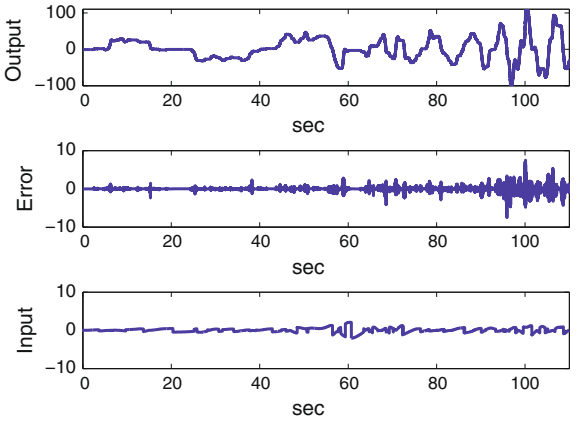

Fig. 10.9 Result of an identification procedure

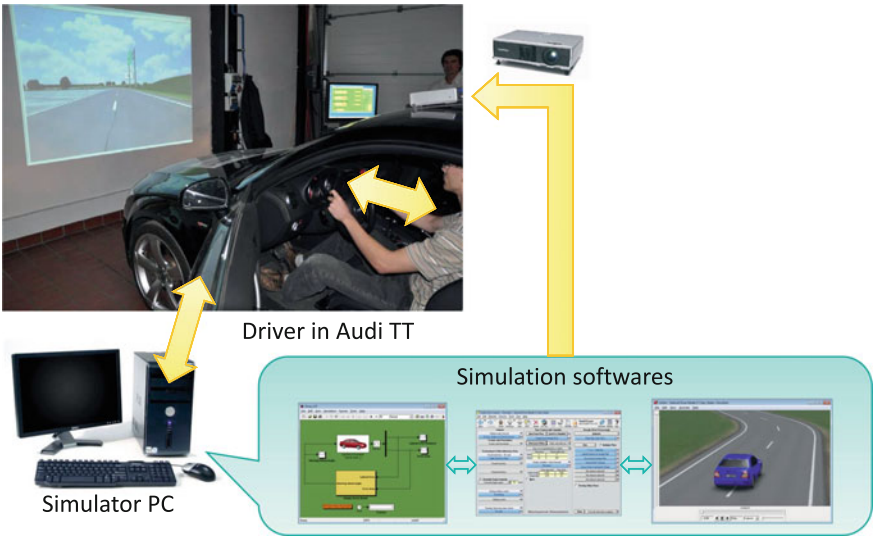

Fig. 10.10 Driver in-the-loop simulation

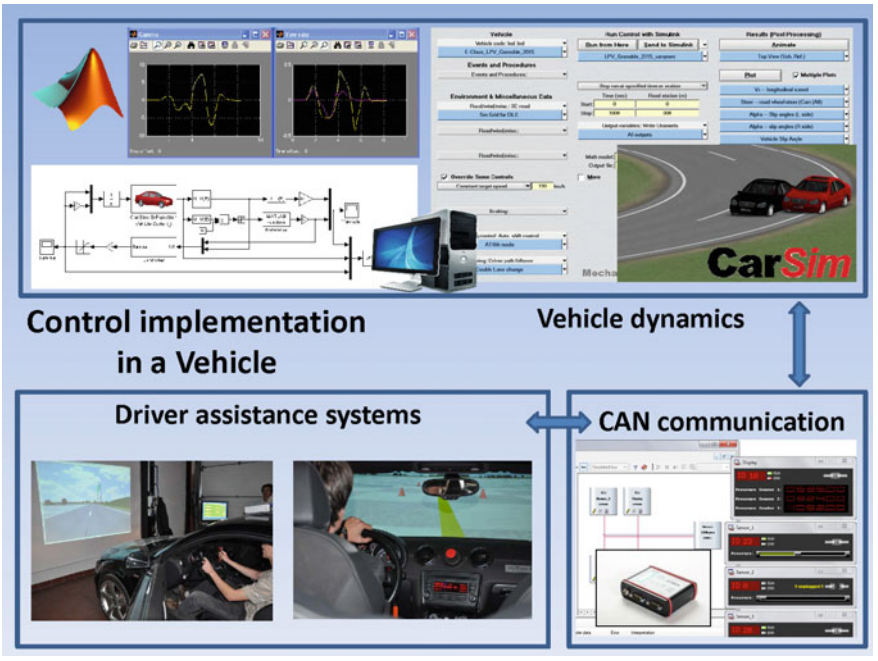

Fig. 10.11 CarSim/CAN simulation and visualization

Based on the identified models, the pole configurations of the driver behavior are analyzed. The test drivers who are traveling with different velocities are compared. Based on a detailed analysis, the activities of the different drivers can be classified and the typical drivers can be modeled, e.g., moderate, aggressive, calm.

The result can be applied in the driver-in-the-loop simulations, see Fig. 10.10.

The scheme of the CarSim-based simulation and visualization environment is illustrated in Fig. 10.11.

Appendix A
Modeling of LPV Systems

A.1 Controllability, Observability, Stabilizability

One of the main questions of system theory is to determine whether the system is controllable and/or is observable. Let us consider the state dynamic s of a controlled linear time-varying (LTV) system:

$$\dot{x}(t) = A(t)x(t) + B(t)u(t), \tag{A.1}$$

where $x(t) \in \mathscr{X} \subset \mathbb{R}^n$ is the state vector, $u(t) \in \mathbb{R}^m$ is the control input while the initial condition is $x_0 = x(t_0)$. The measured signals are obtained by a linear readout map $y(t) = C(t)x(t)$, with $y \in \mathbb{R}^p$.

A state x_0 is said to be controllable at time t_0 if there exists a control function $u(t)$ that steers the system into the origin in finite time; a state x_f is said to be reachable if the system can be steered from the origin into x_f in finite time. If the property holds for every state x and every t_0 then the system will be called controllable (reachable). The system (A.1) is called observable on a finite interval $[t_0, T]$ if any initial state x_0 at t_0 can be determined from knowledge of the system output $y(t)$ and input $u(t)$ over the given interval.

The controllability subspace is denoted by $\mathscr{C}$, while the reachability subspace by $\mathscr{R}$, respectively. For linear systems (complete) controllability and reachability are equivalent, i.e., the system is completely controllable if and only if $\mathscr{C} = \mathscr{R} = \mathscr{X}$.

Analogously $\mathscr{U}$ ($\mathscr{O}$) denotes the unobservability (observability) subspace; $\mathscr{U}$ is the set of all initial states that cannot be recognized from the output function. The system is observable if and only if $\mathscr{U} = 0$, i.e., $\mathscr{O} = \mathscr{X}$.

Our interest in such models is motivated by the fact that nonlinear dynamics can be often cast as an LTV system

$$\dot{x}(t) = A(\rho(y))x(t) + B(\rho(y))u(t) \tag{A.2}$$

P. Gáspár et al., *Robust Control Design for Active Driver Assistance Systems*,
Advances in Industrial Control, DOI 10.1007/978-3-319-46126-7

by choosing a suitable set of scheduling functions ρ that depend only on measured variables y, i.e., its values are available in operational time (qLPV systems).

A special case is when the dependence from the scheduling variables is affine, i.e.,

$$\begin{aligned} A(\rho(t)) &= A_0 + \rho_1(t)A_1 + \cdots + \rho_N(t)A_N, \\ B(\rho(t)) &= B_0 + \rho_1(t)B_1 + \cdots + \rho_N(t)B_N. \end{aligned} \tag{A.3}$$

For the sake of notational simplicity, in what follows, the time dependency of the matrices will be dropped ($A(\rho) := A(\rho(t))$) where it is possible.

Properties of some hybrid dynamics can also be analyzed in this framework: e.g., the class of linear switched systems

$$\dot{x}(t) = A(\sigma(t))x(t) + B(\sigma(t))u(t) \tag{A.4}$$

where $\sigma : \mathbb{R}^+ \to \mathbb{N}$ is a piecewise constant switching function, i.e., the matrices $A(\sigma)$ and $B(\sigma)$ are piecewise constant.

A convenient way to study all solutions of a linear equation on the interval $[\sigma, \tau]$, for all possible initial values simultaneously, is to introduce the corresponding transition matrix $\Phi(\tau, \sigma)$

$$\begin{aligned} x(\tau) &= \Phi(\tau, \sigma)x(\sigma) + \int_\sigma^\tau \Phi(\tau, t)B(t)u(t)\mathrm{d}t = \\ &= \Phi(\tau, \sigma)(x_0 + \int_\sigma^\tau \Phi(\sigma, t)B(t)u(t)\mathrm{d}t). \end{aligned}$$

Recall that $\Phi(t, t_0)$ is nonsingular and $\Phi(t, t_0) = X(t)X^{-1}(t_0)$ with

$$\dot{X}(t) = A(t)X(t), \quad X(t_0) = I, \ X(t) \in \mathbb{R}^{n\times n}.$$

Applying the time-varying coordinate change $z = \Phi(\sigma, t)x$ in the state space, the dynamic equation transforms into $\dot{z} = \Phi(\sigma, t)B(t)u(t)$. Thus in this new coordinate system controllability reduces to the solvability study of the equation $z_0 = -\int_\sigma^\tau \Phi(\sigma, t)B(t)u(t)\mathrm{d}t$ for a suitable finite τ. If we denote by $\mathscr{C}_\tau$ the set of states controllable at τ then $\mathscr{C}_\tau$ is a (closed) subspace, moreover $\mathscr{C}_{\tau_1} \subset \mathscr{C}_{\tau_2}$ for $\tau_1 < \tau_2$. Since the image space of the corresponding integral operator is finite dimensional, if the system is controllable there must be a finite $\bar{\tau} > 0$ such that $\mathscr{C}_{\bar{\tau}} = \mathbb{R}^n$.

Hence, the controllability problem of an LTV system has been reduced to the question wether the finite rank operator $\mathfrak{L} : \mathscr{L}_2([\sigma, \bar{\tau}], \mathbb{R}^m) \to \mathbb{R}^n$ defined as

$$\mathfrak{L}u = \int_\sigma^{\bar{\tau}} \Phi(\sigma, t)B(t)u(t)\mathrm{d}t$$

is onto. These types of linear operators have a nice theory: it is immediate that the adjoint operator $\mathfrak{L}^* : \mathbb{R}^n \to \mathscr{L}_2^*([\sigma, \bar{\tau}], \mathbb{R}^m)$ can be identified with $\mathfrak{L}^* x = B^*(t)\Phi^*(\sigma, t)x$ and that $\mathfrak{L}$ is onto if and only if $\mathfrak{L}\mathfrak{L}^* > 0$. So, the fundamental result Kalman (1960) concerning controllability of the LTV system (A.1) can be stated as the equivalence of the following statements:

Theorem A.1 (Kalman) *There exist a $\tau > 0$ such that*

- *the controllability Grammian $W(\sigma, \tau) = \int_\sigma^\tau \Phi(\sigma, s)B(s)B^*(s)\Phi^*(\sigma, s)\mathrm{d}s$ is positive definite;*
- *there is no nonzero vector $p \in \mathbb{R}^n$ such that $\langle p, \Phi(\sigma, t)b_i(t)\rangle = 0$, for $t \in [\sigma, \tau]$, and $i = 1, \ldots, m$.*

It is a standard result Silverman and Meadows (1967) that one can derive a rank condition that guarantees controllability while it does not involve integration and it can be obtained directly from the initial data matrices $(A(t), B(t))$:

Theorem A.2 *If (A.1) is analytic on an interval J and t is an arbitrary fixed element of J, then the system is completely controllable on every nontrivial subinterval of J if and only if*

$$\operatorname{rank}\left[B_0(t)\ B_1(t)\ \cdots\ B_k(t)\right] = n, \tag{A.5}$$

for some integer k, where

$$B_0(t) := B(t), \quad B_{i+1}(t) := A(t)B_i(t) - \frac{\mathrm{d}}{\mathrm{d}t}B_i(t). \tag{A.6}$$

If the analyticity condition is dropped, then the rank condition is only sufficient.

The problem is that it is hard to compute the rank of a time-varying matrix, and we have no information about how to compute the controllability decomposition of the system. In the framework of LTI theory the question of controllability can be decided by consulting the dimension of the reachability subspace, that can be computed easily from the initial data (A, B) of the problem, i.e.,

$$\mathscr{R} = \sum_{k=0}^{n-1} \operatorname{Im} A^k B. \tag{A.7}$$

Practically, the dimension of $\mathscr{R}$ is equal to the rank of the matrix whose columns are selected properly from those of the matrices $A^k B$, where $k = 1, \ldots, n-1$. This condition is called Kalman rank condition.

Kalman's controllability result also reveals a structural property of linear systems: namely, by applying a suitable—in general time-varying—state transformation these systems decompose into a controllable an a purely uncontrollable part. To see this, let us suppose that there are at most r vectors $p_i \in \mathscr{X}$, $\langle p_i, \Phi(\sigma, s)B(s)\rangle = 0$, $s \in$

$[\sigma, \tau]$. Chose them such that $\Pi^*\Pi = \mathrm{i}_r$, where $\Pi = [\, X^*(\sigma)p_i\,]$. Consider $n-r$ vectors $\lambda_i \in \mathscr{X}$ orthogonal on p_i, such that $\Lambda^*\Lambda = \mathrm{i}_{n-r}$, where $\Lambda = [\, X^*(\sigma)\lambda_i\,]$. Then, the time-varying matrix

$$z = Tx \quad \text{with} \quad T(t) = \begin{bmatrix} \Pi^* \\ \Lambda^* \end{bmatrix} X^{-1}(t)$$

transforms system (A.1) into the controllability decomposition form:

$$\dot{z}_1(t) = 0 \tag{A.8}$$

$$\dot{z}_2(t) = \Lambda^* X^{-1}(t) B(t) u. \tag{A.9}$$

with the uncontrollable mode $z_1(t) = \Pi^* X^{-1}(t)x(t)$ and with the completely controllable mode $z_2(t) = \Lambda^* X^{-1}(t)x(t)$. In other words, the reachable set is invariant to the action of the controlled dynamics. The notion of invariance met in this context plays a central role in the investigations of geometric systems theory and it has been proven very useful in solving a series of control problems.

For LTI systems the reachability set is a subspace and knowing this subspace one can decompose the system in a controllable and an uncontrollable part by using a state transformation that does not depend on t. Moreover, for LTI systems the different stabilizability properties are strictly related to controllability.

Controllability of Linear Affine Systems

For affine time dependency $A(t) = \sum_{i=1}^{N} \rho_i(t) A_i$ the fundamental matrix can be given, at least locally, in terms of the solutions of the Wei–Norman equation, see Wei and Norman (1964):

$$\dot{g}(t) = \Big(\sum_{i=1}^{K} e^{\Gamma_1 g_1} \cdots e^{\Gamma_{i-1} g_{i-1}} E_{ii}\Big)^{-1} \rho(t), \quad g(0) = 0. \tag{A.10}$$

Here $\rho(t) = [\rho_1(t), \ldots, \rho_N(t)]^T$ and $\{\hat{A}_1, \ldots, \hat{A}_K\}$ is a basis of the Lie algebra $\mathscr{L}(A_1, \ldots, A_N)$, the structure matrices $\Gamma_i = [\gamma^l_{i,j}]_{l,j=1,\cdots,K}$ of the algebra are given by $[\hat{A}_i, \hat{A}_j] = \sum_{l=1}^{K} \gamma^l_{i,j} \hat{A}_l$ and E_{ii} is the matrix with a single nonzero unitary entry at the ith diagonal element.

Locally, the fundamental matrix is given by the expression:

$$\Phi(t) = e^{g_1(t)\hat{A}_1} e^{g_2(t)\hat{A}_2} \cdots e^{g_n(t)\hat{A}_n}, \tag{A.11}$$

and generally it is not available in closed form. However, by exploiting the affine structure and using the Peano–Baker formula for the transition matrix one can prove the following result:

Lemma A.1 *For affine linear systems the points attainable from the origin are those from the subspace $\mathscr{R}_{(\mathscr{A},\mathscr{B})}$ given by:*

$$\mathscr{R}_{(\mathscr{A},\mathscr{B})} = \operatorname{span}\{\prod_{j=1}^{J} A_{l_j}^{i_j} B_k \mid J \geq 0,\ l_j, k \in \{0,\dots,N\},\ i_j \in \{0,\dots,n-1\}\}, \tag{A.12}$$

i.e., $\mathscr{R} \subset \mathscr{R}_{(\mathscr{A},\mathscr{B})}$.

Moreover, if one consider the finitely generated Lie algebra $\mathscr{L}(A_0,\dots,A_N)$ which contains the matrices $A_0,\dots,A_N$, and a basis $\hat{A}_1,\dots,\hat{A}_K$ of this algebra, then

$$\mathscr{R}_{(\mathscr{A},\mathscr{B})} = \sum_{l=0}^{N} \sum_{n_1=0}^{n-1} \dots \sum_{n_K=0}^{n-1} \operatorname{Im}(\hat{A}_1^{n_1} \dots \hat{A}_K^{n_K} B_l).$$

A direct consequence of this fact is that if the inclusion $\mathscr{R}_{\mathscr{A},\mathscr{B}} \subset \mathbb{R}^n$ is strict, i.e., if $\mathscr{R}_{\mathscr{A},\mathscr{B}}$ is a proper subspace, then the system (A.1) cannot be completely controllable.

The main question is that under which condition is the reachability set equal to the Lie algebra, i.e., when we have $\mathscr{R} = \mathscr{R}_{\mathscr{A},\mathscr{B}}$. In what follows, if this property holds, then the system will be called *c-excited*. Characterization of this property by using only the initial data seems to be difficult:

Theorem A.3 *A system is c-exciting if and only if the following implication holds: there exist a nonzero $\xi \in \mathbb{R}^n$ such that $B(t)^*\Phi^*(t_0,t)\xi = 0$ for all $t \in [t_0,T]$ implies that $\mathscr{R}^*_{\mathscr{A},\mathscr{B}}\Phi^*(t_0,t)\xi = 0$ for all $t \in [t_0,T]$.*

It is clear, that for c-excited systems controllability is guaranteed if the relation $\mathscr{R}_{\mathscr{A},\mathscr{B}} = \mathbb{R}^n$, i.e., the multivaraiable Kalman rank condition, holds. Moreover, if the rank condition does not hold, for this class of systems one can construct the controllability decomposition by using a time independent state transformation matrix that depends only on the matrix Lie algebra.

In Szigeti (1992) a sufficient condition for a system to be c-excited is given by the following property:

Theorem A.4 (Szigeti) *The system $\dot{x} = A(t)x + Bu$ with affine time dependency is c-persistently excited on $[t_0,T]$ if from the equalities*

$$B^* A_{i_1}^* \cdots A_{i_l}^* A(t)^* \Phi^*(t_0,t)p = 0 \tag{A.13}$$

follows

$$B^* A_{i_1}^* \cdots A_{i_l}^* A_j^* \Phi^*(t_0, t)\, p = 0, \quad j = 0, \ldots, N, \tag{A.14}$$

where p is a no nonzero vector in $\mathbb{R}^n$.

Stabilizability of Completely Controllable Linear Switched Systems

The concept of stabilizability is related to the property that there exists a state-dependent control law (closed-loop) which, starting from any initial state, asymptotically drives the system into the equilibrium (the origin). This concept expresses the requirements imposed by practical applications to an automatic control solution and it is a cornerstone of every control design algorithm.

For controlled LTI and LTV systems controllability is intimately related to stabilizability in that the former implies the later, moreover stabilizability can be achieved by applying a linear state feedback.

For general nonlinear systems, however, there is no such result. Controllability ensures that from every initial state the system can be driven to the origin in finite time by using a suitable control. It is not known, in general, whether among these controls there exists at least one which is uniformly bounded by the norm of the initial condition. If this property holds, the system is called asymptotically controllable. It turns out that asymptotic controllability is not only equivalent to stabilizability but also guarantees—under fairly mild conditions—the existence of a not too pathological feedback and control Lyapunov function, see Kellett and Teel (2004), Rifford (2002).

The zero solution of the differential inclusion $\dot{x} \in A_c(x)$ is called asymptotically weakly stable if there exists a solution $x(t)$ such that for any $\varepsilon > 0$ there is a $\delta > 0$ and $\Delta > 0$ such that if $||x(0)|| < \delta$ then $||x(t)|| < \varepsilon$ holds for all $t \geq 0$ and if $||x(0)|| < \Delta$ then $\lim_{t\to\infty} x(t) = 0$ holds.

Lemma A.2 *A completely controllable linear switching system is globally asymptotically controllable.*

It follows that a completely controllable linear switching system is globally asymptotically controllable, see Szabó (2009), i.e.,

Theorem A.5 *The completely controllable linear switching system is closed-loop stabilizable.*

Connection to the General Nonlinear Theory

Time-varying systems can be viewed as input affine nonlinear systems, by augmenting the state with the time variable as $\xi := [t,\ x^t]^T$ and rewriting the system equations as:

$$\dot{\xi} = g_0(\xi) + \sum_{i=1}^{m} g_i(\xi) u_i,$$

with $g_0(\xi) = \begin{bmatrix} 1 \\ A(t)x \end{bmatrix}$, $g_i(\xi) = \begin{bmatrix} 0 \\ B_i(t) \end{bmatrix}$, and B_i is the ith column of B.

A distribution Δ will be invariant on an open set U under the vector fields g_i if and only if $[g_i, \eta_j] = \frac{\partial \eta_j}{\partial \xi} g_i - \frac{\partial g_i}{\partial \xi} \eta_j \in \Delta(\xi)$, for all $\eta_j \in \Delta$ and $\xi \in U$, where $\eta_j,\ j = 1, \ldots dim(\Delta)$ are vector fields locally spanning Δ, see Isidori (1995).

Controllability depends on the rank of the smallest distribution that contains g and is invariant under the vector field f, given by the following algorithm: $\Delta_0 = g, \quad \Delta_{i+1} = \Delta_i + [f, \Delta_i]$ as the limiting distribution of $\Delta^* = \lim_{i \to \infty} \Delta_i$.

For the linear affine system the distribution Δ_i is spanned exactly by the vectors $B_i(t)$ given by the Silverman–Meadows algorithm.

If Δ^* is involutive, by the Frobenius theorem, one can determine the transformation that decomposes system equations in the controllability form. To do this, it is necessary to solve partial differential equations of the form $(\partial_x \lambda)\delta_j = 0$, where $\{\delta_j\}$ span the distribution Δ^*, for details see Isidori (1995).

Geometry of LTI Systems

For the details concerning the notions and propositions used in this section the interested reader is sent to Basile and Marro (2002) and Wonham (1985).

Let us consider the LTI control system

$$\dot{x} = Ax + Bu$$

with the output

$$y = Cx.$$

It is assumed that columns of the matrix $B \in \mathbb{R}^{n \times m}$ and the rows of the matrix C are linearly independent.

The set of points that lies on the same trajectory with the origin is called the reachability (controllability) subspace. Let us denote the controllability subspace of the pair (A, B) by $\mathscr{R}(A, B)$.

In the absence of control action a subspace of the state space $\mathscr{X}$ is a locus of trajectories if and only if it is an A-invariant set. The extension of this property to

the case in which the control is present and suitably used to steer the state along a convenient trajectory leads to the concept of (A, B)-controlled invariant subspace $\mathscr{V}$ defined as:

$$A\mathscr{V} \subset \mathscr{V} + \mathscr{B}, \quad \mathscr{B} = \text{Im } B.$$

The dual of a controlled invariant subspace is an $(A, C)-$*conditioned invariant* subspace $\mathscr{S}$, which is defined as:

$$A(\mathscr{S} \cap \mathscr{C}) \subset \mathscr{S}, \quad \mathscr{C} = \text{Ker } C.$$

The set of all (A, B)-controlled invariants $\mathscr{V}_{\mathscr{E}}$ contained in a given subspace $\mathscr{E}$ is an upper semilattice that admits a supremum, the maximal $(A, B)-$*controlled invariant* contained in $\mathscr{E}$, which will be denoted by $\mathscr{V}_{\mathscr{E}}^* = max\, V(A, B, \mathscr{E})$. Similarly the set of all (A, C)-conditioned invariants $\mathscr{S}_{\mathscr{D}}$ containing a given subspace $\mathscr{D}$ is a lower semilattice that admits an infimum, the minimal $(A, C)-$*conditioned invariant* containing $\mathscr{D}$, which will be denoted by $\mathscr{S}_{\mathscr{D}}^* = \min S(A, C, \mathscr{D})$. These subspaces can be determined by efficient algorithms in finite steps.

A trajectory of the pair (A, B) can be controlled on $\mathscr{E}$ if and only if its initial state belongs to a controlled invariant contained in $\mathscr{E}$, hence in $\mathscr{V}_{\mathscr{E}}$. In general, for any initial state belonging to a controlled invariant $\mathscr{V}_{\mathscr{E}}$, it is possible not only to continuously maintain the state on $\mathscr{V}_{\mathscr{E}}$ by means of a suitable control action, but also to leave $\mathscr{V}_{\mathscr{E}}$ with a trajectory on $\mathscr{E}$ and to pass to some other controlled invariant contained in $\mathscr{E}$. On the other hand, there exist controlled invariants that are closed with respect to the control, i.e., that cannot be excited by means of any trajectory on $\mathscr{E}$: these will be called self-bounded with respect to $\mathscr{E}$. An (A, B)-controlled invariant $\mathscr{V}$ contained in a subspace $\mathscr{E}$ is said to be self-bounded with respect to $\mathscr{E}$ if $\mathscr{V}_{\mathscr{E}}^* \cap \mathscr{B} \subset \mathscr{V}$.

The duals of the self-bounded controlled invariants are the self-hidden conditioned invariants: an (A, C)-conditioned invariant $\mathscr{S}$ containing a subspace $\mathscr{D}$ is said to be self-hidden with respect to $\mathscr{D}$ if $\mathscr{S} \subset \mathscr{S}_{\mathscr{D}}^* + \mathscr{C}$.

In general, however, it is not possible to reach any point of a controlled invariant from any other point (in particular, from the origin) by a trajectory completely belonging to it. In other words, given a subspace $\mathscr{E}$, by leaving the origin with trajectories belonging to $\mathscr{E}$, hence to $\mathscr{V}_{\mathscr{E}}$, (the maximal (A, B)-controlled invariant contained in $\mathscr{E}$), it is not possible to reach any point of $\mathscr{V}_{\mathscr{E}}$, but only a subspace of it, which is called the reachable set on $\mathscr{E}$ and denoted by $\mathscr{R}_{\mathscr{E}}$. It can be proved that $\mathscr{R}_{\mathscr{E}} = \mathscr{V}_{\mathscr{E}}^* \cap \mathscr{S}$ with $\mathscr{S} = \min \mathscr{S}(A, \mathscr{E}, \mathscr{B})$.

Let us denote by $\mathscr{V}^* = \max \mathscr{V}(A, B, \mathscr{C})$ the maximal (A, B)-controlled invariant subspace contained in $\mathscr{C}$ and by $\mathscr{S}_* = \min \mathscr{S}(A, C, \mathscr{B})$ the minimal (A, C)-conditioned invariant subspace containing $\mathscr{B}$.

Theorem A.6 (Four Map Theorem) *Let us consider the state transformation*

$$\xi = T^{-1}x, \quad \textit{defined by} \quad T = \begin{bmatrix} T_1 & T_2 & T_3 & T_4 \end{bmatrix},$$

with Im $T_1 = \mathscr{V}^* \cap \mathscr{S}_*$ *and* Im $[T_1\, T_2] = \mathscr{V}^*$, Im $[T_1\, T_3] = \mathscr{S}_*$. *Then*

$$T^{-1}AT = \begin{bmatrix} A_{11} & A_{12} & A_{13} & A_{14} \\ 0 & A_{22} & A_{23} & A_{24} \\ A_{31} & A_{32} & A_{33} & A_{34} \\ 0 & 0 & A_{43} & A_{44} \end{bmatrix} \quad T^{-1}B = \begin{bmatrix} B_1 \\ 0 \\ B_3 \\ 0 \end{bmatrix} \quad CT = \begin{bmatrix} 0\, 0\, C_3\, C_4 \end{bmatrix},$$

where $A_{23} = \bar{A}_{23}C_3$ *and* $A_{43} = \bar{A}_{43}C_3$. *Moreover by a suitable feedback* A_{31} *and* A_{32} *can be zeroed out.*

When (A, C) is not observable (reconstructable), the initial or final state can be determined modulo the subspace Ker $\Psi_{(A,B,C)} = \mathscr{Q}$, where $\mathscr{Q}$ denotes the maximal $A-$invariant subspace contained in $\mathscr{C}$, which is called unobservability subspace (unreconstructability subspace). This means that the state canonical projection on $\mathscr{X}/\mathscr{Q}$ can be determined from the output function. $\mathscr{Q}$ is the locus of the free motions corresponding to the output function identically zero. A dynamical system is completely unknown-input state observable by means of differentiators if it is possible to determine its state x when an arbitrary short output segment y is given.

The subspace of unknown input state observability by means of differentiators is

$$\min \mathscr{S}(A^T, \text{Ker } B^T, \text{Im } C^T) = \max \mathscr{V}^{\perp}(A, B, C)$$

and the subspace of functional input observability is $B^T \min \mathscr{S}(A^T, \text{Ker } B^T, \text{Im } C^T)$. The orthogonal projection of the state on the subspace $\mathscr{V}^{*,\perp}$ can be deduced from the output and from its derivatives, moreover this is the greatest subspace where the orthogonal projection of the state can be recognized solely from the output. If the state is known the orthogonal projection of the input can be determined on $B^T\mathscr{V}^{*,\perp}$ and it cannot be recognized a greater subspace (it can be determined modulo $B^{-1,T}\mathscr{V}^*$).

The term system invertibility denotes the possibility of reconstructing the input from the output function. Assume that B has maximal rank. The system (A, B, C) with $x(0) = 0$ is said to be invertible (left-invertible) if, given any output function $y(t)$ defined on $[0, t_1]$, $t_1 > 0$ belonging to Im $\Phi^0_{(A,B,C)}$, there exists a unique input function $u(t)$ such that $\Phi^0_{(A,B,C)}u(t) = y(t)$ holds, i.e., Ker $T^0_{(A,B,C)} = 0$.

The triple (A, B, C), with B having maximal rank, is unknown-state (zero-state) invertible if and only if it is unknown-state, unknown-input (zero-state, unknown-input) completely reconstructable.

A dynamic system exists which, connected to the system output and with initial state suitably set as a linear function of the system state (which is assumed to be known), provides tracking of the system state modulo $\mathscr{S}_*$. This system is not necessarily stable. The observer equations, expressed in the basis that corresponds to the transformation $T = [T_1\, T_2]$, with Im $T_1 = \mathscr{S}_*$, can be written as:

$$\begin{bmatrix} \dot{\eta}_1 \\ \dot{\eta}_2 \end{bmatrix} = \begin{bmatrix} A_{11} & A_{12} \\ 0 & A_{22} \end{bmatrix} \begin{bmatrix} \eta_1 \\ \eta_2 \end{bmatrix} + \begin{bmatrix} B_1 \\ 0 \end{bmatrix} u + \begin{bmatrix} G1 \\ G_2 \end{bmatrix} y,$$

where G is such that $(A + GC)\mathscr{S}_* \subset \mathscr{S}_*$. If the observer initial state is set according to $\eta(0) = T^{-1}x(0)$ a state estimate modulo $\mathscr{S}_*$ is derived.

An algebraic reconstructor with differentiators provides as output a state estimate z_1 modulo $\mathscr{V}^*$ and works if neither the initial state nor the input function is known, while the dynamic tracking device provides as z_2 a state estimate modulo $\mathscr{S}_*$, but requires the initial state to be known. A state estimate modulo $\mathscr{V}^* \cap \mathscr{S}_*$ is obtained as a linear function of the outputs of both devices, i.e., $z = Mz_1 + Nz_2$. This state reconstructor provides the maximal information on the system state when the input function is unknown and the initial state known, by observing the output in any nonzero time interval.

The term functional controllability (right invertibility) denotes the possibility of imposing any sufficiently smooth (piecewise differentiable at least n times) output function by a suitable input function, starting at the zero state.

For multi input single output (MISO) systems a formal definition can be given as:

Definition A.1 Assume that C has maximal rank. The system (A, B, C) is said to be functionally controllable (right-invertible) if there exists an integer $\rho \geq 1$ such that, given any output function y with ρth derivative piecewise continuous and such that $y(0) = 0, \cdots y^{(\rho)}(0) = 0$, there exists at least one input function u such that $\Phi^0_{(A,B,C)}u = y$ holds. The minimum value of ρ satisfying the above statement is called the relative degree of the system.

In order to define the relative degree for MIMO systems in geometric terms the following extension of functional output controllability is introduced:

Definition A.2 (*Constrained Functional Output Controllability*) A subspace $\mathscr{Y}^{(h)}$ is said to be a functional output controllability subspace with respect to the hth derivative if the output of the triple (A, B, C) can be driven along any trajectory y such that $y \in \mathscr{Y}^{(h)}$ with the hth derivative piecewise continuous.

This is possible exactly when there exist an (A, B)-controlled invariant subspace $\mathscr{V}$ such that $\mathscr{Y}^{(h)} = C\mathscr{V}$. Let us consider $\mathscr{E} = C^{-1}\mathscr{Y}^{(h)}$ and $\mathscr{V}^{(h)}_{\mathscr{E}}$, the maximal (A, B)-controlled invariant subspace contained in $\mathscr{E}$ such that the output can be driven on $C\mathscr{V}^{(h)}_{\mathscr{E}}$ along any trajectory y with piecewise continuous hth derivative for all the initial states $x(0) \in \mathscr{V}^{(h)}_{\mathscr{E}}$.

The multivariable relative degree ρ_i of output y_i is defined as $\rho_i = h$ (if exists), where $\mathscr{Y}^{(h)} = C\mathscr{V}^{(h)}_{\mathscr{E}}$ assuming that $\mathscr{Y}^{(h)} = \{y \mid y_k = 0,\ k \neq i\}$.

The functional controller is realizable in exactly the same way as the (left) inverse system, i.e., by a state reconstructor completed with a further differentiator stage and an algebraic part. Its dynamic part is asymptotically stable if and only if all the invariant zeros of (A, B, C) are stable. In this case, however, the input u corresponding to the desired output is not unique, in general. The difference between any two admissible input corresponds to a zero-state motion on $R_{\mathscr{V}^*} = \mathscr{V}^* \cap \mathscr{S}_*$ which does not affect the output, so that the functional controller can be realized to provide any one of the admissible inputs, for instance by setting to zero input components which, expressed in a suitable basis, correspond to forcing actions belonging to $\mathscr{V}^* \cap \mathrm{Im}B$.

Left and right invertibility can be characterized in geometric terms as follows:

Theorem A.7 *Triple* (A, B, C) *is left-invertible if and only if*

$$\mathscr{V}^* \cap \mathscr{B} = 0.$$

Condition of left-invertibility is equivalent to $\mathscr{V}^* \cap \mathscr{S}_* = 0$.

Theorem A.8 *Let* $\mathscr{C} := \operatorname{Ker} C$. *Triple* (A, B, C) *is right-invertible if and only if*

$$\mathscr{S}_* + \mathscr{C} = X.$$

Condition of right-invertibility is equivalent to $\mathscr{V}^* + \mathscr{S}_* = X$.

A.2 Parameter-Varying Invariant Subspaces

For LTI systems the concept of certain invariant subspaces and the corresponding global decompositions of the state equations induced by these invariant subspaces was one of the main thrusts for the development of geometric methods for the solution of a series of relevant problems, see Wonham (1985). Nonlinear systems can be studied using tools from differential geometry, when the central role is played by the concept of invariant distributions. From the geometric viewpoint results of classical linear control can be seen as special cases of more general nonlinear results, for details see Isidori (1995) and Nijmeijer and van der Schaft (1991). Due to the computational complexity involved, these general nonlinear methods have limited applicability in practice.

In order to extend the classical geometric tools used to describe detection filters for LTI systems, consider first the following linear time-varying (LTV) system:

$$\dot{x}(t) = A(t)x(t) + B(t)v(t) \tag{A.15}$$

$$y(t) = Cx(t), \tag{A.16}$$

where $x(t) \in \mathscr{X} \subset \mathbb{R}^n$, $x_0 = x(t_0)$, $u(t) \in \mathbb{R}^m$ and $y(t) \in \mathbb{R}^p$. Special instances of LTV systems are LPV, when the state space matrices depend on time-varying parameters, e.g., $A(t) = A(\rho(t))$. Considering constant C does not restrict generality since by a suitable state transform one can always obtain the desired form.

Restricting the investigations to linear subspaces, as special instances of distributions, then a subspace $\mathscr{V}$ of $\mathbb{R}^n$ will be an invariant distribution for system (A.15) if and only if $A(\rho(t))\mathscr{V} \subset \mathscr{V}$ for all $t \in \mathscr{I}$, where $\mathscr{I}$ is an interval on which the solutions are defined.

This fact motivates the introduction of the following notion for LPV systems: a subspace $\mathscr{V}$ is called parameter-varying invariant subspace for the family of the linear maps $A(\rho)$ (or shortly $\mathscr{A}$-invariant subspace) if

$$A(\rho)\mathscr{V} \subset \mathscr{V} \quad \text{for all } \rho \in \mathscr{P}, \text{ i.e., for all } t \in \mathscr{I}. \tag{A.17}$$

Analogously, let $\mathscr{B}(\rho)$ denote Im $B(\rho)$. Then a subspace $\mathscr{V}$ is called a parameter-varying (A,B)-invariant subspace (or shortly $(\mathscr{A}, \mathscr{B})$-invariant subspace) if for all $\rho \in \mathscr{P}$ either of the following equivalent conditions holds:

$$A(\rho)\mathscr{V} \subset \mathscr{V} + \mathscr{B}(\rho); \tag{A.18}$$

there exists a mapping $F \circ \rho : [0, T] \to \mathbb{R}^{m \times n}$ such that:

$$(A(\rho) + B(\rho)F(\rho))\mathscr{V} \subset \mathscr{V}. \tag{A.19}$$

The dual notion is the following: let $\mathscr{C}(\rho)$ denote Ker $C(\rho)$. Then a subspace $\mathscr{W}$ is called a parameter-varying (C,A)-invariant subspace (or shortly $(\mathscr{C}, \mathscr{A})$-invariant subspace) if for all $\rho \in \mathscr{P}$ either of the following equivalent conditions holds:

$$A(\rho)(\mathscr{W} \cap \mathscr{C}(\rho)) \subset \mathscr{W}; \tag{A.20}$$

there exists a mapping $G \circ \rho : [0, T] \to \mathbb{R}^{n \times p}$ such that:

$$(A(\rho) + G(\rho)C(\rho))\mathscr{W} \subset \mathscr{W}. \tag{A.21}$$

These definitions are suitable for qLPV systems, too.

Let us denote the maximal $\mathscr{A}$-invariant subspace contained in a constant subspace $\mathscr{K}$ by $\langle \mathscr{K} | A(\rho) \rangle$.

For the LPV case (with constant B matrix) one can get the following definition for the controllability subspace: a subspace $\mathscr{R}$ is called parameter-varying controllability subspace if there exists a constant matrix K and a parameter-varying matrix $F : [0, T] \to \mathbb{R}^{m \times n}$ such that

$$\mathscr{R} = \langle \mathscr{A} + B\mathscr{F} | \text{Im } BK \rangle, \tag{A.22}$$

where $\mathscr{A} + B\mathscr{F}$ denotes the system $A(\rho) + BF(\rho)$.

As in the classical case, it can be seen that the family of controllability subspaces contained in a given subspace $\mathscr{K}$ is closed under subspace addition. Hence this family has a maximal element $\mathscr{R}^*$. The dual notion of parameter-varying controllability subspace is the following: a subspace $\mathscr{S}$ is called an unobservability subspace associated to an LPV system if there exists a constant matrix H and a parameter-varying matrix $G : \mathscr{P} \to \mathbb{R}^{n \times p}$ such that

$$\mathscr{S} = \langle \text{Ker } HC | A(\rho) + G(\rho)C \rangle. \tag{A.23}$$

The family of unobservability subspaces associated to an LPV system containing a given subspace $\mathscr{L}$ is closed under subspace intersection. This family has a minimal element denoted by $\mathscr{S}^*$.

From a practical point of view it is an important question to characterize these subspaces associated to an LPV system by a finite number of conditions. A series of efficient algorithms were derived for the computation of these subspaces, for detail see Balas et al. (2003).

If certain conditions are fulfilled, e.g., if the parameter functions are differential algebraically independent, then the parameter-invariant subspaces defined above coincide with the corresponding invariant distribution or codistribution, respectively. However, to give sufficient conditions for the solution of certain state feedback and observer filter design problems it is enough that some decompositions of the state equations could be performed. The parameter-varying versions of these invariant spaces are suitable objects to define the required decompositions, therefore they can play the same role in the solution of the fundamental problems, such as disturbance decoupling, unknown input observer design, fault detection (FPRG), as their counterparts in the time-invariant context.

Computational Algorithms

Let Δ be a distribution defined on an open set U. We are interested in finding the smallest distribution, which is invariant under given vector fields $(\tau_1, \ldots, \tau_q)$ and which is denoted by the symbol $\langle \tau_1, \ldots, \tau_q | \, \Delta \rangle$. Given a distribution Δ and a set $\tau_1, \ldots, \tau_q$ of vector fields we define the nondecreasing sequence of distributions:

$$\Delta_0 = \Delta, \quad \Delta_k = \Delta_{k-1} + \sum_{i=1}^{q} [\tau_i, \Delta_{k-1}], \tag{A.24}$$

i.e., for all k one has that $\Delta_k \subset \langle \tau_1, \ldots, \tau_k | \, \Delta \rangle$. If there exists an integer k^* such that $\Delta_{k^*} = \Delta_{k^*+1}$ then $\Delta_{k^*} = \langle \tau_1, \ldots, \tau_k | \, \Delta \rangle$.

Let Ω be a codistribution defined on an open set U and we are interested in finding the smallest codistribution, which is invariant under the given vector fields $(\tau_1, \ldots, \tau_q)$ and which is denoted by the symbol $\langle \tau_1, \ldots, \tau_q | \, \Omega \rangle$. Given a codistribution Ω and a set $\tau_1, \ldots, \tau_q$ of vector fields we define the dual version, i.e.,

$$\Omega_0 = \Omega, \quad \Omega_k = \Omega_{k-1} + \sum_{i=1}^{q} L_{\tau_i} \Omega_{k-1}. \tag{A.25}$$

Then for all k one has $\Omega_k \subset \langle \tau_1, \ldots, \tau_k | \, \Omega \rangle$ while $\Omega_{k^*} = \langle \tau_1, \ldots, \tau_k | \, \Omega \rangle$ provided that there exists an integer k^* such that $\Omega_{k^*} = \Omega_{k^*+1}$.

In the special case of LTI systems the algorithm (A.24) ends up with the well-known controllable subspace of the system:

$$\Delta_{n-1}(x) = \mathrm{Im}\,[B \;\; AB \;\; \ldots \;\; A^{n-1}B], \qquad x \in \mathbb{R}^n$$

Considering the dual case let Ω_0 be the codistribution spanned by the row vectors $c_1, \ldots, c_p$ of C, the algorithm (A.25) ends up with the subspace:

$$\Omega_{n-1}(x) = \text{Im } (C^T \; A^T C^T \; \ldots \; (A^T)^{n-1} C^T).$$

By duality $\Omega_{n-1}^{\perp}(x)$ is the largest distribution invariant under the vector field f_A and contained in the distribution $\Omega_0^{\perp}(x)$. Moreover, by construction, at each $x \in \mathbb{R}^n$,

$$\Omega_0^{\perp}(x) = \text{Ker } C, \quad \Omega_{n-1}^{\perp}(x) = \text{Ker} \begin{bmatrix} C \\ CA \\ \vdots \\ CA^{n-1} \end{bmatrix}.$$

As far as affine LPV systems are concerned, denoting by $\tau_i(x) = A_i x, \; i = 0, 1, \ldots, m$ one can get

$$\Delta_k = \Delta_{k-1} + \sum_{i=0}^{m} A_i \Delta_{k-1}$$

yielding

$$\Delta_{n-1} = \sum_{l=0}^{n-1} \sum_{j_i \in \{0,\ldots,m\},\; i=1,\ldots,l} A_{j_1} \ldots A_{j_l} \Delta$$

where the algorithm was initialized at a constant distribution Δ.

Starting from the constant codistribution $\Omega_0 = \tilde{\text{Im}}\, C = \text{Im } C^T$, one has

$$\Omega_k = \Omega_{k-1} + \sum_{i=0}^{m} \Omega_{k-1} A_i.$$

Let $p_1(x), \ldots, p_d(x)$ be a set of smooth vector fields defined on an open set U, set $P = \text{span}\{p_1, \ldots, p_d\}$ and consider the nondecreasing sequence of distributions defined as follows:

$$S_0 = \overline{P}, \quad S_k = \overline{S}_{k-1} + \sum_{i=0}^{m} [g_i, \overline{S}_{k-1} \cap \text{Ker } \mathrm{d}h\}],$$

where $\overline{S}$ denotes the involutive closure of S.

Suppose there exists an integer k^* such that $S_{k^*+1} = \overline{S}_{k^*}$ and set $\Sigma_*^P = \overline{S}_{k^*}$. Then Σ_*^P is the minimal conditioned invariant and involutive distribution containing P. This algorithm is called termed as conditioned invariant distribution algorithm.

By setting

$$g_0(x) = Ax, \quad g_1(x) = B, \quad h(x) = Cx$$

one has

$$[g_0, \overline{S}_{k-1} \cap \text{Ker } C](x) = A(S_{k-1} \cap \text{Ker } C),$$

thus one can obtain the well-known (C, A)-invariant subspace algorithm for LTI systems:

$$S_0 = \mathscr{P}, \quad S_k = S_{k-1} + A(S_{k-1} \cap \text{Ker } C).$$

For affine LPV systems, i.e., $g_i(x) = A_i x$ it follows that:

$$S_0 = \mathscr{P}, \quad S_k = S_{k-1} + \sum_{i=0}^{m} A_i(S_{k-1} \cap \text{Ker } C).$$

Using the augmented state space $\xi = [t, x]^T$ one can obtain the algorithm

$$S_0(\xi) = \mathscr{P}, \quad S_k(\xi) = S_{k-1}(\xi) + \left(\frac{\partial}{\partial \text{t}} - A(\pi(t))\right)(S_{k-1}(\xi) \cap \text{Ker } C),$$

for a linear time-varying dynamics, a readout map with constant C matrix and a constant distribution $\mathscr{P}$.

The dual is the controlled invariant distribution algorithm which is defined via codistributions:

$$\Omega_0 = \text{span}dh, \quad \Omega_k = \Omega_{k-1} + \sum_{i=0}^{m} L_{g_i}(\Omega_{k-1} \cap G^{\perp}). \tag{A.26}$$

Suppose there exists an integer k^* such that $\Omega_{k^*+1} = \Omega_{k^*}$. Then $\Omega_k = \Omega_{k^*}$, for all $k > k^*$ and if $\Omega_{k^*} \cap G^{\perp}$ and $\Omega_{k^*}^{\perp}$ are smooth, then $\Omega_{k^*}^{\perp}$ is the maximal controlled invariant smooth distribution contained in Ker dh.

Considering LTI systems, the algorithm

$$\Omega_0 = \tilde{\text{Im}}\ C = \text{Im } C^T, \quad \Omega_k = \Omega_{k-1} + (\Omega_{k-1} \cap \text{Ker } B^T)A,$$

ends up in the minimal (B^T, A^T)-invariant subspace over Im C^T so its dual is the maximal (A, B)-invariant subspace in Ker C.

The derivation of the time-dependent form (in the augmented state space) of the controlled invariant distribution algorithm (A.26) will end up in

$$\tilde{\Omega}_{k+1}(\xi) = \text{span}\{\text{d}h\} + (\tilde{\Omega}_k \cap \mathscr{B}^{\perp})A(\rho),$$

provided that there exists k^* such that $\Omega_{k^*+1} = \Omega_{k*}$. Then $\tilde{\Omega}_{k*}^{\perp}$ will be the maximal controlled invariant distribution in Ker $\{\text{d}h\}$ which contains $G = \text{span}\{g_1, \ldots, g_m\}$. Considering constant codistributions in each step we get

$$\tilde{\Omega}_{k+1} = \text{span}\{\text{d}h\} + \sum_{i=0}^{N} (\tilde{\Omega}_k \cap \mathscr{B}^{\perp}) A_i.$$

Let Θ be a fixed codistribution and define the nondecreasing sequence of codistributions as:

$$Q_0 = \Theta \cap \text{spand}h, \quad Q_{k+1} = \Theta \cap \left(\sum_{i=0}^{m} L_{g_i} Q_k + \text{spand}h \right). \tag{A.27}$$

Suppose that all the codistributions of this sequence are nonsingular, i.e., there exists an integer $k^* \leq n-1$ such that $Q_k = Q_{k^*}$ for all $k > k^*$, set $\Omega^* = Q_{k^*}$ and use the notation $\Omega^* = \text{o.c.a.}(\Theta)$ where o.c.a. stands for observability codistribution algorithm. Then

$$Q_0 = \Omega^* \cap \text{spand}h\}, \quad Q_{k+1} = \Omega^* \cap \left(\sum_{i=0}^{m} L_{g_i} Q_k + \text{spand}h \right).$$

provided that all the codistributions generated by the observability codistribution algorithm are nonsingular. As a consequence $\text{o.c.a.}(\Omega^*) = \Omega^*$ and if Θ is conditioned invariant, so is the codistribution Ω^*.

Ω is said to be a observability codistribution if fulfills the relations:

$$L_{g_i} \Omega \subset \Omega + \text{spand}h, \quad i = 0, 1 \ldots m, \quad \text{o.c.a.}(\Omega) = \Omega.$$

The distribution Δ is called unobservability distribution if its annihilator $\Omega = \Delta^{\perp}$ is an observability codistribution. If the algorithm (A.27) is initialized at $(\Sigma_*^P)^{\perp}$, then $\text{o.c.a.}((\Sigma_*^P)^{\perp})$ is an observability codistribution contained in $\mathscr{P}^{\perp}$. Moreover, it is the largest codistribution having this property.

Let us consider the nonlinear system

$$\dot{x} = A_0 x + \sum_{i=1}^{m} u_i A_i x + l(x) m + \sum_{i=1}^{d} p_i(x) w_i, \quad y = Cx$$

with the assumption that $\mathscr{P} = \text{span}\ \{p_1, \ldots, p_d\}$ is independent of x. Then the observability codistribution algorithm will be read as:

$$Q_0 = \Theta \cap \tilde{\text{Im}}\, C, \quad Q_{k+1} = \Theta \cap \left(\sum_{i=0}^{m} Q_k A_i + \tilde{\text{Im}}\, C \right). \tag{A.28}$$

A.3 Identifiability

Identifiability is a fundamental prerequisite for model identification and it concerns the uniqueness of the model parameters determined from input–output data, under ideal conditions of noise-free measurements and error-free model structure. Identifiability analysis requires one to solve systems of highly nonlinear algebraic equations, the analysis tool being mainly differential algebraic. For details about identifiability, see, e.g., Ljung and Glad (1994); Saccomani et al. (2003) and the references cited therein.

From a practical point of view we can state that a necessary condition for identifiability is that the system representation should be minimal, i.e., (algebraically) observable and controllable. For the decisive role of controllability, see Saccomani et al. (2003).

Let $y = \Phi_{x_0}(u, p)$ be the input–output map of the nonlinear input affine system depending on a vector parameter p:

$$\begin{aligned} \dot{x} &= f(x, p) + g(x, p)u \\ y &= h(u, x, p) \end{aligned} \tag{A.29}$$

started from the initial state $x(0) = x_0$. Then, the parameter p^* is said to be a priori globally identifiable from input–output data if there exists at least one input function u in such a way that the equation $\Phi_{x_0}(u, p) = \Phi_{x_0}(u, p^*)$ has only one solution, i.e., $p = p^*$, for all initial states x_0. A weaker notion is that of the local identifiability, when uniqueness holds only in a neighborhood of p^*.

The solution of the system, i.e., the map Φ usually is not available. However, in some cases, an implicit input–output map, i.e., a relation $\Psi(y, u, p) = 0$ can be determined from the system equations. Since we examine identification in the context of (q)LPV systems, in what follows, the main steps of the identifiability test will be sketched.

Let us consider an LTV system

$$\begin{aligned} \dot{x} &= A(t)x + B(t)u \\ y &= C(t)x, \end{aligned} \tag{A.30}$$

and let us denote it by $\tilde{y} := [\, y \ \dots \ y^{(n-1)} \,]^T$. Then, one has the equation

$$\tilde{y} = \Omega(t)x + \Gamma(t)\tilde{U} \tag{A.31}$$

where $\Omega^T(t) = [\, C_0^T(t) \cdots C_{n-1}^T(t) \,]$ with

$$\begin{aligned} C_0(t) &:= C(t), \\ C_{i+1}(t) &:= C_i(t)A(t) + \frac{d}{dt}C_i(t). \end{aligned} \tag{A.32}$$

Let us denote it by γ^k the row vector defined as:

$$\begin{aligned} \gamma_0^{k+1} &= \gamma_0^k + C_k, \\ \gamma_j^{k+1} &= \gamma_j^k + \dot{\gamma}_{j-1}^k, \quad j = k, \ldots, 1 \\ \gamma_j^k &= 0, \quad j \geq k. \end{aligned} \tag{A.33}$$

Then $\Gamma(t)$ has as rows the vectors γ_k, $k = 0, \ldots n-1$. Let us denote by $U(t) = B(t)u$ and by $\tilde{U} := [\, U \ \cdots \ U^{(n-1)} \,]^T$.

If system (A.30) is analytic on an interval $\mathscr{I}$ and t is an arbitrary fixed element of $\mathscr{I}$, then (A.30) is completely observable on every nontrivial subinterval of $\mathscr{I}$ if and only if rank $\Omega(t) = n$, i.e., one can solve Eq. (A.31) for the state x. It follows that

$$y^{(n)} - C_n(p)\Omega^{\#}(p)\tilde{y} = (\gamma^n(p) - C_n(p)\Omega^{\#}(p)\Gamma(p))\tilde{U}(p), \tag{A.34}$$

where $\Omega^{\#}(p)$ is a generalized inverse of $\Omega(p)$. This equation gives us the implicit map $\Psi(y, u, p) = 0$, with initial conditions given by

$$\tilde{y}(0) = \Omega(0)x(0) + \Gamma(0)\tilde{U}(0). \tag{A.35}$$

Equations (A.34) and (A.35) are usually highly nonlinear in the parameters p, however, they can be re-parametrized using as new parameters the functions $\Pi := [\pi_l(p, x_0)]$. In terms of the new parameters one has a linear equation of the form:

$$\Psi_1(u, y) + \Pi(p, x_0)\Psi_2(u, y) = 0. \tag{A.36}$$

If the map $(p, x_0) \to \Pi(p, x_0)$ is injective, i.e., can be solved uniquely for (p, x_0), then the system is identifiable.

In Ljung and Glad in relation (A.36) the map Π is the identity map. In the identification context that involves mechanical problems the parameter dependence of the state matrices is usually nonlinear, so, in general a simple form for this map cannot be expected.

The input output pairs for which (A.36) can be solved, i.e., such that $\Psi_2(u, y)$ is of full rank, can be called as "persistently exciting" pairs, see Stoica (1989). If the initial condition x_0 is known, then the map $\Pi(p)$ is required to be injective for identifiability. In the setting of discrete time system identification, some of the authors consider systems given already in the discrete variant of (A.34), for details see Bamieh and Giarre (2000, 2002); Bokor and Keviczky (1987) for the continuous-time case see e.g., Kowalczuk and Kozlowski (2000); Soderstrom et al. (1997).

A.4 The Role of the Sampling Time

Finding the unknown parameters usually involves the application of an optimization process that contains some iterations, requiring the solution of certain differential equations, for an overview see Polak (1997). Although we embed the system in the class of (q)LPV systems, in general, we cannot exploit the linear structure in the solution process, and we have to use a general differential equation solver. Recall, that the method that solves a differential equation is a numerical algorithm, which performs an implicit discretization of the system. Sometimes they are implicit schemes with variable step length.

Moreover, since the values of $\rho(t), u(t)$ and $y(t)$ are only available at discrete time instances determined by the sampling period, the original (q)LPV system is embedded in the class of (q)LPV systems that operate on the set of piecewise constant functions. In order to assure that this class is sufficiently close to the original system, one has to impose conditions on the sampling time τ, i.e., it must be sufficiently small. What "sufficiently" means in this context, depends heavily on the differential equation that has to be solved in the identification process.

It is known from the literature that for a certain class of differential equations, i.e., for stiff equations, this condition might be quite stringent, leading to unacceptable small values of the sampling time. The numerical methods designed for this class are quite involved, see Hairer and Wanner (1996), and usually uses a variable step length. This fact causes inherent difficulties in the parameter identification process, i.e., for stiff differential equations the error committed might make impossible the solution of the problem for a given, practically reliable, sampling time.

In the context of optimal control the same problem arises. A feedback law which globally stabilizes a given system in the absence of quantization will in general fail to provide global asymptotic stability of the closed loop system that arises in the presence of state quantization, for details see, e.g., Liberzon (2003). For the observer design of the LTI system the effect of quantization is shown e.g., in Sur and Paden (1998).

Example: Quarter Car, Sprung Mass Estimation

The aim of this demonstration example is to illustrate the identification of the sprung mass m_s of a vehicle by using a quarter car suspension model. At first glance its identification, even from input–output data, seems to be almost trivial. However, due to the inherent nonlinearity of the system, the problem can be really hard from an implementation point of view.

The state space representation of the nonlinear model is:

$$\begin{pmatrix}\dot{x}_1\\ \dot{x}_2\\ \dot{x}_3\\ \dot{x}_4\end{pmatrix} = \begin{pmatrix} 0 & 0 & 1 & 0\\ 0 & 0 & 0 & 1\\ -\frac{k_s^l}{m_s} & \frac{k_s^l}{m_s} & \frac{b_s^l}{m_s} & \frac{b_s^l}{m_s}\\ \frac{k_s^l}{m_u} & -\frac{k_s^l}{m_u} - \frac{k_t}{m_u} & \frac{b_s^l}{m_u} & \frac{b_s^l}{m_u}\end{pmatrix}\begin{pmatrix}x_1\\ x_2\\ x_3\\ x_4\end{pmatrix} +$$
$$+\begin{pmatrix} 0 & 0 & 0\\ 0 & 0 & 0\\ \frac{k_s^{nl}}{m_s} & -\frac{b_s^{sym}}{m_s} & \frac{b_s^{nl}}{m_s}\\ -\frac{k_s^{nl}}{m_s} & \frac{b_s^{sym}}{m_s} & -\frac{b_s^{nl}}{m_s}\end{pmatrix}\begin{pmatrix}\rho_k^3\\ |\rho_b|\\ \sqrt{|\rho_b|}\,\mathrm{sgn}(\rho_b)\end{pmatrix} + \begin{pmatrix}0\\ 0\\ 0\\ \frac{k_t}{m_u}\end{pmatrix} w,$$

see Fig. 2.9 and Sect. 2.5.

The measured outputs are

$$y_1 = x_2 - x_1, \quad y_2 = x_4 - x_3$$

and they can be also selected as scheduling parameters, i.e., $\rho_b = y_2$ and $\rho_k = y_1$. Let us denote by $\phi(\rho_k, \rho_b)$ the column vector

$$\phi(\rho_k, \rho_b) = \begin{bmatrix}\rho_k^3 & |\rho_b| & \sqrt{|\rho_b|}\,\mathrm{sgn}(\rho_b)\end{bmatrix}^T.$$

If one considers $\phi(\rho_k, \rho_b)$ as a fictitious input and denotes by $\mu = m_u/m_s$, the state space equations of the qLPV model can be written as:

$$\dot{x} = \begin{pmatrix} 0 & 0 & 1 & 0\\ 0 & 0 & 0 & 1\\ -\mu\pi_1 & \mu\pi_1 & -\mu\pi_2 & \mu\pi_2\\ \pi_1 & -\pi_1 - \pi_t & \pi_2 & -\pi_2\end{pmatrix} x +$$
$$+\begin{pmatrix} 0 & 0 & 0\\ 0 & 0 & 0\\ \mu\pi_3 & -\mu\pi_4 & \mu\pi_5\\ -\pi_3 & \pi_4 & -\pi_5\end{pmatrix}\phi(\rho_k, \rho_b) + \begin{pmatrix}0\\ 0\\ 0\\ \pi_t\end{pmatrix} w$$

where

$$\pi := [\pi_1\ \pi_2\ \pi_3\ \pi_4\ \pi_5] = [\frac{k_s^l}{m_u}\ \frac{b_s^l}{m_u}\ \frac{k_s^{nl}}{m_u}\ \frac{b_s^{sym}}{m_u}\ \frac{b_s^{nl}}{m_u}],$$

and $\pi_t = \frac{k_t}{m_u}$ are known parameters. Since the value of m_s may vary, the parameter μ is considered to be unknown.

Let us denote by

$$\Lambda(y) = \pi_1 y_1 + \pi_2 y_2 + [\pi_3\ -\pi_4\ \pi_5]\phi(y).$$

Then the identifiability analysis leads to the following input–output map that corresponds to relation (A.34):

$$y_2^{(3)} + (1+\mu)\Lambda^{(2)}(y) + \pi_t y_2^{(2)} + \mu\pi_t \Lambda(y) - \pi_t w^{(2)} = 0.$$

Equation (A.36) can be obtained by successive derivation of this relation, obtaining

$$\Psi_1(u, y) = \begin{pmatrix} y_2^{(3)} \\ y_2^{(3)} \\ y_2^{(3)} \end{pmatrix}, \quad \Pi = \begin{pmatrix} \pi_t \\ \mu\pi_t \\ 1+\mu \end{pmatrix},$$

and

$$\Psi_2(u, y) = \begin{pmatrix} y_2^{(2)} - w^{(2)} & \Lambda(y) & \Lambda^{(2)}(y) \\ y_2^{(3)} - w^{(3)} & \dot{\Lambda}(y) & \Lambda^{(3)}(y) \\ y_2^{(4)} - w^{(4)} & \Lambda^{(2)}(y) & \Lambda^{(4)}(y) \end{pmatrix}.$$

It follows, that if $\Lambda(y)$ is not identically zero, and the input is persistently exciting, then the parameter μ is identifiable. Accidentally, it can be seen, that if π_t were be unknown, then it also could be identified. Since for practical reasons for a true system condition $\Lambda(y) = 0$ cannot hold, we can conclude that the parameter μ is, at least theoretically, identifiable.

As a side remark: if one considers the extension of the system with $\dot{\mu} = 0$, and studies the observability of the extended system, then the same results would be obtained.

The model that we have used in the simulations was described by the following parameters:

$$\pi = \begin{pmatrix} 398.30 & 20.33 & 3.38 & -1.69 & 0.16 \end{pmatrix},$$
$$\mu_0 = 0.2034, \quad \pi_t = 3220.3.$$

It was assumed that the value of μ may vary between $-0.15\mu_0$ and $0.1\mu_0$ around its nominal value μ_0. The true value of $\mu = (1+\alpha)\mu_0$ was set for $\alpha = 0.05$.

In the simulation experiment we have used three sampling times τ_s, namely $0.01, 0.001$ and 0.0001. As an optimization tool the MATLAB®'s *lsqnonlin* routine was applied and for the solution of the differential equation the *lsim* routine was used. Using LMI techniques an observer gain K was computed such that the observer must be stable for all possible values of the parameter. The computed gain was:

$$K^T = \begin{pmatrix} 3.6 & -0.9 & 2.1 & 1116.6 \\ 326.0 & 1121.7 & 214.9 & 226.7 \end{pmatrix}.$$

In the first situation the initial condition was assumed to be known. Parameter estimation was performed based on the original system structure and then on the

Table A.1 Results for α, with known x_0

τ_s	0.01	0.001	0.0001
α, $K = 0$	0.049	0.0501	0.0501
α, K	-0.15	0.0434	0.0545

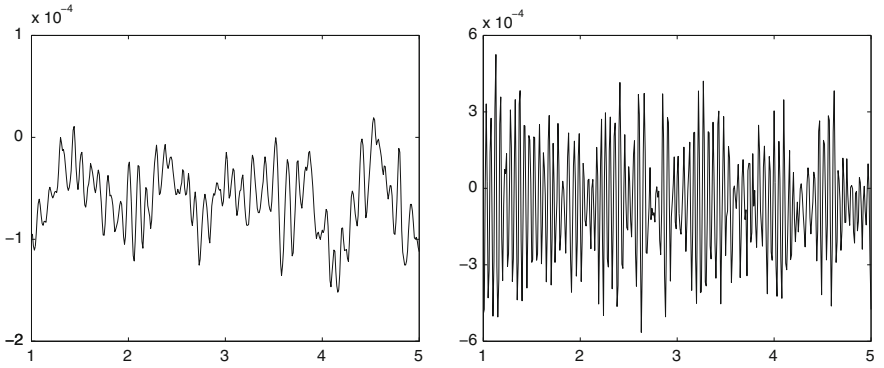

Fig. A.1 Simulation error for the original system (a) and for the observer (o)

observer system structure using measurements that correspond to different values of the sampling time. Values for the computed parameter α are shown in Table A.1. One can observe that in this situation the identification based on the original system structure seems to slightly outperform the results obtained in the case when an observer is to be identified. However, these differences are not significant and can be explained by numerical reasons.

The observer cannot be used for identification for the lowest sampling time. Figure A.1a shows the simulation error of the original system for the nominal value of the parameter, i.e., for $\alpha = 0.05$. The simulation error of the observer is shown in Fig. A.1o. One can observe the loss of stability of this system, which explains the failure of the optimization algorithm in this case.

In the second case, the initial condition was assumed to be unknown and an observer was used for identification purposes. In simulations

$$x_0 = \begin{pmatrix} -0.0024 & -0.0026 & -0.0200 & 0.0408 \end{pmatrix}$$

was set while in the identification process $x_0 = 0$ was used. The computed values for α are shown in Table A.2.

One can observe that the identification scheme based on the original system gives unsatisfactory results, i.e., the computed parameter value is far from the nominal one $\alpha = 0.005$. The observer based scheme performs quite well, given almost the same results as in the situation with known x_0. Figure A.2a shows the simulation error of

Table A.2 Results for α, with unknown x_0

τ_s	0.01	0.001	0.0001
α, $K = 0$	0.0254	0.0260	0.0260
α, K	-0.15	0.0478	0.0474

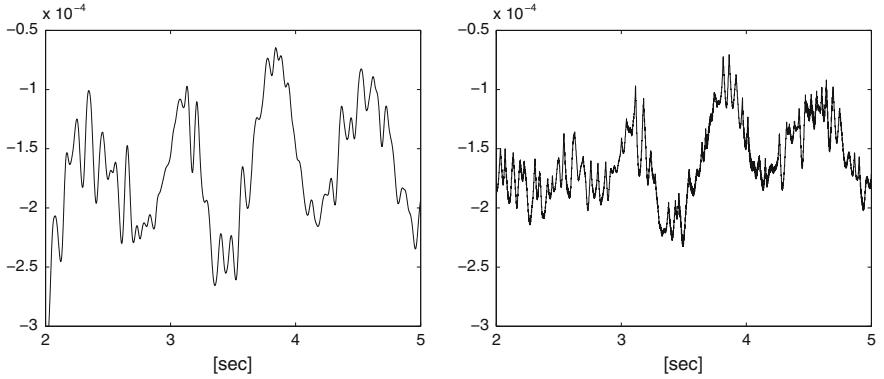

Fig. A.2 Error for the original system (a) and for the observer (o) (unknown x_0)

the original system for the nominal value of the parameter α. Comparing it with the simulation error of the observer system, shown in Fig. A.2o, one can see an increase in the magnitude of the errors.

A.5 Adaptive Observers for (q)LPV Systems

The class of systems considered in this section will be the following:

$$\dot{x} = A(\rho(t))x + B_u(\rho(t))u + B_p\varphi(\rho(t), y)p \tag{A.37}$$

$$y = Cx \tag{A.38}$$

where p is a parameter vector, $\rho(t)$ is a known vector of time-varying scheduling parameters, which basically depends on measured outputs, i.e., $\rho(t) = \rho(y)$, and $\varphi(\rho(t), y)$ is a known, possibly nonlinear, function of its arguments. The objective of our investigations is to compute the unknown parameter p for system (A.38) from input–output measurements, in other words, to solve a grey-box identification problem.

The approach presented in Zhang and Alleyne (2002) proposes the following globally exponentially convergent adaptive observer scheme for the estimation of the parameter p:

$$\dot{\hat{x}} = A(t)\hat{x} + B_u(t)u + B_p\varphi(t)\hat{p} + (K(t) + \Omega(t)G(t))(y - C\hat{x}) \quad (A.39)$$

$$\dot{\Omega}(t) = (A(t) - K(t)C)\Omega(t) + B_p\varphi(t), \quad (A.40)$$

with $\dot{\hat{p}} = G(t)(y - C\hat{x})$ and $G(t) = \Gamma(t)\Omega^T(t)C^T\Sigma(t)$. Here, the gain matrix $K(t)$ should be chosen such that the system defined by $A(t) - K(t)C$ is exponentially stable and it is assumed that the so-called persistency condition holds, i.e., there are positive constants α, β, T and there is a bounded positive definite matrix such that

$$\alpha I \leq \int_t^{t+T} \Omega^T(\tau)C^T\Sigma(\tau)C\Omega(\tau)d\tau \leq \beta I, \quad (A.41)$$

for all t.

Typically $\Gamma(t)$ is chosen as a positive diagonal matrix.

Unfortunately currently there are no results available for an optimal design and the algorithm should be tuned through trials. In our identification oriented applications we find that it is hard to tune the algorithm properly, i.e., to find suitable matrices $\Sigma(t)$ and $\Gamma(t)$ in order to achieve acceptable performances.

Convergence

In our applications we often consider systems that can be cast in the form:

$$\dot{x} = A(t)x + B_u(t)u + B_p\varphi(y)p \quad (A.42)$$

$$y = Cx \quad (A.43)$$

where p is a parameter vector and $\varphi(y)$ is a known, possibly nonlinear. Assuming that there exists a symmetric and positive definite matrix P, a gain matrix $K(t)$, a matrix M and $\mu > 0$ such that

$$PA_o(t) + A_o^T(t)P \leq -\mu I, \quad PB_p = C^T M, \quad (A.44)$$

where $A_o(t) = A(t) - K(t)C$ holds, and that the signals φ are persistently exciting. Then, the adaptive observer is defined as:

$$\dot{\hat{x}} = A(t)\hat{x} + B_u(t)u + B_p\varphi(t)\hat{p} + K(t)(y - C\hat{x}) \quad (A.45)$$

$$\dot{\hat{p}} = -\varphi^T(t)P(y - C\hat{x}). \quad (A.46)$$

In what follows, we highlight the main ideas of the proof for the global convergence of the scheme. Let us denote by $e = \hat{x} - x$ and by $e_p = \hat{p} - p$. Then, the error system will be:

$$\dot{e} = A_o(t)e + B_p\varphi(t)e_p \quad \dot{e}_p = -\varphi^T(t)M^T Ce. \quad (A.47)$$

Let us consider the candidate Lyapunov function

$$V(e, e_p) = e^T P e + e_p^T e_p. \tag{A.48}$$

It follows that

$$\dot{V}(e, e_p) = e^T (P A_o(t) + A_o^T(t) P) e \leq \mu e^T e. \tag{A.49}$$

This implies that $||e||$ and $||e_p||$ are bounded, hence $\|\dot{e}\|$ is also bounded. From Barbalat's lemma follows $\lim_{t\to\infty} \|e\| = 0$. Furthermore, since φ is persistently exciting, then it also follows that $\lim_{t\to\infty} \|e_p\| = 0$.

In applications the measurements are corrupted by noise or bounded disturbance, i.e., $\bar{y} = y + w$, where $\|w\| < c_w$.

Let us use the form $\bar{\varphi}(t) = \varphi(\bar{y}) = \varphi(t) + \Delta_\varphi$, then the error equation will be:

$$\dot{e} = A_o(t) e + B_p \bar{\varphi}(t) e_p + \zeta(t) \tag{A.50}$$

$$\dot{e}_p = -\bar{\varphi}^T(t) M^T C e - \Delta_\varphi^T M^T w, \tag{A.51}$$

where $\zeta(t) = K(t) w + B_p \Delta_\varphi p$. It is reasonable to suppose a Lipschitz property for φ, i.e., $\|\|\Delta_\varphi\|\| \leq c\|w\|$.

It follows that

$$\dot{V}(e, e_p) = -\mu e^T e + e^T P \zeta - w^T M \Delta_\varphi e_p, \tag{A.52}$$

i.e., there are suitable positive numbers $\mu_1,\ \mu_2,\ \mu_3$ such that

$$\dot{V}(e, e_p) \leq -\mu_1 \|e\|^2 + \mu_2 \|\zeta\|^2 + \mu_3 \|\zeta\| \|e_p\|, \tag{A.53}$$

provided that $\mu \geq \mu_1 + \frac{\lambda_{max}(P)}{\mu_2}$.

Applying the extended persistency of excitation lemma, see Marino and Santosuosso (1999), it follows that the error system is Input to State Stable and the origin is its globally exponentially stable equilibrium point, when $\zeta = 0$, provided that $\varphi(\bar{y})$ satisfy the persistency excitation condition of type (A.41).

A.6 Geometric Approach for qLPV FDI Design

Let us consider the class of linear parameter-varying (LPV) systems of m inputs and p outputs that can be described as:

$$\dot{x}(t) = A(\rho(t)) x(t) + B(\rho(t)) v(t) \tag{A.54}$$

$$y(t) = C x(t) \tag{A.55}$$

where

$$A(\rho(t)) = A_0 + \rho_1(t)A_1 + \cdots + \rho_N(t)A_N, \tag{A.56}$$

$$B(\rho(t)) = B_0 + \rho_1(t)B_1 + \cdots + \rho_N(t)B_N, \tag{A.57}$$

and the dimension of the state space is supposed to be n.

It is assumed that each parameter ρ_i ranges between known extremal values $\rho_i(t) \in [\underline{\rho}_i, \overline{\rho}_i]$ and the parameter set that contains all $(\rho_1(t), \cdots, \rho_N(t))$, where $t \in [0, T]$ will be denoted by $\mathscr{P}$. For the sake of notational simplicity the time dependency of the matrices will be omitted $(A(\rho) := A(\rho(t)))$ where it is possible.

Inversion of qLPV Systems

It is not hard to figure out that if some technical conditions for the parameter functions (persistency) are fulfilled, then $T_x Z^* = \mathscr{V}^*$, where $\mathscr{V}^*$ is the maximal $(\mathscr{A}, \mathscr{B})$-invariant subspace contained in Ker C. The invertability conditions reduce to

$$\text{dimIm } B = m, \quad \mathscr{V}^* \cap \text{Im } B = 0.$$

Let us observe, that if these conditions are fulfilled, one can always choose a coordinate transform of the form

$$z = Tx, \text{ where } \quad T = \begin{bmatrix} \mathscr{V}^{*\perp} \\ \Lambda \end{bmatrix}, \ \Lambda \subset (\text{Im } B)^{\perp}.$$

Accordingly, the system will be decomposed to:

$$\dot{\xi} = A_{11}(t)\xi + A_{12}(t)\eta + B\nu \tag{A.59}$$

$$\dot{\eta} = A_{21}(t)\xi + A_{22}(t)\eta \tag{A.60}$$

$$y = C_1\xi. \tag{A.61}$$

It follows that applying a suitable feedback

$$\nu = F_2(\rho(t))\eta + v, \tag{A.62}$$

such that $\mathscr{V}^*$ is $(\mathscr{A} + \mathscr{B}F, \mathscr{B})$ invariant, one can obtain the system:

$$\dot{\xi} = A_{11}(t)\xi + Bv \tag{A.63}$$

$$y = C_1\xi. \tag{A.64}$$

By the maximality of $\mathscr{V}^*$ follows that both ξ and v can be expressed as functions of y and its derivatives.

With $\tilde{y} = S\xi$, where

$$\tilde{y} = \left[y_1, \cdots, y_1^{(\gamma_1)}, \cdots, y_p, \cdots, y_p^{(\gamma_p)} \right]^T$$

one has

$$v = B^{-1}S^{-1}(\dot{\tilde{y}} - \dot{S}S^{-1}\tilde{y} - S\bar{A}_{11}S^{-1}\tilde{y}),$$

i.e.,

$$\begin{aligned} \dot{\eta} &= A_{22}\eta + A_{21}\xi \\ v &= F_2\eta + \bar{B}^{-1}S^{-1}(\dot{\tilde{y}} - (\dot{S}S^{-1} + SA_{11}S^{-1})\tilde{y}). \end{aligned}$$

For details, see Szabó et al. (2003).

Detection Filter Design for qLPV Systems

Let us consider to the following LPV system:

$$\begin{aligned} \dot{x}(t) &= A(\rho)x(t) + B(\rho)u(t) + L_1(\rho)m_1(t) + L_2(\rho)m_2(t) \\ y(t) &= Cx(t). \end{aligned} \tag{A.65}$$

The task of designing a residual generator that is sensitive to the fault associated with the L_1 direction and insensitive to the fault associated with the L_2 direction is called the fundamental problem of residual generation (FPRG). More precisely, one has to design a residual generator, let us denote its output by r_1, such that if $\nu_1 \neq 0$ then $r_1 \neq 0$ and if $\nu_1 = 0$ then $\lim_{t\to\infty} \|r_1(t)\| = 0$, i.e., a stability condition requirement on the residual generator.

It turns out that the fundamental problem of residual generation has a solution if and only if $\mathscr{S}^* \cap \mathscr{L}_1 = 0$, moreover, if the problem has a solution, the dynamics of the residual generator can be assigned arbitrary.

For LPV systems given in Eq. (A.65) one can design a—not necessarily stable—residual generator of type

$$\dot{w}(t) = N(\rho)w(t) - G(\rho)y(t) + F(\rho)u(t) \tag{A.66}$$

$$r(t) = Mw(t) - Hy(t), \tag{A.67}$$

if for the smallest unobservability subspace (associated to an LPV system) $\mathscr{S}^*$ containing $\mathscr{L}_2$ one has $\mathscr{S}^* \cap \mathscr{L}_1 = 0$, where $\mathscr{L}_i = \sum_{j=0}^{N} \operatorname{Im} L_{i,j},\ i = 1, 2$.

One can compute an acceptable $\hat{G}(\rho)$ as follows: let us consider a splitting of $A(\rho)$ and C according to the projection $P : \mathscr{X} \to \mathscr{X}/\mathscr{S}^*$ and $P^{\perp}$, respectively, and let us consider $A_{12}(\rho) := PA(\rho)P^{\perp}$ and $C_{12} := CP^{\perp}$. Then one has

$$\hat{G}(\rho) = \begin{bmatrix} -A_{12}(\rho)C_{12}^{(-1)} \\ 0 \end{bmatrix},$$

where $C_{12}^{(-1)}$ is a pseudoinverse.

In order to achieve that the condition $\mathscr{S}^* \cap \mathscr{L}_1 = 0$ become necessary and sufficient the subspace $\mathscr{S}^*$ has to be the minimal unobservability codistribution containing $\mathscr{L}_2$. If the components of the parameter function ρ are differential algebraically independent then this property holds.

The Question of Stability

Recall, that an affine LPV system is said to be quadratically stable if there exists a matrix $P = P^T > 0$ such that

$$A(\rho)^T P + PA(\rho) < 0 \tag{A.68}$$

for all the parameters $\rho \in \mathscr{P}$. A necessary and sufficient condition for a system to be quadratically stable is that the condition in Eq. (A.68) holds for all the corner points of the parameter space, i.e., one can obtain a finite system of LMI's that has to be fulfilled for $A(\rho)$ with a suitable positive definite matrix P.

In order to obtain a quadratically stable residual generator one can set $N_{stable}(\rho) = N(\rho) + G(\rho)M$ in Eq. (A.66), where $N(\rho) = (A(\rho) + \hat{G}(\rho)C)|_{\mathscr{X}/\mathscr{S}^*}$, and $G(\rho) = G_0 + \rho_1 G_1 + \cdots \rho_N G_N$ is determined such that the LMI defined in Eq. (2.91), i.e.,

$$(N(\rho) + G(\rho)M)^T P + P(N(\rho) + G(\rho)M) < 0$$

holds for suitable $G(\rho)$ and $P = P^T > 0$. By introducing the auxiliary variable $K(\rho) = G(\rho)P$, one has to solve the following set of LMIs on the corner points of the parameter space:

$$N(\rho)^T P + PN(\rho) + M^T K(\rho)^T + K(\rho)M < 0.$$

In certain cases one can find $\mathrm{Ker}C \subset \mathscr{S}^*$. Then one can choose $G(\rho)$ such that the matrix $N(\rho)$ becomes constant, since the equation $G(\rho)CU = UT - A(\rho)U$ has a solution for arbitrary T, where U is the insertion map of $\mathscr{X}/\mathscr{S}^*$. The matrix T is a design parameter that contains the information about the desired poles.

Robustness Issues

A fundamental problem of model-based designs is that the model is not a fidel copy of reality, hence there are uncertainties that an efficient fault detection has to cope with. The problem is more accentuated for nonlinear models when the design algorithms usually contain operations that depend in a highly nonlinear way on the uncertainties, e.g., the maps that define certain diffeomorphisms in order to realize desired variable changes.

To achieve robustness in the presence of disturbances and uncertainty, optimization-based FDI schemes have been proposed where an appropriately selected performance index is chosen to enhance sensitivity to the faults and simultaneously attenuate disturbances. The methods that try to enhance the robustness of the detection filters against perturbations and model uncertainties via eigenstructure assignment applied in the linear context, e.g., for parity space methods (Patton and Chen 1996) or observer-based methods (Douglas and Speyer 1996; Chen and Speyer 2002), are not applicable in the general nonlinear setting. In the LPV setting, however, the robustness issue can be handled in certain circumstances using $\mathscr{H}_\infty$ theory, see, e.g., Ganguli et al. (2002); Grenaille et al. (2008).

Applying an inversion based design if additional outputs are available such that the system with “eliminated" unknown inputs is observable (i.e., by eliminating the inputs through the algebraic relation $A(x)v = B(x)$) and it is possible to construct an observer then one has an inverse (not reduced). In such situations derivatives of the output are still needed but the stability of the zero dynamics does not play any role. For this class robustness issues can be handled Edelmayer et al. (2004, 2009).

If the design criteria are met the LPV/FPRG method can be used to obtain fault detection filters that are robust against parametric variations and noise, see e.g., Szászi et al. (2005).

Often the FDI filter design has been considered as a separate task from the design of feedback controllers. Optimal integrated design is equal to the optimal separate design of the controller and detection filter if there is no model uncertainty. When there is uncertainty an integrated approach is more favorable for the trade-off between performance and robustness, for the linear case see, e.g., Stoustrup and Grimble (1996), Stoustrup and Niemann (2002) and Weng et al. (2008) for the LPV case, respectively.

Appendix B
Robust Control of LPV Systems

B.1 Structured Uncertainty

Structured uncertainties arise when the plant is subject to multiple perturbations. Multiple perturbations occur when the plant contains a number of uncertain parameters or when the plant contains multiple unstructured uncertainties. In practice many systems involve parametric uncertainties that are real. In this case real parametric and complex uncertainties should be divided, see Fig. B.1. The mixed real and complex μ involve three types of blocks: repeated real scalar, repeated complex scalar and full blocks. S_r represents the number of repeated real scalar blocks, S_c the number of repeated complex scalar blocks and F the number of full blocks. They satisfy the following: $\sum_{i=1}^{S_r} k_i + \sum_{j=1}^{S_c} r_j + \sum_{k=1}^{F} m_k = n$. The ith repeated real scalar block is $k_i \times k_i$, the jth repeated complex scalar block is $r_j \times r_j$ and the kth full block is $m_k \times m_k$. The admissible set of uncertainties $\Delta \subset \mathbb{C}^{nxn}$ is defined as

$$\begin{aligned}\nabla = \{&\text{diag}\left(\Phi_1 I_{k_1}, \ldots, \Phi_{S_r} I_{k_{S_r}}, \delta_1 I_{r_1}, \ldots, \delta_{S_c} I_{r_{S_c}}, \Delta_1, \ldots, \Delta_F\right) : \\ &\Phi_i \in \mathbb{R}, \delta_j \in \mathbb{C}, \delta_k \in \mathbb{C}^{m_k \times m_k}\}.\end{aligned} \tag{B.1}$$

Definition B.1 (*The definition of* μ) For a matrix $M \in \mathbb{C}^{n\times n}$ the $\mu_{\tilde{\Delta}}$ function is then defined as:

$$\mu_{\nabla}(M) := \frac{1}{\min\{\bar{\sigma}(\Delta) : \Delta \in \nabla,\ \det(I - M\Delta) = 0\}} \tag{B.2}$$

unless no $\Delta \in \nabla$ makes $I - M\Delta$ singular, in which case $\mu_{\nabla}(M) = 0$, see Doyle (1985).

Thus $1/\mu_{\nabla}(M)$ is the "size" of the smallest perturbation Δ, measured by its maximum singular value, which makes $\det(I - M\Delta) = 0$. Directly from the definition of μ we can state that the lower and the upper bounds of μ are the following:

P. Gáspár et al., *Robust Control Design for Active Driver Assistance Systems*,
Advances in Industrial Control, DOI 10.1007/978-3-319-46126-7

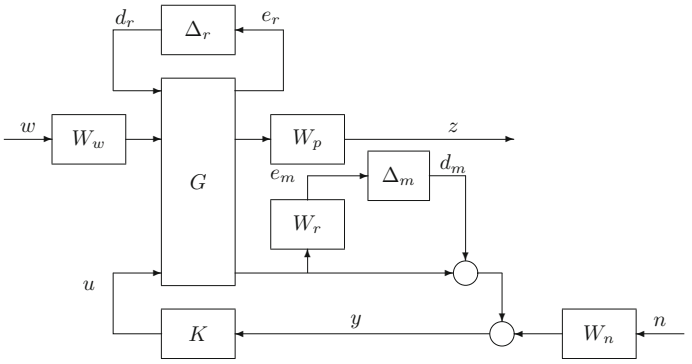

Fig. B.1 The feedback configuration with parametric and unstructured uncertainties

$$\rho(M) \leq \mu_{\nabla}(M) \leq \bar{\sigma}(M). \tag{B.3}$$

However, these bounds are not sufficient for control design, because the gap between ρ and $\bar{\sigma}$ can be arbitrarily large. They are refined by considering transformations on M that do not affect $\mu_{\nabla}(M)$, but do affect ρ and $\bar{\sigma}$. To do this, define the following three subsets:

$$\mathbb{Q} = \left\{\Delta \in \Delta : \Phi_i \in \left[-1\ 1\right], |\delta_i| = 1, \Delta_i \Delta_i^* = I_{mi}\right\}, \tag{B.4}$$

$$\mathbb{D} = \left\{ \begin{array}{l} \operatorname{diag}\left[\tilde{D}_1, \ldots, \tilde{D}_{sr}, D_1, \ldots, D_{sc}, d_1 I_{m1}, \ldots, d_{F-1} I_{mF-1}, I_{mF}\right] : \\ \tilde{D}_i \in \mathbb{C}^{k_i \times k_i}, \tilde{D}_i = \tilde{D}_i^* > 0, D_i \in \mathbb{C}^{r_i \times r_i}, D_i D_i^* > 0, d_j \in \mathbb{R}, d_j > 0 \end{array} \right\}, \tag{B.5}$$

$$\mathbb{G} = \left\{\operatorname{diag}\left[\tilde{G}_1, \ldots, \tilde{G}_{sr}, 0, \ldots, 0, 0\right] : G_i = G_i^* \in \mathbb{C}^{k_i \times k_i}\right\}. \tag{B.6}$$

Unfortunately, the lower bound can have multiple local maxima that are not global. Thus local search cannot guarantee to obtain μ. The upper bound can be reformulated as a convex optimization problem, so the global minimum can be found. Unfortunately, the upper bound is not always equal to μ:

$$\mu_{\Delta}(M) \leq \inf_{D \in \mathbb{D}} \bar{\sigma}(DMD^{-1}). \tag{B.7}$$

A better upper bound can be obtained for the mixed μ by exploiting the phase information of the real parameters in the following way.

Theorem B.1 *Let $M \in \mathbb{C}^{n \times n}$ and $\Delta \in \Delta$. Then*

$$\mu_{\Delta}(M) \leq \inf_{D \in \mathbb{D}, G \in \mathbb{G}} \min_{\beta} \operatorname{diag}\left[\beta : M^* D M + j(GM - M^* G) - \beta^2 D \leq 0\right]. \tag{B.8}$$

See Fan et al. (1991); Young and Doyle (1996).

The scaling G allows one to exploit the phase information about the real parameters so that a better upper bound can be obtained. An alternative characterization of the upper bound that uses a different scaling strategy ($D - G - K$ scheme) is given in the following result.

Theorem B.2 *Given $\beta > 0$, there exist $D \in \mathbb{D}$ and $G \in \mathbb{G}$ such that*

$$M^* DM + j(GM - M^* G) - \beta^2 D \leq 0$$

if and only if there are $D_1 \in \mathbb{D}$ and $G_1 \in \mathbb{G}$ such that

$$\bar{\sigma}\left[(\frac{D_1 M D_1^{-1}}{\beta} - jG_1)(I + G_1^2)^{-\frac{1}{2}} \leq 1\right]. \tag{B.9}$$

See Zhou et al. (1996).

Theorem B.3 (Robust stability) *The loop is well posed and internally stable for all $\Delta(.) \in \nabla$ with $\|\Delta\|_\infty < \frac{1}{\beta}$ and $\beta > 0$ if and only if*

$$\sup_{\omega \in \Re} \mu_\nabla(M(j\omega)) \leq \beta. \tag{B.10}$$

Hence the peak value on the μ plot of the frequency response determines the size of perturbations. Consequently, the loop is robustly stable. See Zhou et al. (1996).

The robust performance problem can be converted into an equivalent robust stability problem by appending an uncertainty block to the system. This block connects the performance output with the disturbance input as shown in Fig. B.2. The system in Fig. B.1 meets the performance robustness objectives if and only if the system in Fig. B.2 is robustly stable. The system is stable for all perturbations of the following kind: $\Delta_p(s) = \text{diag}\,[\Delta(s), \Delta_o(s)]$ such that $\|\Delta_p(s)\|_\infty \leq 1$.

Theorem B.4 (Robust performance, see Zhou et al. (1996)) *The loop is well posed and internally stable and $\|F_u(G_P, \Delta)\|_\infty \leq \beta$ for all $\Delta(s) \in \mathbb{M}(\Delta)$ with $\|\Delta\|_\infty < \frac{1}{\beta}$ and $\beta > 1$ if and only if*

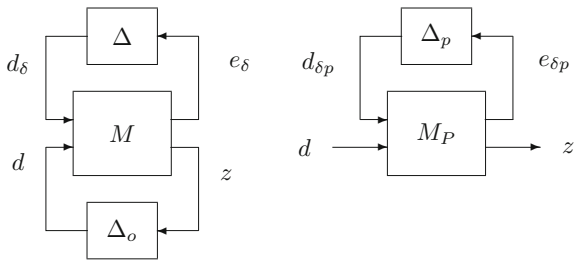

Fig. B.2 Structured uncertainty incorporating the performance block

$$\sup_{\omega\in\Re} \mu_{\Delta P}(M_P(j\omega)) \le \beta. \tag{B.11}$$

Suppose we have a stabilizing controller K, which is absorbed in the feedback loop to achieve the closed-loop system, $F_\ell(P, K)$. The generalized closed-loop system is a 2×2 block-structured transfer function matrix M_P between $\left[d_{\delta p}\ d\right]^T$ and $\left[e_{\delta p}\ z\right]^T$, see on the right-hand side of Fig. B.2:

$$\begin{bmatrix} e_{\delta p} \\ z \end{bmatrix} = \begin{bmatrix} M_{P11} & M_{P12} \\ M_{P21} & M_{P22} \end{bmatrix} \begin{bmatrix} d_{\delta p} \\ d \end{bmatrix} \tag{B.12}$$

From the above results a nonconservative, necessary and sufficient condition for robust performance is derived by Doyle (1984).

Theorem B.5 (General analysis theorem)

1. *Nominal performance is satisfied if and only if* $\bar{\sigma}(M_{P22}(j\omega) < 1, \forall\omega$.
2. *Stability is robust if and only if* $\bar{\sigma}(M_{P11}(j\omega) < 1, \forall\omega$.
3. *Performance is robust if and only if* $\mu(M_P(j\omega)) < 1, \forall\omega$.

B.2 Control Design Based on Nonlinear $\mathscr{H}_\infty$ Methods

The Problem of the Nonlinear $\mathscr{H}_\infty$ Control

The nonlinear $\mathscr{H}_\infty$ control is the extension of the $\mathscr{H}_\infty$ methods to nonlinear systems. In the nonlinear $\mathscr{H}_\infty$ synthesis, the objective is to find a possible nonlinear controller such that the $\mathscr{L}_2$ gain of the closed-loop system from the disturbance input w to the performance output z is minimized and the closed-loop is internally stable. An upper bound on the $\mathscr{L}_2$ gain from w to z can only be found by using a positive number γ. The bounded real lemma has a corresponding nonlinear version, too.

Lemma B.1 (Bounded real lemma) *Consider the time-invariant nonlinear system:*

$$\dot{x} = f(x) + g(x)w, \quad x(0) = 0, \tag{B.13}$$

$$z = h(x), \tag{B.14}$$

where $f(x)$ is locally Lipschitz and $g(x)$, $h(x)$ are continuous over $\mathscr{R}^n$. The functions f and h vanish at the origin, i.e., $f(0) = 0$ and $h(0) = 0$. Let γ be a positive number and suppose there is a continuously differentiable and positive semidefinite function $V(x)$ that satisfies the following partial differential inequality:

$$\mathscr{H}(V, f, g, h, \gamma) = \frac{\partial V}{\partial x} f(x) + \frac{1}{2\gamma^2} \frac{\partial V}{\partial x} g(x) g^T(x) (\frac{\partial V}{\partial x})^T + \frac{1}{2} h^T(x) h(x) \le 0 \tag{B.15}$$

for all $x \in \mathscr{R}^n$. Then, for each $x_0 \in \mathscr{R}^n$ the $\mathscr{L}_2$ gain of the system is less than or equal to γ. See Khalil (2000).

Inequality (B.15) is known as the Hamilton–Jacobi inequality (HJI), or the Hamilton–Jacobi equation (HJE) when ($\leq$) is replaced by ($=$). The search for a function $V(x)$ that satisfies (B.15) essentially requires the solution of a partial differential equation, which might be difficult to solve. Much of the research in nonlinear $\mathscr{H}_\infty$ controller synthesis is focused on how to solve inequality (B.15). This is a nontrivial task, and the problem increases dramatically with the state space dimension.

The analogy with the $\mathscr{H}_\infty$ synthesis for LTI systems becomes obvious comparing (B.15) with the real algebraic Riccati equation: consider a linear time invariant system $\dot{x} = Ax + Bw$ and $z = Cx$ and suppose there is a positive semidefinite solution P to the Riccati equation $PA + AP^T + \frac{1}{\gamma^2} PBB^T P + C^T C = 0$ for some $\gamma > 0$. Taking $V(x) = \frac{1}{2} x^T Px$ and using the expression $\frac{\partial V}{\partial x} = x^T P$, it can be seen that $V(x)$ satisfies the HJE: $\mathscr{H}(V, Ax, B, Cx, \gamma) = x^T PAx + \frac{1}{2\gamma^2} x^T PB^T BPx + \frac{1}{2} x^T C^T Cx = 0$. Hence, the system is finite-gain $\mathscr{L}_2$ gain stable and its $\mathscr{L}_2$ gain is less than or equal to γ.

In this chapter the nonlinear $\mathscr{H}_\infty$ control problem in state space for a class of nonlinear systems is examined following the results of Lu and Doyle, see Lu and Doyle, see Lu and Doyle (1993, 1994, 1995, 1996, 1997, 2002).

Consider the nonlinear plant P with two sets of inputs: the exogenous disturbance input d and the control input u, and two sets of outputs: the measured output y and the regulated output z (Fig. 3.1). K is the controller to be designed. Both P and K are time-invariant and can be realized as affine state space equations.

The state space representation (SSR) of the plant is as follows:

$$\dot{x} = f(x) + g_1(x)d + g_2(x)u, \tag{B.16}$$

$$z = h_1(x) + k_{11}(x)d + k_{12}(x)u, \tag{B.17}$$

$$y = h_2(x) + k_{21}(x)d + k_{22}(x)u, \tag{B.18}$$

where $f, g_i, h_i, k_{ij} \in \mathscr{C}^2$, $h_1(0) = 0$, $h_2(0) = 0$.

The SSR of the controller is as follows:

$$\dot{x}_k = a(x_k) + b(x_k)y, \tag{B.19}$$

$$u = c(x_k) + d(x_k)y, \tag{B.20}$$

with $a, b, c, d \in \mathscr{C}^2$ and $a(0) = 0, c(0) = 0$. The initial states for both plant and controller are $x(0) = 0$ and $x_k(0) = 0$. The closed-loop system is denoted as nonlinear operator $\Omega(P, K)$ which represents the input/output relation $z = \Omega(P, K)d$.

Problem B.1 (*The nonlinear $\mathscr{H}_\infty$ control problem*) The problem setup of the design of a $\mathscr{H}_\infty$ controller is the following. Let us denote $\Omega(P, K)$ the fraction representation of operator G on operator K. Find an output feedback controller K for system

P, if any exist, such that the closed-loop system $\Omega(P, K)$ is asymptotically stable with $w = 0$ and has $\mathscr{L}_2$-gain ≤ 1, that is

$$\int_0^T (\|d(t)\|^2 - \|z(t)\|^2)dt \geq 0, \tag{B.21}$$

for all $T \in \mathbb{R}^+$.

The following assumptions are made:

1. $\left[h_1(x),\, f(x)\right]$ and $\left[h_2(x),\, f(x)\right]$ are zero-detectable.
2. $k_{12}^T(x)\left[h_1(x)\ k_{12}(x)\right] = \left[0\ I\right]$.
3. $\begin{bmatrix} g_1(x) \\ k_{21}(x) \end{bmatrix} k_{21}^T(x) = \begin{bmatrix} 0 \\ I \end{bmatrix}$.
4. $k_{11}(x) = 0, k_{22}(x) = 0$.

It is known that a large class of nonlinear systems can be simplified to satisfy the above assumption when the $\mathscr{H}_\infty$ control problem is considered, see Safonov and Limebeer (1988).

The Solution of the Nonlinear $\mathscr{H}_\infty$ Control

The solvability of the output feedback $\mathscr{H}_\infty$ control problem is based on two quantities, which are linked to the full information (FI) and the full control (FC) problems by using the similar idea to the linear case.

In the full information (FI) problem the plant has the following form:

$$\dot{x} = f(x) + g_1(x)d + g_2(x)u, \tag{B.22}$$

$$z = h_1(x) + k_{12}(x)u, \tag{B.23}$$

$$y = \begin{bmatrix} x \\ 0 \end{bmatrix} + \begin{bmatrix} 0 \\ I \end{bmatrix} d \tag{B.24}$$

and the controller is provided with information from the state and the disturbance, i.e., $y = \left[x\ d\right]^T$. The FI $\mathscr{H}_\infty$ control problem was first explicitly introduced by Van der Schaft Van der Schaft der Schaft (1993). The solution to the FI $\mathscr{H}_\infty$ control problem is related to the following HJI:

$$\begin{aligned} \mathscr{H}_{FI}(V, x) = \frac{\partial V}{\partial x}(x) f(x) + \frac{1}{4}\frac{\partial V}{\partial x}(x)(g_1(x)g_1^T(x) - \\ - g_2(x)g_2^T(x))\frac{\partial V}{\partial x}^T(x) + h_1^T(x)h_1(x) \leq 0 \end{aligned} \tag{B.25}$$

Theorem B.6 (The solvability of the FI problem) *$\mathscr{H}_{FI}(V,x) \le 0$ has a C^3 solution $V(x)$ with $V(0) = 0$ if and only if there is $F(x)$ such that*

$$\frac{\partial V}{\partial x}(x)(f(x) + g_2(x)F(x)) + \frac{1}{4}\frac{\partial V}{\partial x}(x)(g_1(x)g_1^T(x)\frac{\partial V^T}{\partial x}(x)+ (h_1(x) + k_{12}(x)F(x))^T(h_1(x) + k_{12}(x)F(x)) \le 0 \tag{B.26}$$

Moreover, if $V(x)$ satisfies $\mathscr{H}_{FI}(V,x) \le 0$ with $V(0) = 0$, then $F(x)$ can be taken as $F_0(x) = -\frac{1}{2}g_2^T\frac{\partial V^T}{\partial x}(x)$. See der Schaft (1993); Lu and Doyle (1995).

Theorem B.7 (The solution of the FI problem) *Suppose there exists C^3 positive definite function $V(x) \ge 0$ such that $\mathscr{H}_{FI}(V,x) \le 0$ with $V(0) = 0$. Then the $\mathscr{H}_\infty$ control problem for FI is solvable. Moreover, such state feedback FI $\mathscr{H}_\infty$ controller is given by $u = -\frac{1}{2}g_2^T\frac{\partial V^T}{\partial x}(x)$.*

In the full control (FC) problem the plant has the following form:

$$\dot{x} = f(x) + g_1(x)d + \begin{bmatrix} I & 0 \end{bmatrix} u, \tag{B.27}$$

$$z = h_1(x) + \begin{bmatrix} 0 & I \end{bmatrix} u, \tag{B.28}$$

$$y = h_2(x) + k_{21}(x)d \tag{B.29}$$

The solution to the FC $\mathscr{H}_\infty$ control problem is related to the following HJI:

$$\mathscr{H}_{FC}(U,x) = \frac{\partial U}{\partial x}(x)f(x) + \frac{1}{4}\frac{\partial U}{\partial x}(x)(g_1(x)g_1^T(x))\frac{\partial U^T}{\partial x}(x)+ +h_1^T(x)h_1(x) - h_2^T(x)h_2(x) \le 0 \tag{B.30}$$

Theorem B.8 (The solvability of the FC problem) *$\mathscr{H}_{FC}(U,x) \le 0$ has a C^3 solution $U(x)$ with $U(0) = 0$ if and only if there is $L(x)$ such that*

$$\frac{\partial U}{\partial x}(x)(f(x) + L(x)h_2(x)) + h_1^T(x)h_1(x)+ \frac{1}{4}\frac{\partial U}{\partial x}(x)(g_1(x) + L(x)k_{21}(x))(g_1(x) + L(x)k_{21}(x))^T\frac{\partial U^T}{\partial x}(x) \le 0 \tag{B.31}$$

Moreover, if $U(x)$ satisfies $\mathscr{H}_{FC}(U,x) \le 0$ with $U(0) = 0$, then $L(x)$ can be taken as $\frac{\partial U}{\partial x}(x)L_0(x) = -2h_2^T(x)$. See Lu and Doyle (1995).

Theorem B.9 (The solution of the FC problem) *Suppose there exists C^3 positive definite function $U(x) \ge 0$ such that $\mathscr{H}_{FC}(U,x) \le 0$ with $U(0) = 0$. If*

$$\frac{\partial U}{\partial x}(x)L_0(x) = -2h_2^T(x)$$

holds for some $L_0(x)$, then the $\mathscr{H}_\infty$ control problem for FC is solvable. Moreover, such a controller is given by output injection $u = \begin{bmatrix} L_0(x) \\ 0 \end{bmatrix} y$. See Lu and Doyle (1994).

Next, the output feedback $\mathscr{H}_\infty$ control problem is considered.

Theorem B.10 (The solvability of the nonlinear $\mathscr{H}_\infty$ problem) *Consider G in form (B.16) and the quantities for the FI and the FC problems in forms (B.25) and (B.30). If there is some $\psi(x) \geq 0$ with $\psi(0) = 0$ such that*

- *There exists a positive definite $V(x)$ which solves the HJE of the FI problem:*

$$\mathscr{H}_{FI}(V, x) + \psi(x) = 0 \tag{B.32}$$

  with $V(0) = 0$.
- *There exists a positive definite $U(x)$ which solves the HJI of the FC problem:*

$$\mathscr{H}_{FC}(U, x) + \psi(x) \leq 0 \tag{B.33}$$

  with $U(0) = 0$, moreover, $\mathscr{H}_{FC}(U, x) + \psi(x)$ has nonsingular Hessian matrix at 0.
- *$U(x) - V(x) \geq 0$ is positive definite.*

Moreover, the following equation has a solution $L_0(x)$:

$$\left(\frac{\partial U}{\partial x}(x) - \frac{\partial V}{\partial x}(x)\right) L_0(x) = -2h_2^T(x). \tag{B.34}$$

Then the output feedback $\mathscr{H}_\infty$ control problem is (locally) solvable. The form of the controller is the following:

$$\dot{x}_k = f_K(x_k) + L_0(x_k)h_2(x_k) - L_0(x_k)y, \tag{B.35}$$
$$u = F_0(x_k), \tag{B.36}$$

where

$$f_K(x_k) = f(x_k) + g_1(x_k)F_1(x_k) + g_2(x_k)F_0(x_k), \tag{B.37}$$
$$F_0(x) = -\frac{1}{2}g_2^T(x)\frac{\partial V^T}{\partial x}(x), \tag{B.38}$$
$$F_1(x) = \frac{1}{2}g_1^T(x)\frac{\partial V^T}{\partial x}(x). \tag{B.39}$$

See Lu and Doyle (1993).

Theorem B.11 (Solution of the nonlinear $\mathscr{H}_\infty$ problem) *Consider P satisfying the condition in Theorem B.10. If an addition $L_1(x)$ satisfies*

$$\left(\frac{\partial U}{\partial x}(x) - \frac{\partial V}{\partial x}\right) L_1(x) = -2h_1^T(x), \tag{B.40}$$

then the controller $u = \Omega(M, Q)y$ with M given by

$$\dot{x}_k = f_K(x_k) - L_0(x_k)y + (g_2(x_k) + L_1(x_k)u_0, \tag{B.41}$$
$$u = F_0(x_k) + u_0, \tag{B.42}$$
$$y_0 = h_2(x_k) - y, \tag{B.43}$$

for all Q also (locally) solves the output feedback $\mathscr{H}_\infty$ control problem. See Lu and Doyle (1994).

An equivalent version of the nonlinear $\mathscr{H}_\infty$ problem was obtained by Isidori (1992). Note that $\mathscr{H}_\infty$ controllers have separation structures. The separation principle for the $\mathscr{H}_\infty$ performance in nonlinear systems was confirmed by Ball et al. (1993). A more complete treatment of the nonlinear extensions of the $\mathscr{H}_\infty$ synthesis can be found in Helton and James (1999).

From Nonlinear $\mathscr{H}_\infty$ to Gain Scheduling

Since the solution of Hamilton–Jacobi inequality (HJI) (B.25) leads to highly nonlinear partial differential equations in $\frac{\partial V}{\partial x}$, it is almost impossible to solve in practice. Moreover, it would be desirable to have a solution in closed form in order to implement the controller. Thus, it would be convenient to obtain conditions that lead to suboptimally satisfactory but computationally reliable solutions.

The first important step to obtain a desired controller synthesis methodology is to convert HJI into a form which is linear and convex in $\frac{\partial V}{\partial x}$. Using a Schur complement argument the following inequality is equivalent with (B.15):

$$\begin{bmatrix} \frac{\partial V}{\partial x} f(x) + h^T(x)h(x) & \frac{1}{2}\frac{\partial V}{\partial x} g(x) \\ \frac{1}{2} g^T(x) \frac{\partial V^T}{\partial x} & -\gamma^2 I \end{bmatrix} \leq 0, \tag{B.44}$$

Inspired by the success of quadratic type functions in the linear context, it seems to be reasonable to consider the quasi-linear model structure. Write the nonlinear system as:

$$\dot{x} = A(x)x + B(x)w, \quad x(0) = 0, \tag{B.45}$$
$$z = C(x)x,$$

where $A(x)$, $B(x)$ and $C(x)$ are reminiscents of the LTI system matrices. Note that this form is not unique since using $E(x) = M(x)(x^T x I - x x^T)$ one has $A(x)x = (A(x) + E(x))x$.

If there is a storage function $V(x) > 0$ such that $\frac{\partial V}{\partial x} = 2xP(x)$ for some positive definite matrix function $P(x)$ then the HJI (B.25) can be written as

$$\begin{bmatrix} A^T(x)P(x) + P(x)A(x) & P(x)B(x) \\ B^T(x)P(x) & -\gamma I \end{bmatrix} \leq 0. \tag{B.46}$$

It is similar to the LMI conditions of the LTI setting. It cannot be ensured that the storage function is positive. The other problem is that since the optimal state is not known in advance one cannot obtain a closed form solution. This method is closely related to the state-dependent Riccati equation (SDRE) method, see Cloutier (1997); Shamma and Cloutier (2003). In order to achieve a closed form solution one must impose additional restrictions on the model set and the form of the storage function.

Next, the quasi-linear model class (B.45) is selected in such a way that the state matrices depend on the measured quantities, e.g., $A(x) = A(y)$. In this structure the form of the storage function is selected as $\frac{\partial V}{\partial x} = x^T P(t)x$. This selection leads to the gain scheduling and the LPV methods.

The Gain Scheduling Strategy

In this chapter, we introduce gain scheduling, a method that can extend the validity of the linearization approach to a range of operating points. Usually the change of the system dynamics between operating points is known. It might be possible to model the system in such a way that the operating points are parameterized by one or more variables, i.e., by scheduling variables. Thus, the nonlinear system dynamics can be approximated by a family of linearized model at several equilibrium points. Then controllers are designed at each point, and finally the family of linear controllers are implemented as a single controller. The scheduling variables are monitored in order that the controller is able to adapt to the current operating conditions. This means that the controller must be able to determine the controller parameters via the gain schedule from the command signal and the measured output.

The classical approach to gain scheduling consists of the following steps:

1. The nonlinear system is approximated using standard linearization locally in a set of operating (equilibrium) points, thus a family of linear models is constructed.
2. A controller synthesis is performed for the local models to achieve the specified performance such that a family of linear controllers are obtained. This step involves standard linear system controller synthesis where the closed-loop specifications are expressed in the same way as in the standard controller synthesis for linear systems.

3. The nonlinear controller is formulated. The closed-loop system under the gain-scheduled controller has the same equilibrium point as the closed-loop system under the fixed gain controller. The controller parameters are interpolated at intermediate operating points. In this step the local controllers are mapped together to obtain a nonlinear controller such that the entire operating range is covered. This interpolation process is usually ad hoc in nature and relies on physical insight.

LPV technique provides a superset of the gain scheduling approach in adding stability guarantee of the design by a suitable application of the linear robust control design paradigm.

B.3 An LFT Based qLPV Controller Design

In what follows the control design problem is set in the framework presented in Scherer (2001), that strongly exploits the available LMI techniques. As opposed to the gain scheduling technique these approaches provide a design algorithm that starts from an analysis equation that guarantees a certain (quadratic) performance level and the designed controller is supposed to fulfill the robust stability and performance requirements.

A main characteristic of the LPV framework is that the design is performed in time-domain based on a dissipativity approach applied to a $P - K - \Delta$ structure, where P and K are the LTI part of the (generalized) plant and of the controller, respectively, while $\Delta = \Delta_c \oplus \Delta_u$. The scheduling variables of the plant and (possibly) of the controller are contained in Δ_c while the uncertainties are placed in Δ_u.

The open loop generalized plant is defined as:

$$\left(\begin{array}{c} \dot{x}(t) \\ \hline z_u(t) \\ z_p(t) \\ y(t) \end{array}\right) = \left(\begin{array}{c|ccc} A & B_u & B_p & B \\ \hline C_u & D_{uu} & D_{up} & E_u \\ C_p & D_{pu} & D_{pp} & E_p \\ C & F_u & F_p & 0 \end{array}\right) \left(\begin{array}{c} x(t) \\ \hline w_u(t) \\ w_p(t) \\ u(t) \end{array}\right)$$

$$\begin{pmatrix} w_u(t) \\ z_u(t) \end{pmatrix} \in \mathscr{S}(\Delta(t)) \subset \mathbb{R}^{m_u + k_u} \tag{B.47}$$

with the time-varying parameters satisfying $\Delta(t) \in \nabla$. It is assumed that $\mathscr{S}(\Delta)$ admits the explicit description $\mathscr{S}(\Delta) = \mathrm{Im}(\mathbf{S}(\Delta))$ with a continuous matrix function $\mathbf{S}(\Delta)$ of full column rank. Furthermore, we suppose that (B.47) is well posed, and that there exists a nominal value $\Delta_0 \in \nabla$ for which $\mathrm{Im} \begin{pmatrix} 0 \\ I_{k_u} \end{pmatrix} \in \mathscr{S}(\Delta_0)$, see Scherer (2001).

An output-feedback LPV controller for (B.47) is described as

$$\left(\begin{array}{c}\dot{x}_c(t)\\ \hline u(t)\\ z_c(t)\end{array}\right) = \left(\begin{array}{c|cc}A_c & B_{c1} & B_{c2}\\ \hline C_{c1} & D_{c11} & D_{c12}\\ C_{c2} & D_{c21} & D_{c22}\end{array}\right)\left(\begin{array}{c}x_c(t)\\ \hline y(t)\\ w_c(t)\end{array}\right)$$
$$\begin{pmatrix} w_c(t)\\ z_c(t)\end{pmatrix} \in \mathscr{S}_c(\Delta(t)) \subset \mathbb{R}^{m_c+k_c} \tag{B.48}$$

and consists of an LTI system in which the online measured parameter $\Delta(t)$ enters via an implicit constraint imposed by $\mathscr{S}_c(\Delta)$. Here $\mathscr{S}_c(\Delta)$ is a subspace that depends continuously on $\Delta \in \nabla$ and that satisfies $\mathrm{Im}\begin{pmatrix}0\\ I_{k_c}\end{pmatrix} \in \mathscr{S}_c(\Delta_0)$.

The controller should fulfill the quadratic performance index:

$$\int_0^\infty \begin{bmatrix} w\\ z\end{bmatrix}^T \begin{bmatrix} Q_p & S_p\\ S_p^T & R_p\end{bmatrix}\begin{bmatrix} w\\ z\end{bmatrix} \le -\varepsilon\|w\|^2, \tag{B.49}$$

e.g., for an $\mathscr{L}_2$–gain specification one has $Q_p = -\gamma^2 I$, $S_p = 0$ and $R_p = I$. For these problems the performance index γ is an indicator on the quality of the controller.

Theorem B.12 (LPV analysis) *There exist a controller (B.48) such that closed-loop system is well-posed and stable if and only if there exist X, Y, multipliers $P = \begin{pmatrix} Q & S\\ S^T & R\end{pmatrix}$ and $\tilde{P} = \begin{pmatrix}\tilde{Q} & \tilde{S}\\ \tilde{S}^T & \tilde{R}\end{pmatrix}$ with $P > 0$ on $\mathscr{S}(\Delta)$ and $\tilde{P} < 0$ on $\mathscr{S}(\Delta)^\perp$ for all $\Delta \in \nabla$ that satisfy the matrix inequalities*

$$\begin{pmatrix} X & I\\ I & Y\end{pmatrix} \ge 0, \tag{B.50}$$

$$\Psi^T \left(\begin{array}{c}*\\ *\\ \hline *\\ *\\ \hline *\\ *\end{array}\right)^T \left(\begin{array}{cc|cc|cc} 0 & X & 0 & 0 & 0 & 0\\ X & 0 & 0 & 0 & 0 & 0\\ \hline 0 & 0 & Q & S & 0 & 0\\ 0 & 0 & S^T & R & 0 & 0\\ \hline 0 & 0 & 0 & 0 & Q_p & S_p\\ 0 & 0 & 0 & 0 & S_p^T & R_p\end{array}\right)\left(\begin{array}{ccc} I & 0 & 0\\ A & B_u & B_p\\ \hline 0 & I & 0\\ C_u & D_{uu} & D_{up}\\ \hline 0 & 0 & I\\ C_p & D_{pu} & D_{pp}\end{array}\right)\Psi < 0, \tag{B.51}$$

$$\Phi^T \left(\begin{array}{c}*\\ *\\ \hline *\\ *\\ \hline *\\ *\end{array}\right)^T \left(\begin{array}{cc|cc|cc} 0 & Y & 0 & 0 & 0 & 0\\ Y & 0 & 0 & 0 & 0 & 0\\ \hline 0 & 0 & \tilde{Q} & \tilde{S} & 0 & 0\\ 0 & 0 & \tilde{S}^T & \tilde{R} & 0 & 0\\ \hline 0 & 0 & 0 & 0 & \tilde{Q}_p & \tilde{S}_p\\ 0 & 0 & 0 & 0 & \tilde{S}_p{}^T & \tilde{R}_p\end{array}\right)\left(\begin{array}{ccc} -A^T & -C_u^T & -C_p^T\\ I & 0 & 0\\ \hline -B_u^T & -D_{uu}^T & -D_{pu}^T\\ 0 & I & 0\\ \hline -B_p^T & -D_{up}^T & -D_{pp}^T\\ 0 & 0 & I\end{array}\right)\Phi > 0, \tag{B.52}$$

where $\Phi = \mathrm{Ker}\begin{pmatrix} B^T & E_u^T & E_p^T\end{pmatrix}$ and $\Psi = \mathrm{Ker}\begin{pmatrix} C & F_u & F_p\end{pmatrix}$.

According to our experiences the design can be facilitated considerably by adding to the analysis LMIs (B.50), (B.51), (B.52) conditions $X < \kappa_x I$ and $Y > \kappa_y I$, where

$\kappa_x, \kappa_y > 0$ are tunable parameters. In the H_∞ setting the value of γ can be influenced by these parameters.

Controller synthesis starts with the solution of the analysis LMIs of Theorem B.12 which usually involves a relaxation step.

Relaxation

LMI conditions on the scaling matrices P and $\tilde{P}$ must hold on an infinite set. In order to make the problem tractable a so-called relaxation technique, i.e., sufficient conditions that must hold on a finite set, is needed. This might lead, however, to a conservative design, hence in general we want to reduce the relaxation "gap".

In this paper a convex relaxation is used in which the relevant LMIs are imposed at the vertices of the polytope defined by the scheduling variables. The price of this relaxation is that restriction of the multipliers P and $\tilde{P}$ of Theorem B.12 to those that have the blocks $Q < 0$ and $\tilde{R} > 0$ is needed.

The choice of a proper relaxation scheme is the cornerstone of a successful control design. For the role of the choice of the convex-hull and other related relaxations schemes that can also be applied, see Szabó et al. (2010).

Extension

Using the results of the analysis stage one can obtain from X and Y the Lyapunov matrix X_e of the closed-loop system:

$$X_e = \begin{pmatrix} X & Z \\ Z^* & [Z^*(X - Y^{-1})Z]^{-1} \end{pmatrix}, \tag{B.53}$$

where $\mathrm{Im} Z = \mathrm{Im}(X - Y^{-1})$.

In general, the multiplier $\mathscr{P}$, corresponding to the scheduling variables, can be obtained from P and $\tilde{P}$ as follows:

$$P_e := \begin{pmatrix} P & UT \\ (UT)^T & T^T[U^T(P - \tilde{P}^{-1})U]^{-1}T \end{pmatrix}.$$

U is an orthogonal matrix such that $\mathrm{Im} U = \mathrm{Im} P - \tilde{P}^{-1}$ and T is a suitable nonsingular matrix.

For the convex relaxation chosen in this paper one has

$$P_e := \begin{pmatrix} P & T \\ T^T & T^T N T \end{pmatrix}, \tag{B.54}$$

with $N = (P - \tilde{P}^{-1})^{-1}$ and $T = (T_1\, T_2)$ having the blocks $T_1 = TW$, $T_2 = T\tilde{W}$, where $W = \begin{pmatrix} I \\ 0 \end{pmatrix}$, $\tilde{W} = \begin{pmatrix} 0 \\ I \end{pmatrix}$. These blocks are chosen to fulfill the conditions

$$T_1^T(N - WQ^{-1}W^T)T_1 < 0,\ T_2^T(N - \tilde{W}R^{-1}\tilde{W}^T)T_2 > 0, \tag{B.55}$$

see Scherer (2000).

The LTI Part of the Controller

The LTI part of the LPV controller can be obtained by solving the quadratic matrix inequality:

$$\begin{pmatrix} I_m \\ \mathscr{C} + \mathscr{A}\mathscr{X}\mathscr{B} \end{pmatrix}^T \mathscr{M} \begin{pmatrix} I_m \\ \mathscr{C} + \mathscr{A}\mathscr{X}\mathscr{B} \end{pmatrix} < 0, \tag{B.56}$$

where $\mathscr{C} \in \mathbb{R}^{n\times m}$, $\mathscr{A} \in \mathbb{R}^{n\times k}$, $\mathscr{B} \in \mathbb{R}^{l\times m}$ are matrices that depend on the system matrices of the generalized plant M. The unknown is $\mathscr{X} = \begin{pmatrix} A_c & B_c \\ C_c & D_c \end{pmatrix} \in \mathbb{R}^{k\times l}$ contains the state matrices of the controller. The multiplier $\mathscr{M}$ contains X_e, P_e and the performance multiplier $P_p = \begin{pmatrix} -\gamma I & 0 \\ 0 & I \end{pmatrix}$, for details see, e.g., Scherer (2001).

In order to obtain the controller one has to solve the synthesis equation (B.56). It turns out that finding an $\mathscr{X}$ that satisfies (B.56) boils down to obtain a maximal negative graph subspace of a symmetric matrix $\mathscr{M}_s$, i.e., find a $\mathscr{Z}$ such that

$$\begin{pmatrix} I_q \\ \mathscr{Z} \end{pmatrix}^* \mathscr{M}_s \begin{pmatrix} I_q \\ \mathscr{Z} \end{pmatrix} < 0, \tag{B.57}$$

where $\mathscr{M}_s \in \mathbb{F}^{(q+p)\times(q+p)}$ with inertia $in(P_s) = (q, 0, p)$.

The existence of a solution for (B.57) has been proved by a regularization argument and involves the inverse of a perturbed nonsingular matrix. While this approach is satisfactory for the theory, in practice it is not reliable for numerical computations. A numerically reliable algorithm and a parametrization of the solutions of this inequality were given by the authors in Szabó et al. (2012):

Proposition B.1 *Let $\mathscr{M}_s$ be a symmetric matrix such that there is a nonsingular matrix M for which $\mathscr{M}_s = M^{-T}JM^{-1}$, where $J = \mathrm{diag}(-I_m, I_n)$. Then all solutions of (B.57) are given by*

$$Z = T_M(K) \tag{B.58}$$

for K is an arbitrary contraction ($\|K\| < 1$) in $\mathrm{dom}(T_M)$.

For a matrix M partitioned as

$$M = \begin{pmatrix} M_{11} & M_{12} \\ M_{21} & M_{22} \end{pmatrix} \tag{B.59}$$

the Möbius transformation T_M is defined by the equation

$$T_M(L) = (M_{21} + M_{22}L)(M_{11} + M_{12}L)^{-1} \tag{B.60}$$

for $L \in \mathrm{dom}(T_M) = \left\{ L \,:\, \exists (M_{11} + M_{12}L)^{-1} \right\}$.

Thus, the parametrization relies on describing $\mathrm{dom}(T_M)$.

This can be done by using the generalized singular value decomposition (GSVD), of M_{11} and M_{12}, i.e.,

$$M_{11} = Q\Sigma_1 U^T, \quad M_{12} = Q\Sigma_2 V^T,$$

where Σ_1 and Σ_2 has the form:

$$\begin{aligned} &\Sigma_1 = C, \quad \Sigma_2 = \begin{pmatrix} S & 0 \end{pmatrix}, && \text{if } n > m; \\ &\Sigma_1 = C, \quad \Sigma_2 = S, && \text{if } n = m; \\ &\Sigma_1 = \begin{pmatrix} C & 0 \\ 0 & I \end{pmatrix}, \quad \Sigma_2 = \begin{pmatrix} S \\ 0 \end{pmatrix}, && \text{if } n < m, \end{aligned}$$

where the matrices Σ_1 and Σ_2 have the following form

$$C = \begin{pmatrix} I & 0 & 0 \\ 0 & \bar{C} & 0 \\ 0 & 0 & 0 \end{pmatrix}, \quad S = \begin{pmatrix} 0 & 0 & 0 \\ 0 & \bar{S} & 0 \\ 0 & 0 & I \end{pmatrix}.$$

Partition $\bar{X} = V^* X U$ as

$$\bar{X} = \begin{pmatrix} \tilde{X} \\ \hat{X} \end{pmatrix}, (n > m); \ \bar{X} = \tilde{X}, (n = m); \ \bar{X} = \begin{pmatrix} \tilde{X} & \hat{X} \end{pmatrix}, (n < m).$$

With these notations one has:

Proposition B.2 *The set* $\mathscr{X}_{M_{11},M_{12}} = \{X \mid M_{11} + M_{12}X \text{ nonsingular}\}$ *is given by*

$$\mathscr{X}_{M_{11},M_{12}} = \{X \mid V\bar{X}U^T\} \tag{B.61}$$

such that

$$\begin{pmatrix} \tilde{X}_{22} & \tilde{X}_{23} \\ \tilde{X}_{32} & \tilde{X}_{33} \end{pmatrix} = N - \begin{pmatrix} \bar{C}\bar{S}^{-1} & 0 \\ 0 & 0 \end{pmatrix}, \quad N \text{ nonsingular.} \tag{B.62}$$

$\mathscr{X}_{M_{11},M_{12}}$ has elements with arbitrarily small, and also elements with arbitrarily big norm, i.e., $\mathrm{dom}(T_M) \neq \emptyset$.

Observe that considering $\hat{X} = 0$ if necessary, for sufficiently small κ the matrix $\bar{X}(\kappa)$, hence $X(\kappa)$, is a contraction. This choice is robust in the sense that it provides a solution independently of the actual values of Σ_1 and Σ_2.

The matrices T_1, T_2 that fulfill (B.55) can also be chosen by using the result of Proposition B.2.

Choice of the Scheduling Variables

The procedure to construct the scheduling variables in the general case is described in Scherer (2001). Under the conditions adopted in this paper there is a much simpler construction that are more favorable for implementation.

By permuting the blocks of P_e one has the partitioning $\begin{pmatrix} Q_e & S_e \\ S_e^T & R_e \end{pmatrix}$ with $Q_e < 0$ and $R_e > 0$. The scheduling block Δ_c of the controller can be obtained from the condition

$$\left(\begin{array}{cc|cc} U_{11} & U_{12} & (W_{11}+\Delta)^T & W_{21}^T \\ U_{21} & U_{22} & W_{12}^T & (W_{22}+\Delta_c)^T \\ \hline W_{11}+\Delta & W_{12} & V_{11} & V_{12} \\ W_{21} & W_{22}+\Delta_c & V_{21} & V_{22} \end{array}\right) > 0,$$

where

$$U = R_e - S_e^T Q_e^{-1} S_e,\ V = -Q_e^{-1},\ W = Q_e^{-1} S_e,$$

as

$$\Delta_c = -W_{22} + \begin{pmatrix} W_{21} & V_{12} \end{pmatrix} \begin{pmatrix} U_{11} & W_{11}^T + \Delta^T \\ W_{11} + \Delta & V_{11} \end{pmatrix}^{-1} \begin{pmatrix} U_{12} \\ W_{12} \end{pmatrix},$$

for additional details see Scherer (2000).

References

Abe M (1994) A study on effects of roll moment distribution control in active suspension on improvement of limit performance of vehicle handling. Int J Veh Des 15:326–336

Ackermann J, Bünte T (1998) Handling improvements of robust car steering. In: Proceedings of the international conference on advances in vehicle control and safety, Amiens, France

Ackermann J, Odenthal D (1999) Damping of vehicle roll dynamics by gain scheduled active steering. In: Proceedings of European control conference, Karlsruhe, Germany

Ackermann J, Guldner J, Sienel W, Steinhauser R (1995) Linear and nonlinear controller design for robust automatic steering. IEEE Trans Control Syst Technol 3:132–142

Alam A, Martensson J, Johansson K (2013) Look-ahead cruise control for heavy duty vehicle platooning. In: Proceedings of 16th IEEE annual conference on intelligent transportation systems, The Hague

Alberding MB, Tjønnås J, Johansen TA (2014) Integration of vehicle yaw stabilisation and rollover prevention through nonlinear hierarchical control allocation. Veh Syst Dyn 52(12):1607–1621

Alleyne A, Hedrick J (1992) Nonlinear control of a quarter car active suspension. Proceedings of the American control conference 1:21–25

Alleyne A, Hedrick J (1995) Nonlinear adaptive control of active suspensions. IEEE Trans Control Syst Technol 94–101

Alleyne A, Liu R (2000) A simplified approach to force control for electro-hydraulic systems. Control Eng Pract 8:1347–1356

Ambuhl D, Guzzella L (2009) Predictive reference signal generator for hybrid electric vehicles. IEEE Trans Veh Technol 58(9):4730–4740

Anderson B, Liu Y (1989) Controller reduction: concepts and approaches. IEEE Trans Autom Control 34(8):802–812

Anwar S (2005) Yaw stability control of an automotive vehicle via generalized predictive algorithm. In: American control conference, Minneapolis

Apkarian P, Adams R (1998) Advanced gain-scheduling techniques for uncertain systems. IEEE Trans Control Syst Technol 6:21–32

Apkarian P, Gahinet P (1995) A convex characterization of gain-scheduled $\mathscr{H}_\infty$ controllers. IEEE Trans Autom Control 40(5):853–864

Apkarian P, Tuan H (2000) Parameterized LMIs in control theory. SIAM J Control Optim 38:1241–1264

Apkarian P, Gahinet P, Becker G (1995) Self-scheduled $\mathscr{H}_\infty$ control of linear parameter-varyng systems: a design example. Automatica 31(9):1251–1261

P. Gáspár et al., *Robust Control Design for Active Driver Assistance Systems*,
Advances in Industrial Control, DOI 10.1007/978-3-319-46126-7

Asadi B, Vahidi A (2011) Predictive cruise control: utilizing upcoming traffic signal information for improving fuel economy and reducing trip time. IEEE Trans Control Syst Technol 19(3):707–714
Attia R, Orjuela R, Basset M (2014a) Combined longitudinal and lateral control for automated vehicle guidance. Veh Syst Dyn 52(2):261–279
Attia R, Orjuela R, Basset M (2014b) Nonlinear cascade strategy for longitudinal control in automated vehicle guidance. Control Eng Pract 29:225–234
Bae HS, Ruy J, Gerdes J (2001) Road grade and vehicle parameter estimation for longitudinal control using GPS. In: 4th IEEE conference on intelligent transportation systems, Oakland, California
Balas G, Fialho I, Lee L, Nalbantoglu V, Packard A, Tan W, Wolodkin G, Wu F (1997) Theory and application of linear parameter varying control techniques. In: Workshop notes: American control conference
Balas G, Bokor J, Szabó Z (2003) Invariant subspaces for LPV systems and their applications. IEEE Trans Autom Control 48(11):2065–2069
Ball J, Helton J, Walker M (1993) $\mathscr{H}_\infty$ control for nonlinear systems with output feedback. IEEE Trans Autom Control 38:546–559
Bamieh B, Giarre L (2000) Identification for a general class of LPV models. In: Proceedings of the IFAC sytem identification
Bamieh B, Giarre L (2002) Identification of linear parameter varying models. Int J Robust Nonlinear Control 12:841–853
Baranyi P (2004) TP model transformation as a way to LMI based controller design. IEEE Trans Ind Electr 51(2):387–400
Baranyi P, Tikk D, Yam Y, Patton RJ (2003) From differential equations to PDC controller design via numerical transformation. Comput Ind Elsevier Sci 51:281–297
Bardawil C, Talj R, Francis C, Charara A, Doumiati M (2014) Integrated vehicle lateral stability control with different coordination strategies between active steering and differential braking. In: 17th international conference on intelligent transportation systems, pp 314–319
Basile GB, Marro G (2002) Controlled and conditioned invariants in linear system theory. Prentice Hall, Englewood Cliffs, NJ
Becker G, Packard A (1994) Robust performance of linear parametrically varying systems using parametrically-dependent linear feedback. Syst Control Lett 23:205–215
Becker G, Packard A, Philbrick D, Balas G (1993) Control of parametrically dependent linear systems: a single quadratic Lyapunov approach. In: Proceedings of the American control conference, San Francisco, pp 2795–2799
Besancon G (2000) Remarks on nonlinear adaptive observer design. Syst Control Lett 41(4):271–280
Bokor J, Balas G (2004) Detection filter design for LPV systems: a geometric approach. Automatica 40:511–518
Bokor J, Balas G (2005) Linear parameter varying systems: a geometric theory and applications. In: 16th IFAC world congress, Prague
Bokor J, Keviczky L (1987) Arma canonical forms obtained from constructibility invariants. Int J Control 45:861–873
Borrelli F, Bemporad A, Fodor M, Hrovat D (2001) Hybrid systems: computation and control, vol 2034. Springer, Berlin, pp 162–174 (chap A hybrid system approach to traction control)
Braghin F, Cheli F, Melzi S, Sabbioni E (2008a) Race driver model. Comput Struct 86:1503–1516
Braghin F, Cimatti F, Sabbioni E (2008b) Development of a variable kinematics suspension system. In: 11th mini conference on vehicle system dynamics, identification and anomalies, Budapest
Briat C, Sename O, Lafay J (2009) Delay-scheduled state-feedback design for time-delay systems with time-varying delays: a LPV approach. Syst Control Lett 58:664–671
Burgio G, Zegelaar P (2006) Integrated vehicle control using steering and brakes. Int J Control 79:534–541
Cairano S, Tseng HE, Bernardini D, Bemporad A (2013) Vehicle yaw stability control by coordinated active front steering and differential braking in the tire sideslip angles domain. IEEE Trans Control Syst Technol 21(4):1236–1248

Castro R, Araújo RE, Tanelli M, Savaresi SM, Freitas D (2012) Torque blending and wheel slip control in EVs with in-wheel motors. Veh Syst Dyn 50:71–94
Chen B, Peng H (2001) Differential-braking-based rollover prevention for sport utility vehicles with human-in-the-loop evaluations. Veh Syst Dyn 36:359–389
Chen J, Patton R (1999) Robust model based fault diagnosis for dynamic systems. Kluwer
Chen R, Speyer J (2002) Robust multiple-fault detection filter. Int J Robust Nonlinear Control 12(8):675–696
Chen Y, Wang J (2011) Adaptive vehicle speed control with input injections for longitudinal motion independent road frictional condition estimation. IEEE Trans Veh Technol 60(3):839–848
Cloutier J (1997) State-dependent Riccati equation techniques: an overview. In: Proceedings of the American control conference, New Mexico, pp 932–936
Cole D (2001) Fundamental issues in suspension design for heavy road vehicles. Veh Syst Dyn 35:319–360
Cole DJ (2012) A path-following driver-vehicle model with neuromuscular dynamics, including measured and simulated responses to a step in steering angle overlay. Veh Syst Dyn: Int J Veh Mech Mobil 50(4):573–596
Daafouz J, Bernussou J, Geromel JC (2008) On inexact LPV control design of continuous-time polytopic systems. IEEE Trans Autom Control 53(7):1674–1678
Daniel L, Cabrera S (2010) Active tilt and steer control for a narrow tilting vehicle. PhD Thesis, Politecnico di Torino
Delorme D, Song B (2001) Human driver model for smartahs. California PATH Research Report pp 1–12
Diop S, Grizzle JW, Chaplais F (2000) On numerical differentiation algorithms for nonlinear estimation. Proceedings of the 39th IEEE conference on decision and control, Australia, Sydney, pp 1133–1138
Dorling R (1996) Integrated control of road vehicle dynamics. PhD Thesis, University of Cambridge
Douglas R, Speyer J (1996) Robust fault detection filter design. J Guid Control Dyn 19(1):214–218
Doumiati M, Sename O, Martinez J, Dugard L, Gáspár P, Szabo Z (2013) Integrated vehicle dynamics control via coordination of active front steering and rear braking. Eur J Control 19(2):121–143
Doyle J (1984) Lecture notes in advances in multivariable control. Honeywell Workshop, Mineapolis
Doyle J (1985) Structured uncertainties in control system design. In: Proceedings of the conference on decision and control, Landerdale, pp 260–265
Du H, Zhang N (2007) $\mathscr{H}_\infty$ control of active vehicle suspensions with actuator time delay. J Sound Vib 301:236–252
Ebnre A, Hermann R (2001) A self-organized radio network for automotive applications. In: 8th world congress on intelligent transportation systems, Sydney, Australia
Edelmann J, Plochl M, Reinalter W, Tieber W (2007) A passenger car driver model for higher lateral acceleration. Veh Syst Dyn 45:1117–1129
Edelmayer A, Bokor J, Szabó Z, Szigeti F (2004) Input reconstruction by means of system inversion: a geometric approach to fault detection and isolation in nonlinear systems. Int J Appl Math Comput Sci 14(2):189–199
Edelmayer A, Bokor J, Szabó Z (2009) Inversion-based residual generation for robust detection and isolation of faults by means of estimation of the inverse dynamics in linear dynamical systems. Int J Control 82(8):1526–1538
Enache M, Glaser L, Nouveliere, (2009) Composite lyapunov based vehicle longitudinal control assistance. European control conference, Budapest, Hungary
Eriksson A, Steén M (2003) Styrning av växling i motorfordon. Swedish patent, SE 520(228):C2
Evers W, van der Knaap A, Besselink I, Nijmeijer H (2008) Analysis of a variable geometry active suspension. In: International symposium on advanced vehicle control, Kobe, Japan
Fallah MS, Bhat R, Xie WF (2009) New model and simulation of macpherson suspension system for ride control applications. Veh Syst Dyn 47(2):195–220
Fan M, Tits A, Doyle J (1991) Robustness in the presence of mixed parametric uncertainty and unmodelled dynamics. IEEE Trans Autom Control 36(1):25–38

Fen W, Yang XH, Packard A, Becker G (1996) Induced $\mathscr{L}_2$ norm control for LPV systems with bounded parameter variation rates. Int J Nonlinear Robust Control 6:983–998
Fergani S, Sename O, Dugard L (2015) An LPV/Hinf integrated vehicle dynamic controller. IEEE Trans Veh Technol 15(3):566–580
Festag A, Hessler A, Baldessari R, Le L, Zhang W, Westhoff D (2008) Vehicle-to-vehicle and road-side sensor communication for enhanced road safety. In: 15th world congress on intelligent transport systems
Fialho I, Balas G (2002) Road adaptive active suspension design using linear parameter-varying gain-scheduling. IEEE Trans Control Syst Technol 10(1):43–54
Frank P, Palkovics L, Gianone L (2000) Using wheel speed and wheel slip information for controlling vehicle chassis systems. In: Proceedings of the 5th international symposium on advanced vehicle control, Ann Arbor
Fujiwara Y, Fujihira T, Ishiwa S, Adachi S (2004) Control design of driver support system using multiple driver models. SICE annual conference, Sapporo, Japan, pp 2443–2448
Gahinet P, Apkarian P (1996) Explicit controller formulas for LMI-based $\mathscr{H}_\infty$ synthesis. Automatica 32:1007–1014
Ganguli S, Marcos A, Balas G (2002) Reconfigurable LPV control design for Boeing 747-100/200 longitudinal axis. In: Proceedings of the 2002 American control conference, Anchorage, Alaska, vol 5, pp 3612–3617
Gáspár P, Bokor J (2004) Fault-tolerant rollover prevention system based on an LPV method. Int J Veh Des 42(3–4):392–412
Gáspár P, Bokor J (2005) Improving handling of vehicles with active suspension. Int J Veh Auton Syst 3(2–4):134–151
Gáspár P, Németh B (2015) Design of look-ahead cruise control using road and traffic conditions. American control conference, Chicago, pp 3447–3452
Gáspár P, Németh B (2016) Integrated control design for driver assistance systems based on LPV methods. Int J Control (in print)
Gáspár P, Palkovics L, Bokor J (1998) Iterative design of vehicle combinations for stability enhancement. Veh Syst Dyn Suppl 28:451–461
Gáspár P, Szabó Z, Bokor J (2003a) Estimating road roughness by using a linear parameter varying model. In: 4th IFAC symposium on robust control design, Milan
Gáspár P, Szászi I, Bokor J (2003b) Active suspension design using linear parameter varying control. Int J Veh Auton Syst 1:206–221
Gáspár P, Szászi I, Bokor J (2003c) Braking control to prevent the rollover of heavy vehicles based on a linear parameter varying model. In: Proceedings of the European conference of control, Cambridge
Gáspár P, Szászi I, Bokor J (2003d) The design of a combined control structure to prevent the rollover of heavy vehicles. Proc Eur J Control 10(2):1–15
Gáspár P, Szászi I, Bokor J (2003e) Rollover avoidance for steer-by-wire vehicles by using linear parameter varying methods. In: Proceedings of the mediterranean conference on control and automation, Rhodes
Gáspár P, Szászi I, Bokor J (2004a) Improving rollover stability with active suspensions by using an LPV method. In: Proceedings of the intelligent autonomous systems, Lisbon
Gáspár P, Szászi I, Bokor J (2004b) Rollover stability control for heavy vehicles by using linear parameter varying model. In: Proceedings of the IFAC symposium on advances in automotive control, Salerno
Gáspár P, Szabó Z, Bokor J (2005a) The design of an integrated control system in heavy vehicles based on an LPV method. In: Conference on decision and control, Sevilla
Gáspár P, Szabó Z, Bokor J (2005b) Estimation of the friction coefficient for road vehicles. In: American control conference, Minneapolis
Gáspár P, Szászi I, Bokor J (2005c) Reconfigurable control structure to prevent the rollover of heavy vehicles. Control Eng Pract 13(6):699–711

Gáspár P, Szászi I, Bokor J (2005d) Rollover stability control in steer-by-wire vehicles based on an LPV method. Int J Heavy Veh 13(1–2):125–143
Gáspár P, Szabó Z, Bokor J, Sename O, Dugard L (2010) Design of a reconfigurable global chassis control. FISITA Congress, Budapest
Gáspár P, Bokor J, Mihály A, Szabó Z, Fülep T, Szauter F (2015) Robust reconfigurable control for in-wheel electric vehicles. 9th IFAC symposium on fault detection, supervision and safety for technical processes (SAFEPROCESS'15), Paris, pp 36–41
Gerdes J, Hedrick J (1997) Vehicle speed and spacing control via coordinated throttle and brake actuation. Control Eng Pract 5(11):1607–1614
Gertler JJ (1998) Fault detection and diagnosis in engineering systems. Marcel and Dekker, New York
Gillespie T (1992) Fundamentals of vehicle dynamics. Society of Automotive Engineers Inc
Goodarzia A, Oloomia E, Esmailzadehb E (2010) Design and analysis of an intelligent controller for active geometry suspension systems. Veh Syst Dyn 49(1):333–359
Gordon T, Howell M, Brandao F (2003) Integrated control methodologies for road vehicles. Veh Syst Dyn 40:157–190
Gough V, Shearer G (1956) Front suspension and tyre wear. The Institution of Mechanical Engineers, Proceedings of the automobile division, pp 171–216
Grenaille S, Henry D, Zolghadri A (2008) A method for designing fault diagnosis filters for LPV polytopic systems. J Control Sci Eng
Gustafsson F (1997) Slip-based tire-road friction estimation. Automatica 33(6):1087–1099
Gustafsson N (2006) The use of positioning systems for look-ahead control in vehicles
Hac A (1987) Adaptive control of vehicle suspension. Veh Syst Dyn 16(2):57–74
Hahn J, Rajamani R, You S, Lee K (2004) Real-time identification of road-bank angle using differential GPS. IEEE Trans Control Syst Technol 12:589–599
Hairer E, Wanner G (1996) Solving ordinary differential equations II: Stiff and differential algebraic problems, Springer
Hedrick J, Uchanski M (2001) Brake system modeling and control. PATH Project Proposal, Berkeley, USA
Hedrick J, Gerdes J, Maciuca D, Swaroop D (1997) Brake system modelling, control and integrated brake/throttle switching. PATH Project Proposal, Berkeley, USA
Hellström E, Ivarsson M, Åslund J, Nielsen L (2009) Look-ahead control for heavy trucks to minimize trip time and fuel consumption. Control Eng Pract 17(2):245–254
Hellström E, Åslund J, Nielsen L (2010) Horizon length and fuel equivalents for fuel-optimal look-ahead control. Munich
Helton J, James M (1999) Extending $\mathscr{H}_\infty$ control to nonlinear systems. SIAM Adv Des Control
Henry D, Zolghadri A (2004) Robust fault diagnosis in uncertain linear parameter-varying systems. In: Proceedings of the IEEE international conference on systems. man and cybernetics, The Hague, Netherlands, pp 5165–5170
Hess RA, Modjtahedzadeh A (1990) A control theoretic model of driver steering behavior. Control Syst Mag 3–8
Hirano Y, Harada H, Ono E, Takanami K (1993) Development of an integrated system of 4WS and 4WD by H_∞ control. SAE J 79–86
Hoogendoorn RG (2010) Longitudinal driving behavior under adverse weather conditions: adaptation effects, model performance and freeway capacity in case of fog. 13th IEEE international conference on intelligent transportation systems. Funchal, Portugal, pp 450–455
Hori N, Mori T, Nikiforuk P (1992) A new perspective for discrete-time models of a continuous-time systems. IEEE Trans Autom Control 37:1013–1017
Hu JS, Yin D (2011) Mtte-based motion stabilization control for in-wheel motor electric vehicles. In: SICE annual conference, September 13-18, 2011, Tokyo, Japan
Hwang S, Park Y (1995) Active roll moment distribution based on predictive control. Int J Veh Des 16:15–28

Ifedi C, Mecrow B, Brockway S, Boast G, Atkinson G, Kostic-Perovic D (2013) Fault tolerant in-wheel motor topologies for high performance electric vehicles. IEEE Trans Ind Appl 49:1249–1257

Isidori A (1992) Dissipation inequalities in nonlinear $\mathscr{H}_\infty$ control. In: Proceedings of the conference on decision and control, Tucson, pp 3265–3270

Isidori A (1995) Nonlinear control systems. Springer

Iwasaki T, Hara S (1998) Well-posedness of feedback systems: insights into exact robustness analysis and approximate computations. IEEE Trans Autom Control 43(5):619–630

Iwasaki T, Shibata G (2001) LPV system analysis via quadratic separator for uncertain implicit systems. IEEE Trans Autom Control 46(8):1195–1208

Jiang W, Canudas-de Wit C, Sename O, Dumon J (2011) A new mathematical model for car drivers with spatial preview. IFAC world congress. Milano, Italy, pp 1139–1144

Jianyong W, Houjun T, Shaoyuan L, Wan F (2007) Improvement of vehicle handling and stability by integrated control of four wheel steering and direct yaw moment. In: Proceedings of 26th Chinese control conference, Zhangjiajie

Junaid K, Shuning W, Usman K, Wencheng T (2005) Intelligent longitudinal cruise control by quadratic minimization and robust synthesis. IEEE international conference on vehicular electronics and safety. Xi'an, China, pp 182–187

Kageyama I, Arai A, Nomura T (2000) Analysis of driverís control algorithm using neural network modeling. Veh Syst Dyn 33:122–130

Kalman RE (1960) Contributions to the theory of optimal control. Boletin de la Sociedad Matematica Mexicana 5:102–119

Katriniok A, Maschuw J, Christen F, Eckstein L, Abel D (2013) Optimal vehicle dynamics control for combined longitudinal and lateral autonomous vehicle guidance. IEEE European control conference. Zurich, Switzerland, pp 974–979

Katsuyama E (2013) Decoupled 3d moment control using in-wheel motors. Vehi Syst Dyn 51:18–31

Kawashima K, Uchida T, Hori Y (2009) Rolling stability control based on electronic stability program for in-wheel-motor electric vehicle. World Electr Veh J 3:1–8

Kellett C, Teel A (2004) Discrete-time asymptotic controllability implies smooth control-Lyapunov function. Syst Control Lett 52:349–359

Kesting A, Treiber M, Helbing D (2007) Extending adaptive cruise control to adaptive driving strategies. Transp Res Rec 16–24

van Keulen T, de Jager B, Foster D, Steinbuch M (2010) Velocity trajectory optimization in hybrid electric trucks. In: American control conference, pp 5074–5079

Khalil H (2000) Nonlinear systems. Pearson Education Int Inc, Newy Jersey

Khorshidi S, Karim M (2009) Modified AIC and FPE criteria for autoregressive (AR) model order selection by using LSFB estimation method. In: International conference on advances in computational tools for engineering applications, Lebanon

Kiencke U (1995) Integrated vehicle control systems. In: Proceedings of the intelligent components for autonomous and semi-autonomous vehicle, Toulouse

Kiencke U, Nielsen L (2000) Automotive control systems for engine, driveline and vehicle. Springer

Kiencke U, Majjad R, Kramer S (1999) Modeling and performance analysis of a hybrid driver model. Control Eng Pract 7:985–991

Kim D, Peng H, Bai S, Maguire J (2007) Control of integrated powertrain with electronic throttle and automatic transmission. IEEE Trans Control Syst Technol 15(3):474–482

Kim H, Park Y (2004) Investigation of robust roll motion control considering varying speed and actuator dynamics. Mechatronics 14:35–54

Kolmanovsky I, Filev D (2010) Terrain and traffic optimized vehicle speed control. In: IFAC advances in automotive control conference, Munich, Germany

Kowalczuk Z, Kozlowski J (2000) Continuous-time approaches to identification of continuous-time systems. Automatica 36:229–236

Labayrade R, Aubert D, Tarel J (2002) Real time obstacle detection in stereovision on non flat road geometry through "v-disparity" representation. Intell Veh Symp IEEE 2:646–651

Langbort C, Chandra RS, D'Andrea R (2004) Distributed control design for systems interconnected over an arbitrary graph. IEEE Trans Autom Control 49(9):1502–1519
Larish C, Piyabongkarn D, Tsourapas V, Rajamani R (2013) A new predictive lateral load transfer ratio for rollover prevention systems. IEEE Trans Veh Technol 62(7):2928–2936
Lattemann F, Neiss K, Terwen S, Connolly T (2004) The predictive cruise control: a system to reduce fuel consumption of heavy duty trucks. SAE Technical Paper. doi:10.4271/2004-01-2616
Lee K, Peng H (2004) Identification and verification of a longitudinal human driving model for collision warning and avoidance systems. Int J Veh Auton Syst 2(1):3–17
Lee L, Poola K (1996) Identification of linear parameter-varying systems via lfts. In: Proceedings of the 35th IEEE CDC, Kobe, vol 2, pp 1545–1550
Lee L, Poola K (1999) Identification of linear parameter varying systems using nonlinear programming. ASME J Dyn Syst Meas Control 121:71–78
Lee UK, Lee SH, Han CS, Hedrick K, Catala A (2008) Active geometry control suspension system for the enhancement of vehicle stability. Proc IMechE Part D: J Automob Eng 222(6):979–988
Lefebvre D, Chevrel P, Richard S (2003) An H-infinity-based control design methodology dedicated to the active control of vehicle longitudinal oscillations. IEEE Trans Control Syst Technol 11(6):948–956
Lefevre S, Carvalho A, Gao Y, Tseng HE, Borrelli F (2015) Driver models for personalised driving assistance. Veh Syst Dyn 53(12):1705–1720
Leith D, Leithead W (2000) Survey of gain-scheduling analysis and design. Int J Control 73(11):1001–1025
Levant A (2003) Higher-order sliding modes, differentiation and output feedback control. Int J Control 76(9/10):924–941
Li S, Li K, Rajamani R, Wang J (2011) Model predictive multi-objective vehicular adaptive cruise control. IEEE Trans Control Syst Technol 19(3):556–566
Li S, Li K, Wang J (2013) Economy-oriented vehicle adaptive cruise control with coordinating multiple objectives function. Veh Syst Dyn 51(1):1–17
Liberzon D (2003) Hybrd feedback stabilization of systems with quantized signals. Automatica 39:1543–1554
Lin R, Cebon D, Cole D (1996) Optimal roll control of a single-unit lorry. Proc IMechE J Automob Eng 44–55
Lingman P, Schmidtbauer B (2002) Road slope and vehicle mass estimation using Kalman filtering. Veh Syst Dyn Suppl 37:12–23
Ljung L (2001) Estimating linear time invariant models of non-linear time-varying systems. Eur J Control 7:203–219
Ljung L, Glad T (1994) On global identifiability for arbitrary model parametrizations. Automatica 30:265–276
Lu J, Filev D (2009) Multi-loop interactive control motivated by driver-in-the-loop vehicle dynamics controls: the framework. Joint 48th IEEE conference on decision and control and 28th Chinese control conference, Shanghai
Lu J, Messih D, Salib A, Harmison D (2007) An enhancement to an electronic stability control system to include a rollover control function. SAE Trans 2007-01-0809 116:303–313
Lu W, Doyle J (1993) $\mathscr{H}_\infty$ control of nonlinear systems: a class of controllers. In: Proceedings of the conference on decision and control, pp 166–171
Lu W, Doyle J (1994) $\mathscr{H}_\infty$ control of nonlinear systems via output feedback: controller parametrization. IEEE Trans Autom Control 39:2517–2521
Lu W, Doyle J (1995) $\mathscr{H}_\infty$ control of nonlinear systems: a convex charcterization. IEEE Trans Autom Control 40:1668–1675
Lu W, Doyle J (1996) Stabilization of uncertain linear systems: an LFT approach. IEEE Trans Autom Control 41:50–64
Lu W, Doyle J (1997) Robustness analysis and synthesis for nonlinear uncertain systems. IEEE Trans Autom Control 42:1654–1662

Lu W, Doyle J (2002) On robust $\mathscr{H}_\infty$ control for nonlinear uncertain systems. Commun Inf Syst 2:255–264
Lu X, Hedrick J (2005) Heavy-duty vehicle modelling and longitudinal control. Veh Syst Dyn 43(9):653–669
Macadam C (2003) Understanding and modeling the human driver. Veh Syst Dyn 40:101–134
Maciuca D (1996) Design, modelling and control of steering and braking for an urban electric vehicle. PATH Project Proposal, Berkeley, USA
Mammar S, Koenig D (2002) Vehicle handling improvement by active steering. Veh Syst Dyn 38:211–242
Marcos A, Balas G (2001) Linear parameter varying modeling of the Boeing 747-100/200 longitudinal motion. In: AIAA guidance, navigation and control conference, American Institute of Aeronautics and Astronautics, pp AIAA–01–4347
Marino R, Santosuosso GL (1999) Robust adaptive observers for nonlinear systems with bounded disturbances. Proceedings of the 38th IEEE conference on CDC. Phoenix, Arizona, pp 5200–5205
Markkula G, Benderius O, Wahde M (2014) Comparing and validating models of driver steering behaviour in collision avoidance and vehicle stabilisation. Veh Syst Dyn 52(12):1658–1680
Martinez J, Canudas-de-Wit C (2007) A safe longitudinal control for adaptive cruise control and stop-and-go scenarios. IEEE Trans Control Syst Technol 15(3):246–258
Mastinu G, Babbel E, Lugner P, Margolis D (1994) Integrated controls of lateral vehicle dynamics. Veh Syst Dyn 23:358–377
Mehrabi N, Razavian RS, McPhee J (2015) Steering disturbance rejection using a physics-based neuromusculoskeletal driver model. Veh Syst Dyn 53(10):1393–1415
Menhour L, Lechner D, Charara A (2009) Steering control based on a two-level driver model: experimental validation and robustness tests. 18th IEEE international conference on control applications. Saint Petersburg, Russia, pp 125–130
Merritt H (1967) Hydraulic control systems. Wiley and Sons
Muenchhof M, Beck M, Isermann R (2009) Fault-tolerant actuators and drives structures, fault detection principles and applications. Annu Rev Control 33:136–148
Muniandy V, Samin P, Jamaluddin H (2015) Application of a self-tuning fuzzy PI-PD controller in an active anti-roll bar system for a passenger car. Veh Syst Dyn 53(11):1641–1666
Na X, Cole DJ (2013) Linear quadratic game and non-cooperative predictive methods for potential application to modelling driver-afs interactive steering control. Veh Syst Dyn 51(2):165–198
Nagai M, Hirano Y, Yamanaka S (1998) Intergated robust control of active rear wheel steering and direct yaw moment control. Veh Syst Dyn 28:416–421
Németh B, Gáspár P (2011) Integration of control design and variable geometry suspension construction for vehicle stability enhancement. In: Proceedings of the conference on decision and control, Orlando, Fl
Németh B, Gáspár P (2012) Mechanical analysis and control design of mcpherson suspension. Int J Veh Syst Model Test 7(2):173–193
Németh B, Gáspár P (2013a) Control design of variable-geometry suspension considering the construction system. IEEE Trans Veh Technol 62(8):4104–4109
Németh B, Gáspár P (2013b) Design of vehicle cruise control using road inclinations. Int J Veh Auton Syst 11(4):313–333
Németh B, Gáspár P (2014) Optimised speed profile design of a vehicle platoon considering road inclinations. IET Intell Transp Syst 8:200–208
Németh B, Gáspár P, Orjuela R, Basset M (2015a) Robust $\mathscr{H}_\infty$ design of an automotive cruise control system. In: IFAC workshop on engine and powertrain control, simulation and modeling, Columbus
Németh B, Varga B, Gáspár P (2015b) Hierarchical design of an electro-hydraulic actuator based on robust LPV methods. Int J Control 88(8):1429–1440
Nemirovsky A, Gahinet P (1994) The projection method for solving linear matrix inequalities. In: Proceedings of the American control conference, Baltimore

Nesterov Y, Nemirovsky A (1993) Interior point polynomial methods in convex programming: theory and applications. SIAM
Nijmeijer H, van der Schaft A (1991) Nonlinear dynamical control systems. Springer
Nuevo J, Parra I, Sjoberg J, Bergasa L (2010) Estimating surrounding vehicles' pose using computer vision. In: 13th IEEE conference on intelligent transportation systems, pp 1863–1868
Odenthal D, Bźnte T, Ackermann J (1999) Nonlinear steering and bring control for vehicle rollover avoidance. In: Proceedings European control conference, Karlsruhe
Ono E, Hattori Y, Muragishi Y, Koibuchi K (2006) Vehicle dynamics integrated control for four-wheel-distributed steering and four-wheel-distributed traction/braking systems. Veh Syst Dyn 44(2):139–151
Pacejka HB (2004) Tyre and vehicle dynamics. Elsevier Butterworth-Heinemann, Oxford
Packard A (1994) Gain scheduling via linear fractional transformations. Syst Control Lett 22:79–92
Packard A, Becker G (1992) Quadratic stabilization of parametrically dependent linear systems using parametrically dependent linear feedback. Adv Robust Nonlinear Control Syst 43:29–36
Packard A, Wu F (1993) Control of linear fractional transformations. In: Proceedings of the conference on decision and control, pp 1036–1040
Palkovics L, Fries A (2001) Intelligent electronic systems in commercial vehicles for enhanced traffic safety. Veh Syst Dyn 35:227–289
Palkovics L, Semsey A, Gerum E (1999) Roll-over prevention system for commercial vehicles. Veh Syst Dyn 32:285–297
Passenberg B, Kock P, Stursberg O (2009) Combined time and fuel optimal driving of trucks based on a hybrid model. In: European control conference, Budapest
Patton RJ, Chen J (1996) Robust fault detection and isolation FDI systems. Contr Dyn Syst 74:176–224
Pauwelussen J (2012) Dependencies of driver steering control parameters. Veh Syst Dyn: Int J Veh Mech Mobil 50(6):939–959
Piyabongkarn D, Keviczky T, Rajamani R (2004) Active direct tilt control for stability enhancement of a narrow commuter vehicle. Int J Autom Technol 5(2):77–88
Polak E (1997) Optimization. Springer, Algorithm and Consistent Approximations
Poussot-Vassal C, Sename O, Dugard L, Gáspár P, Szabó Z, Bokor J (2008) A new semi-active suspension control strategy through LPV technique. Control Eng Pract 16(12):1519–1534
Poussot-Vassal C, Sename O, Dugard L, Gáspár P, Szabó Z, Bokor J (2011) Attitude and handling improvements through gain-scheduled suspensions and brakes control. Control Eng Pract 19(3):252–263
Prohaska R, Devlin P (1997) Combined brake and steering actuator for automatic vehicle research. In: Proceedings of the American control conference, New Mexico, pp 1603–1607
Rajamani R (2005) Vehicle dynamics and control. Springer
Rajamani R, Piyabongkarn DN (2013) New paradigms for the integration of yaw stability and rollover prevention functions in vehicle stability control. IEEE Trans Intell Transp Syst 14(1):249–261
Rajamani R, Tan H, Law B, Zhang W (2000) Demonstration of integrated longitudinal and lateral control for the operation of automated vehicles in platoons. IEEE Trans Control Syst Technol 8:695–708
Rifford L (2002) Semiconcave control-Lyapunov functions and stabilizing feedbacks. SIAM J Contr Optim 41(3):659–681
Ringdorfer M, Horn M (2011) Development of a wheel slip actuator controller for electric vehicles using energy recuperation and hydraulic brake control. IEEE international conference on control applications. Denver, USA, pp 313–318
Rossa FD, Gobbi M, Mastinu G, Piccardi C, Previati G (2014) Bifurcation analysis of a car and driver model. Veh Syst Dyn 52(Supplement 1):142–156
Saccomani M, Audoly S, D'Angio L (2003) Parameter identifiability of nonlinear systems: the role of initial conditions. Automatica 39:619–632

Saerens B, Rakha H, Diehl M, den Bulck EV (2013) A methodology for assessing eco-cruise control for passenger vehicles. Transp Res Part D 19:20–27
Safonov M, Limebeer D (1988) Simplifying the $\mathscr{H}_\infty$ theory via loop shifting. In: Proceedings of the conference on decision and control, Austin
Sakai Y, Kanai M, Yamakita M (2010) Torque demand control by nonlinear mpc for speed control of vehicles with variable valve lift engine. In: IFAC AAC advances in automotive control, Munich, Germany
Salvucci D, Mandalia H, Kuge N, Yamamura T (2007) Lane-change detection using a computational driver model. Hum Fact 43:532–542
Sampson D (2000) Active roll control of articulated heavy vehicles. PhD Thesis, University of Cambridge
Sampson D, Cebon D (1998) An investigation of roll control system design for articulated heavy vehicles. Proceedings of the international symposium on advanced vehicle control. Nagoya, Japan, pp 311–316
Sampson D, Cebon D (2003) Active roll control of single unit heavy road vehicles. Veh Syst Dyn 40:229–270
Sancibrian R, Garcia P, Viadero F, Fernandez A, De-Juan A (2010) Kinematic design of double-wishbone suspension systems using a multiobjective optimisation approach. Veh Syst Dyn 48(7):793–813
Savaresi S, Poussot-Vassal C, Spelta C, Sename O, Dugard L (2010) Semi-active suspension control for vehicles. Elsevier—Butterworth Heinemann
Sayers M (1986) Characteristic power spectral density functions for vertical and roll components of road roughness. In: Symposium on simulation and control of ground vehicles and transportation systems, Anaheim, pp 113–139
van der Schaft AJ (2000) L2-gain and passivity techniques in nonlinear control. Springer, Berlin
der Schaft AV (1993) Nonlinear state space $\mathscr{H}_\infty$ control theory. In: Trentelman HL, Willems JC (eds) Essays on control: perspectives in the theory and its applications. Birkhauser, Boston
Scherer C, Weiland S (2000) Lecture notes DISC course on linear matrix inequalities in control. Delft University of Technology, Delft, Netherlands
Scherer C, Gahinet P, Chilali M (1997) Multiobjective output-feedback control via LMI optimization. IEEE Trans Autom Control 42(7):896–911
Scherer CW (2000) Recent advances on LMI methods in control. SIAM, chap Robust mixed control and LPV control with full block scalings, pp 187–208
Scherer CW (2001) LPV control and full block multipliers. Automatica 27(3):325–485
Sciarretta A, De Nunzio G, Ojeda L (2015) Optimal ecodriving control: energy-efficient driving of road vehicles as an optimal control problem. IEEE Control Syst 35(5):71–90
Sepulchre R, Jankovic M, Kokotovic P (1997) Constructive nonlinear control. Springer
Shamma J (1992) Gain scheduling: potential hazards and possible remedies. IEEE Control Syst Mag 12:101–107
Shamma J, Athans M (1990) Analysis of gain scheduled control for nonlinear plants. IEEE Trans Autom Control 35:898–907
Shamma J, Athans M (1991) Guaranteed properties of gain sheduled control of linear parameter-varying plants. Automatica 27:559–564
Shamma J, Cloutier J (2003) Existence of sdre stabilizing feedback. IEEE Trans Autom Control 48:513–517
Sharp R (1998) Variable geometry active suspension for cars. IEEE Comput Control Eng J 9(5):217–222
Sharp R, Casanova D, Symonds P (2000) A mathematical model for driver steering control, with design, tuning and performance results. Veh Syst Dyn 33:289–326
Shibahata Y, Shimada K, Tomari T (1993) Improvement of vehicle maneuverability by direct yaw moment control. Veh Syst Dyn 22(5–6):465–481

Shuai Z, Zhang H, Wang J, Li J, Ouyang M (2013) Lateral motion control for four-wheel-independent-drive electric vehicles using optimal torque allocation and dynamic message priority scheduling. Control Eng Pract 24:55–66
Silverman LM, Meadows HE (1967) Controllability and observability in time-variable linear systems. SIAM J Control 5:64–73
Soderstrom T, Stoica P (1989) System identification. Prentice Hall, Englewood Cliffs NJ
Soderstrom T, Fan H, Carlsson B, Bigi S (1997) Least squares parameter estimation of continuous-time arx models from discrete-time data. IEEE Trans Autom Control 42:659–673
Song P, Tomizuka M, Zong C (2015) A novel integrated chassis controller for full drive-by-wire vehicles. Veh Syst Dyn 53(2):215–236
Stoustrup J, Grimble M (1996) Integrated control and fault diagnosis design: a polynomial approach. IEE Modelling and Signal Processing for Fault Diagnosis, Leicester, UK
Stoustrup J, Niemann H (2002) Fault estimation: a standard problem approach. Int J Robust Nonlinear Control 12(8):649–674
Sun X, Postlethwaite I (1998) Affine LPV modeling and its use in gain-scheduled helicopter control. Conference publication of UKACC international conference on control 455:1504–1509
Sur J, Paden BE (1998) State observer for lti systems with quantized output. ASME J Dyn Syst Meas Control 120:423–426
Szabó Z (2009) Geometric control theory and linear switched systems. Eur J Control 15(3–4):378–388
Szabó Z, Bokor J, Balas G (2003) Inversion of LPV systems and its application to fault detection. In: Proceedings of the 5th IFAC Symposium on fault detection supervision and safety for technical processes (SAFEPROCESS'03), Washington, USA, pp 235–240
Szabó Z, Gáspár P, Nagy S, Baranyi PZ (2008) Tp model transformation for control-oriented qLPV modeling. Austral J Intell Inf Process Syst 10(2):36–53
Szabó Z, Gáspár P, Bokor J (2010) A novel control-oriented multi-affine qLPV modeling framework. Proceedings of the 18th mediterranean conference on control and automation. Marrakesh, Marocco, pp 1019–1024
Szabó Z, Biró Z, Bokor J (2012) All controllers for an LPV robust control problem. In: 7th IFAC symposium on robust control design, Aalborg, Denmark
Szászi I, Marcos A, Balas G, Bokor J (2005) LPV detection alter design for a Boeing 747–100/200 aircraft. AIAA J Guid Dyn Control 28(3):461–470
Szigeti F (1992) A differential algebraic condition for controllability and observability of time varying linear systems. Proceedings of the 31st IEEE conference on decision and control. Tucson, USA, pp 3088–3090
Takagi T, Sugeno M (1985) Fuzzy identification of systems and its application to modelling anf control. IEEE Trans Syst Man Cybern 15:116–132
Takahashi H, Kidokoro H, Shiratori A (1998) Controlling vehicular driving force in anticipation of road situation on which vehicle is to run utilizing vehicular navigation system. United States patent, US 5(832):400
Takano S, Nagai M (2001) Dynamics control of large vehicles for rollover prevention. In: Proceedings of the IEEE international vehicle electronics conference, pp 85–89
Trachtler A (2004a) Integrated vehicle dynamics control using active brake, steering and suspension systems. Int J Veh Des 36:1–12
Trachtler A (2004b) Vehicle dynamic management. Benefits of integrated control of active brake, active steering and active suspension systems. Technical Report, Robert Bosch Gmbh 36:1–12
Ungoren AY, Peng H (2005) An adaptive lateral preview driver model. Veh Syst Dyn 43:245–260
Vahidi A, Stefanopoulou A, Peng H (2005) Recursive least squares with forgetting for online estimation of vehicle mass and road grade: theory and experiments. Veh Syst Dyn 43(1):31–55
Varga A (2008) On computing nullspace bases: a fault detection perspective. Proceedings of the 17th world congress the international federation of automatic control. Seoul, Korea, pp 6296–6300
Varga B, Németh B, Gáspár P (2015) Design of anti-roll bar systems based on hierarchical control. Strojniški vestnik J Mech Eng 61(6):374–382

Vasiljevic LK, Khalil H (2006) Differentiation with high-gain oservers the presence of measurement noise. Proceedings of the 45th IEEE conference on decision and control. San Diego, CA, USA, pp 4717–4722

Verdult V, Verhaegen M (2002) Subspace identification of multivariable linear parameter-varying systems. Automatica 38:805–814

Wang B, Huang X, Wang J, Guo X, Zhu X (2014a) A robust wheel slip ratio control design combining hydraulic and regenerative braking systems for in-wheel-motors-driven electric vehicles. J Frankl Inst 50:71–94

Wang R, Wang J (2012) Fault-tolerant control for electric ground vehicles with independently-actuated in-wheel motors. J Dyn Syst Meas Control 134

Wang R, Jing H, Yan F, Karimi HR, Chen N (2015) Optimization and finite-frequency $\mathscr{H}_\infty$ control of active suspensions in in-wheel motor driven electric ground vehicles. J Frankl Inst 352(2):468–484

Wang Y, Nagai M (1996) Integrated control of four-wheel-steer and yaw moment to improve dynamic stability margin. In: Proceedings 35th conference on decision and control, Kobe

Watanabe Y, Sharp RS (1999) Mechanical and control design of a variable geometry active suspension system. Veh Syst Dyn 32(2):217–235

Watts A, Vallance A, Whitehead A, Hilton C, Fraser A (2010) The technology and economics of in-wheel motors. SAE Int J Passeng Cars Electr Electr Syst 37–57

Wei J, Norman E (1964) On the global representations of the solutions of linear differential equations as a product of exponentials. Proc Am Math Soc 15:327–334

Weng Z, Cui P, Patton J (2008) Integrated design of robust controller and fault estimator for linear parameter varying systems. Proceedings of the 18th IFAC world congress. Seoul, Korea, pp 4535–4539

de Wit CC, Tsiotras P, Claeys X, Yi J, Horowitz R (2003) Friction tire/road modelling, estimation and optimal braking control. In: Johansson, Rantzer (eds) Nonlinear and hybrid systems in automotive control, pp 125–146

Wonham WM (1985) Linear multivariable control: a geometric approach, 3rd edn. Springer, New York

Wu F (1995) Control of linear parameter varying systems. PhD Thesis, Mechanical Engineering, University of California at Berkeley

Wu F (2001) A generalized LPV system analysis and control synthesis framework. Int J Control 74(7):745–759

Wu F, Yang X, Packard A, Becker G (1996) Induced L_2 norm controller for LPV systems with bounded parameter variation rates. Int J Robust Nonlinear Control 6:983–988

Wu FK, Yeh TJ, Huang CF (2013) Motor control and torque coordination of an electric vehicle actuated by two in-wheel motors. Mechatronics 23:46–60

Xiong L, Yu Z, Wang Y, Yang C, Meng Y (2012) Vehicle dynamics control of four in-wheel motor drive electric vehicle using gain scheduling based on tyre cornering stiffness estimation. Veh Syst Dyn 50:831–846

Xu Z, Ioannu P (1994) Adaptive throttle control for speed tracking. Veh Syst Dyn 23(1):293–306

Yang YP, Lo CP (2008) Current distribution control of dual directly driven wheel motors for electric vehicles. Control Eng Pract 16:1285–1292

Yim S, Jeon K, Yi K (2012) An investigation into vehicle rollover prevention by coordinated control of active anti-roll bar and electronic stability program. Int J Control Autom Syst 10(2):275–287

Young P, Doyle J (1996) Properties of the mixed μ problem and its bound. IEEE Trans Autom Control 41(1):155–159

Yu F, Li D, Crolla D (2008) Integrated vehicle dynamics control: state-of-the art review. In: IEEE vehicle power and propulsion conference, Harbin, China

Zhang S, Zhang T, Zhou S (2009) Vehicle stability control strategy based on active torque distribution and differential braking. In: Conference on measuring technology and mechatronics automation, Zhangjiajie, China

Zhang Y, Alleyne A (2002) A practical and effective approach to active suspension control. In: Proceedings of the international symposium on advanced vehicle control, Hiroshima

Zhao H, Gao B, Ren B, Chena H (2014) Integrated control of in-wheel motor electric vehicles using a triple-step nonlinear method. J Frankl Inst 352(2):519–540

Zhou K, Doyle J, Glover K (1996) Robust and optimal control. Prentice Hall

Zin A, Sename O, Gáspár P, Dugard L, Bokor, (2005) An LPV/$\mathscr{H}_\infty$ active suspension control for global chassis technology: design and performance analysis. American control conference, Minneapolis

Zin A, Sename O, Gáspár P, Szabó Z, Dugard L, Bokor J (2008) An LPV/Hinf active suspension control for global chassis technology: design and performance analysis. Veh Syst Dyn 46:889–912

Zomotor A (1991) Fahrwerktechnik. Vogel Verlag Und Druck, Fahrverhalten

Zulkarnain N, Imaduddin F, Zamzuri H, Mazlan S (2012) Application of an active anti-roll bar system for enhancing vehicle ride and handling. In: IEEE colloquium on humanities, science and engineering research, pp 260–265

Index

P. Gáspár et al., *Robust Control Design for Active Driver Assistance Systems*,
Advances in Industrial Control, DOI 10.1007/978-3-319-46126-7